SUBSURFACE INITIATED FATIGUE BEHAVIOR OF RAIL STEELS

Hua Li

B.S. from Northeastern University, China, 1982

M.S. from Beijing University of Science & Technology, China, 1988

A dissertation submitted to the faculty of the
Oregon Graduate Institute of Science & Technology
in partial fulfillment of the
requirements for the degree
Doctor of Philosophy
in
Materials Science

October, 1996

The dissertation "Subsurface Initiated Fatigue Behavior of Rail Steels" by Hua Li has been examined and approved by the following Examination Committee:

Paul Clayton, Thesis Adviser
Professor

Milton Scholl
Assistant Professor

Dr. Oscar Orringer
Lecturer, Tufts University

David Atteridge
Professor

TABLE OF CONTENTS

ACKNOWLEDGMENTS

At the Wear Group, my thanks first go to Dr. Paul Clayton, my thesis advisor, for his support, unfailing patience, and constructive criticism. When I came to OGI, he accepted me as his student; in the past four years, he has guided my work every step of the way. Dr. Milt Scholl helped to get the experimental equipment ready, kept an eye on the progression of this research and offered perceptive views throughout. I owe thanks to him. Also, I am thankful to Dr.Vivek Dikshit, Dr.Yuding Jia and Dr. Nong Jin for their help.

For the perspective in monitoring this research and reviewing this thesis, I am grateful to Dr. Oscar Orringer of Tufts University. Also sitting on my dissertation committee, Dr. David Atteridge, Professor in this department, deserves my thanks for his advice and valuable time.

For his deep understanding, I am especially indebted to Hui Su, my fellow student, who was always willing to listen whenever I talked of this research program in excitement or frustration.

Finally, special thanks go to Doug Davis, the manager of the machine shop. Over the years, his instant help kept my work running.

This research was funded by the Federal Railroad Administration, DOT, with William R. Paxton and Jerry Deiley as technical monitors.

LIST OF TABLES

LIST OF FIGURES

SUBSURFACE INITIATED FATIGUE BEHAVIOR OF RAIL STEELS

ABSTRACT

Hua Li

Supervising Professor: Paul Clayton

Oregon Graduate Institute of Science & Technology

In free rolling contact the maximum shear stresses occur at a certain depth below the surface, making the subsurface the most vulnerable to fatigue. The rail shell is a subsurface initiated fatigue crack. Both contact stresses and tensile residual stresses are driving forces for nucleation and propagation of the shell. Oxide inclusions play a role in initiation. Previous field investigations have shown that the incidence of the shell is a function of the characteristics of the oxide inclusions and rail hardness. The current work investigated the conditions under which subsurface initiated fatigue could be produced in a laboratory test and studied the relationships between fatigue failures, contact load, and material properties and inclusion properties.

A statistical procedure for assessing the cleanliness of a rail was developed, and six rail steels evaluated. A statistical sample of 20 random specimens from a rail is large enough to assess rail cleanliness. Subsurface initiated fatigue in five rail steels was investigated. The normalized contact pressure, P_o/k, was a key factor in determining fatigue mode. The limits of P_o/k to achieve subsurface fatigue in the rail steels were defined by the tests. The experimental findings revealed that not only oxide inclusions but also manganese sulfides participated in initiating fatigue cracks. A statistical model that uses measurable material properties has been advanced for predicting the probability of subsurface fatigue.

INTRODUCTION

Railroading dates back to the year 1803 with the great steam-puffing "iron horse" invented in Great Britain. About 30 years later, America's first chartered railroad was built and put into operation. Almost from its beginning the railroads of the United States became the dominant all-purpose land carrier of both freight and passengers, as a reliable, low cost, high-volume system of land transportation, and had primacy in land transportation for several decades. As the other transportation means, such as automotive highway, air, pipeline, and modern water transport have emerged and grown, railroad transportation has played a changed but specialized role. In this country, highway and air services have almost completely taken over the transportation of passengers, except that in urban areas, highway trucks perform most of the freight transportation at distances of less than 300 miles, and pipelines carry most of the petroleum products as well as other commodities. Nevertheless, the railroads of the United States carries a substantially greater volume of intercity freight transportation, compared to the other transportation means. Approximate 40 percent of the nation's freight is transported by railroad. As a result of the United States railroads' efforts to survive and develop, rail productivity rose by an incredible 57 percent from 1983 to 1993. [1] The rail freight business is booming in the United States.

To improve the economy of rail transportation, heavy axle loads and high speed have been the two major implementations. Freight car wheel loads increased from 12-15 kip to 25-30 kip in the past two decades; train speeds rose to more than 100 miles per hour.[2] Currently, some cars with 39 kip wheel loads are already in service, and over the next several years the maximum wheel load of a unit train is expected to climb to above 40 kips.[3] As wheel loads increase, however, the incidence of fatigue defects increases too. The trend to increasing axle load demands rail steels of high wear resistance and high fatigue endurance, compelling rail manufacturers to enhance the strength, hardness, and cleanliness of rail steels. Although the quality of tracks has continued to be improved in the past decades, premature failures of service rails due to wear and rolling contact fatigue (RCF) are still major problems tarnishing the economy of tracks.

Compared to the counterparts of other countries, the railroad industry of the United States undergoes especially severe RCF damage because of its heavier axle loads and denser traffic on the main lines. RCF damage to service rails is a major railroad industry concern in the United States, and it becomes prominent particularly when rail wear is alleviated by using lubricants. An investigation of 200,000 annually replaced defective rails showed that the majority of defects were traceable to the cause of RCF. [4] According to Orringer's report, [5] detail fractures, which originate from rail shells, have become the second greatest factor in causing rail defect-related train accidents, and will dominate the population of rail defects. Furthermore, another survey on service rails in six locations demonstrated that shells and shell-related defects accounted for nearly three-quarters of the detected defects. [6] In some heavy haul railroads shell-related defects were more dominant. [7] Undisputably, shells and shell-related defects are responsible for the premature replacement of rails in the USA. [8]

RCF initiated at the surface or subsurface of rail subjected to wheel loads is conventionally categorized into surface-initiated and subsurface-initiated. The modes of RCF—— surface initiated or subsurface initiated fatigue —— are governed by responses of rail steels to rolling contact as well as contact loads. [9, 10] Unlike surface initiated fatigue, subsurface initiated fatigue usually results in longitudinal and transverse defects such as shells, detail fractures, and spalls. [11,12]

To cope with an increasing incidence of rail defects, the railroad industry of the United States practices a combinationof tactics, redesigning the profile of rail / wheel to reduce contact stresses, increasing the strength of rail steels, and improving the cleanliness of rail steels. This practice actually aims at suppressing the initiation of RCF so that understanding the formation mechanism of RCF failures is essential. Therefore, considerable work needs to be done on mechanical engineering and metallurgical engineering of rail steels. Whereas previous work revealed that service lives of rails depend on both contact loads and metallurgical properties of rail steels, [13] current research and investigation activities are concentrating on RCF mechanisms, influences of both material properties and contact loads upon RCF life, and potential relations between properties of rail steels and the propensity of rail steels to RCF.

Chapter 1

A REVIEW OF SUBSURFACE INITIATED FATIGUE AND METALLURGICAL PROPERTIES OF RAIL STEELS

1.1 Distributions of Contact Stresses in Rail

1.1.1 The stress distribution in free rolling elements

When two metal cylinders are rolled together, the contact area between them is small but stresses are quite large in that location. The distribution of stresses in rolling contact is much more complex than stress distributions in standard bending or axial pulling. So far only an elastic solution to the stress distribution of two circular cylinders in line contact is well established. R_1 and R_2, two elastic solid cylinder bodies lying parallel to each other, are pressed in normal contact by a force N per unit length on a long strip of width 2b. Within the contact region, compressive stress P_o and principal stresses (σ_y, σ_z), which are induced by the contact load N, are given by equations 1-1 and 1-2, respectively: [14, 15]

$$P_0 = 0.418\ [\frac{N * E * (R_1 + R_2)}{R_1 * R_2}]^{\frac{1}{2}}, \qquad (1\text{-}1)$$

$$\sigma_y = -\frac{P_0}{b}\left[(1+2z^2)(b^2+z^2)^{-\frac{1}{2}} - 2z\right],$$
$$\sigma_z = -\frac{P_0}{b}(b^2+z^2)^{-\frac{1}{2}}. \tag{1-2}$$

Therefore, the principal shear stress τ_1 stands as:

$$\tau_1 = -\frac{P_0}{b}\left[z - z^2(b^2+z^2)\right]^{-\frac{1}{2}}. \tag{1-3}$$

The distributions of the surface compressive stress and subsurface stresses in ideal line contact are illustrated in Figures 1.1 and 1.2. The subsurface stresses vary with the depth underneath the contact surface, and the shear stress τ_1 reaches its maximum at a depth of 0.78b. When a loaded element rolls over a point on the surface (Figure 1.3), the shear stress on the *z* axis varies between 0 and τ_{max} If the element rolls in the direction of the *y* axis, then the shear stress in the *yz* plane underneath the contact surface changes from negative to positive for values of either *y* less or greater than zero respectively, so the shear stress field reverses itself. By the stress distribution on the free rolling condition, the subsurface is apparently the most vulnerable to fatigue. However, Hertzian theory is only applicable to frictionless counterformal surfaces where contact occurs over a very small patch relative to the undeformed surfaces. [16] Once surface traction is taken into account, the stress field becomes more complicated because of the presence of friction. [17] As shown in Figure 1.4, the shear stress on rolling and sliding contact is the combination of the sliding component and the rolling component; the alternating shear stress beneath the contact surface increases in magnitude but moves nearer to the surface. A quantitative determination of the subsurface stresses induced by both normal and tangential loads is still unresolved because of its extreme complexity.

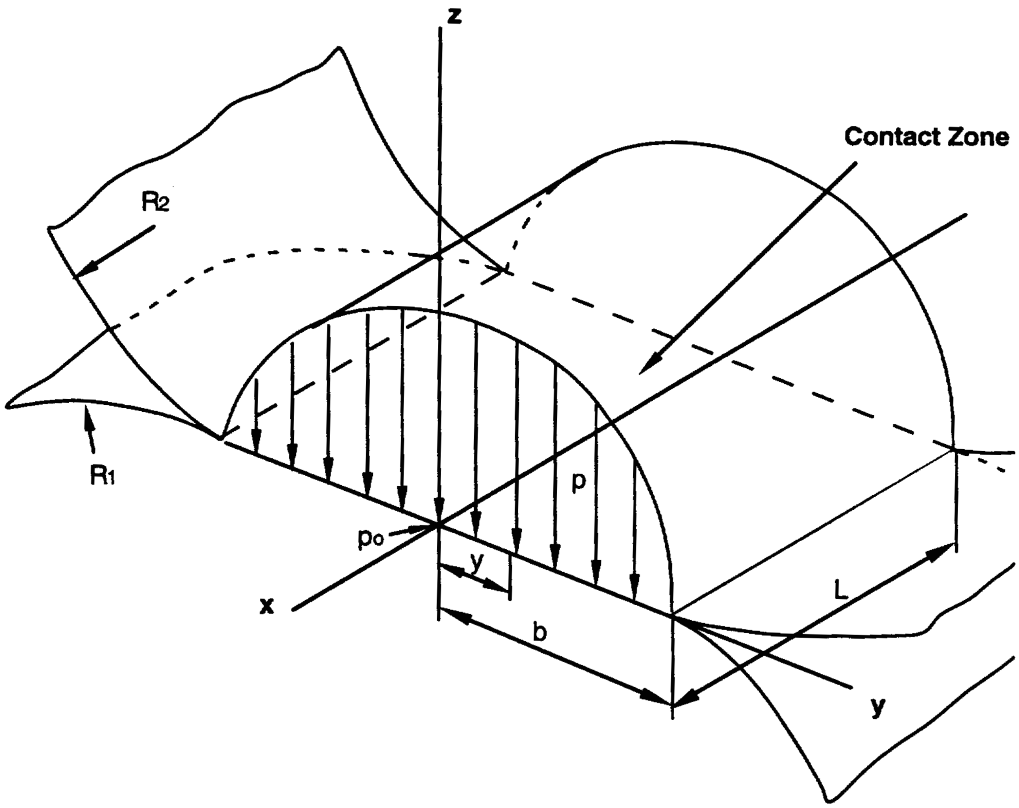

Figure 1.1 Surface compressive stress in ideal line contact.

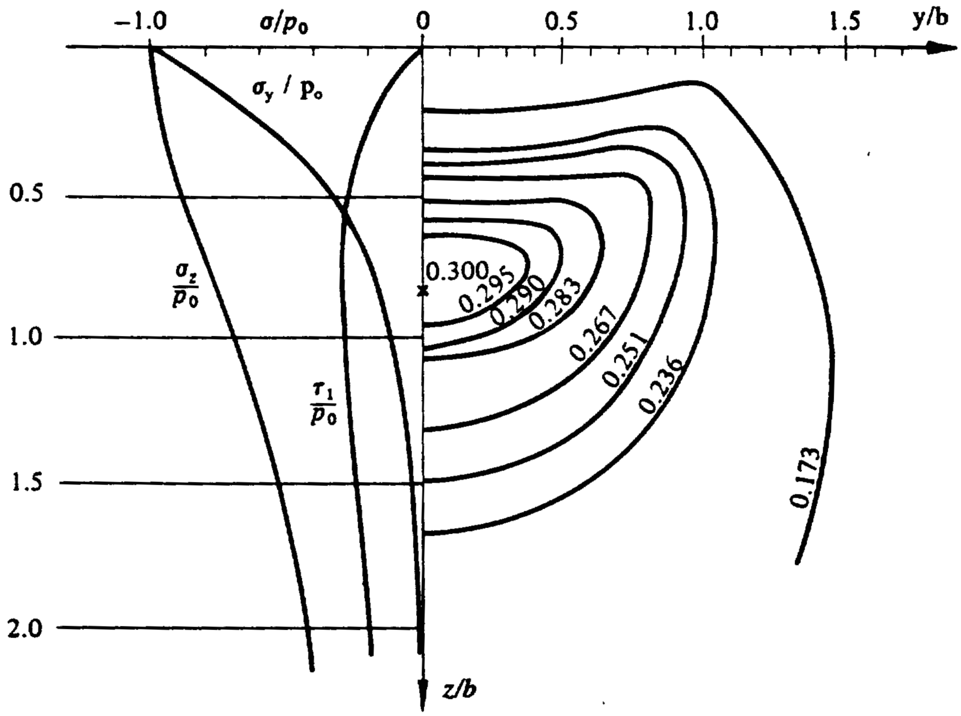

Figure 1.2 Subsurface stresses along the axis of symmetry and contours of principal shear stress τ_1.

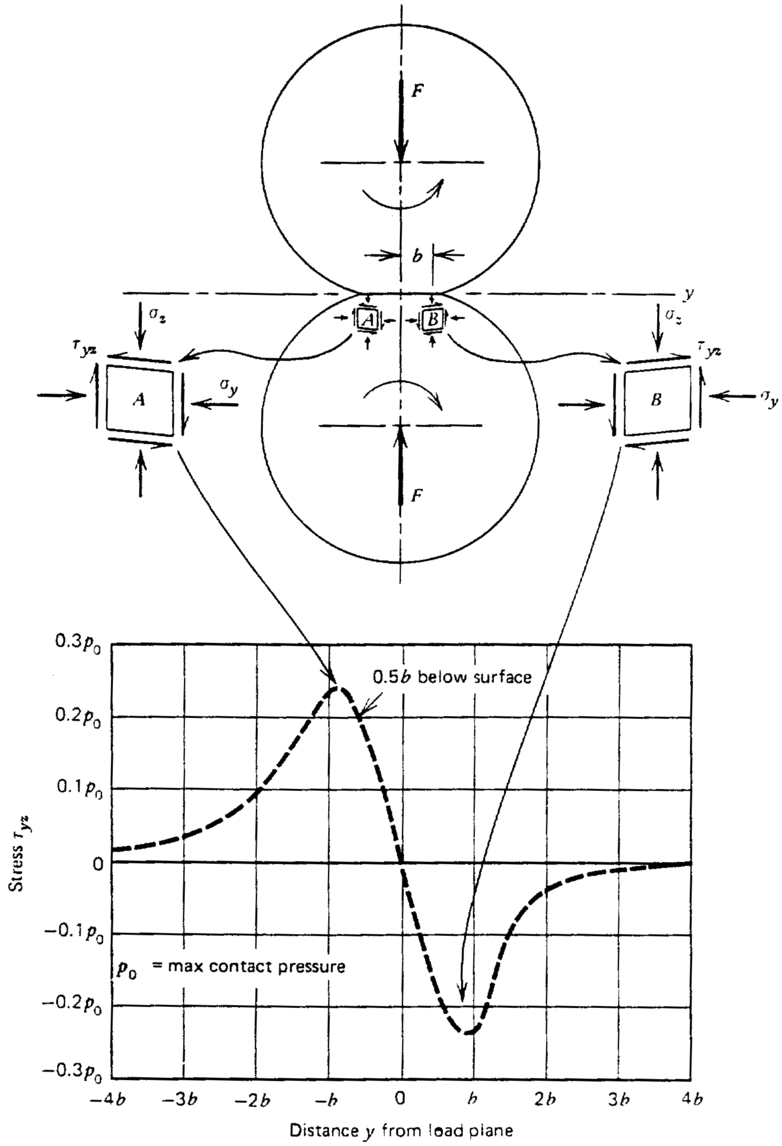

Figure 1.3 Shear stresses produced by a cylindrical roller below the surface.

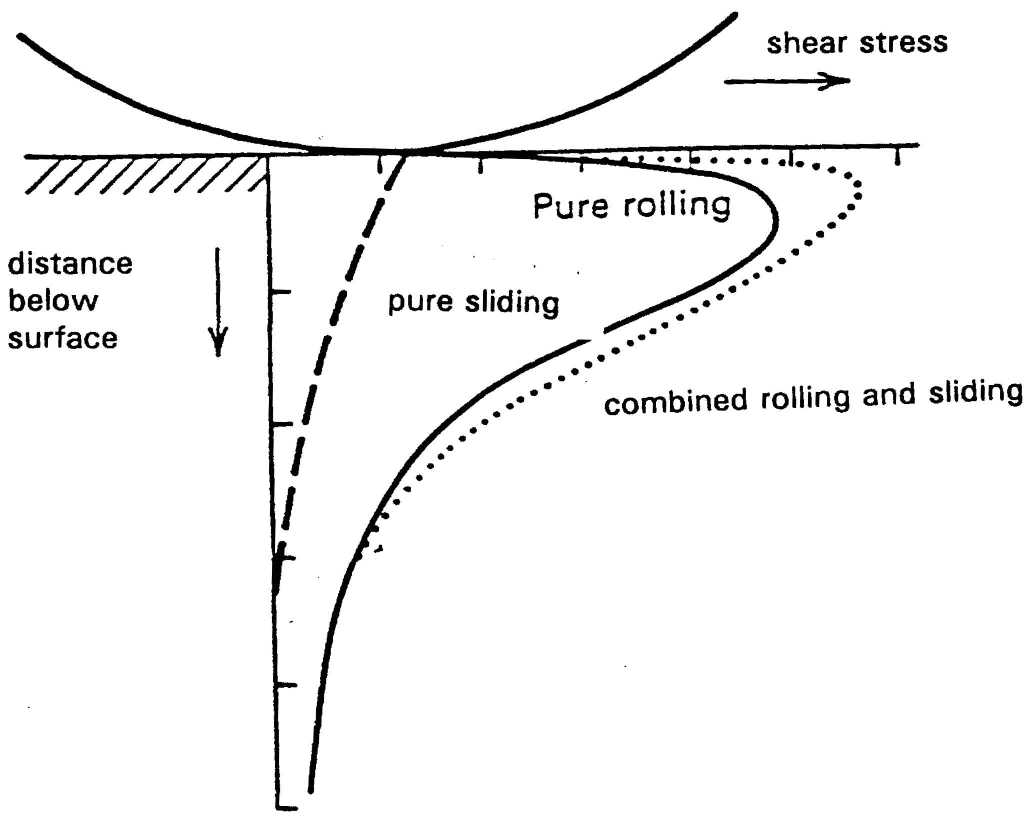

Figure 1.4 A schematic stress pattern in rolling and sliding conditions.

1.1.2 Stresses in service rail

Wheel/rail contact is a typical case of rolling contact. Hertz's contact theory is the foundation of wheel/rail contact although this theory is based on some idealized assumptions. Field rails are stressed by wheel contact load, plastic deformation, and beam flexural action. [18, 19] The contact load produces Hertzian pressure and induces shear stresses; the plastic deformation, which occurs when local shear stresses in the contact region exceed plastic limits of materials, develops residual stresses; vertical bending of rail causes flexural stresses. Compared to contact stresses and residual stresses, flexural stress is so insignificant in magnitude that its role in causing RCF is negligible. Contact stresses below the running surface of a rail are illustrated in Figure 1.5, and the region affected by residual stresses extends into the subsurface of rail (Figure 1.6). As in free rolling, the maximum stresses in rails are situated in the subsurface rather than on the surface. Even for actual rolling contact of wheel/rail, where sometimes large tangential stresses are exerted on rails by wheels, the subsurface region is still the most susceptible to yielding and fracture; [20] residual stresses in rails compound effects of shear stresses, participating in driving the subsurface to fatigue. [21]

The distribution of stresses in rail suggests that RCF tends to initiate at the subsurface affected by contact stresses and residual stresses. But the pattern of stresses alone provides little quantitative information about fatigue life of rail. Life prediction needs to consider both stress distributions in rail and fatigue properties of rail steels. Therefore, a reliable quantitative model that incorporates factors of stresses and materials and thus can be used to predict the probability of rail subsurface fatigue is needed not only for understanding metallurgical causes of subsurface initiated fatigue but also for controlling RCF failures.

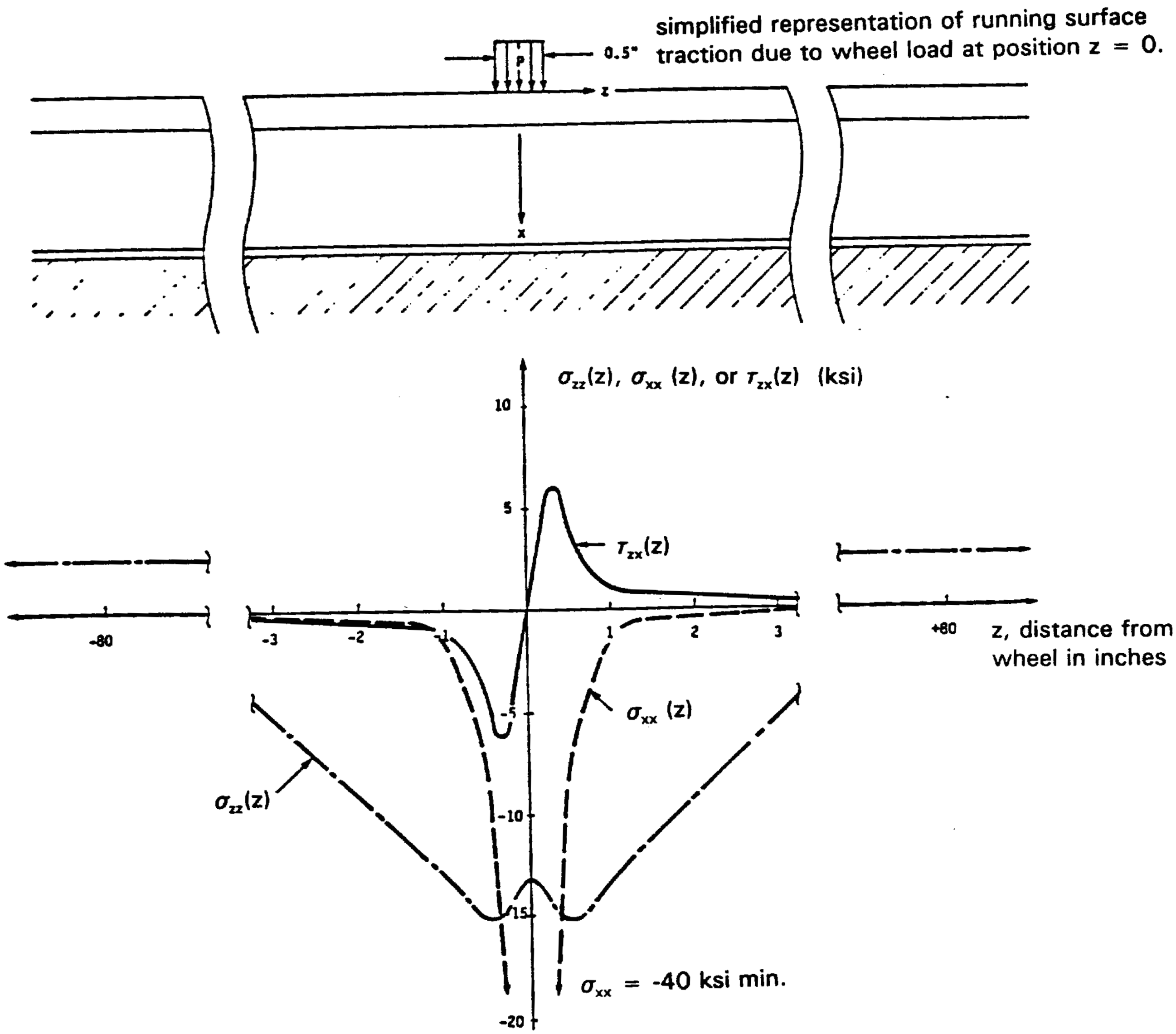

Figure 1.5 Distributions of contact stresses in a service rail.

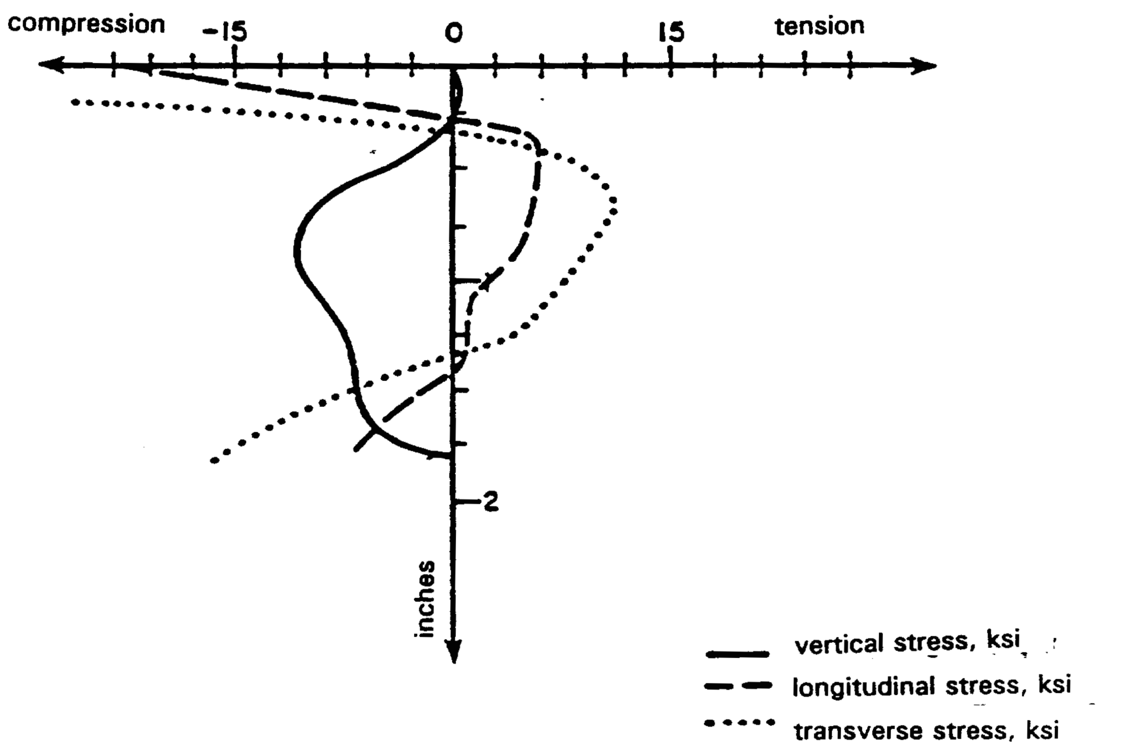

Figure 1.6 Longitudinal, vertical and transverse residual stresses under the centerline of contact.

1.1.3 Tensile residual stresses

Under the action of a cyclic load, even if nominal stresses are well below the elastic limit of a material, local stresses at inclusions or other material defects may be raised above the yield limit, resulting in plastically deformed material being surrounded by elastic material. The plastic deformation underneath the running surface leads to an attempted expansion of the plastically deformed top layer but this expansion will be constrained by the elastic material above, so residual compressive stresses are built up. [38, 103] Because the residual compressive stresses need to be equilibrated internally, tensile residual stresses must accordingly be induced below the plastically deformed top layer. As a result, a residual stress state that is highly compressive near the surface but tensile at greater depths is established. The residual tensile stresses are believed to play a critical part in nucleation and propagation of subsurface fatigue cracks. [22]

1.2 Materials Response to Rolling Contact

1.2.1 Microstructure change

Before materials fail in fatigue, changes in the material microstructure reflect responses of materials to rolling contact. Voskamp and Swahn et al. [23, 24] observed the three aspects of microstructural changes in steel subjected to rolling contact. These changes were characterized by DER (dark etching region), DER + 30° bands, and DER + 30° bands + 80° bands, respectively. These microstructural changes were dependent on the stress levels and rolling cycles; the higher the contact loads and the longer the rolling contact duration, the more striking the change in microstructure. However, none of the observed microstructure changes was identified as failure-initiating characteristics. It is difficult to relate such microstructural changes to the onset of subsurface fatigue or the nucleation of subsurface fatigue defects. Although similar changes in microstructure were observed too in a rolling contact test of rail steels, [25] the lack of features that indicate the imminence of subsurface fatigue makes it difficult to define the onset of subsurface fatigue in rail steels. In research on subsurface fatigue, the absence of such a criterion is an obstacle in testing.

1.2.2 Shakedown behavior of materials in rolling contact

Depending on the magnitude of rolling contact stresses, responses of materials subjected to cyclic loads can be perfectly elastic, elastic and plastic shakedown, or ratchetting. [26] If the maximum stresses during cycling are below the yield stress, materials will be perfectly elastic. Otherwise, if the maximum stresses during the first cycle exceed the elastic limit of materials, then plastic deformation occurs and thereby induces residual stresses. In the case of wheel/rail contact, once contact stresses at some locations exceed the elastic limit of a rail steel, residual stresses are induced. In a subsequent passage of contact loads rail is then subjected to an interaction of contact stresses and residual stresses. After a few passes, residual stresses can be built up to such a level at which the rail steel will resume its elastic behavior during following passes of loads; the system shakes down to a resultant state of stresses in which the responses of the rail steel to contact loads are entirely elastic. The maximum load at which the system shakedown takes place is defined as the shakedown limit, an important parameter for study on the behavior of subsurface initiated fatigue. From the perspective of material properties, shakedown is a self-stabilization of material when stresses caused by cyclically applied loads exceed the flow stress of material. Clearly, cumulative plastic flow in material cannot occur unless contact loads exceed the shakedown limit. Plastic deformation amplitudes vary with distance below the running surface and increase as the contact pressure goes up. The accumulation of plastic deformation at some susceptible locations, e.g., nonmetallic inclusions in steel, is the root cause of subsurface fatigue failure.

Johnson[27] found that the shakedown limit of materials in line contact was four times the shear yield strength of materials, $P_o = 4k$ (Figure 1.7). The shear yield strength k is related to the yield stress σ by $k = \sigma_{y\mathrm{s}} / 3^{1/2}$. [28] Since kinematic behavior materials have the same shakedown limit as that of elastic-perfect-plastic materials, [29] the relationship $P_o = 4k$ is also applicable to rail steels.

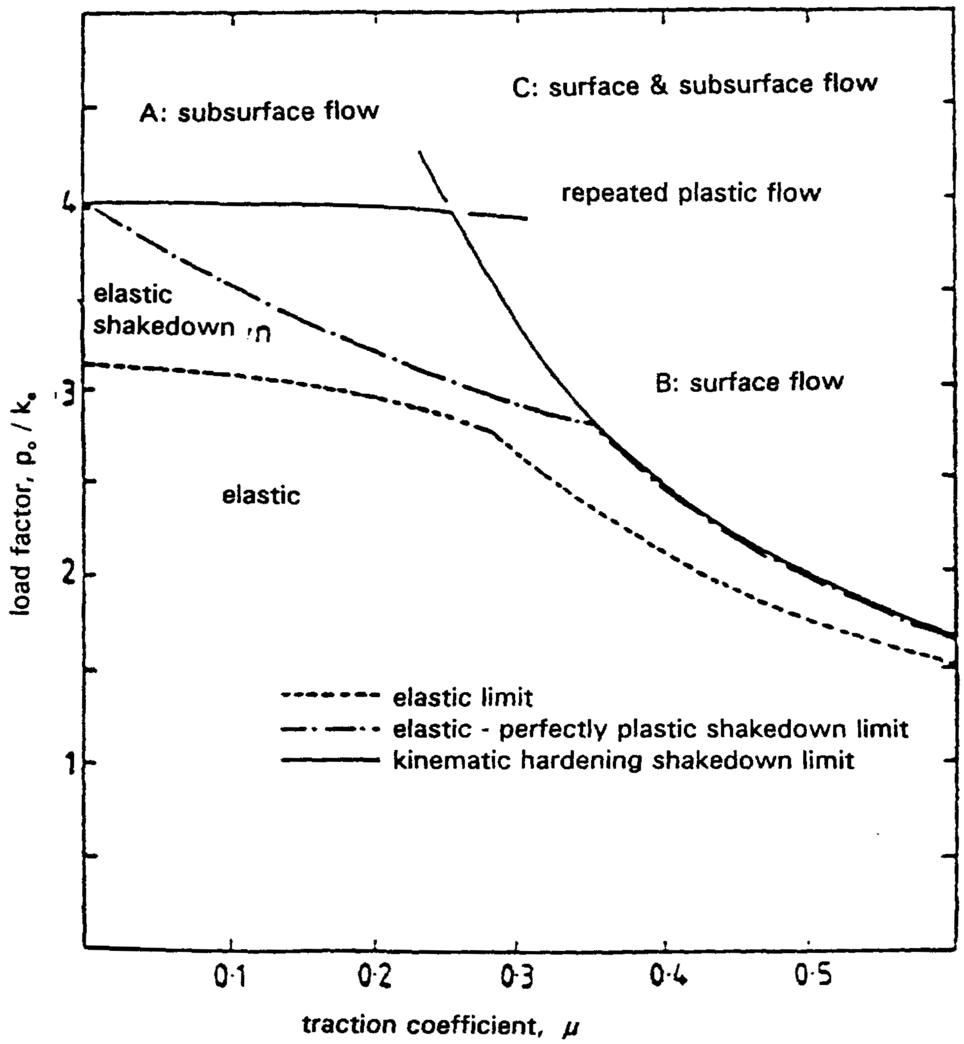

Figure 1.7 Map of shakedown limits.

1.3 Subsurface initiated fatigue defects of rails

1.3.1 Shells in rails

A shell is a progressive horizontal separation that generally is initiated at 5-15 mm depth underneath the running surface of a rail. The rail shell is a common type of fatigue defect caused by RCF, and regarded as the source of other subsurface fatigue failures such as spalls and detail fractures. [30, 31]

Shells originate in the transition zone between the deformed surface zone and the undeformed interior of railheads, [9, 22, 32] and the initiation area is approximately 20-30 mm^2. [11, 33] Driven by both contact and residual stresses, shells either propagate parallel to the running surface or turn down to form transverse defects.[16] On the one hand, many investigations have shown that this type of defect actually tended to initiate at oxide inclusions, [32, 34, 35, 36] and grew in the lateral direction.[11, 12] On the other hand, some investigators, according to the absence of inclusions in some uncapped shell defects, disagreed that rail shells are nucleated at oxide inclusions and suspected that those shells could develop from microcracks nucleated through an intrusion-extrusion mechanism. [37] However, the intrusion-extrusion mechanism is effective when fatigue cracks are nucleated on the surface or free surface, and this mechanism is probably not applicable to the formation of a subsurface initiated shell defect. In fact, shells are initiated internally and do not grow from surface initiated headchecks although shells may eventually link with them. [33]

1.3.2 Effects of contact stresses

In principle, fatigue cracks are all started by the simultaneous action of three necessary elements: cyclic stress, tensile stress and plastic strain. Without exception, the formation of shell defects is the result of interaction of the three elements.

Under contact of wheel/rail, cyclic shear stresses, residual stresses and compressive stress occur in the affected zone of a railhead. Effects of rail stresses upon subsurface initiated fatigue cracks were modeled by Leis [38] and Lieurade et al. [28] According to Lundberg and

Palmgren's rolling fatigue theory for ball bearings, which considers that a fatigue crack is initiated at a point below the surface where a large-magnitude alternating shear stress coincides with the weak point in material, [39] some rail investigators used also to emphasize the effect of shear stresses on shelling. [40, 41, 42] However, shells usually occur at the depth where contact shear stresses are not at their maximum, strongly suggesting that shells can be caused by other stresses than shear stresses. Work by Rice et al. and Tokuda [22, 43] provided a clue that residual stresses tended to build up around typical locations of shelling initiation. Recent work demonstrated that residual stresses actually had a dominant effect upon the initiation of a shell. [32, 44] Marich et al. [45] contended that residual tensile stresses and cyclic compressive stress are responsible for the occurrence of a shell whereas cyclic shear stresses did not play a role. Within the stress contours illustrated in Figure 1.8, the residual stresses are tensile but beyond the contour they become compressive. Both the cyclic compressive stress and residual tensile stress are normal to the crack plane. Thus, the interaction between the compressive stress and residual tensile stress is able to nucleate a subsurface crack. Subjected to the residual tensile stress, a shell either grows longitudinally or develops into a transverse defect.

Shelling is a subsurface fatigue phenomenon of rails in rolling contact. Under ideal rolling contact conditions or with negligible surface friction, rail fatigue tends to occur in the subsurface, resulting in subsurface cracks, subsurface-deformed bands, and voids. [10] The induced residual stress in the subsurface is the driving force for the shell to occur and grow.

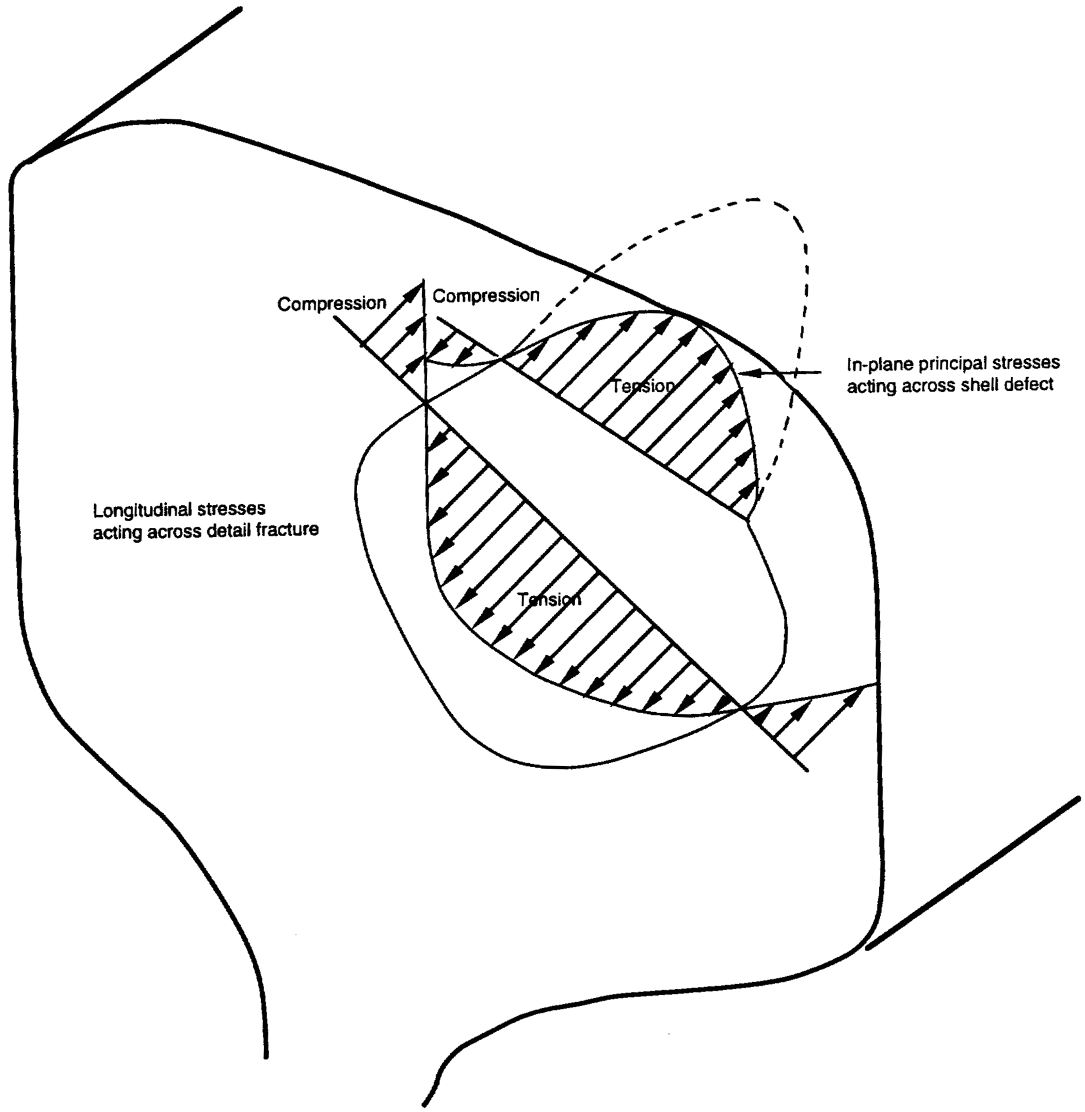

Figure 1.8 Schematic distribution of residual stresses in rail head.

1.3.3 Effects of nonmetallic inclusions

In some cases, shells were originated at the regions where both shear stresses and residual stresses were not at the maximum.[8, 44] Therefore, the occurrence of these shell defects might be ascribed to other factors than the stresses. As many investigations found, most shell defects were traceable to the cause of nonmetallic inclusions and steelmaking slag. Marich and Sonon demonstrated that complex oxides could act as fatigue crack initiators of transverse defects.[45] In particular, work in Australia[46, 47] has identified oxide inclusions as a significant factor. This finding has been largely supported by work carried out in the United States.[48, 49, 50] The results of the FAST (Facility for Accelerated Service Testing) experiments at Pueblo, Colorado, have led Clayton and Brave to conclude that the incidence of defects appears to be directly proportional to the logarithm of the volume fraction of oxide inclusions as well as a measure of clustered oxide inclusions divided by some function of the hardness.[48] Work by Sugino et al[51] has also rated alumina clusters a primary factor in causing rail shell defects while manganese sulfides did not take a part in the formation of shells. Now it is well recognized that oxide inclusions in rails, as stress-raisers and micro-crack providers, potentially are origins of shell nucleation. A number of railroads, including Norfolk Southern, Canadian National and British Rail, have already specified a maximum level of inclusions for rails. One of the current activities of the European Railway Research Institute Committee D173 is to define a standard method of determining inclusion levels and recommend limits for new rail steel specifications.[52] While, in principle, the approach is reasonable, there are very few data with which to quantify the effect of inclusions on rail performance. A further concern is what method to use in determining the content of nonmetallic inclusions in rails.

The content of sulfide inclusions in rail steel accounts approximately for 80% of total nonmetallic inclusions. Yet none of the investigations has provided solid evidence linking the occurrence of shell defects to the presence of sulfide inclusions.[33] In view of this fact, researchers seem to agree that sulfide inclusions would be benign as crack initiation sites.[2] But sulfide inclusions interrupt the continuity of a steel matrix, deteriorating the fatigue resistance of the local material. Whether or not sulfide inclusions are involved with the cause of subsurface defects needs to be verified by future work. Moreover, not only do the properties of inclusions influence the occurrence of rail shells, but also their size, morphology and distribution of inclusions.

1.4 Theories of subsurface initiated fatigue defects

1.4.1 Criteria of void nucleation

Since little work has been aimed at investigating subsurface initiated fatigue in rolling contact, the formation mechanisms of subsurface initiated fatigue defects are very obscure and there are no established criteria for judging the onset of subsurface initiated fatigue. In contrast, defect nucleation processes in uniaxial tension or in pure shear have been extensively investigated. Although the state of stress and strain in rolling contact is different from that in uniaxial tension and pure shear, the nucleation of a fatigue defect is somewhat similar in the two cases. [53] Therefore, reviewing theories or models about defect nucleation at simple uniaxial loads is helpful in understanding the process of subsurface initiated fatigue in rolling contact.

The energy criterion, the local stress criterion, and the local strain criterion have been advanced for defining the conditions at which a fatigue defect is nucleated around an particle. Based on the local strain energy density and local stress field around a particle, the energy criterion was first proposed by Garland and Plateau. [54] The critical stress σ, required for debonding at the interface between the particle and matrix, is expressed by this criterion as:

$$\sigma \geq \frac{1}{C}\left[\frac{12 W_{ad} E_{w}}{d}\right]^{\frac{1}{2}}$$

where C is the stress concentration factor; d the diameter of a particle; E_w a weighted elastic modulus of the particle and the matrix; and W_{ad} the surface energies of the particle, the matrix, and the interface respectively. The equation gives a prediction that the critical stress required for debonding increases as the size of a particle decreases.

The stress criterion was proposed by Ashby. [55] In his theory a defect can be nucleated at a point along a particle-matrix interface if a tensile radial stress at that point exceeds the cohesive strength of the interface, i.e.,

$$\sigma_{rr}\big|_{max} \geq \sigma_c$$

The energy and stress criteria of defect nucleation signify that debonding at the particle-matrix interface does not occur until the local strain energy in and around the particle is greater than the work of interface adhesion and that the magnitude of the tensile radial stress at some point along the particle-matrix interface exceeds the interfacial bond strength. For a nucleation of voids around hard particles in a deformed matrix, the energy criterion must be satisfied and also a larger tensile stress than the interfacial strength must be developed.

As Argon et al [56] pointed out, the energy criterion is always satisfied in a pure elastic situation as long as particles are larger than 25 nm. But in many instances many larger particles remain attached to a matrix even at strains much larger than the yield strain, suggesting that the energy criterion is only a necessary but not a sufficient condition of crack nucleation. Since the energy criterion is always satisfied for large particles, the stress criterion becomes the necessary and sufficient condition for the nucleation of voids at the interface between particles and matrix. After analyzing the process of defect nucleation around circular cross-section inclusions embedded in an elastic-plastic matrix in plane strain, Argon et al [57] concluded that the maximum interfacial tensile stress at the boundary due to pure shear is equal to the yield strength of a material and that the maximum interfacial tensile stress caused by accumulative plastic strain is equal to 1.7 times that of the pure yield strength k, or $3^{1/2}k$.

1.4.2 Mechanisms of subsurface-initiated fatigue cracks

In rolling contact, subsurface deformation is highly localized around oxide inclusions. [58] Because of stress and strain concentration, subsurface fatigue tends to initiate at material defects such as voids, inclusion/matrix interfaces, and grain boundaries. Although in a plastically deformed region it is possible that microcracks are nucleated through several mechanisms, the nucleation in an elastically deformed region is always attributed to localized microplastic deformation. The nucleation is through one of plastic nucleation processes such as dislocation pileups, twin intersections and strain incompatibility.[59]

As carriers of deformation, driven by shear stresses, dislocations and vacancies in materials move during repetitive stressing, with dislocations piling up at material defects.[60] Accordingly, the accumulation of plastic micro-strains occurs at the defects. As the dislocation density increases, a crack embryo will finally be nucleated. Hence, the piling-up of dislocations at material defects is crucial for the formation of subsurface initiated fatigue cracks.[61, 62, 63]

The formation of a subsurface initiated fatigue crack can be summarized as:

Step 1, dislocations in the subsurface are piled up at material defects, resulting in dislocation cell structure;

Step 2, voids or microcracks are initiated in the regions of the maximum stress or near to discontinuities in the microstructure such as grain boundaries, preexisting porosity or inclusion/matrix interfaces;

Step 3, microcracks in the subsurface grow and propagate.

In regard to the nucleation of subsurface-initiated fatigue, however, some researchers argued that subsurface cracks could be nucleated in locations free of material defects and nonmetallic inclusions. Ruppen et al.[64] contended that the initiation of cracks in the subsurface could be a result of dislocation-microstructural interactions only, not involved with other material defects. But nobody has ever attempted to address how subsurface initiated fatigue cracks could be nucleated at defect-free regions. As to the formation of subsurface initiated fatigue defects in rail steel, the question of whether the formation of dislocation cells in rail steels necessitates the presence of nonmetallic inclusions has never been addressed. In Ti-6Al-4V material Gilbert[65] and Neal[66] discovered that dislocation cells could form in region without nonmetallic inclusions. Furthermore, the formation of dislocation cells in the AISI-310 stainless steel did not hinge on the presence of any nonmetallic inclusions.[67] It is tempting to conjecture that dislocation cells in rail steels may be formed at regions free of nonmetallic inclusions.

Obviously, extensive work is required to understand fully how dislocation cells are formed in rail steels and how dislocation cells cause the nucleation of subsurface initiated fatigue cracks.

1.5 Manufacture and Metallurgy of Rail Steels

1.5.1 Manufacture processes

Today's rail steels are manufactured in either basic oxygen or electric arc furnace processes. The preferred route is by basic oxygen steel making in which liquid blast furnace iron is partially refined to rail steel, and then the liquid rail steel is degassed in a vacuum and fully refined with the temperature and composition controlled in a ladle. The combination of basic oxygen melting, secondary refining and vacuum degassing processes give extremely fine control of all aspects of the steel. Finally, the liquid steel is preferably continuously cast under gas shrouded conditions into low segregation, surface-defect free blooms. Possibly having risked an increase in hydrogen at the beginning of steel teeming, some cast blooms are required to be slowly cooled for hydrogen removal. While still at 600 °C blooms are placed in insulated boxes and cooled at a rate of 1 °C per hour for a period of three to five days. This treatment coupled with prior vacuum degassing can reduce the hydrogen content in finished rails to about 0.5 ppm, ultimately eliminating the hydrogen damage that previously brought about many rail problems. By vacuum degassing, in-ladle trimming and controlled cooling, modern rail steel making technologies can produce high quality steel with strictly controlled composition, lower levels and more modified oxide and sulphide inclusions, and minimum segregation.

The trend toward greater wheel loads in North America necessitates a continuing effort to improve durability of rail steels and coax more life out of rails. Historically, one of the two traditional strategies of extending rail life has been strengthening of rail steels by alloying and heat treatment. This strategy is implemented by replacing matrix pearlitic microstructure with some other constituent, either bainite or tempered martensite, and by decreasing the content of nonmetallic inclusions. Contemporary rail production techniques provide more options for rail users than ever before.

1.5.2 Sources of oxide inclusions in rail steels

Nonmetallic inclusions naturally fall into two groups —— those of indigenous origin and those of exogenous origin. The indigenous group contains inclusions resulting from deoxidization reactions in the molten or solidifying steel bath, whereas the exogenous origin group includes trappings of slags, refractories or other materials with which the molten steel comes in contact. Indigenous inclusions, as a result of homogenous reactions in liquid steel, are composed primarily of oxides and sulfides. Reactions producing indigenous inclusions are induced either by additives to steel or simply by a change in solubility during solidification of steel.

Commonly observed alumina and calcium aluminates in rails stem primarily from the deoxidation of liquid steels although some complex oxide inclusions may come from trappings of steel making slag and furnace-lining materials. The content of nonmetallic inclusions in current rail steels is estimated to be a range of 0.04-0.2 area per cent while the content of oxides alone varies from 0.0004 to 0.017 area per cent. [11, 51, 68] When a rail steel is being produced, a decision has to be made as to what level and types of oxides will be in the final rail products. The composition, size, morphology, and aggregation of oxide inclusions are determined largely by the type of metals or metal alloys used in deoxidizing liquid steels:

$$2[Al] + 3[O] = (Al_2O_3)$$

$$[Ca] + [O] = (CaO)$$

$$M(Al_2O_3) + N(CaO) = MAl_2O_3.NCaO$$

Aluminum and its alloys have been commonly used in deoxidation of rail steels. Al_2O_3 and $MAl_2O_3 \cdot NCaO$ appear in separate particles in steel, but actually they join one another in three-dimension configurations and form clusters.[69, 70] Alumina and calcium aluminates are undeformable within a steel matrix and vulnerable to being broken into stringers during a heavy plastic forming process. The deoxidization of liquid steel by aluminum suppresses the formation of carbon monoxide during solidification and hence eliminates blowhole defects, but the deoxidization results in clusters of undesirable broken aluminates. Other methods of deoxidation are often preferred to using pure aluminum, such as by using Si-Ca-V, Si-Ca-Ba, and Si-Ca-Mg-V for deoxidation and by vacuum carbon deoxidation. [71] Unfortunately, not only are these compound deoxidizers more expensive than aluminum metal, but also their deoxidizing capacities are inferior to that of aluminum. In addition, unlike aluminum and its alloys they cannot refine the grain size of steel, and small grains are required for enhancing fatigue resistance of rail steel. Therefore, aluminum will probably continue to be a primary deoxidizer of rail steels in future although it produces the troublesome product Al_2O_3.

As an inherent byproduct of deoxidizing liquid rail steel, oxide inclusions worsen the fatigue resistance of rail steels. Because of unavoidable secondary oxidation in solidification of liquid steel, oxide inclusions cannot be eliminated from rails even though the alternative process of vacuum carbon deoxidation is applied. An effective approach to alleviating detrimental effects of oxide inclusions is by modifying them in composition and morphology. [72]

1.5.3 Characteristics of inclusions

Nonmetallic inclusions interrupt the continuity of a steel matrix, and are detrimental to the fatigue resistance of steels. In rail steels, spherical non-deformable calcium aluminates and stringered alumina inclusions are the most harmful while sulfide inclusions are relatively benign. [12] Although the behavior of inclusions in rails subjected to rolling contact has been seldom investigated, knowledge of the behavior of nonmetallic inclusions in ball bearing steels provides an insight into the properties and the behavior of nonmetallic inclusions. The factors that impinge upon fatigue properties of steel are the quantity, size, shape, distribution and inter-distance of nonmetallic inclusions.

Properties and behavior

Nonmetallic inclusions' plasticity relative to a steel matrix is a critical factor in influencing the fatigue resistance of steel. The plasticity of inclusions is evaluated with the index of deformability (ν) [73]

$$\nu = \frac{2}{3} * \frac{\log\lambda}{\log h},$$

where $\log \lambda$ is a measure of true elongation of inclusion, and $\log h$ an expression for the true elongation of steel. Al_2O_3 and calcium aluminates (CA, CA_2, CA_6) are hard at all possible temperatures of rail forming, and their deformability indices are therefore zero. The hardness, elasticity, and thermal contraction of alumina and calcium aluminates are radically different from those of rail steels. In a steel rolling process, the difference in the thermal contractions of oxide inclusions and a steel matrix results in textural stresses around inclusions. These stresses could participate in crack initiation so as to deteriorate the fatigue resistance of the matrix. [74] Since brittle alumina and calcium aluminates are harder than steel, they are hardly deformed during rolling and thus cannot transfer locally built-up residual stresses. Stresses around hard inclusions are raised above the flow stress of the matrix; the local material contiguous with the particles are plastically deformed. As a result, nonmetallic inclusions tend to debond at matrix /particle interfaces, or nonmetallic inclusions themselves are broken up to be oxide stringers, creating subsurface micro-cracks. [75]

Sulphide inclusions have a high index of deformability at all temperatures. During the hot rolling of steel sulfides participate in the matrix deformation of different stages, changing their shape with the steel matrix. Therefore, throughout the plastic deformation cycle, interface bonds between inclusions and matrix are hardly broken and no microcracks are generated.

Inclusion size

Undoubtedly, the larger the size of an inclusion, the more detrimental its effects. However, the question of whether an inclusion smaller than a threshold size would have an effect on fatigue properties of steel is still unresolved, although many research workers have tried hard to establish the threshold.

Artificially implanting Al_2O_3 particles, Duckworth and Ineson carried out a fundamental study of size effect. [76] Their findings showed that if an inclusion was larger than a critical size and was not situated in the steel surface, the strength-reducing effect (K_f) of the Al_2O_3 inclusion was proportional to the cube root of the inclusion diameter. Besides, only oxide inclusions bigger than a threshold value were able to affect fatigue properties of steel. Uhrus [77] determined a critical size of oxide inclusions in a ball bearing steel as 30 μm in diameter. But conclusions on the critical size of inclusions in rail were not unanimous, dependent upon individual investigators and their research methods. Skinner, [33] by investigating rail shell defects, determined that only oxide clusters larger than 80 μm were able to initiate rail shells, whereas Barsom et al [78] contended that the critical size of stringer oxides in rails was 25 μm in width. It seems that the concept critical size of oxide inclusions hinges on how it is defined and what methods are used to determine it —— quite subjective. Work in Australia, correlating diameters of oxide inclusions to an incidence of defects in rails, considered 100 μm to be the threshold. [79] Below this threshold, changes in inclusion diameter slightly impinged on the incidence. However, recent work presented a significantly different result: all inclusions larger than 5 μm normally had an adverse effect on fatigue life. [80] Although Kiessling [81] insisted on an inclusion limit of inclusions and advocated making an effort to determine it, the critical limits cited above are so various that one suspects any practical significance of the concept itself.

A critical size of inclusions rests on so many influential factors. For example, actual locations of inclusions in steel and a distance of the location below the steel surface are crucial factors in evaluating effects of the inclusion. Johnson et al [82] found that the critical size increased from 10 μm to 30 μm if the position of an inclusion was down to 100 μm from just below the surface. Therefore, there is not an absolute size limit below which inclusions would not render a detrimental effect. Even though all inclusions had a uniform size, their influences vary significantly with the type of inclusions and locations relative to the surface. In effect, influence of the size of inclusions is actually not so crucial in initiation of microcracks as the aggregation and plasticity of inclusions. [83]

Stringered oxides

The distribution and morphology of oxide inclusions also affect their involvement in the nucleation of a microcrack. An investigation of defective rails revealed that aluminate inclusions associated with shell defects were a stringer type in the longitudinal direction of rail. [45] Alumina and calcium aluminate stringers result from clusters of inclusions during solidification of liquid steel. During the rolling of rails these clusters are broken off in the direction of the rolling, producing aligned stringers. Alumina and calcium aluminate stringers are more detrimental in nucleation of microcracks than isolated inclusions of the same type, because stringer inclusions or roughly-aligned separate inclusions facilitate both the nucleation of individual shells and the coalescence of fine adjacent cracks around them. [74, 84] According to work by Andrews and Turkdogan, [70, 85] the stress field around an isolated inclusion affects an area of radius 4r - 5r from the inclusion center so that stringered inclusions can enhance void nucleations by superimposing the stress effects arising from one another. [86] Therefore, the spacing between individual inclusions of stringers also govern effects of inclusions. Some researchers [87] even proposed the ratio of the size to the inter-spacing as a criterion for evaluating effects of inclusions. Sugino [51] defined a stringer number, which is a measure of effects of oxide stringers in rails, for correlating a relationship among inclusion inter-spaces, stringer lengths, and the incidence of rail shells. Besides, stringered inclusions play a role in growth of transverse cracks, detouring the growth of shell defects and boosting the propagation of the transverse crack. [45]

1.5.4 Microstructure of rail steels and their effects

The microstructure of North American rail steels is fully pearlitic, a microstructure that is characterized with a high resistance to plastic flow and wear. Attempts have been made to introduce alternative microstructures such as bainite or tempered martensite near to eutectoid composition carbon rail steels. [88, 89, 90] However, these trials showed that pearlite of the same hardness as that of the alternative constituent microstructure has significantly better wear and RCF resistances and that martensitic structure is unsuitable because of its inadequate toughness and ductility. Thus, the microstructure of rail steels will continue to be pearlitic until alternative bainitic steel proves convincingly better than pearlitic steel in wear, fatigue, and weldability.

The metallurgical microstructure of rail steels controls yield strength, endurance limit, toughness, and other fatigue-related parameters of rail steels. Influences of pearlitic microstructure are rendered by the sizes of pearlite colonies and the interspacing of cementite lamellae. The critical size of colonies is approximately as large as 15 μm. [91] If a pearlite colony is greater than this limit, the size of a colony is a controlling factor of steel fatigue properties. Otherwise, the spacing and thickness of lamellae take the control. Basically, the smaller the interlamellar spacing and the thinner the lamellae, the higher the fatigue resistance. The flow stress of pearlitic steel is also related to interlamellar spacing between ferrite and cementite in pearlite. Thus the interspacing is a significant factor in influencing fatigue properties of pearlitic rail steels. [91, 92] This relationship is

$$\sigma_{\text{yield stress}} = \sigma_i + K_y\, S^{-1/2}, \quad [63]$$

where σ_i is the friction stress required for dislocations to move through the lattice, and K_y the Hall-Petch slope related to grain size.

In effect, the hardness of a material represents the material resistance to plastic flow, and it is a comprehensive, measurable indicator of fatigue properties. The hardness of pearlitic steels is a function of the interspacing of lamellae too, and so it can be considered an indicator of the material microstructure's effect on RCF. For low and medium strength steels, the relationship between the fatigue limit and the hardness is

$$\sigma \approx 1.6\,Hv \pm 0.1\,Hv \quad (\mathrm{Hv} \leq 400\ \mathrm{Hv}).$$ [94]

A recent study [95] that was conducted on the relationship between the microstructure and the tensile properties of a fully pearlitic steel confirmed a strong influence of interlamellar spacing on yield and flow properties; a threefold decrease in interlamellar spacing produced a doubling in yield strength. The wider the interspacing, the higher the stress necessary for moving a dislocation between two impenetrable cementite plates. To assess the effect of microstructure on fatigue behavior of the same steel, parallel studies showed that the interlamellar spacing slightly influenced the fatigue limit of the steel, suggesting that fatigue limit is not controlled by yield strength. In fact, the fatigue behavior of pearlite is directly related to dislocation configurations in cyclically deformed pearlite with various interlamellar spacing. Under fatigue conditions dislocations are generated predominantly at cementite/ferrite interfaces and largely confined to the interfacial regions. The dislocation sources are likely activated by the development of elastic incompatible stresses between cementite and ferrite. In addition, work by Dollar et al [96] also proved that the fatigue limit of pearlite does not so significantly depend on the interlamellar spacing as do the strength and ductility of fully pearlitic steel. Dollar et al ascribed the different responses to the difference between the dislocation configuration that could be formed during monotonic deformation and the dislocation configuration that was formed during cyclic deformation.

Although pearlite is a relatively simple microstructure and its mechanical properties have been extensively investigated, the yielding, work hardening and fracture behaviors of pearlite are far from understood. Regarding the influences of pearlite microstructure — pearlite interlamellar spacing, pearlite colony size, and prior austenite grain size — on the flow and fracture behaviors of pearlitic steels, a detailed review was given by Alexander and Berstein. [97]

1.6 Quantitative Assessment of Nonmetallic Inclusions

1.6.1 Standard assessment methods

Among assessment methods for evaluating nonmetallic inclusions in steel, the most popular is the microscopic assessment because it enables investigators to reach a complete determination of the type, size, shape and distribution of nonmetallic inclusions. The content of inclusions can be rated by comparison with a standard chart — a counting method — and by volume fraction measurement according to point counting, lineal analysis, or computer-aided image analysis. No matter what assessment procedure is taken, the accuracy of assessment always depends on these factors: sample preparation, examined areas per field and per sample, field selection, the number, location, and orientation of samples.

Standard chart comparison

Standard charts are designed to determine the size, distribution, number and types of inclusions. These charts pictorially illustrate different types, quantities, and distributions of inclusions so as to rate the cleanliness of steels. The ASTM E-45 method is the most common procedure in North America, [98] and the German DIN 50 602 method K is currently favored in Europe. Standard chart methods are relatively simple to apply; an analysis can be performed in a reasonably short time. However, they do have a number of drawbacks that seriously affect the accuracy and reproducibility of measurements.

Manually rating inclusions

The problems inherent in standard chart methods fostered the development of manual rating methods. Although these methods are based on quantitative metallographic techniques, the stereo-theoretical principle has not always been rigorously complied with. Of many standard methods, only the Japanese Specification JIM-G-0555 fully incorporates the stereoscopic principles. [99] In the Japanese method inclusions are divided into three categories —— A-type inclusions, B-type inclusions and C-type inclusions. The A-type are plastically deformed inclusions including sulfides and silicates; the B-type are discontinuously elongated inclusions; the C-type are randomly scattered undeformable inclusions. A magnification of 400 x is recommended in this method. The percentage of area occupied by inclusions is determined by using the following equation

$$d = \frac{n}{p * f} * 100,$$

in which d is the percentage index of cleanliness; n is the number of grid points occupied by inclusions; p is the total number of grid points on the reticle; f is the number of fields. But the standard JIM-G-0555 has not recommended how many of the fields needs to be surveyed. Koyanagi et al. [100] suggested that the number of measurement fields be from 30 to 60.

Computer-aided image analysis

Compared to manual counting methods, a computer-aided image analysis greatly reduces the subjectiveness of inclusion ratings while its speed permits obtaining acceptable statistical data within a reasonable time. An image analyzer detects and discriminates inclusions according to differences of light reflectivities between one type of inclusion and another or the steel matrix. It is reported [101] that the reflectivity of a hardened steel surface yields 59% and the reflectivity of oxide inclusions varies within 10-25% while sulfides have 35-40 % of reflectivity.

Also, the standard practice E 1245-89 for determining inclusion content by automatic image analysis recommends neither a magnification nor the number of survey fields. [102] In practice, the selection of a magnification is a compromise between the surface area examinable in a given time frame and the microscopic resolution. An operator has to decide both a magnification of a microscope and the number of examination fields. The Standard E 1245-89 requires that the polished surface be large enough for the measurements of at least 100 fields at a necessary magnification and a minimum polished surface area be as large as 160 mm^2 or 0.25 $inch^2$. In Rege et al's study, [103] the estimates of inclusion volume fractions with 50, 90 or 190 fields had good correlations with a 1000 field estimate. Thus, under a certain magnification 40 fields probably are enough to yield satisfactory statistical data.

1.6.2 Evaluating the effects of inclusions in rail

Recent improvements in steel-making techniques have significantly decreased the content of nonmetallic inclusions in rail steels. The content of oxygen in rail steels made by modern steel making technologies is about 20 ppm so the number and size of oxide inclusions in steels decrease accordingly. [71] The chance that a large number of oxide inclusions exists on a microscopic field becomes very low. In view of this fact, conventional methods of evaluating inclusions such as JIS or ASTM methods may lose their effectiveness, and the evaluated results of these method may not be reliable. [105]

Tests conducted at FAST under 100T capacity cars revealed that both the volume fraction of aluminum oxide and the stringer length had a direct effect on the incidence of shell defects. [106] It is easy to argue that inclusions have a deleterious effect on rail performance and therefore their presence should be minimized. The cleanliness of rails made from a continuous casting process may vary within a small range, but the cleanliness of rails made from an ingot casting process can show a significant difference from each other. [107] Therefore, the essential question is how to determine the content of inclusions and how to correlate the content of inclusions with rail performance. To characterize variations in amount and distribution of inclusions in rail, a statistical assessment procedure that is developed strictly according to the characteristics of inclusion population is required. Besides, data analysis must be based on statistical distribution models. In this regard similar practices for determining the content of inclusions in ball bearings have given a good lesson. It is well known that rolling element bearings also suffer from subsurface fatigue defects initiated at oxide inclusions. The initial attempts to correlate the ASTM method of inclusion assessment with bearing fatigue performance have not been successful, [108] primarily because the ASTM recommendation of six specimens in a cleanliness assessment resulted in a very small volume of material being examined. An alternative, non destructive method of using ultrasonics has been devised to inspect large volumes of material. [109] A good correlation between the level of aluminum stringers and fatigue performance has been achieved.

While the metallographic determination of oxide inclusion levels for rail steels can follow different routes, the number of specimens required to obtain a reasonable and reproducible oxide content or a statistical sample size is of general concern.

1.7 Prediction of Subsurface Fatigue Life

1.7.1 Tests on service and laboratory scales

The goals of research on subsurface fatigue are to understand the mechanism of subsurface initiated fatigue, to predict the occurrence of this type of fatigue, and to minimize its damage. Strategies of minimizing fatigue damage rely on a quantified assessment of damage under particular operating conditions, no matter how approximate this assessment may be. It is, therefore, important to quantify the reduction of track life caused by the traffic. In the field, however, quantifying rail damage is often hindered by an enormous variety of axle loads, vehicle speeds, wheel-rail contact geometries, track curvatures, and designs. To counter these uncontrollable variables requires an exclusive testing facility. The Facility for Accelerated Service Testing (FAST) at Pueblo, Colorado, is the only one of its kind in North America, by which service scale testing can be conducted. A lot of valuable work has done at FAST.

To study the effects of rolling contact conditions upon fatigue properties of rail steels, laboratory scale testing nevertheless is needed because laboratory simulation can control the plethora of variables in a quick and relatively cheap manner. Meanwhile, laboratory simulation of rail RCF allows variables to be changed in a much more controlled manner than service trials. Provided the relevance of laboratory testing results to track performance is regularly assured by comparison with field data, laboratory scale testing is a rapid route to exploring the mechanisms of RCF failures.

RCF tests, designed to evaluate materials under conditions of cyclic loading, have been described extensively in the literatures. [10, 11, 125] The common theme of these tests is that test pieces are small and have relatively simple geometry, permitting statistical characterization of materials.

1.7.2 Models for predicting RCF life

One of the purposes of rail material-oriented investigations is to investigate how metallurgical properties of rail steels affect rail performance and to establish relations between fatigue behavior of rail steels and their measurable metallurgical parameters such as cleanliness, inclusion distribution and hardness. Work aimed at relating subsurface initiated fatigue to metallurgical characteristics of rail steels is highly valuable but difficult. Since subsurface fatigue lives of rail steels are strongly statistical in nature, a dependence of subsurface fatigue life on metallurgical properties and contact loads can sometimes be so complicated that potential relations often do not present themselves straightforwardly.[76] A comprehensive and quantitative model, which is able to predict subsurface fatigue life from the measurable parameters —— contact load, cleanliness, oxide inclusion distribution and plasticity —— has not been established. Even a simple quantitative correlation between the content of inclusions and RCF life of rail steels has not been developed. In this regard, the existing formulas or models that can provide an insight into influences of nonmetallic inclusions were achieved in investigation of ball bearing steels.

Empirical models

The fatigue life of SAE 52100 ball bearing steel is dependent on the content of oxides and nitrides: [110]

$$Fatigue\ life \propto Number\ of\,[Al_2O_3 + SiO_2 + \frac{TiN}{2}]^{-1}$$

For a particular steel of 0.95-1.05% C, 1.30-1.60% Cr and 0.30-0.60% Mn, the relationship is [111]

$$\log N_f = 1.718 - 0.035\,[SiO_2] - 0.079\,[Al_2O_3]$$

$$\log N_f = 1.428 - 0.059\,[Al_2O_3]$$

In addition to considering the content of inclusions, the formula developed by Atkinson and Murakami [112, 113] incorporated the hardness of steels to characterize the role of inclusions acting as the origin of fatigue. In their models an inclusion would be a fracture origin if a stress amplitude at the location was greater than the predicted fatigue limit σ_w. In the case that fatigue was initiated at an inclusion near to the surface, the predictive limit σ_w is defined as:

$$\sigma_w \approx 1.43\,(H_v + 120)A_i^{\frac{1}{12}}$$

But in case fatigue was initiated at an internal inclusion, σ_w is given by:

$$\sigma_w \approx 1.56\,(H_v + 120)A_i^{\frac{1}{12}}$$

Analytical models

Strain-life, stress-life, and fracture mechanics are three approaches to predicting the fatigue life of a component. The Manson-Coffin strain-life approach, coupled with Neuber's law, probably ought to be a primary way to evaluating subsurface initiated RCF life.

Among others, Chiu et al. [114] advanced a model to predict the occurrence of subsurface initiated RCF in contacting bodies. On the assumption that subsurface cracks would initiate solely from defects, i.e. nonmetallic inclusions, and that the life of a rolling element terminates when a spall forms on the rolling surface, Chiu's model attributes the subsurface fatigue life as a function of the plastic micro-strain at nonmetallic inclusions, matrix strength properties, material defect types and number, and macro-stress field. If the shortest life of subsurface defects is considered to be the rolling element life to the point of first spalling, this model stands as:

$$N_I = \frac{f_I(A_P)}{f_1(\gamma_p, D)},$$

where f_I and f_I are unknown functions; A_P is a crack size at the limit of self-propagation; γ_p is the plastic strain at a defect; D is the local ductility measuring the material's capacity to accommodate plastic strain. Compared to other similar models, [39] Chiu's model takes into account both effects of contact stresses and influences of material defects —— a comprehensive approach. With the severity of subsurface defects being characterized as the density, shape, and elasticity of nonmetallic inclusions, this model demonstrates how to correlate subsurface fatigue life with the metallurgical characteristics of steel.

1.7.3 Models for predicting rail fatigue life

Predicting the occurrence of subsurface fatigue in rail used to take two approaches: one considered the effects of contact stresses and the other focused on the influence of material defects. The quantification of the rail stress environment is the first problem that the former approach needs to deal with. The stress environment is involved not only with cyclic stresses arising from live loads of passing trains but also with residual stresses, which initially result from a rail forming process and subsequently developed from wheel / rail contact, and thermal stresses. [115] Considering the effects of the stresses on subsurface fatigue, the Phoenix model established by the AAR [21] shows responses of service rails under the combined action of varying three-dimensional contact stresses, flexural stresses and steady residual stresses, and it predicts the fatigue life by the Sines Criterion

$$\Sigma_{eff}=C_1\sqrt{\sum(\Delta\sigma_{ij}^{amp})^2}+C_2\sum\sigma_i^{steady}$$

in which, I and j designate the principal stress, $I, j = 1...3$ and $I \neq j$; $\Delta\sigma_{ij}^{amp}$ is the difference between the principal stress amplitude; σ_i^{steady} is the steady principal stress including the mean stresses of the varying stress ranges; C_1 and C_2 are constants. This model evaluates the actual life of rail at each of the evaluation depths by calculating the damage fraction for each load in a load histogram:

$$DF=\sum_L \frac{N}{N_f}$$

where N is the number of cycles in a block of load L only; N_f is the total number of cycles expected to cause fatigue for a specified life percentile at the total stress state associated with load L.

To rate the influence of nonmetallic inclusions, Sugino et al [51] used a count of oxide stringers with which to separate acceptable from unacceptable inclusion levels based on field experience with different rail steels. The Sugino number, which counts the length of stringered oxide inclusions in a certain size sample, simplifies the complicated relations between the presence of oxide inclusions and the occurrence of shell defects, but is unable to predict the occurrence of rail defects. As reviewed in the previous sections, rail subsurface fatigue is a process that is governed by properties of rail steels, loading mode and nonmetallic inclusions. The Sugino number does not take into account fatigue resistance of rail steels and effects of a contact load, and thus is hardly used in predicting the occurrence of fatigue in rails. As an improvement, Shell Index —— defined by Clayton [48] for rating the susceptibility of rails to shelling —— includes the cleanliness of rail steels and characterizes influences of the microstructure with hardness:

$$Shell\ Index = Ln\left[\frac{Oxide\ Volume\ Fraction\ x\ Stringer\ Length}{Hardness^2}\right]$$

where the oxide volume fraction is expressed as a percentage; the stringer length is the total length of oxide stringers in a 200 mm^2 section, as defined by Sugino et al; [51] hardness is measured with a Brinell machine. The Shell Index was derived from FAST experiments and represents the first attempt to quantify interactions of metallurgical factors on susceptibility to shell initiation. It quantitatively correlates the occurrence of shells to the measurable parameters of rail steels, e.g., hardness, inclusions content and their morphology so that the Shell Index is practical. To be an operative model for predicting the imminence of subsurface failures in field rails, the Shell Index apparently should include wheel contact loads. Besides, when the Shell Index was defined, only a single specimen and 30 fields were measured manually. It was recognized that the inclusion measurement was not statistically satisfactory and that when second or third specimens were examined the scatter was considerable. Further work will be required to remodel the interaction of both contact loads and metallurgical factors upon the propensity of rail or rail steels to subsurface fatigue.

1.8 Summary

1. In free rolling the maximum contact stresses occur at a certain depth of the subsurface, and consequently the subsurface is the most vulnerable to fatigue. RCF defects tend to initiate in the subsurface. The modes of RCF, surface initiated or subsurface initiated, are related to contact stresses, fatigue properties of materials, and characteristics of nonmetallic inclusions.

2. The rail shell is a type of subsurface initiated RCF defect and the origin of other rail defects such as spalls and detail fractures. Both contact stresses and tensile residual stresses are driving forces for nucleation and propagation of shells. Oxide inclusions in rails, especially stringer types, participate in causing rail shells while manganese sulfides seem not to play a part in this regard. Previously investigated results have shown that the rate of shell defects is a function of the content of oxide inclusions.

3. The content and type of oxide inclusions in rail steels are controlled by steel making processes, particularly the method of deoxidization.

4. The Shell Index, the first attempt to correlate the incidence of rail shells with metallurgical properties of rail steels, has provided a raw model of predicting subsurface initiated RCF failures. However, since the model was derived from the examination of defective rails and lacking in the complement of necessary laboratory tests, it cannot predict the propensity of subsurface initiated RCF by measurable parameters. Further laboratory tests are obviously necessary in order to accomplish a modified Shell Index. To continue this work, laboratory testing of subsurface initiated fatigue and characterizing the content and distribution of nonmetallic inclusions are the starting points of the entire work.

Chapter 2

SUBSURFACE INITIATED FATIGUE EXPERIMENTS

2.1 Experimental conditions and methods

2.1.1 Testing materials

Materials used in the experiments of assessing nonmetallic inclusions and conducting rolling contact tests were old standard carbon rail steels and standard carbon rail steels, which were produced by the three manufacturers —— Bethlehem, Colorado Fuel & Iron (CF&I), and Rodange —— by ingot or continuous casting. An old standard carbon rail steel that was made by CF&I in 1979 using ingot-casting was denoted as M1-I79 while the other CF&I steel was denoted as M1-I90, and made in 1990 by vacuum-degassing and ingot casting processes. M1-I90 steel was further subcategorized into M1-I90B steel and M1-I90C steel in accordance with their positions in the ingot. The former was the upper part of an ingot, and the latter the lower part of the ingot. The products of both Bethlehem and Rodange were produced through vacuum degassing and continuous casting processes. Bethlehem's products were denoted as M2-C88 and M2-C90 according to the year of manufacture, and steel made by Rodange was denoted as M3-C90. The mechanical properties and chemical compositions of the five steels are presented in Tables 2-1 and 2-2. The microstructure of these rail steels is fully pearlitic (Figure 2.1~ Figure 2.4), with MnS inclusions elongated in the rolling direction. The morphology of the pearlite appears identical in all cases.

Table 2-1 Chemical compositions of the rail steels

steel\content	C	Mn	P	S	Si	Cu	Ni	Cr	Mo	V
M1-I79	.77	1.00	.023	.032	.19	///	0.072	///	///	///
M2-C88	.75	1.02	.011	.026	.29	///	.129	.182	///	///
M1-I90	.77	.88	.009	.013	.24	.25	.07	.22	.014	.003
M2-C90	.78	1.00	.022	.013	.17	.21	.07	.20	.014	.004
M3-C90	.78	.81	.014	.024	.19	.03	.03	.03	.003	.003

Table 2-2 Mechanical properties of the rail steels

properties	M1-I79	M3-C90	M2-C90	M1-I90
HB	265	293	289	270
$Yield_{0.2\%}$, N/mm^2	482	669	444	529
Tensile, N/mm^2	937	1193	998	1023
Elongation, %	9.5	12.71	10.23	10.71

Note: all data except the hardness are from AAR's internal communication.

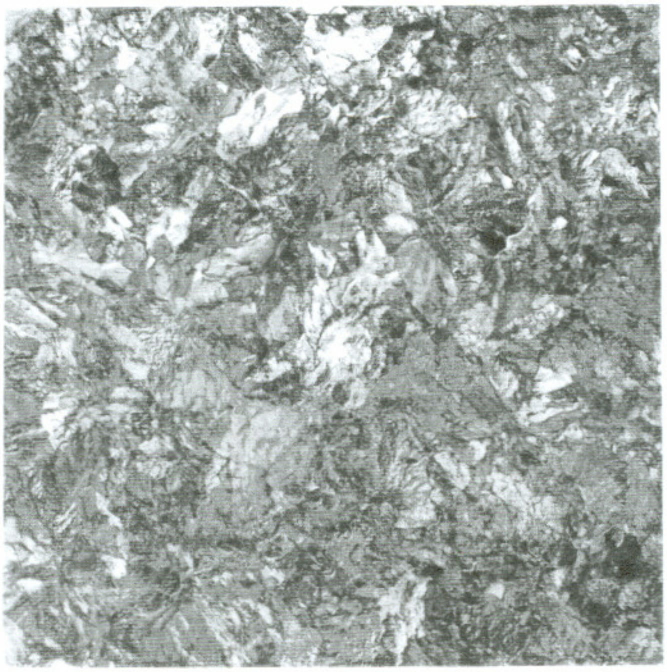

Figure 2.1a Microstructure of M1-I79 steel at a magnification of 100x.

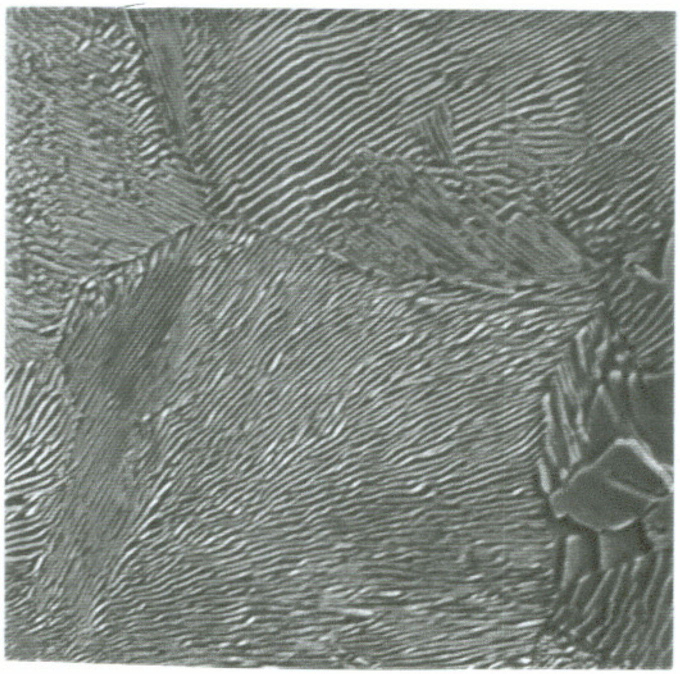

Figure 2.1b Pearlitic structure of M1-I79 steel at a magnification of 3000x.

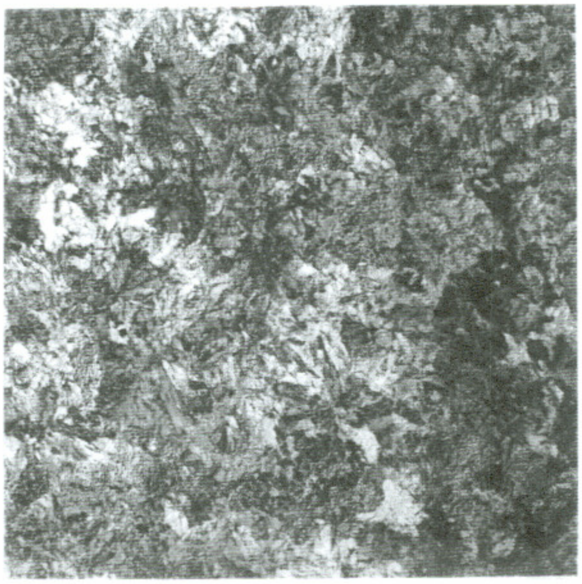

Figure 2.2a Microstructure of M2-C88 steel at a magnification of 100x.

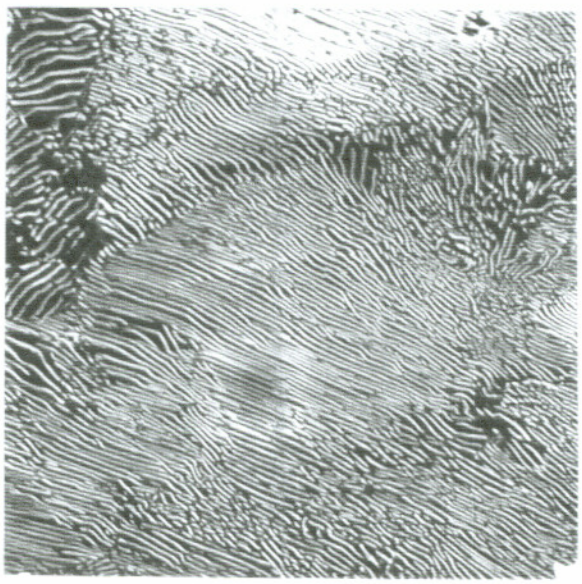

Figure 2.2b Pearlitic structure of M2-C88 steel at a magnification of 3000x.

Figure 2.3a Microstructure of M2-C90 steel at a magnification of 100x.

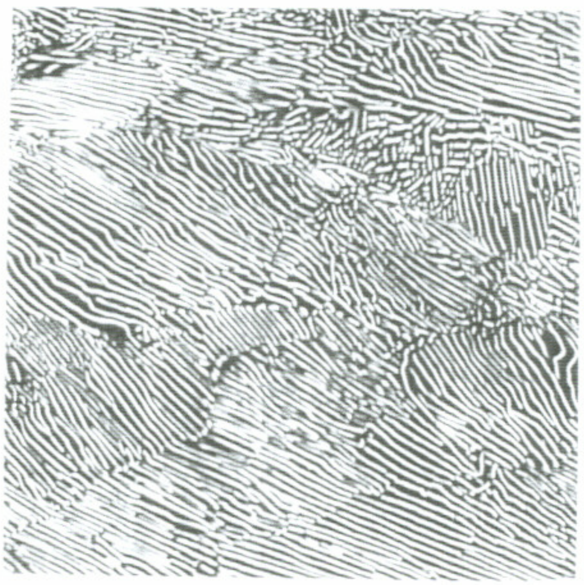

Figure 2.3b Pearlitic structure of M2-C90 steel at a magnification of 3000x.

Figure 2.4a Microstructure of M3-C90 steel at a magnification of 100x.

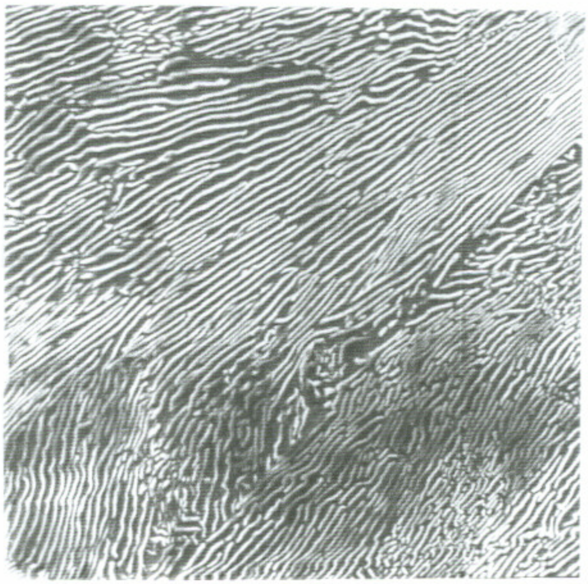

Figure 2.4b Pearlitic structure of M3-C90 steel at a magnification of 3000x.

2.1.2 Test equipment

The test equipment was a geared roller test machine (GRTM), illustrated in Figure 2.5. Power input is through the lower shaft. The speed of the drive motor is a constant, 1,800 rpm. Test rollers are mounted on the two parallel horizontal shafts. The three-inch center distance between the upper and lower shafts is maintained by the rollers. The upper shaft is mounted in a frame and driven from the lower shaft. The upper frame is hinged at one end to the base that holds the lower shaft to form a nutcracker type of mechanism. It can be pivoted upward for installation or inspection of test specimens. The entire assembly is housed in the test box which, as an oil reservoir, is channeled to an oil cooling system. Oil is supplied by the circulatory cooling system at a controlled temperature. The load is applied to the free end of the upper frame through a lever arrangement, which is actuated by a pneumatic Rotochamber. The top roller is midway between the pivot point and the point of load application. Pressurized air from an external source is filtered ahead of the pressure regulator controlling the load. However, the actual load is determined with the aid of a calibrated, strain-gaged load rod. A solenoid-operated dump valve allows quick loading and unloading once the pressure regulator has been set at a desired level. Pressure changes in the air line and the oil line will shut the machine down in the event of a preselected pressure drop in either. In addition, the machine is shut off automatically when excessive vibration occurs during a test.

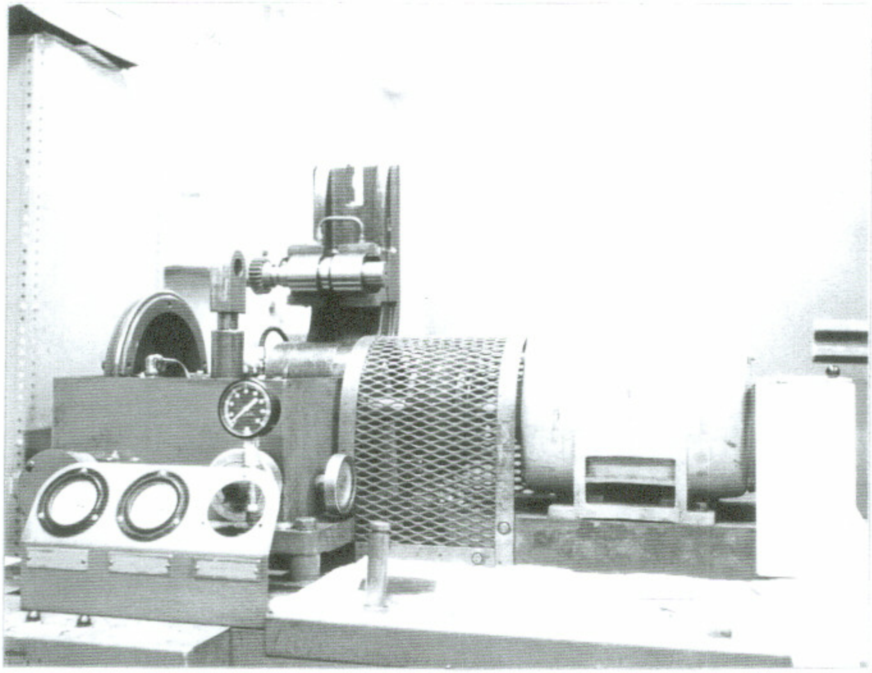

Figure 2.5 Geared roller test machine used in the experiments.

2.1.3 Test specimens

Test specimens were cut from the head and base of used rails. Those specimens that came from the rail head were used as the top rollers of the GRTM while those specimens that came from the rail base used as the bottom rollers. The position from which top rollers were cut from the rail head corresponded with the position at which the metallographic specimens for assessing nonmetallic inclusions were taken. Two specimen geometries, illustrated in Figure 2.6, were used in the tests. The standard geometry was the cone-on-flat configuration while a few tests of the M1-I79 steel used the flat-on-flat configuration. The top roller was as large as 2.8" in diameter, with a 3.2" diameter for the bottom roller chosen to maintain the 3-inch clearance between the axis of top and bottom rollers as required by the test apparatus. The tread widths of the top and bottom rollers were 0.25" and 0.5" respectively. The initial roughness of the rolling surface was 0.8 μm R_a, unless stated otherwise.

2.1.4 Lubricant and lubrication

RCF tests were conducted in free rolling and oil lubricated conditions. SAE 40 and 50 engine oils were used both as lubricant and coolant. The minimum kinematic viscosity of SAE 40 oil is 157 mm^2/s at 105°F; the minimum kinematic viscosity of SAE 50 oil is 169 mm^2/s at 105°F. In lubricating, oil was sprayed onto the contact interface between the top and bottom rollers and circulated through the cooling system. In some tests of the M3-C90 specimens lubrication was implemented differently in that the contact interface of the rollers was entirely immersed in oil. Unless stated otherwise, lubricating was always by oil spray. The temperature of oil was kept below 100 °F in a test.

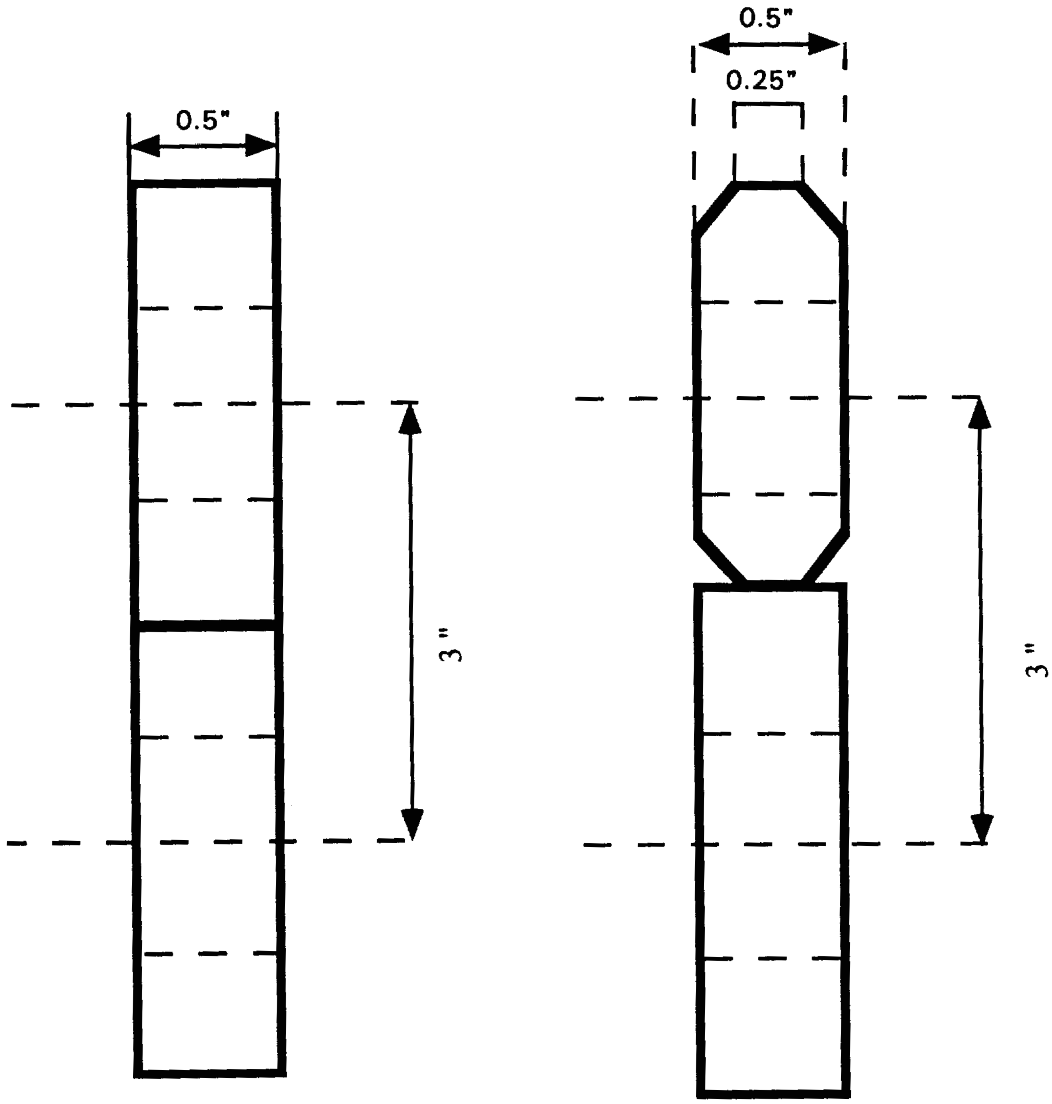

(a)

flat on flat configuration

(b)

cone on flat configuration

Figure 2.6 Two configurations of top and bottom rollers

2.1.5 Metallographic examination

First the rolling surface of a full-size tested roller was examined by a *Nikon* stereoscope. Surface defects such as cracks and spalls were photographed. Afterwards the roller was sectioned into 10 segments of equal size for further examination (Figure 2.7). The preparation of metallographic specimens complied with conventional metallographic sample preparation procedures. Every effort was made to assure that the edges of the segments were not rounded during grinding and polishing. The subsurfaces of the segments were carefully examined using a *Nikon* optical microscope at a magnification of 400x. Rolling contact cracks and voids associated with nonmetallic inclusions in the subsurface were photographed. Some specimens of interesting features were further examined by SEM. In addition, EDX was applied to detect the composition of nonmetallic inclusions from which cracks initiated or were associated. Every top roller was examined in this way.

The polished specimens were etched with 2% nital or 2% nital + picral (50:50) for delineating plastic flow in the subsurface. The deformed zone of the subsurface was investigated both by an optical microscope and by SEM.

2.1.6 Trials for counting the incidence of subsurface defects

Ten longitudinal planes of each tested roller were surveyed at a magnification of 400x using an optical microscope, with each plane being divided into 10 equal size segments. In effect, 100 different locations of a test roller were examined. The number and locations of subsurface-initiated fatigue cracks were documented. As long as a single subsurface initiated fatigue defect was observed on a segment, the plane to which the segment belonged was marked as a fatigue-defective plane.

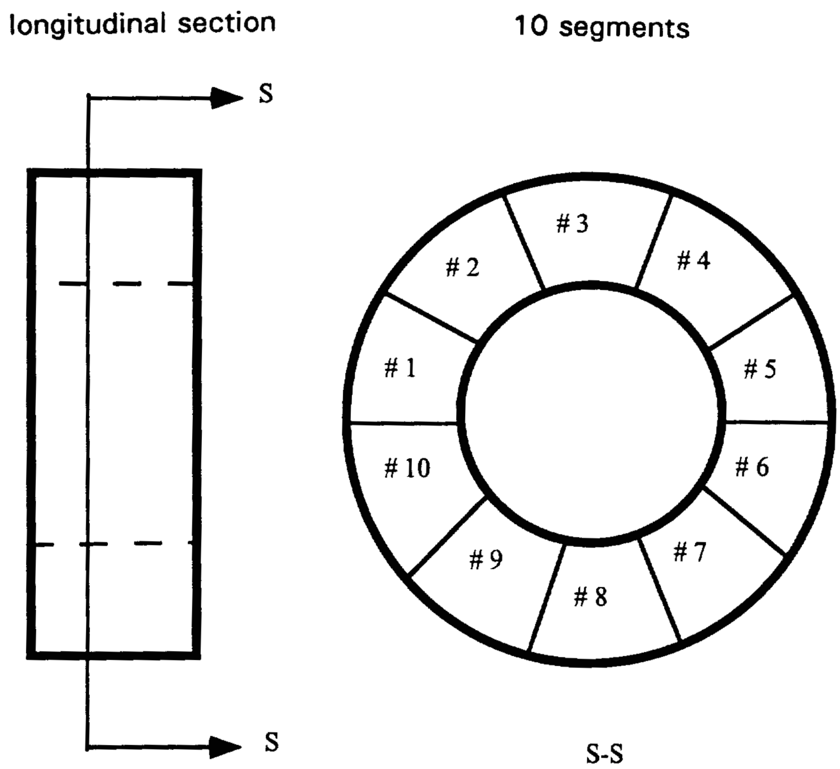

Figure 2.7 Schematics of the sectioning and segmenting of a roller

2.1.7 Brinell hardness and micro hardness measurements

Under guidance of ASTM E384 and ASTM E10, [118, 119] Brinell hardness measurements were conducted with a Wilson Brinell hardness tester. Multiple measurements were made on every test specimen in order to minimize measurement errors. Microhardness of the subsurface was measured using a Leco™ DM-400. At least five sets of microhardness data were acquired from the subsurface of each specimen.

2.2 Rolling contact tests

2.2.1 Tests of M1-I79 steel

As a pilot experiment, M1-I79 steel was tested in order to explore whether subsurface initiated fatigue could be generated with the GRTM and under what range of test parameters. Since the research has no precedent, the test procedure of M1-I79 steel was purely based on trial and error. The contact loads of tests were selected on the principle that a high contact load should be applied provided the rollers could sustain that load with no occurrence of gross deformation. The test parameters used are presented in Table 2-3.

Table 2-3 Rolling contact tests of M1-I79 steel

test #	P, MPa	P_o/k	P_o/HB	rolling cycles	observation
M1-7901	1906	6.9	7.2	1,200,000	spalls
M1-7902	2007	7.2	7.6	20.000	severe deformation
M1-7903	1906	6.9	7.2	1,200,000	spalls
M1-7904	1906	6.9	7.2	1,860,000	spalls
M1-7905	1906	6.9	7.2	1,000,000	no defects on the surface
M1-7906	1722	6.2	6.5	800,000	spalls
M1-7907	1906	6.9	7.2	1,200,000	spalls and cracks
M1-7908	1906	6.9	7.2	10,000	severe deformation
M1-7909	1644	5.9	6.2	1,000,000	cracks on the surface
M1-7910	1683	6.0	6.3	11,129	severe deformation
M1-7911	1683	6.0	6.3	15,239	severe deformation
M1-7912	1645	6.0	6.3	5,321	severe corrugation
M1-7913	1665	6.0	6.3	6,500	severe corrugation
M1-7914	1620	5.8	6.1	21,320	severe corrugation
M1-7915	1578	5.7	5.9	752,000	spall and vibration
M1-7916	1578	5.7	5.9	1,000,000	no surface defects
M1-7917	1578	5.7	5.9	13,920	severe corrugation
M1-7918	1578	5.7	5.9	1,000,000	spalls
M1-7919	1535	5.5	5.9	1,000,000	no defects on the surface

The contact loads of the first seven tests were initially low and gradually scaled up to the desired levels within 100,000 cycles after the start of the tests. Under this loading mode the rollers of the first seven tests experienced loads as high as up to 5400 lb, which corresponds to 1906 MPa and yields $P_o/k = 6.9$. After each test reached 500,000 rolling cycles, the top roller was removed every 100,000 cycles to examine the surface condition. When surface defects such as spalls or cracks were, at a magnification of 30x, observed with the binocular scope, the test ended. Spalls were observed on the M1-7901 roller when the test achieved 1.2 million cycles. The M1-7902 test was carried out at a higher contact load, but the test was prematurely terminated at 20,000 cycles with the deformed top roller causing the machine to vibrate. The post-test examination revealed the presence of subsurface initiated fatigue in the M1-I7901 roller. Accordingly, the contact loads applied in the following five tests, M1-I7902 ~ M1-I7907, were reduced to $P_o/k = 6.9$, and these tests ended in spalling on the rolling surface. The M1-I7904 test was shut off automatically at 1.86 million cycles because spall failures caused severe vibration. The post-test examination proved that subsurface initiated fatigue had been generated at the load of $p_o/k = 6.9$; in the rollers that suffered spalling, subsurface initiated fatigue cracks were found. However, the number of rolling cycles at which spalls were observed varied from 0.8 to 1.86 million, indicating the stochastic nature of spalling. To make the following tests more comparable and avoid any influence of the scaled-up loading mode upon the properties of the testing material, the M1-I7908 ~ M1-I7919 tests were scheduled for 1 million cycles of contact, and the desired contact loads applied to the rollers at the start of the tests. The M1-7908 test failed prematurely at 1,000 cycles, with the top roller deformed. In view of this outcome, the contact load applied to the M1-7909 roller was reduced to 4000 lb or 1644 Mpa. This test achieved 1 million cycles, resulting in microcracks on the surface. The M1-7915 test ended in spalling. The M1-7917 test failed to reach 1 million cycles because of a premature shut-off. The M1-7919 test achieved one million cycles, with no defects occurring on the rolling surface. The post-test examination revealed the presence of subsurface initiated cracks not only in rollers M1-I7909 and M1-I7916 but also in the M1-I7918 roller, which did not suffer spalling on its surface.

2.2.2 Determining test procedure for the four FAST rail steels

The tests of M1-I79 steel provided basic guidance for selecting the test parameters. From the test conditions and consequences presented in Table 2-3, the pilot experiment demonstrated that with both loading modes subsurface initiated fatigue was generated. There existed the upper and lower limits of contact loads that were able to induce subsurface fatigue. The fact that subsurface initiated cracks were found in the spalled rollers suggested that under the conditions of free rolling and oil lubrication spalling might be related to subsurface initiated fatigue. But subsurface initiated cracks were also observed in rollers that had not experienced any surface defects, indicating that subsurface fatigue had initiated before spall failures were formed. Therefore, the experimental design to evaluate the four FAST rail steels in subsurface fatigue was performed with one-step loading mode for 1 million contact cycles. The tests were stopped at 1 million cycles, whether spall failures or cracks occurred. The testing of each steel started with determining the maximum load applicable to the steel. The minimum implemented load was $P_o/k = 4.0$, which is, theoretically, the lowest level of the contact load that can initiate subsurface fatigue.[14] The applied contact loads, rolling cycles and outcome of each test are presented in Tables 2-4 ~ 2-7.

Table 2-4 Rolling contact tests of M3-C90 steel

test	P, MPa	P_o/k	P_o/HB	rolling cycles	observation
M3-9001	1761	4.6	6.0	1,000,000	cracks and spalls on the surface
M3-9002	1835	4.8	6.3	<10,000	severe surface damage, corrugation, spalls
M3-9003	1835	4.8	6.3	<10,000	severe corrugation
M3-9004	1835	4.8	6.3	<10,000	severe and fatal corrugation
M3-9005	1886	4.90	6.4	<35,000	severe surface cavities
M3-9006	1761	4.6	6.0	348,612	severe surface cavities
M3-9007	1924	5.0	6.6	186,366	bottom roller deformation
M3-9008	1924	5.0	6.6	96,560	bottom roller deformation

Table 2-5 Rolling contact tests of M2-C90 steel

test #	P, MPa	P_o/k	P_o/HB	rolling cycles	observation
M2-9001	1761	6.9	6.1	2,500,000	spalls
M2-9002	1919	7.5	7.2	4,239	severe corrugation, spalls
M2-9003	1886	7.4	6.5	41,001	severe corrugation
M2-9004	1792	7.0	6.2	1,000,000	no surface defects
M2-9005	1535	6.0	5.3	1,000,000	no surface defects
M2-9006	1279	5.0	4.4	1,000,000	no surface defects
M2-9007	1024	4.0	3.5	1,000,000	no surface defects
M2-9008	1792	7.0	6.2	29,693	severe corrugation
M2-9009	1665	6.5	5.8	1,000,000	no surface defects
M2-9010	1665	6.5	5.8	1,000,000	no surface defects
M2-9011	1665	6.5	5.8	1,000,000	no surface defects

Table 2-6 Rolling contact tests of M1-I90C steel

test	P, MPa	P_o/k	P_o/HB	rolling cycles	observation
M1-9001C	1835	6.0	6.8	50,000	surface damage
M1-9002C	1761	5.8	6.5	216,000	corrugation, spalls
M1-9003C	1524	5.0	5.6	1,000,000	spalls
M1-9004C	1739	5.7	6.4	1,000,000	spalls
M1-9005C	1220	4.0	4.5	1,000,000	no surface defects
M1-9006C	1677	5.5	6.2	1,000,000	no surface defects
M1-9007C	1739	5.7	6.4	1,000,000	no surface defects
M1-9008C	1677	5.5	6.2	1,000,000	no surface defects
M1-9009C	1739	5.7	6.4	1,000,000	no surface defects
M1-9010C	1677	5.5	6.2	1,000,000	spalls

Table 2-7 Rolling contact tests of M1-I90B steel

roller	P, MPa	P_o/k	P_o/HB	rolling cycles	observation
M1-9001B	1798	5.9	6.6	45,000	severe corrugation
M1-9002B	1739	5.7	6.4	10,000	severe corrugation
M1-9003B	1739	5.7	6.4	<100,000	spalls
M1-9004B	1739	5.7	6.4	1,000,000	no surface defects
M1-9005B	1798	5.9	6.6	34,342	severe corrugation
M1-9006B	1644	5.4	6.0	6,800	severe corrugation
M1-9007B	1524	5.0	5.6	1,000,000	no surface defects
M1-9008B	1835	6.0	6.8	13,207	severe corrugation
M1-9009B	1677	5.5	6.2	1,000,000	no surface defects
M1-9010B	1739	5.7	6.4	1,000,000	spalls
M1-9011B	1220	4.0	4.5	1,000,000	no surface defects
M1-9012B	1677	5.5	6.2	1,000,000	no surface defects
M1-9013B	1739	5.7	6.4	1,000,000	no surface defects

2.3 Results of the rolling contact tests

2.3.1 Characteristics of subsurface initiated cracks

M1-I79 steel

Subsurface fatigue cracks were initiated at 50 μm ~ 150 μm underneath the rolling surface, propagating either parallel or normal to the rolling surface (Figures 2.8 and 2.9). Although these cases did not provide any evidence that initiations of the subsurface cracks were caused by nonmetallic inclusions, SEM examination did verify that other subsurface cracks were initiated by calcium aluminate inclusions (Figures 2.10 and 2.11). Figures 2.12 and 2-13 illustrate the subsurface cracks observed in the rollers M1-I7916 and M1-I7918. Multiple coarse cracks were formed in the subsurface of the M1-7908 roller (Figure 2.14).

M3-C90 steel

Subsurface initiated defects were found in the M3-9001 roller (Figure 2.15). Of all the subsurface cracks observed, the deepest was situated at a depth of 350 μm (Figure 2.16).

M2-C90 steel

Although M2-C90 steel was tested at a wide range of P_o/k, most of the tests resulted in no subsurface defects. Subsurface cracks were found only in the rollers of M2-9001 and M2-9004. Whereas one subsurface crack was apparently initiated by oxide inclusions in the subsurface (Figure 2.17), another appeared to have been initiated by surface defects (Figure 2.18).

M1-I90C steel

Subsurface cracks existed in the rollers subjected to contact loads of P_o/k greater than 5. The subsurface crack shown in Figure 2.19 was at a 120 μm depth beneath the surface, and had already grown to about 500 μm. Subsurface cracks were found in rollers M1-9003C and M1-9004C. The subsurface crack in the M1-9004C roller is shown in Figure 2.20, but its subsurface initiated characteristics were not so evident as that M1-9006C.

M1-I90B steel

At a 100 μm depth of the M1-9007B roller, a subsurface crack grew as long as 1.4 mm (Figure 2.21). In the M1-9019B roller one subsurface crack was initiated at 80 μm depth, while another crack was 50 μm deep; both were propagating parallel to the rolling surface (Figure 2.22). In the M1-9010B roller multiple subsurface cracks were observed, whose morphology and orientation are shown in Figures 2.23. Interestingly, these subsurface cracks were all initiated at about 100 μm in depth and propagated in parallel. A large subsurface crack in the M1-9012B roller grew to 0.7 mm in length (Figure 2.24).

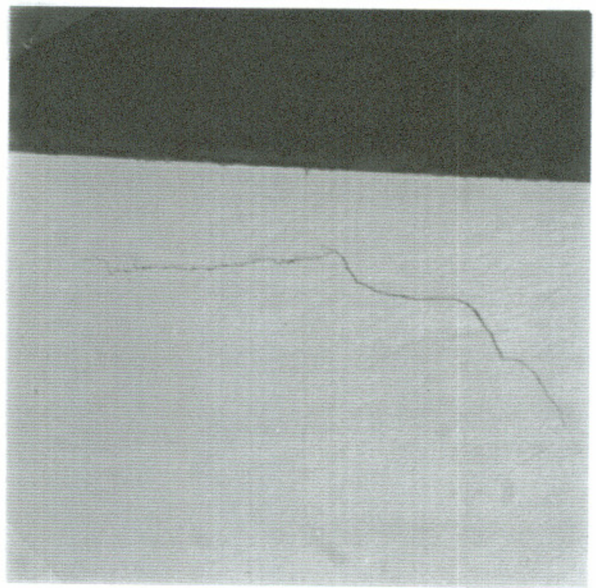

Figure 2.8 A subsurface crack parallel to the rolling surface (roller M1-7907). Magnification 400x.

Figure 2.9 A subsurface crack normal to the rolling surface (roller M1-7904). Magnification 1000x.

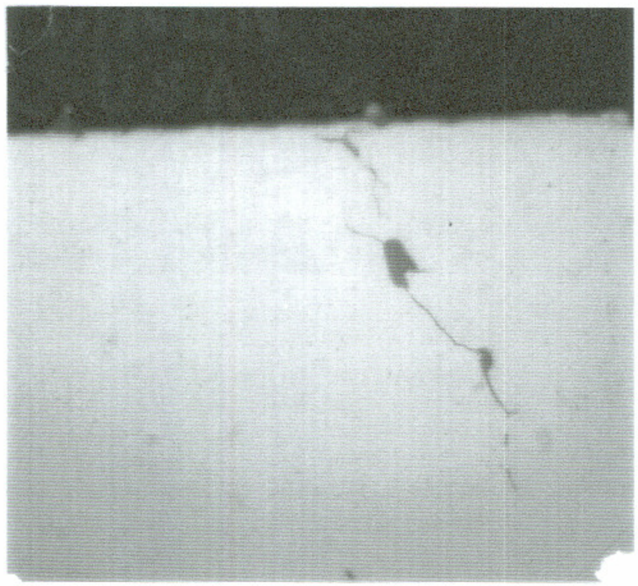

Figure 2.10 A subsurface crack initiated by an oxide inclusion. Magnification 1000x.

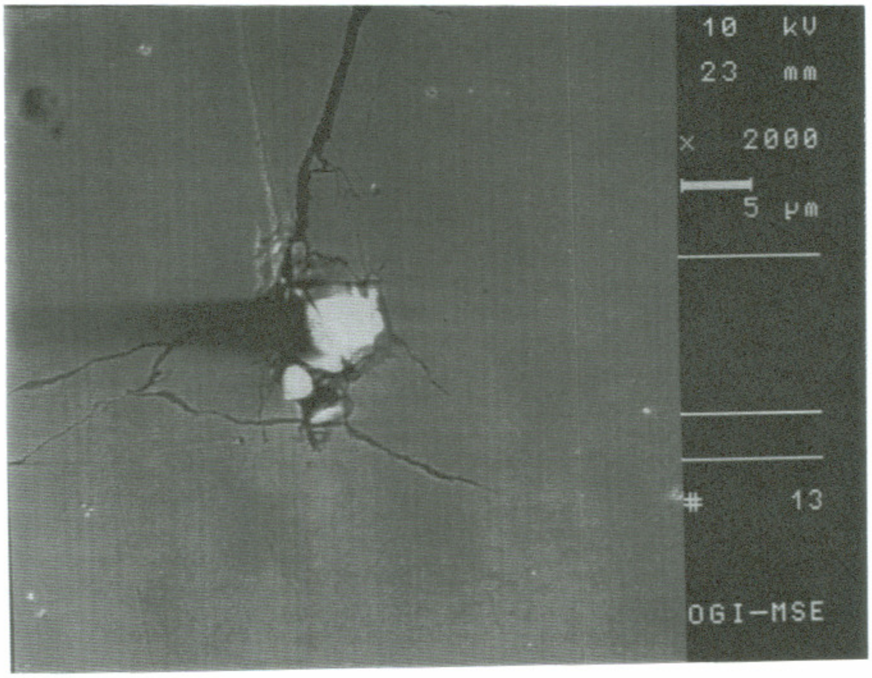

Figure 2.11 A subsurface crack was associated with a compound oxide inclusion. Magnification 2000x.

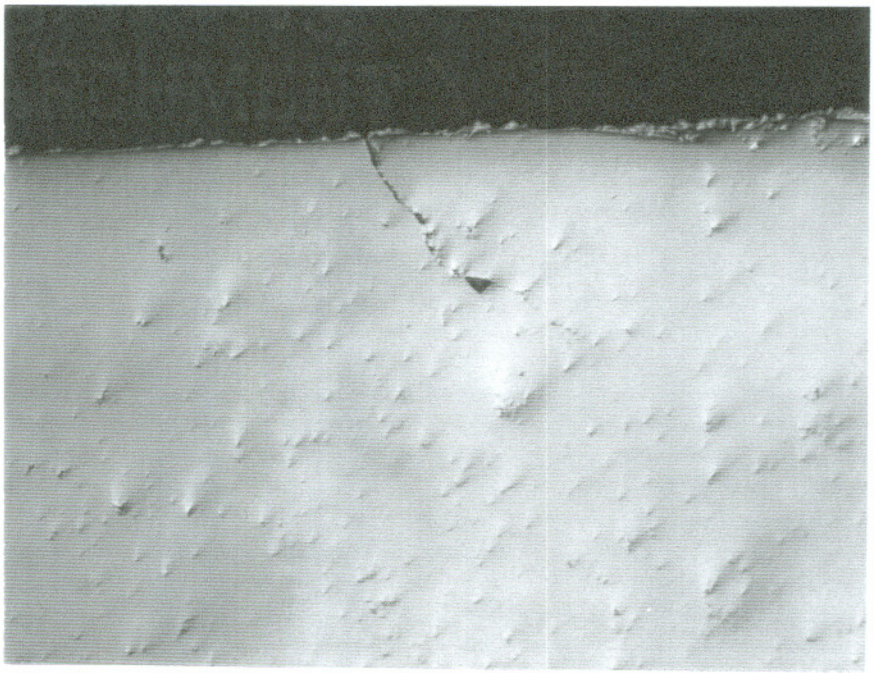

Figure 2.12 A crack was linked to an oxide inclusion in roller M1-7916. Magnification 400x.

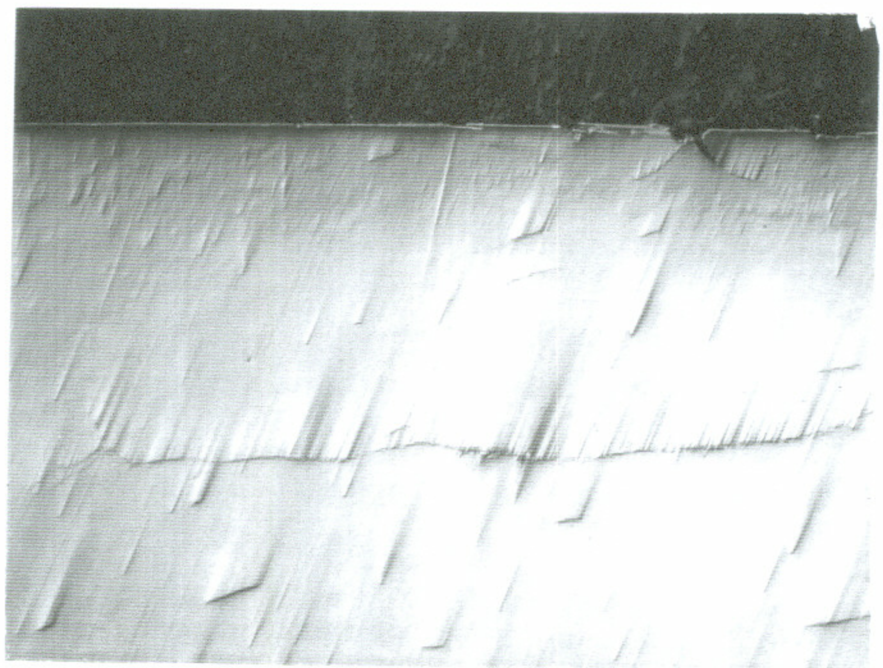

Figure 2.13 A subsurface crack in roller M1-7918. Magnification 200x.

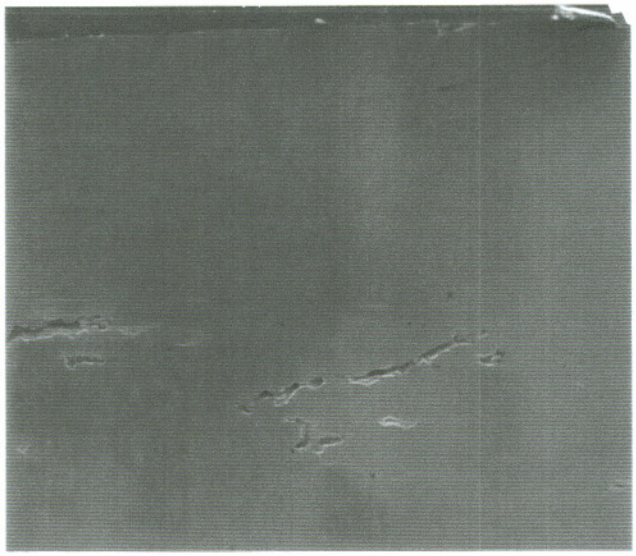

Figure 2.14a Multiple cracks initiated in the subsurface of roller M1-7908. Magnification 40.

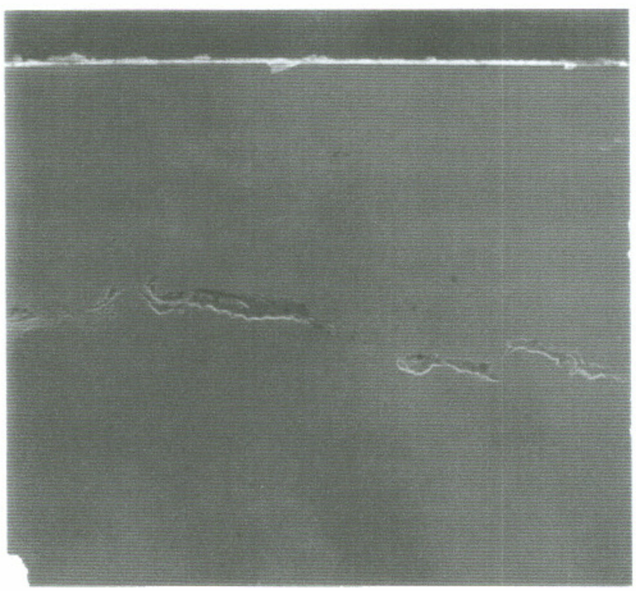

Figure 2.14b Multiple cracks initiated in the subsurface of the roller. Magnification 35.

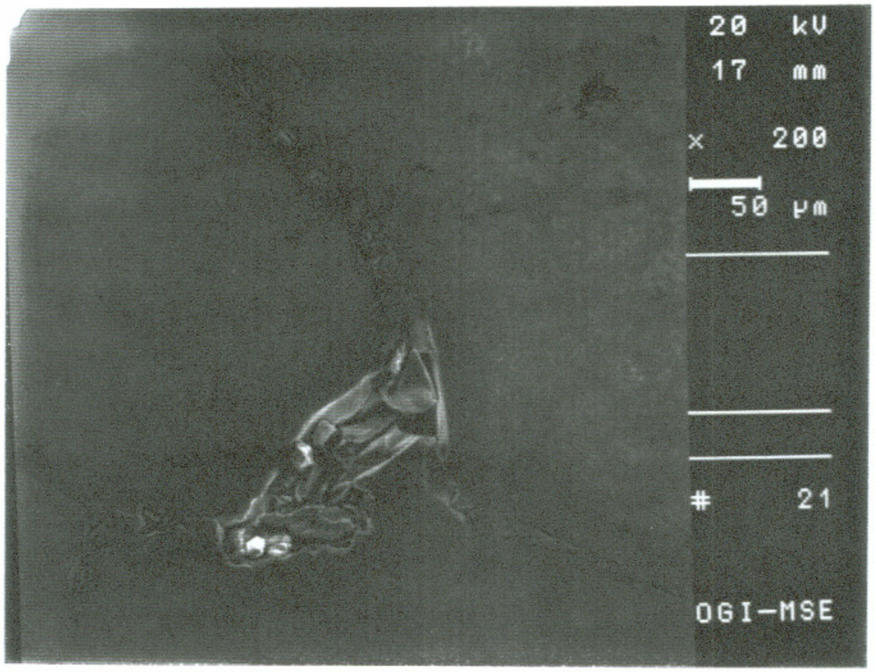

Figure 2.15 A subsurface failure in roller M3-9001.

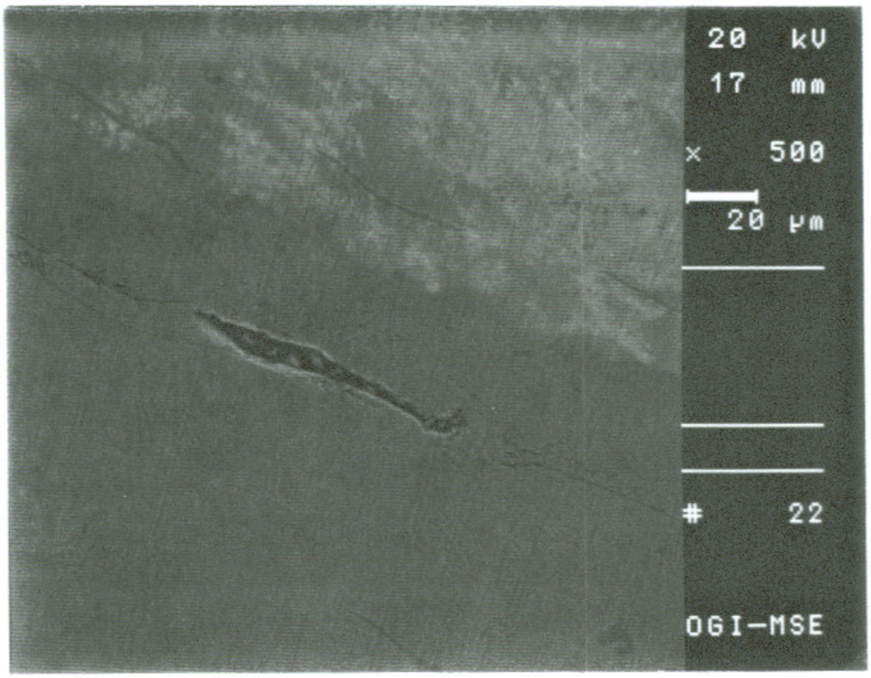

Figure 2.16 A subsurface crack in a depth of 350 μm below the surface of roller M3-9005.

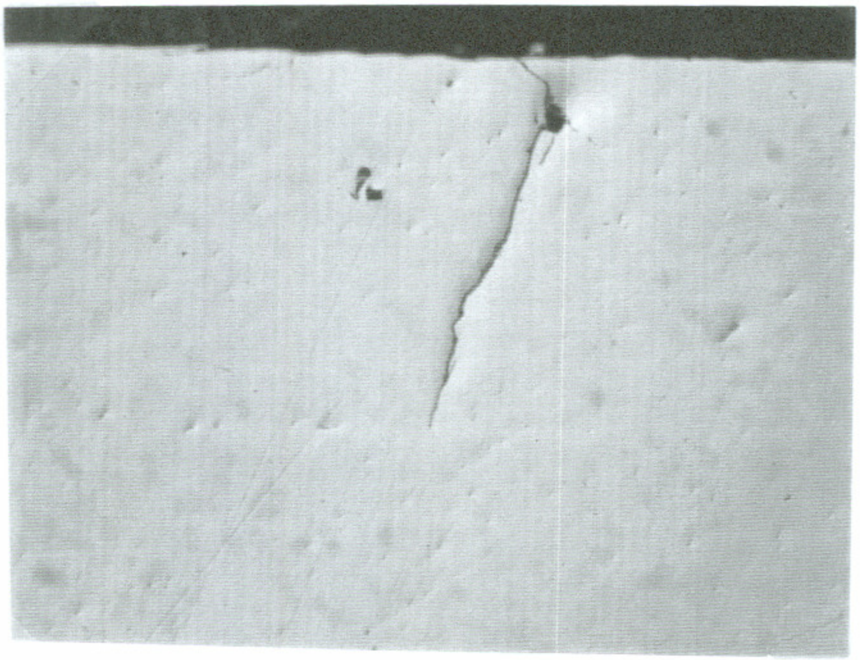

Figure 2.17 A subsurface crack initiated by an inclusion in the subsurface of roller M2-9001. Magnification 400x.

Figure 2.18 A subsurface crack appeared to have been initiated by a surface inclusion. Magnification 400x.

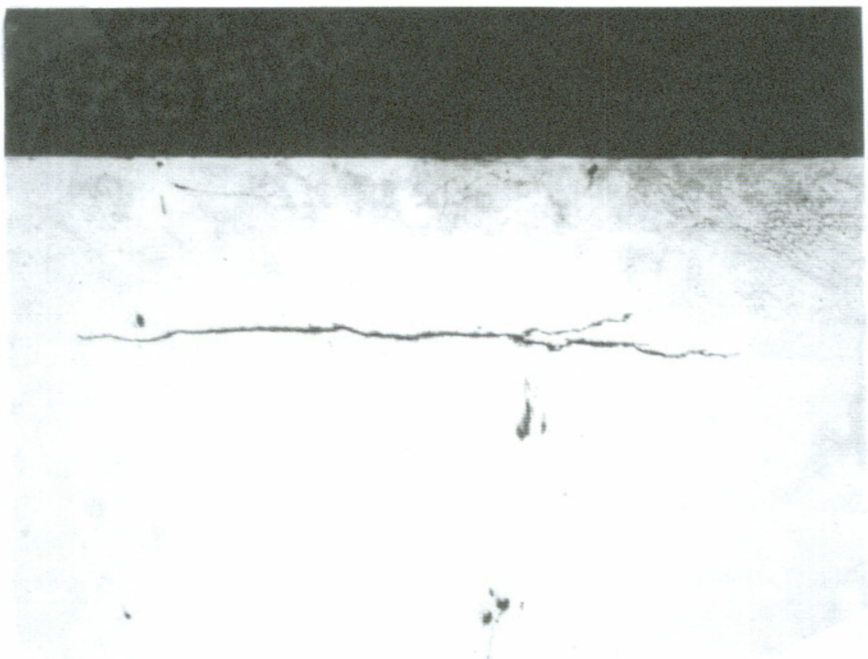

Figure 2.19 A subsurface crack in roller M1-9006C. Magnification 200x.

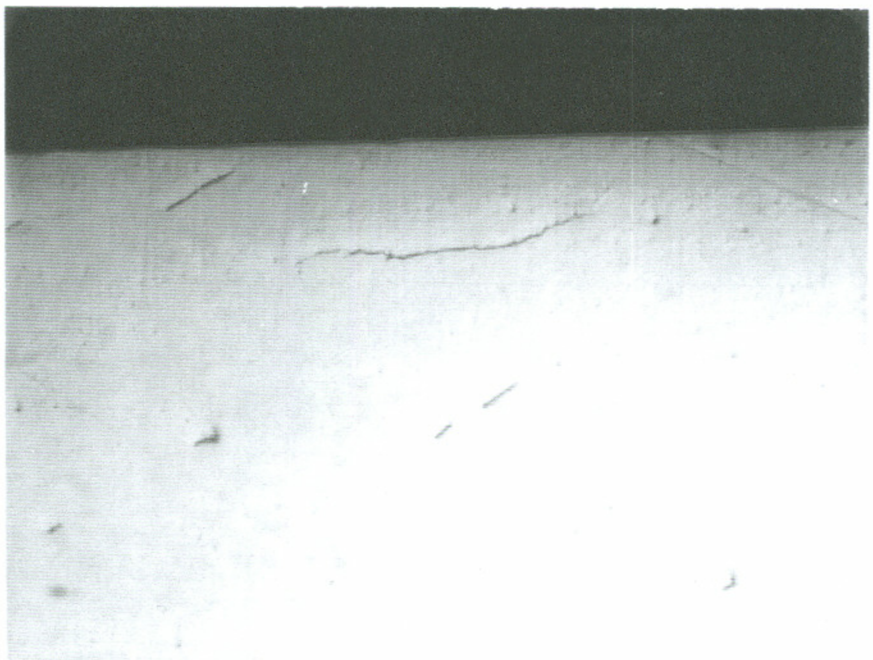

Figure 2.20 A subsurface crack in roller M1-9004C. Magnification 200x.

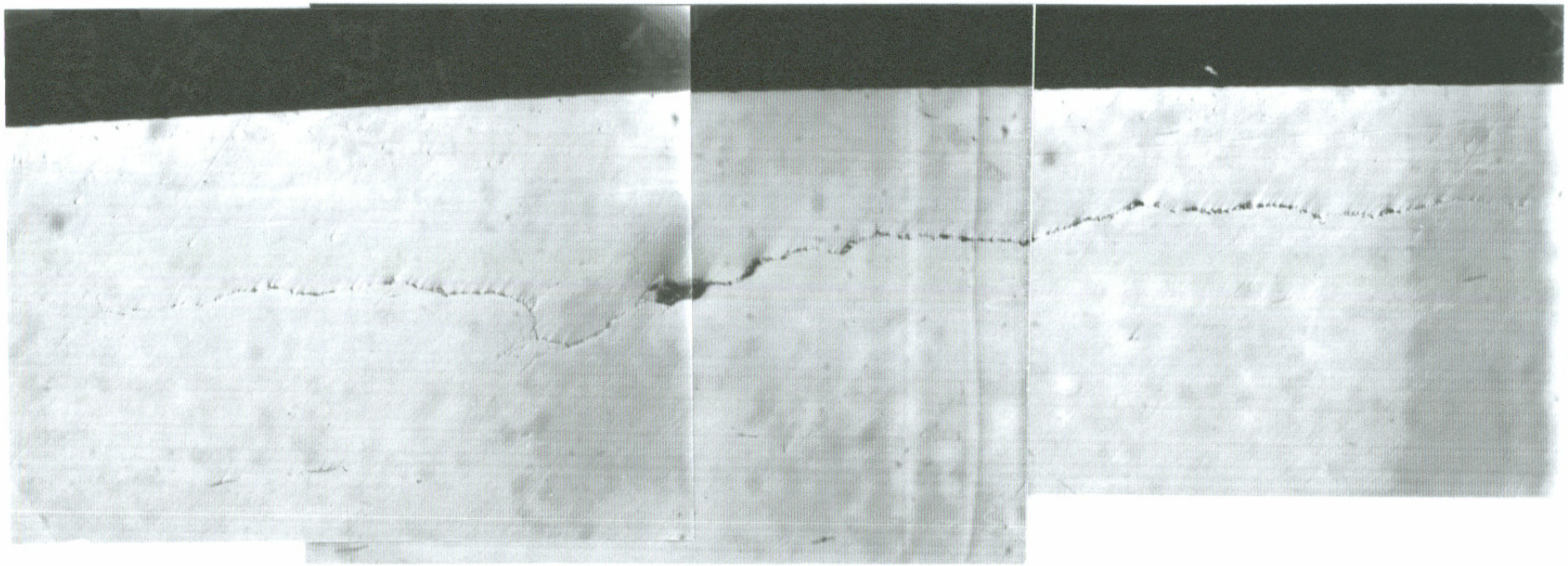

Figure 2.21 A long subsurface crack in roller M1-9007B. Magnification 200x.

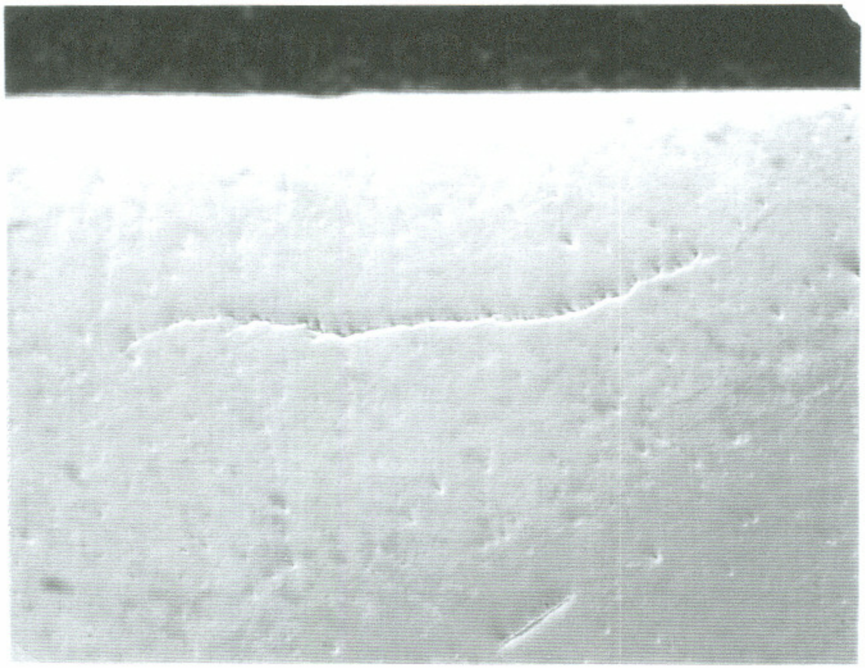

Figure 2.22a A subsurface crack in roller M1-9019. Magnification 400x.

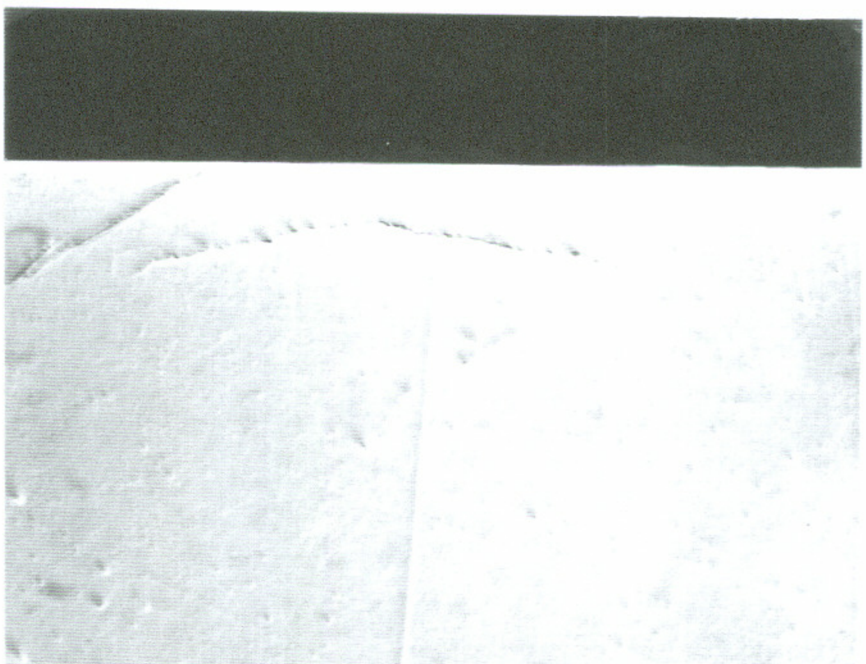

Figure 2.22b Another subsurface crack in the same roller. Magnification 200x.

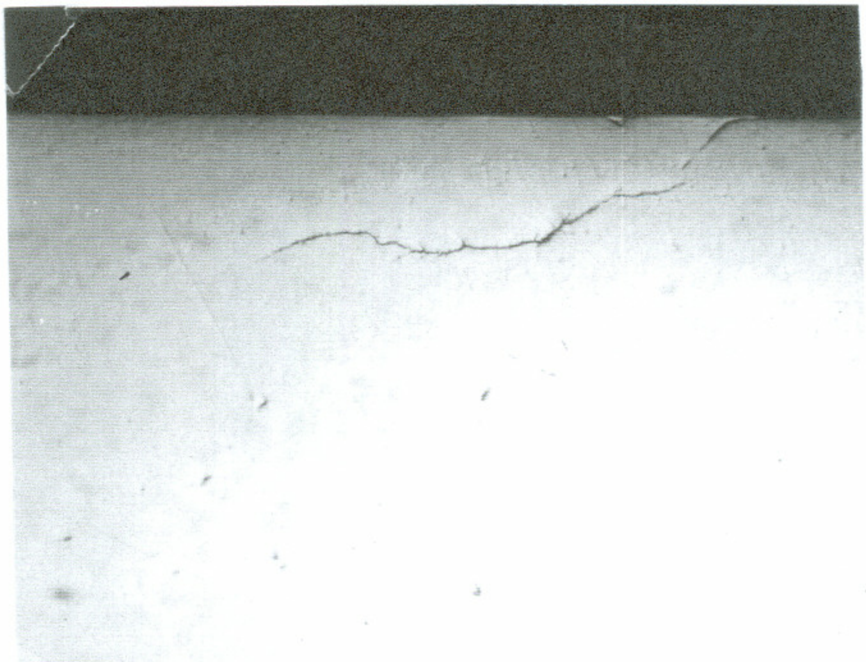

Figure 2.23a A subsurface crack in roller M1-9010B. Magnification 200x.

Figure 2.23b Another subsurface crack in the same roller. Magnification 200x.

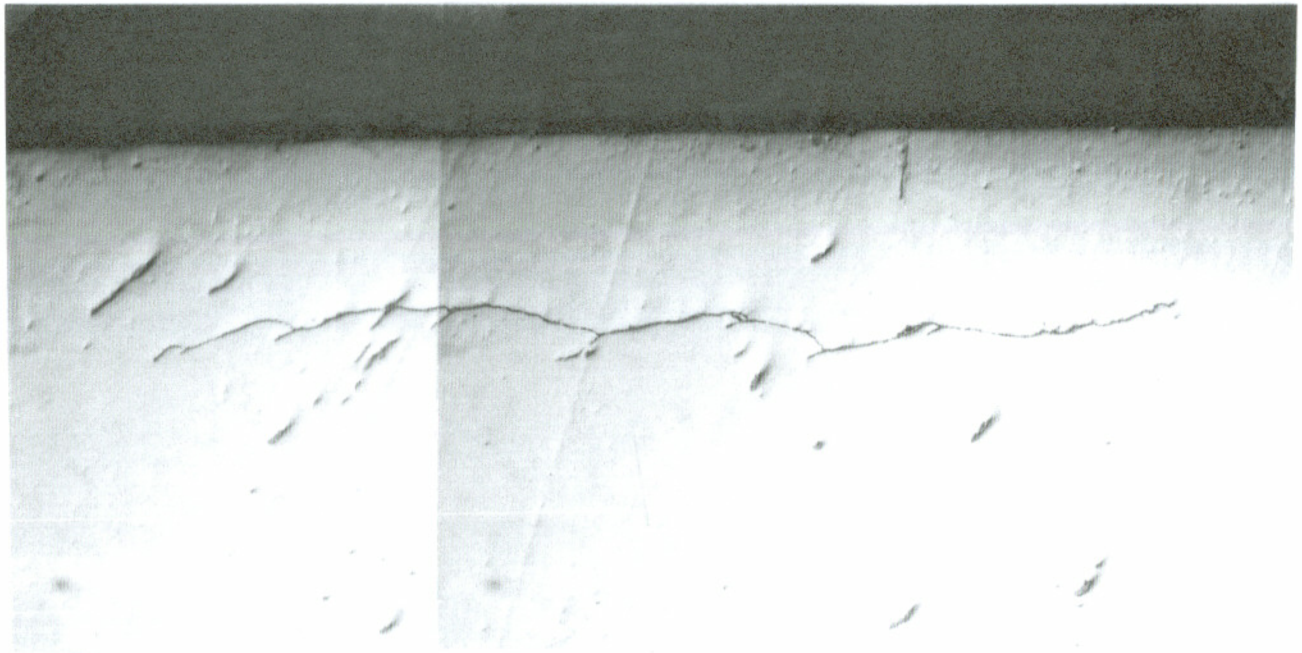

Figure 2.24 A subsurface crack parallel to the rolling surface of roller M1-9012. Magnification 200x.

2.3.2 Evidence for nonmetallic inclusions as crack initiators

Challenging the commonly accepted belief that sulphide inclusions would not participate in initiating subsurface cracks, the experimental findings proved that not only hard oxide inclusions, such as alumina and calcium aluminate, but also manganese sulfides were able to initiate subsurface cracks. When manganese sulfides happened to locate in the stressed subsurface, it was possible for them to nucleate microcracks. Subsurface cracks nucleated by manganese sulfides propagated in all directions. A crack exhibited in Figure 2.25 originated at the tip of the sulfide inclusion, which was elongated normal to the surface, and grew along the orientation of the sulfide. In the case shown in Figure 2.26, a crack initiated from both edges of an elongated sulfide but propagated normal to the orientation of the sulfide. The more interesting case was one in which a subsurface crack started from a sulfide inclusion, which was parallel to the rolling surface, and propagated perpendicularly to the rolling surface (Figure 2.27).

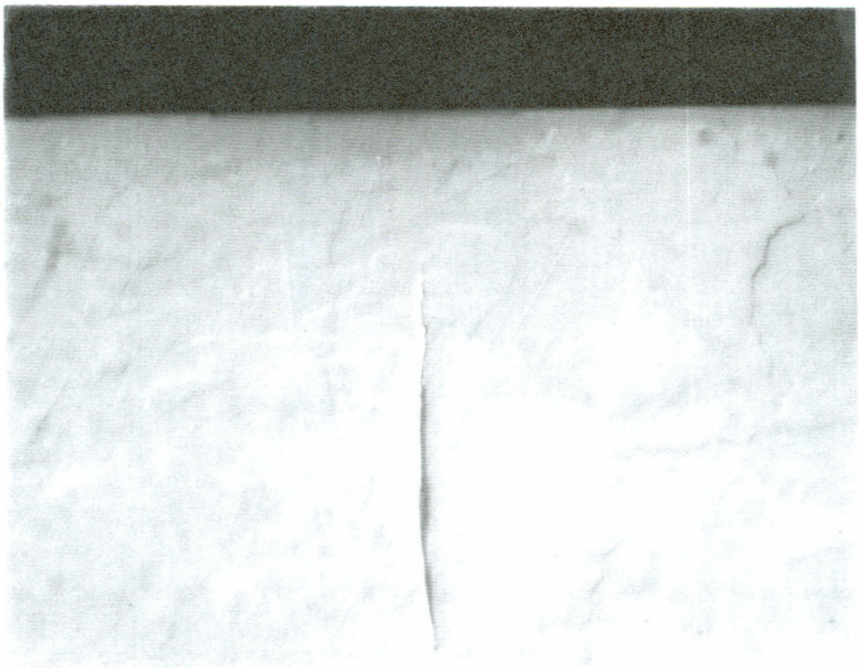

Figure 2.25a A crack initiated from the tip of a sulfide inclusion.

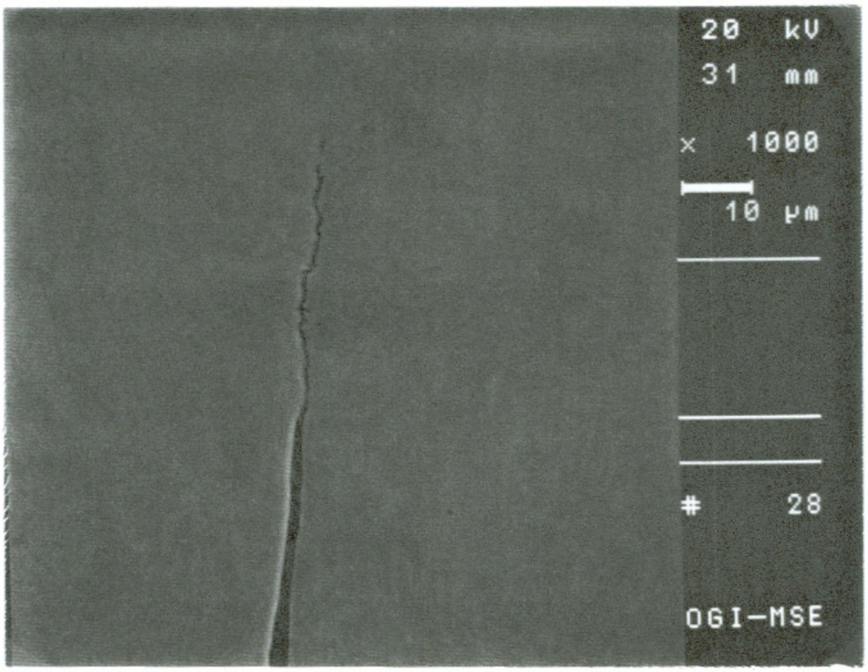

Figure 2.25b Close-up view.

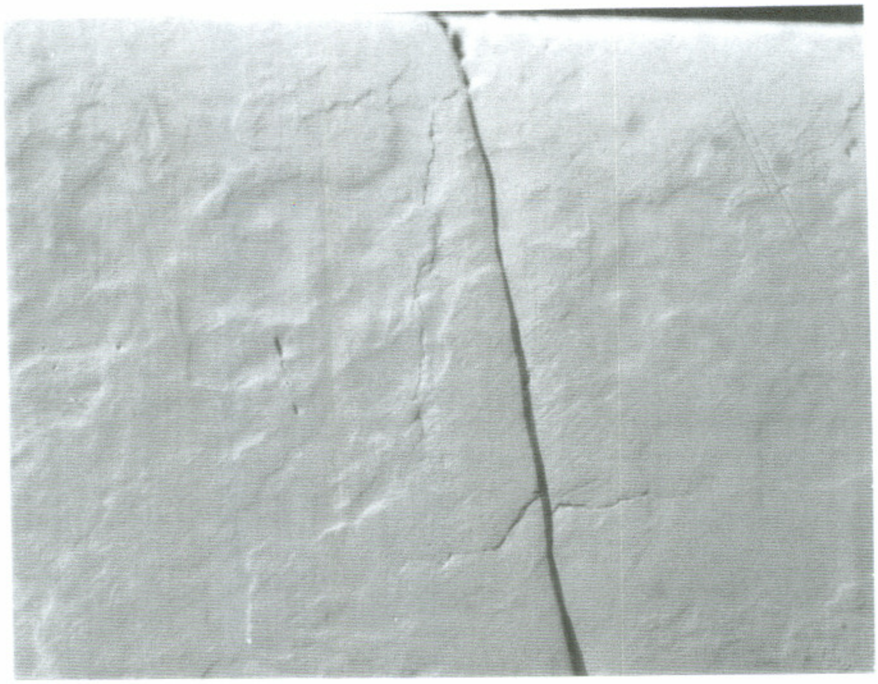

Figure 2.26a A subsurface crack emanated from a sulfide inclusion. Magnification 400x.

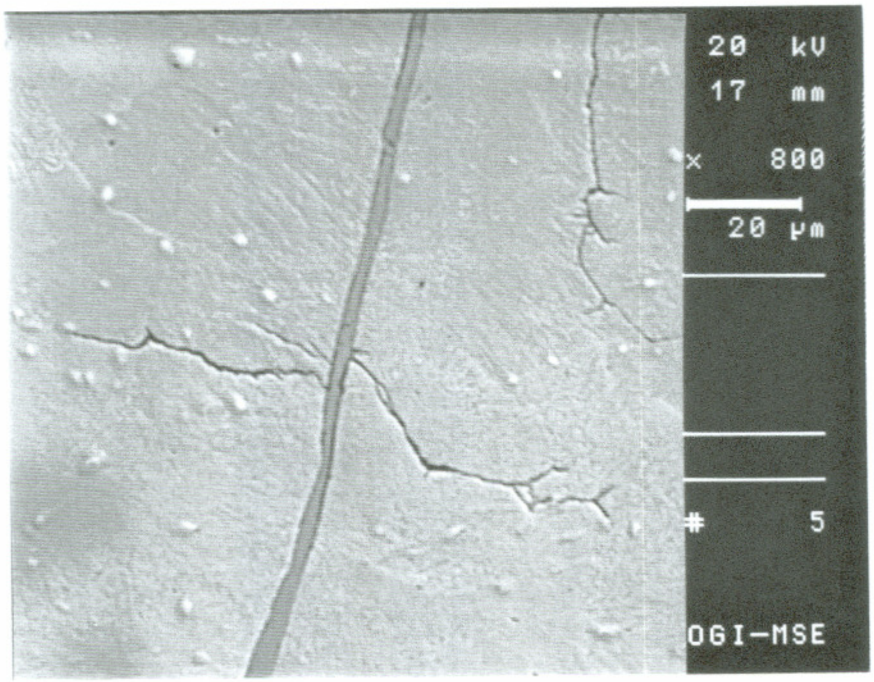

Figure 2.26b Close-up view. Magnification 800x.

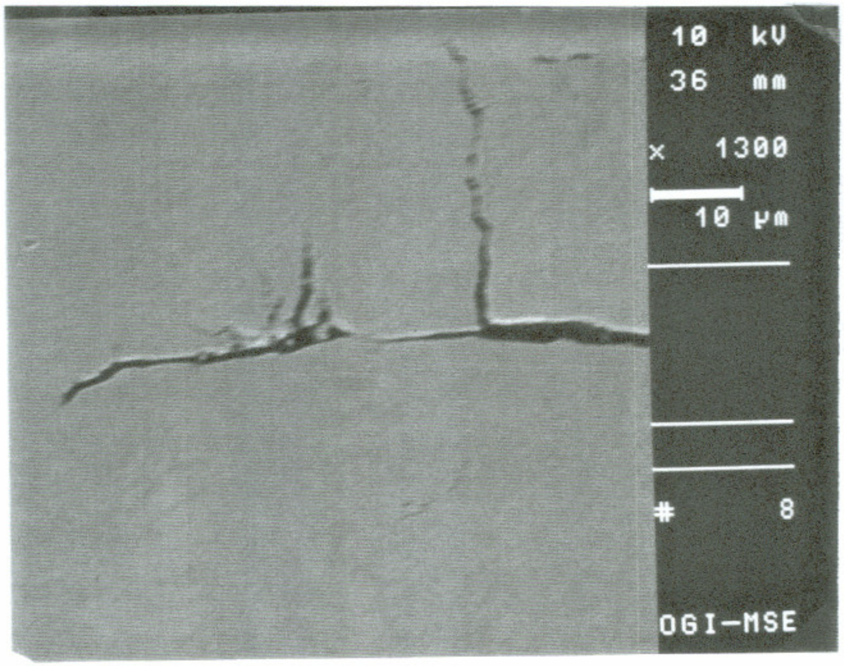

Figure 2.27 Multiple subsurface cracks initiated at sulfide inclusions.

2.3.3 Frequencies of subsurface crack occurrence

Subsurface cracks did not occur in all rollers tested at loads of $P_o/k \geq 4$. To investigate the frequency of subsurface crack occurrence with respect to contact load, the painstaking metallographic work provided an insight into the propensity of the rail steels to subsurface fatigue. Figure 2.28 is the examination record of the M2-9004 roller; only one plane out of 10 planes, the 5th plane, contained a subsurface crack. Figures 2.29~2.34 are the examination records of the M1-I79, M1-I90B and M1-I90C rollers. According to these findings, the frequencies of subsurface crack occurrence were estimated and are presented in Table 2-8. In terms of the frequency, M2-C90 steel proved to be least susceptible to subsurface fatigue whereas M1-I79 steel was the most vulnerable.

Table 2-8 Frequencies of subsurface crack occurrence

P_o/k	$f_{M3\text{-}C90}$	$f_{M2\text{-}C90}$	$f_{M1\text{-}I90B}$	$f_{M1\text{-}I90C}$	$f_{M1\text{-}I79}$
4	0/10	0/10	0/10	0/10	0/10
5	///	0/10	0/10	1/10	0/10
5.5	///	///	1/10	2/10	3/6
5.7	///	///	2/10	4/10	6/10
6	///	0/10	///	///	///
7	///	1/10	///	///	///

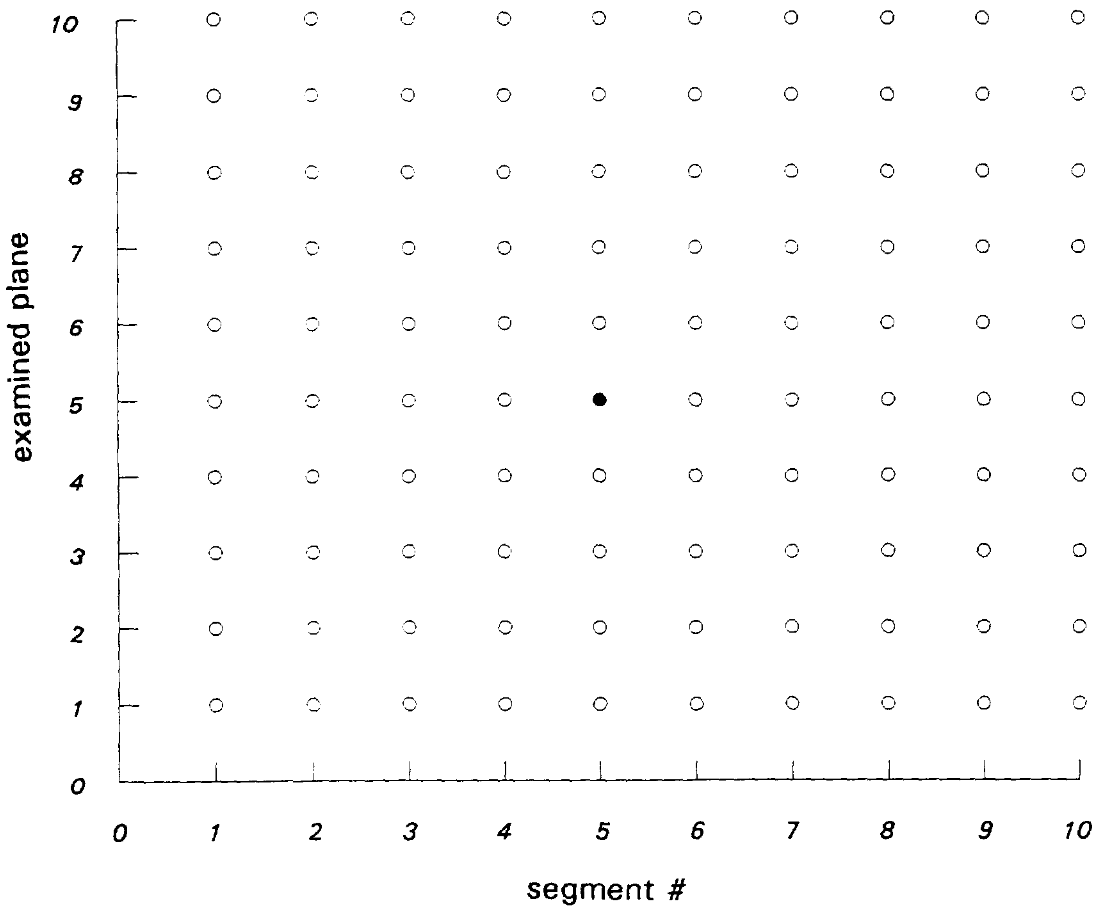

Figure 2.28 A subsurface crack was found on the 5th segment of the 5th plane. Roller M2-9004 at $P_o/k = 7.0$

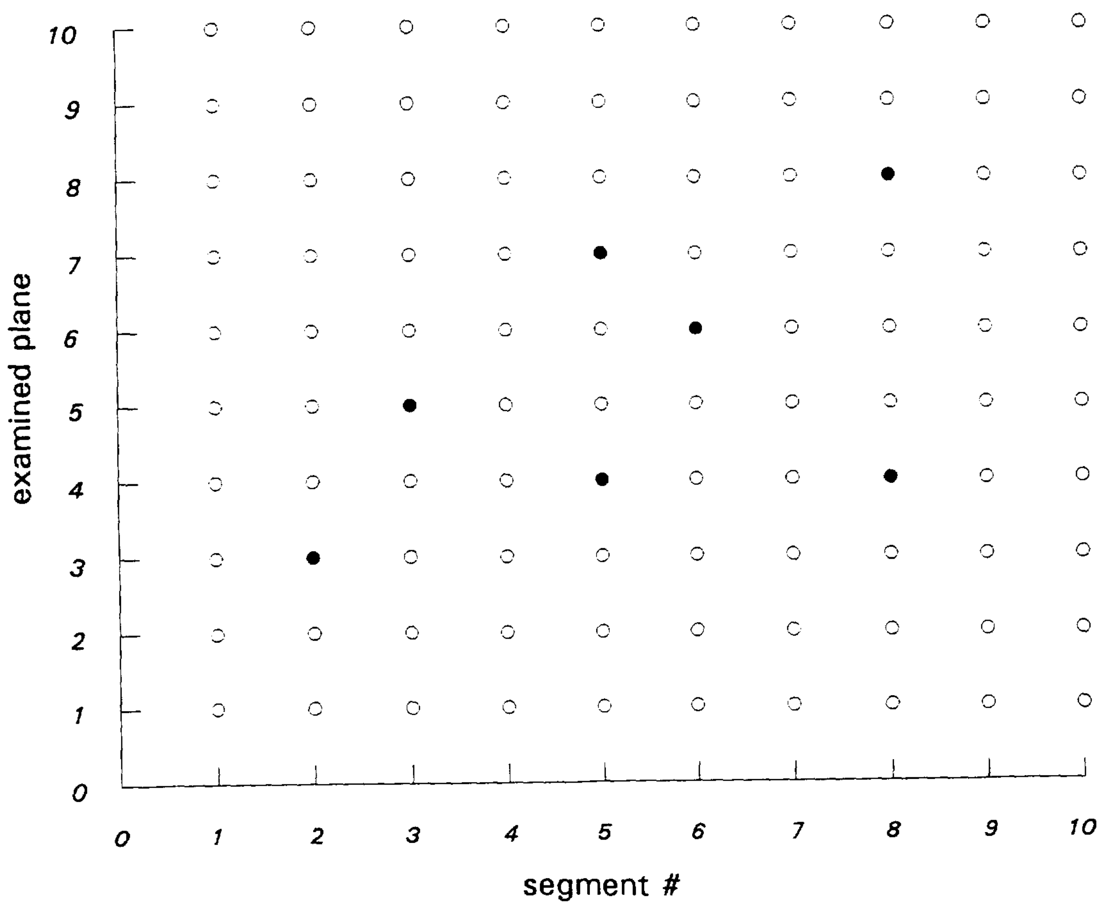

Figure 2.29 Subsurface cracks were found on the six planes of roller M1-I7915, $P_o/k = 5.7$.

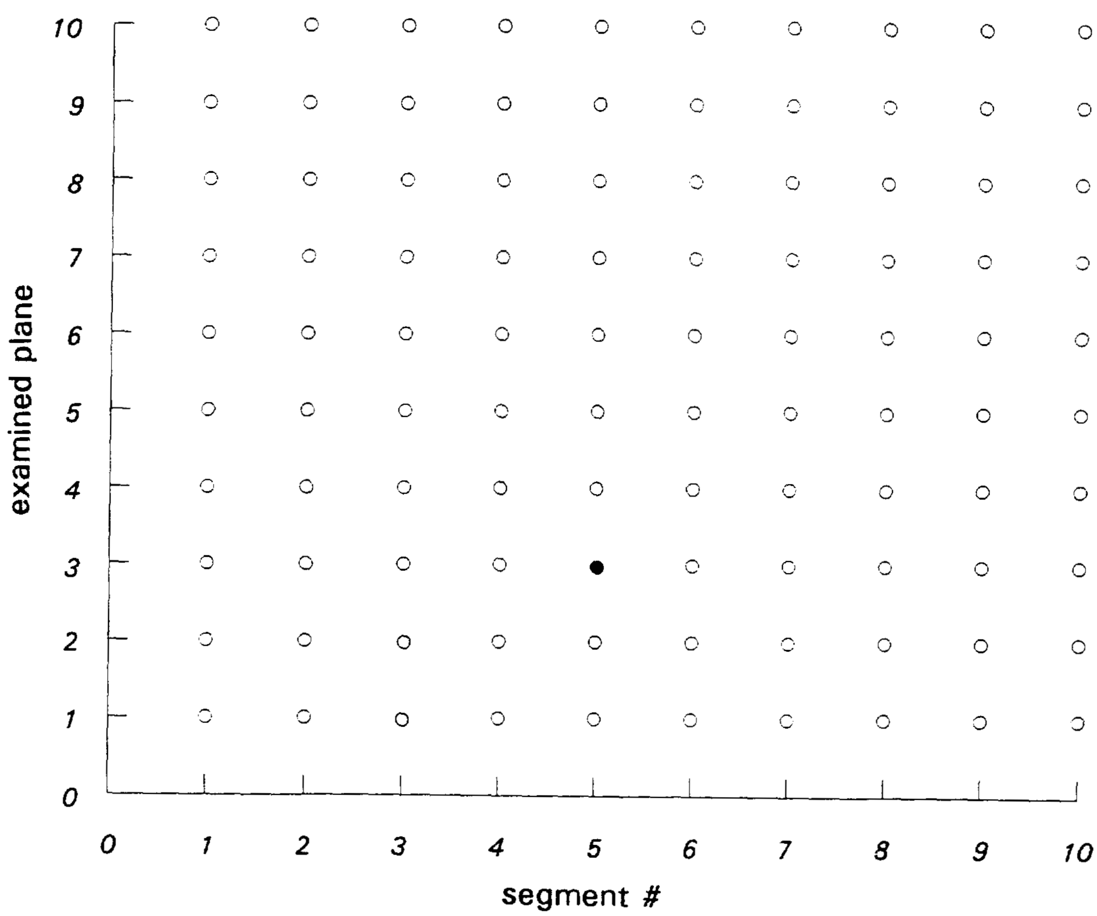

Figure 2.30 A subsurface crack was found on the third plane of roller M1-9003C, $P_o/k = 5.0$.

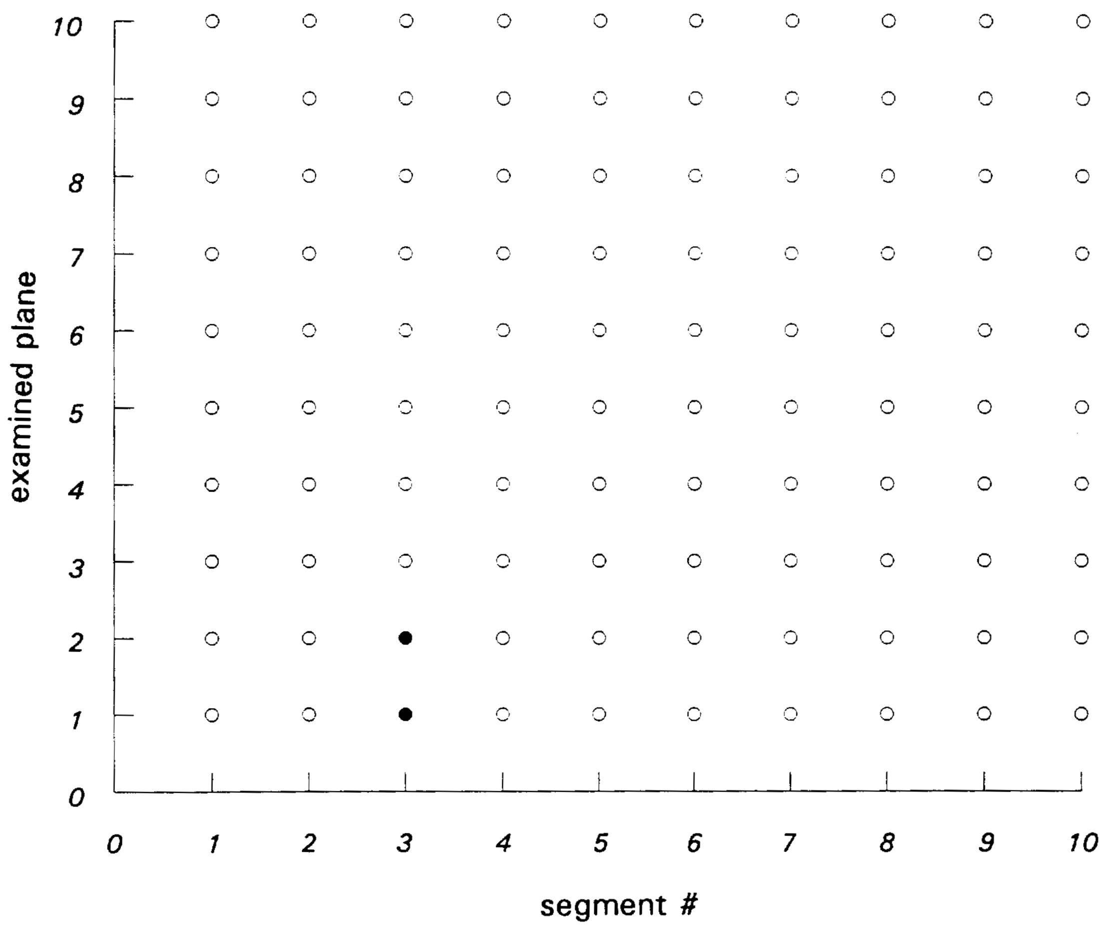

Figure 2.31 Subsurface cracks were found on the planes of roller M1-9006C, $P_o/k = 5.5$.

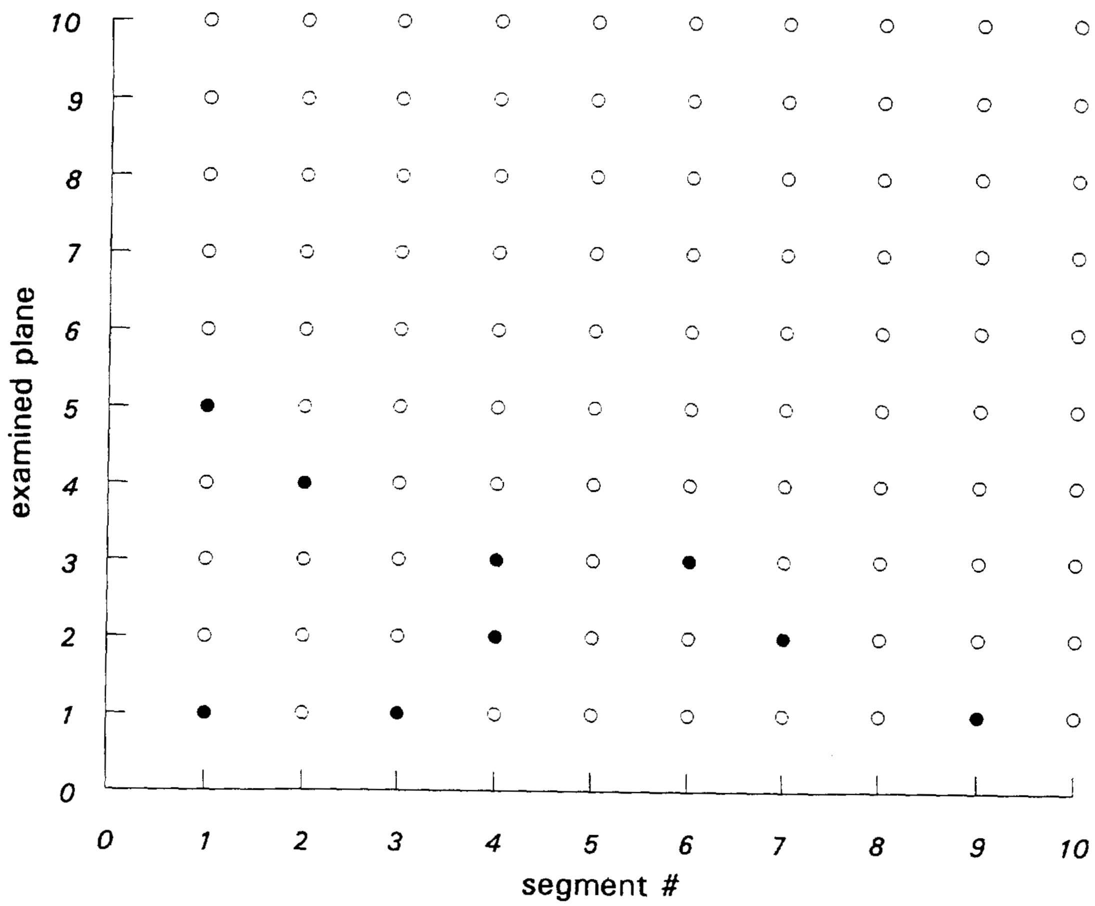

Figure 2.32 Subsurface cracks were found on the planes of roller M1-9004C, $P_o/k = 5.7$.

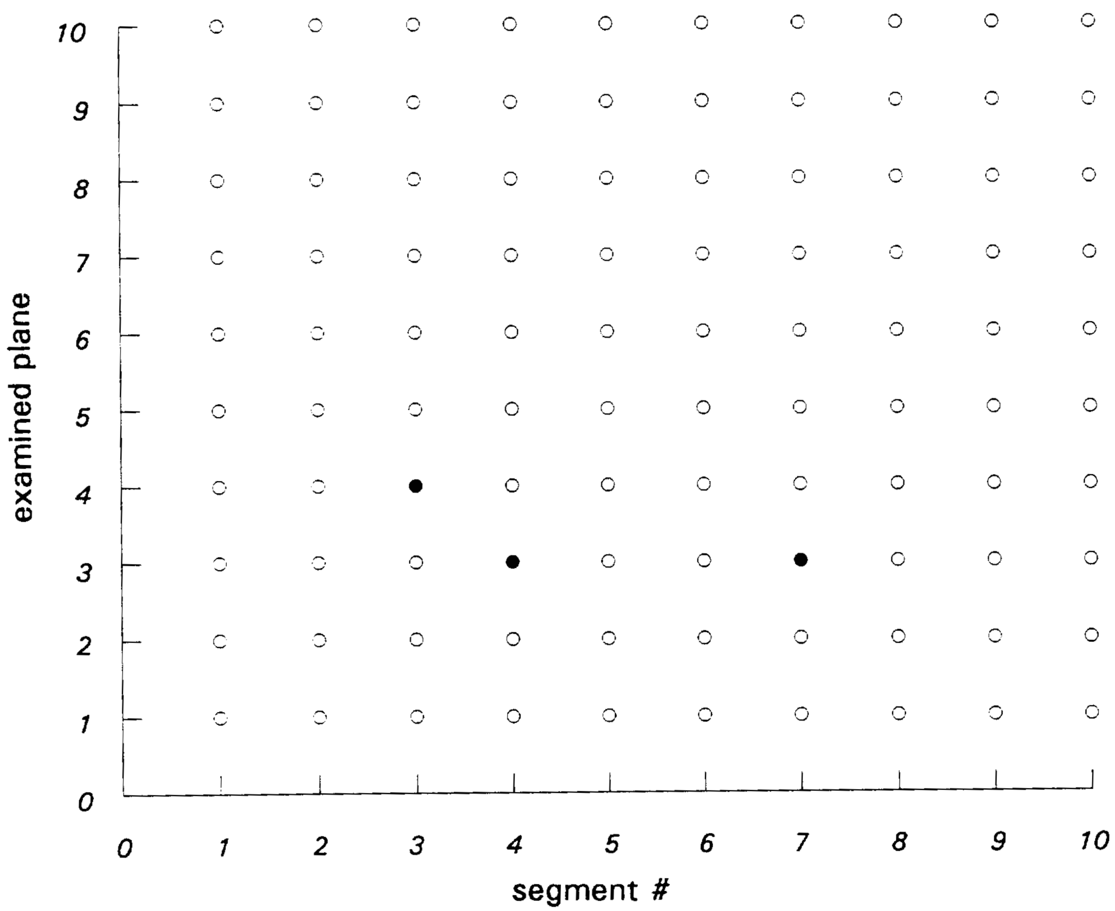

Figure 2.33 Subsurface cracks were found on the planes of roller M1-9012B, $P_o/k = 5.7$.

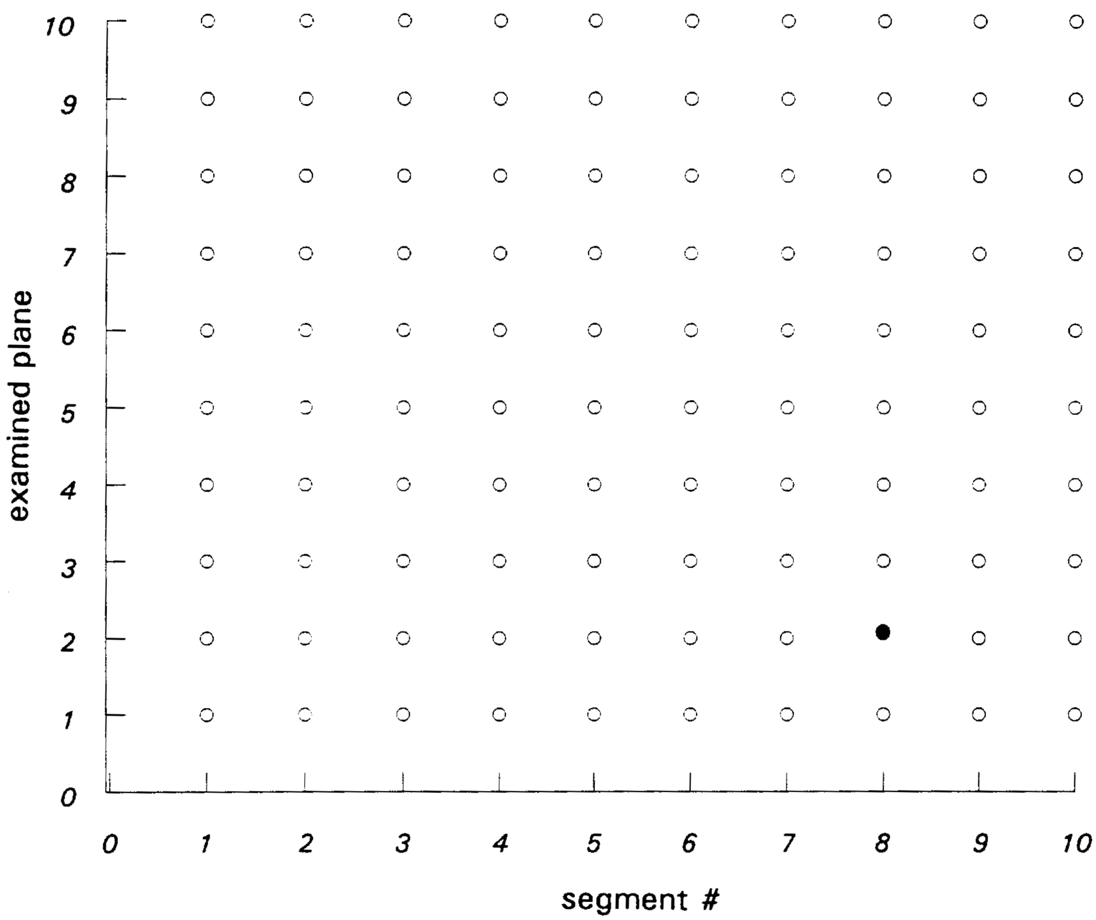

Figure 2.34 A subsurface crack was found on the second plane of roller M1-9009B, $P_o/k = 5.5$.

2.3.4 Plastic deformation and work hardening in the subsurface

plastic deformation

Due to contact stresses one of the changes in the subsurface structure was plastic deformation. In the etched samples of tested rollers, subsurface plastic deformation was characterized by the formation of plastic flow with orientation along the rotation direction of a top roller. The typical characteristics of subsurface plastic deformation are shown in Figure 2.35a. The plastic flow took the same orientation as the roller rotated; the flow zone was discernible at the location of 0.3 mm beneath the surface, and went inwards by 0.9 mm below the surface. On appearance, the entire subsurface zone distinguished itself as four characteristic zones: low plastic top layer (0~0.3 mm), high plastic zone (0.3~0.9 mm), low plastic bottom layer (0.9~1.2 mm), and elastic zone (1.2 mm ~). Within the top layer and the bottom zone, the orientation of plastic flow was obscure while in the high plastic zone plastic flow showed a clear-cut orientation—— the rotation direction of the top roller, with the original pearlitic grain structure distorted (Figure 2.35b). Except for the distorted grain structure, however, SEM examination did not identify any other features that could mark the onset of subsurface fatigue. Beyond the low plastic bottom zone, the structure was virtually unaffected, and the pearlitic grain structure remained intact.

The texture of etched samples has also shown that the severity of subsurface plastic deformation and its depth were related to materials properties, contact loads and contact cycles. Subsurface plastic deformation in the four FAST rail steels (Figures 2.36 ~ 2.37), never developed to the extent of that in the M1-I79 steel. At P_o/k = 5.0, the subsurface appeared not to have been affected by rolling contact. With the contact loads increased to P_o/k = 5.7, the bands of subsurface deformation became discernible, but the orientation of plastic flow was still not clear.

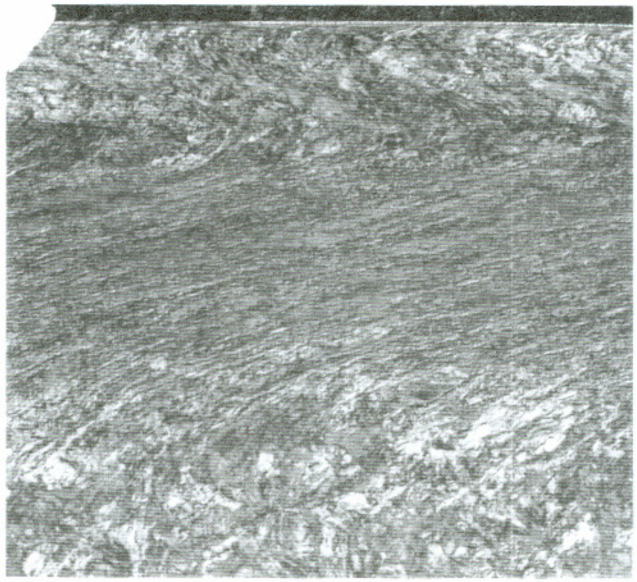

Figure 2.35a Subsurface plastic flow of roller M1-7908. Magnification 50x.

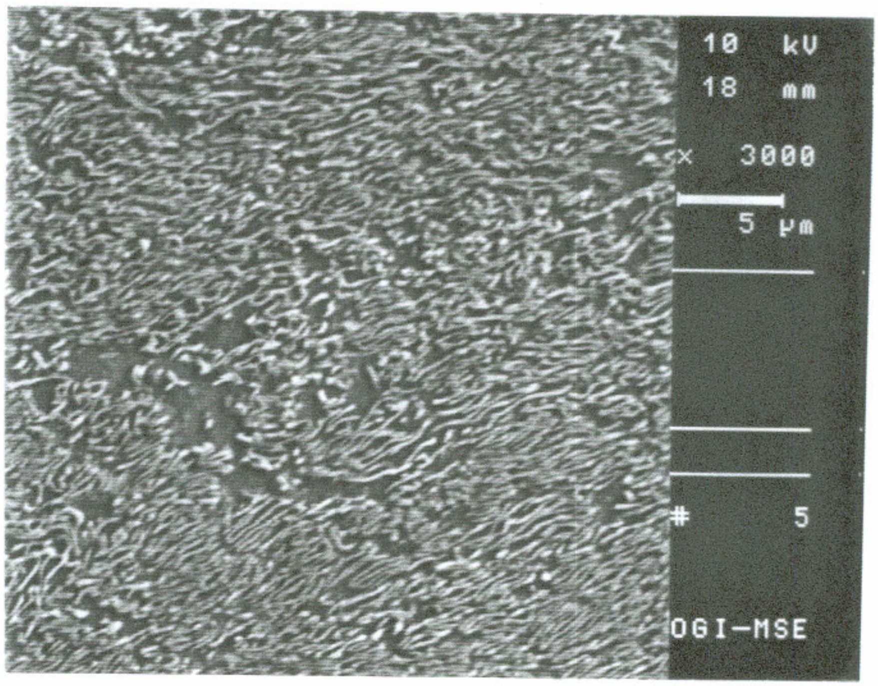

Figure 2.35b Distorted pearlitic structure in the deformed subsurface of the roller.

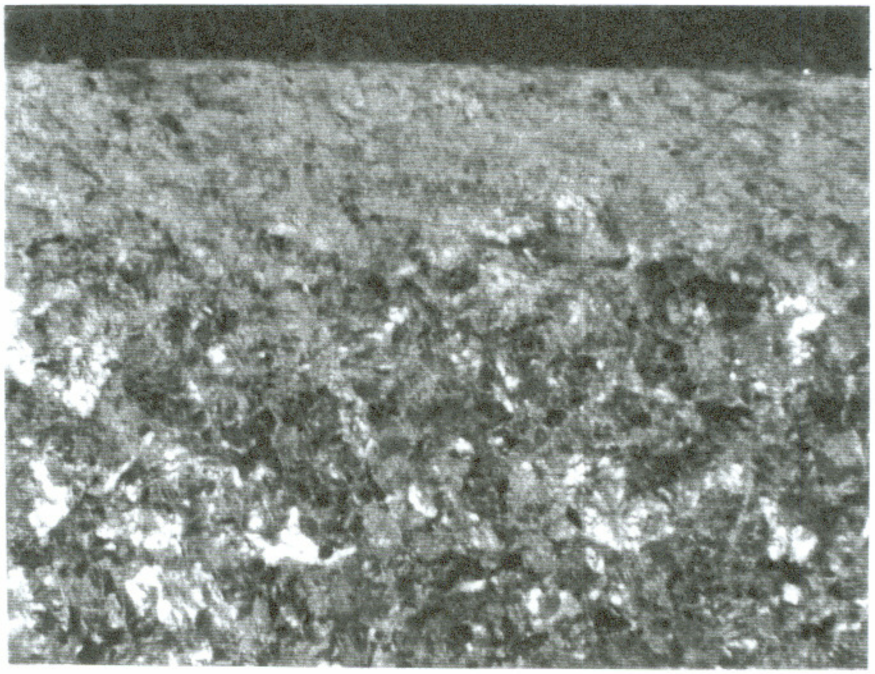

Figure 2.36a Subsurface structure of roller M2-9004, $P_o/k = 7$. Magnification 50x.

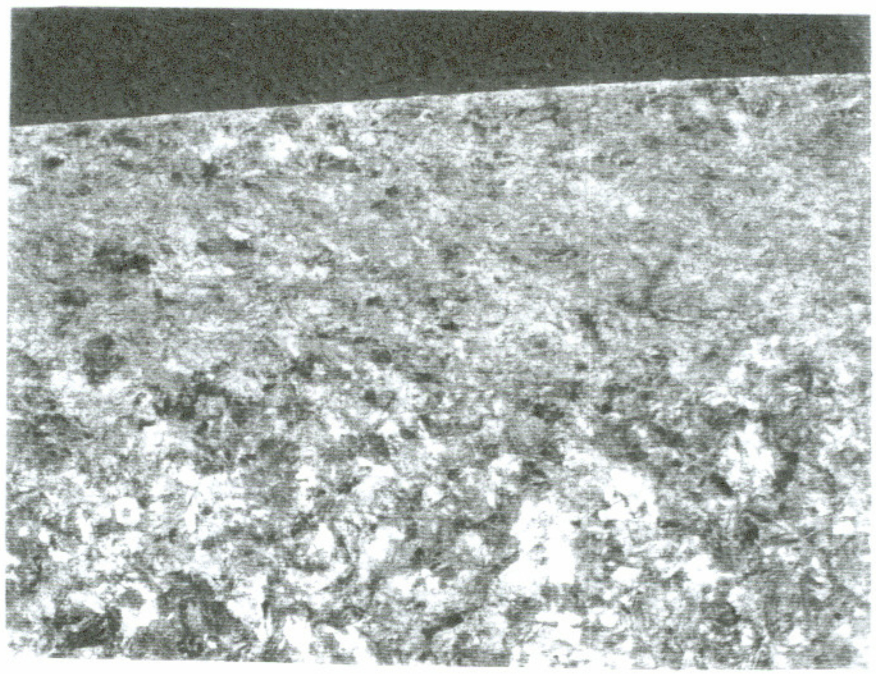

Figure 2.36b Subsurface structure of roller M2-9005, $P_o/k = 7.5$. Magnification 50x.

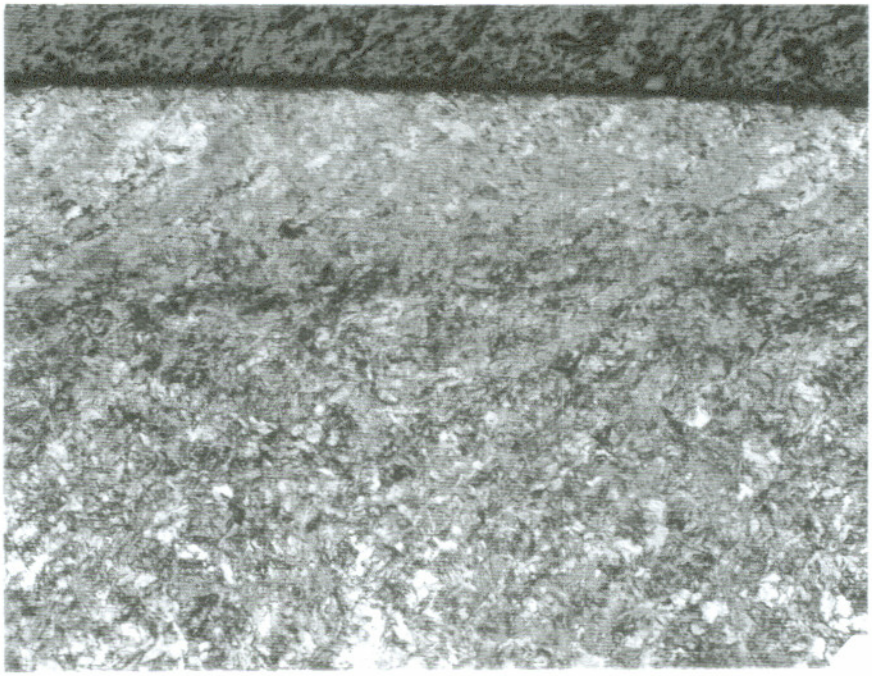

Figure 2.37a Subsurface structure of roller M1-9003C, $P_o/k = 5$. Magnification 30x.

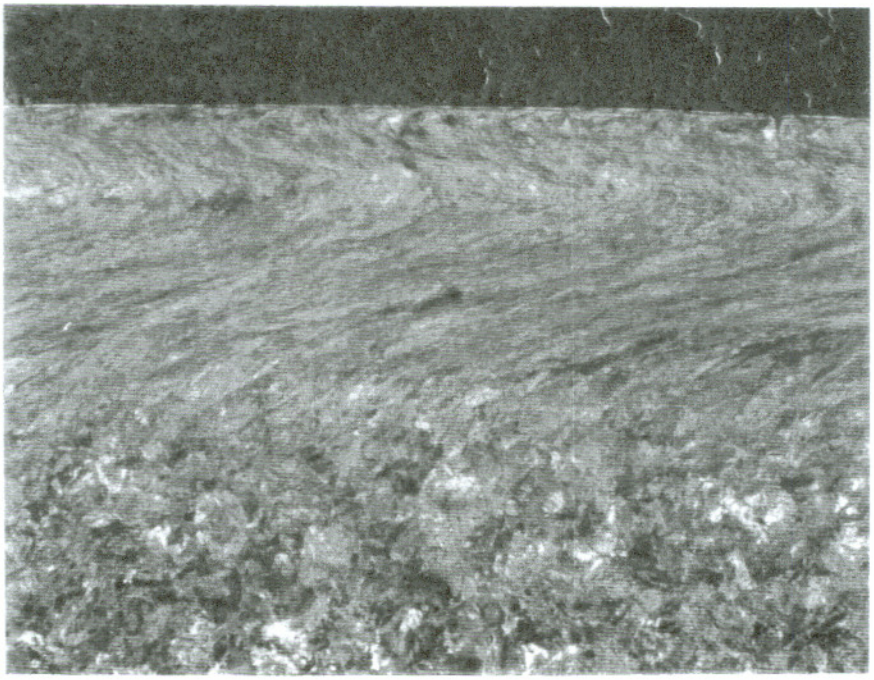

Figure 2.37b Subsurface structure of roller M1-9009C, $P_o/k = 5.7$. Magnification 50x.

Work hardening

Corresponding to the plastic deformation in the subsurface, work hardening caused an increase in microhardness. This phenomenon was observed in all rollers. Even in the rollers where etching failed to delineate plastic flow in the subsurface, microhardness measurements still confirmed the effect of work hardening upon the subsurface. Also, a change in microhardness of the subsurface was a function of the applied contact loads, rolling contact durations and properties of the steels. The relationship between the maximum microhardness in the subsurface of the rail steels and P_o/k is exhibited in Figure 2.38. Except for the case in which the M1-I90C steel was subjected to the load of $P_o/k = 5$, the effect of work hardening was in proportion to the contact loads. The effect of the rolling contact duration is demonstrated in Figures 2.39 and 2.40. The steels subjected to lower loads but longer contact duration had a higher hardness across the subsurface than steels subjected to higher loads but shorter contact duration. The variations in microhardness under the various circumstances are all presented in Figures 2.41～2.43. As the contact loads increased, the work hardening-affected zones in the subsurface grew larger; the location of the micro hardness peak was 0.3 mm beneath the rolling surface.

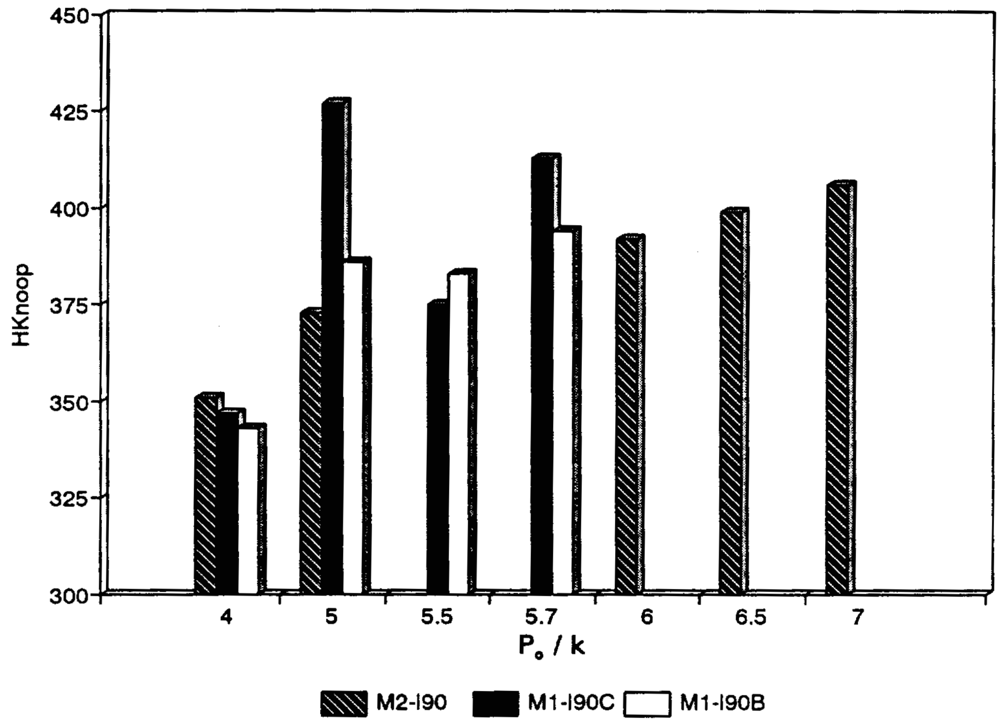

Figure 2.38 Comparison of the maximum microhardness in the subsurface.

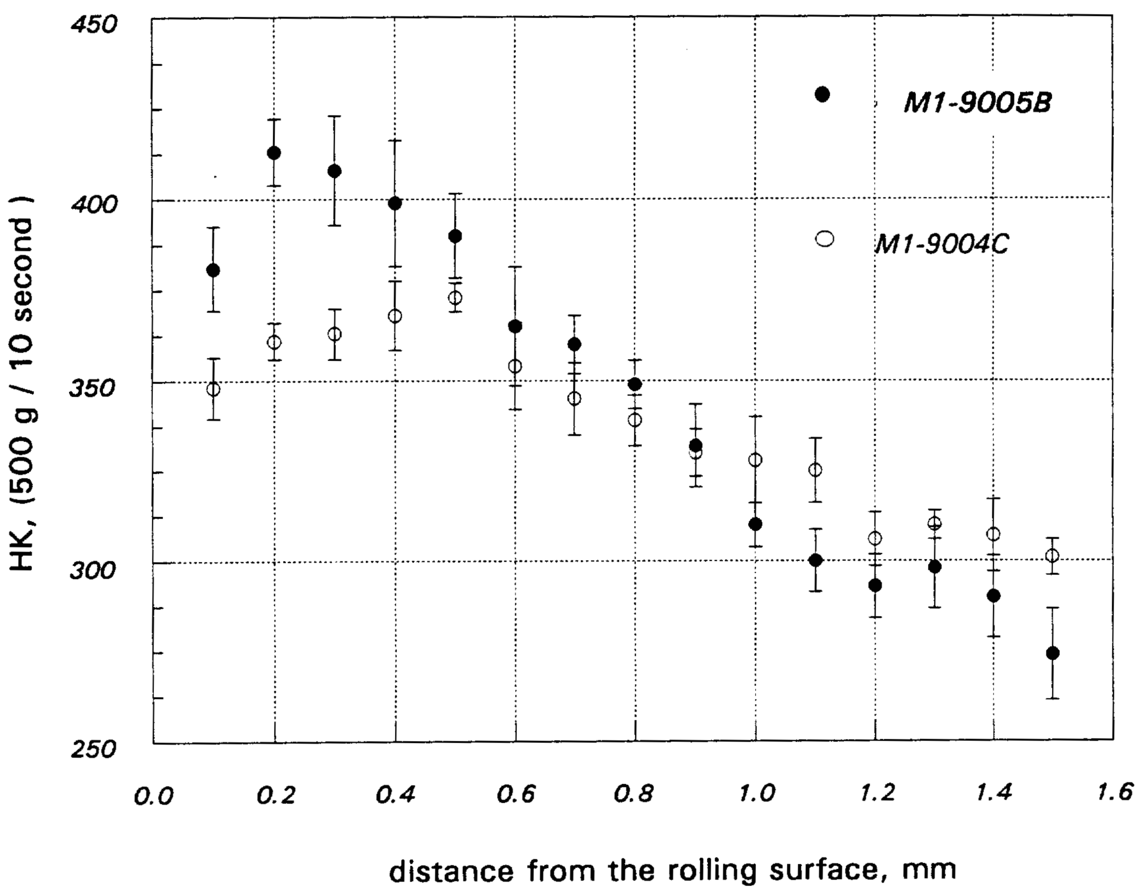

Figure 2.39 Variations in microhardness across the subsurface of rollers M1-9005B and M1-9004C.

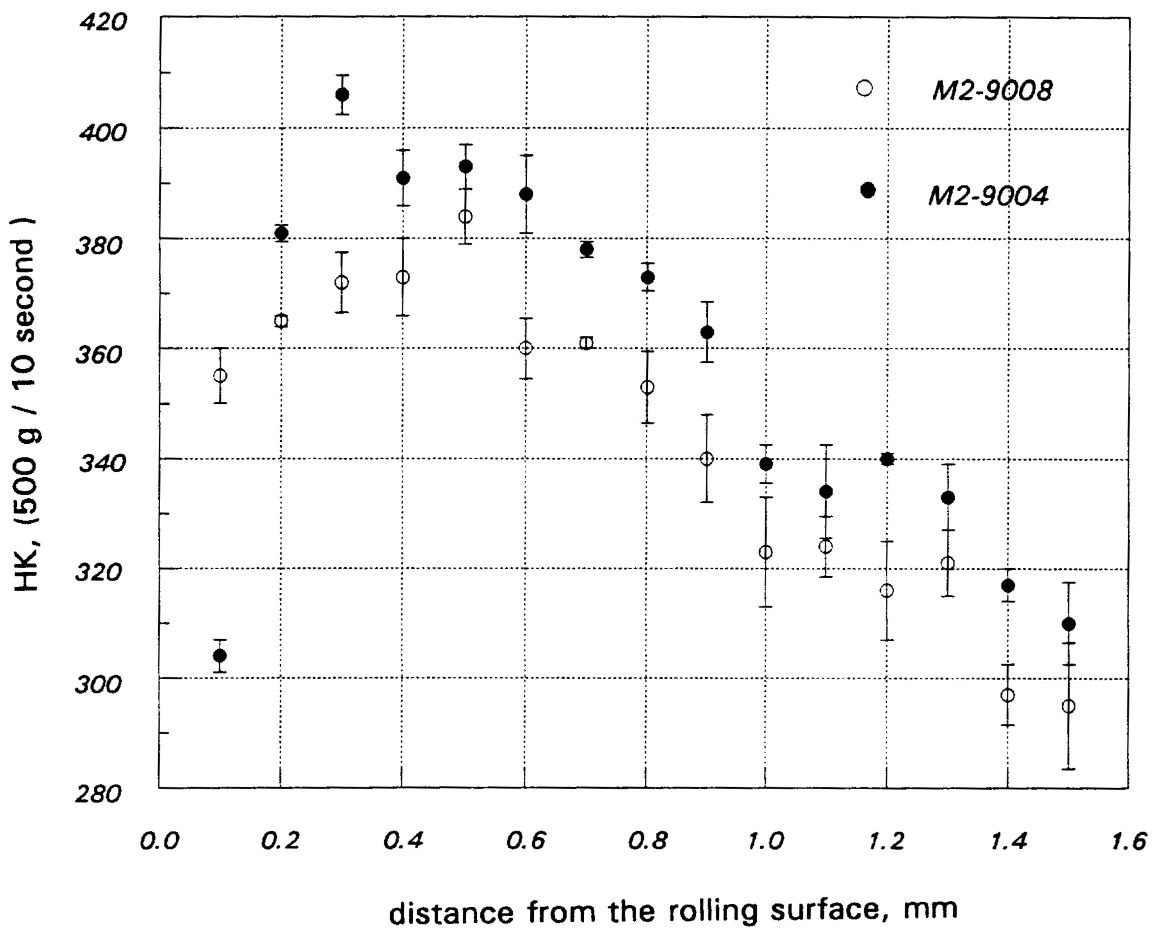

Figure 2.40 Comparison of the microhardness across the subsurface of rollers M2-9008 and M2-9004.

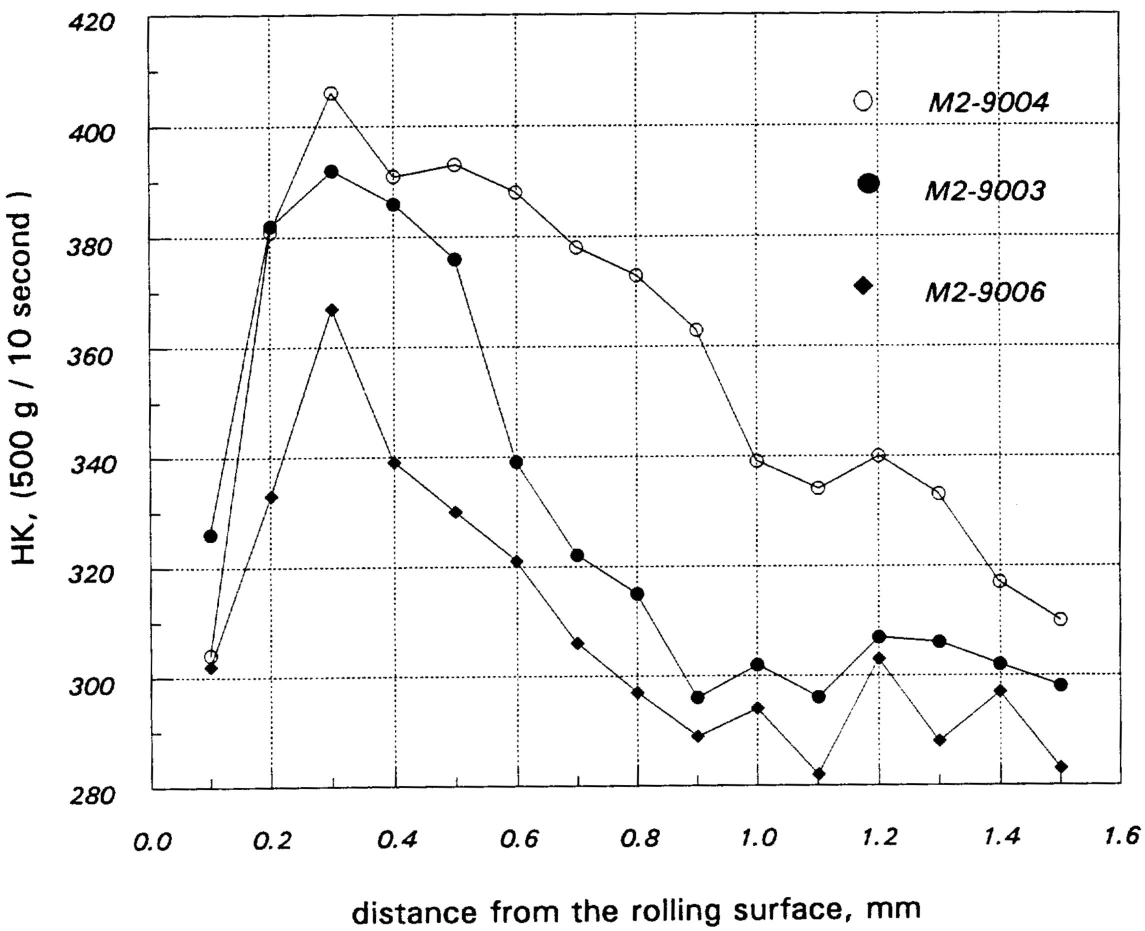

Figure 2.41 Subsurface microhardness profiles of M2-C90 rollers.

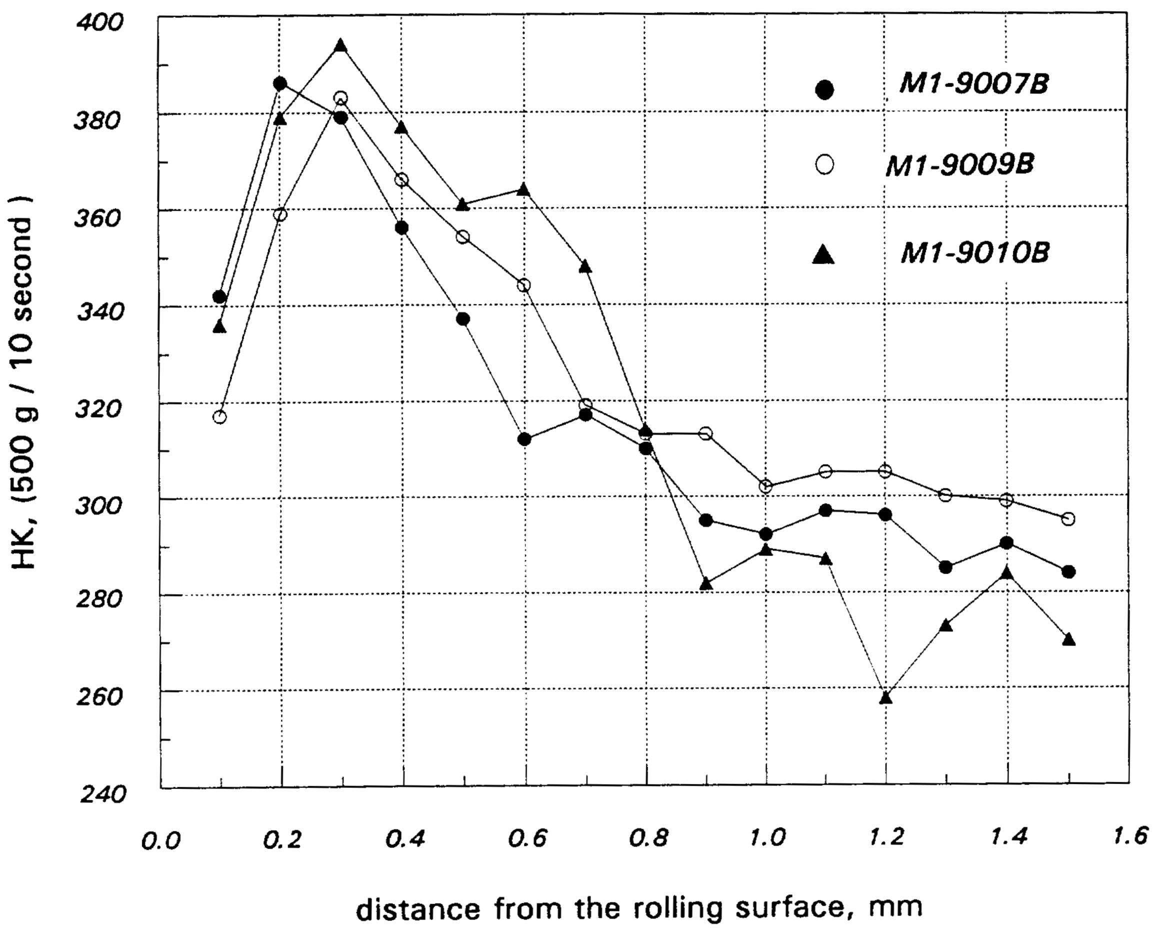

Figure 2.42 Subsurface microhardness profiles of M1-I90B rollers.

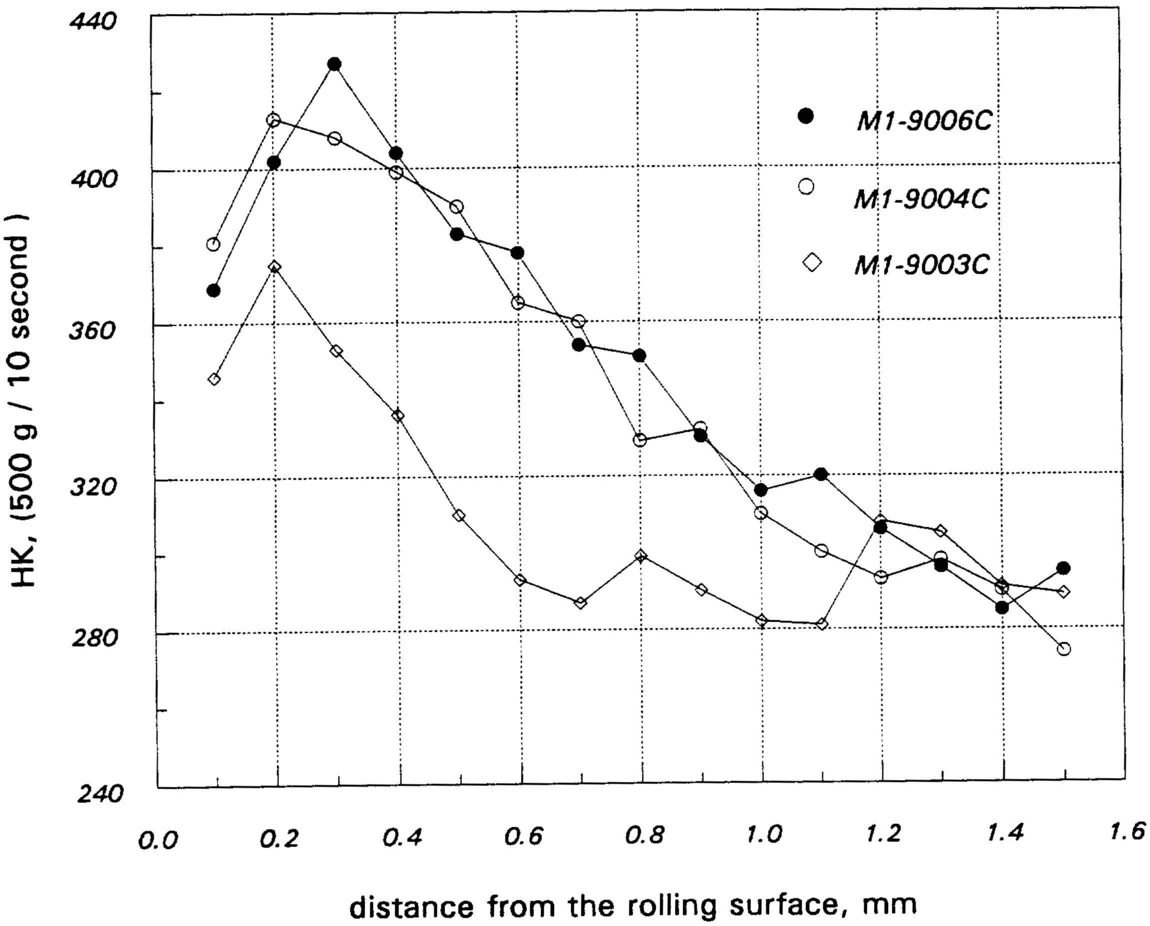

Figure 2.43 Subsurface microhardness profiles of M1-I90C rollers.

2.3.5 Characteristics of spall defects

Spalls were a primary defect observed on the rolling surface. Usually this type of defect emerged late in the rolling contact process, and tended to initiate on the edges of the tread, although they occasionally occurred on the central rolling surface. By morphology, spall defects can be categorized into types I and II. A type I spall was characterized with a round or oblong craterlike cavity with steep walls (Figure 2.44a); in the central deep bottom existed an intergranular, radially oriented crack (Figure 2.44b). The local surface in the vicinity of the spall was smooth and shiny. Figure 2.45 shows both the top view and circumferentially cut view of another typical type I spall; in the subsurface of as deep as 0.6 mm a crack propagated parallel to the rolling surface. The metal in some locations of the bottom was smeared, whereas other locations were characterized with flaps of parabolic tongue (Figure 2.46). As opposed to the type I spalls, type II spalls had a dull V-apexed appearance that distinguished between a leading edge and a trailing edge. A longitudinally cut view showed that a main crack propagated, from the surface, inward through the subsurface at a shallow angle 20°-30° between the crack and the surface (Figure 2.47). The local surface round the type II spall was already deformed, pitted, and cracked. The bottom of the type II spall was featureless (Figure 2.48). Figure 2.49 exhibits the early stage of the formation of a type II spall, with unbroken-off debris still on the top of the cavity.

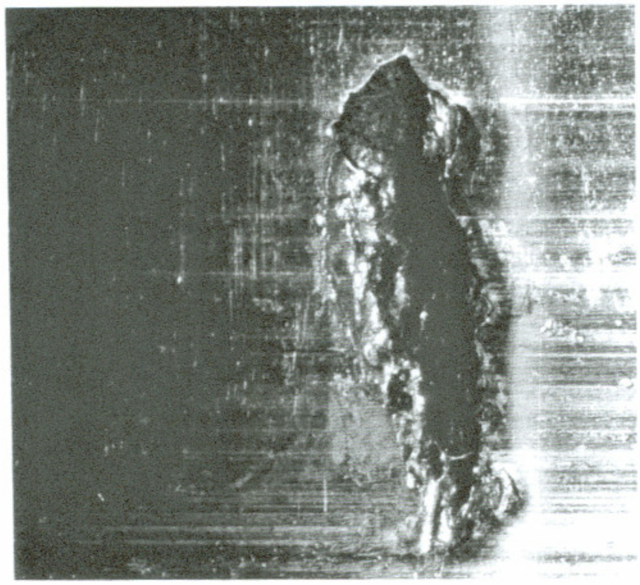

Figure 2.44a A typical type I spall on the rolling surface. Magnification 30x.

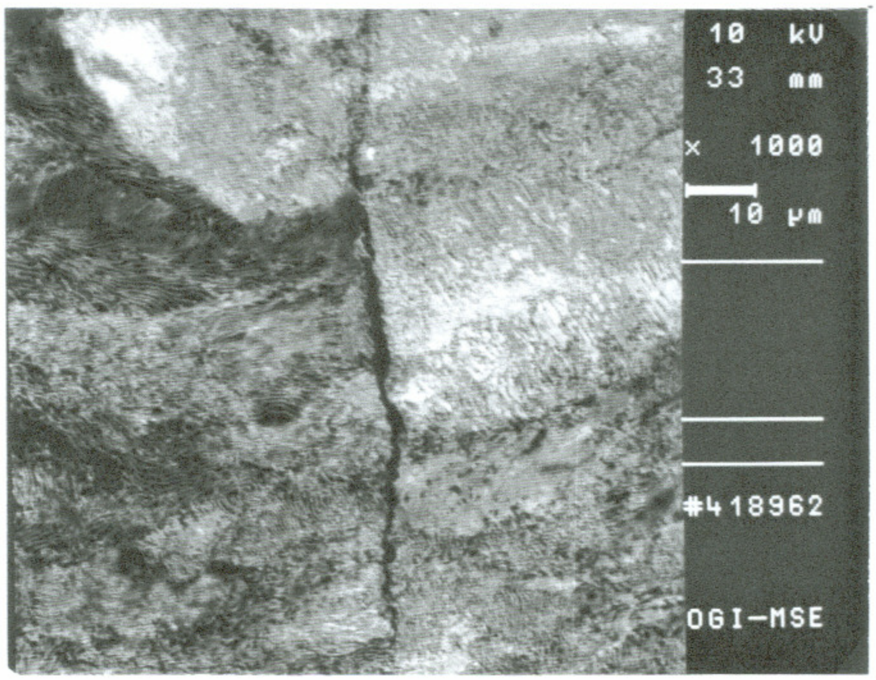

Figure 2.44b The side view of a vertical transverse crack in the bottom of the spall. Magnification 1000.

Figure 2.45a Another typical type I spall. Magnification 15x.

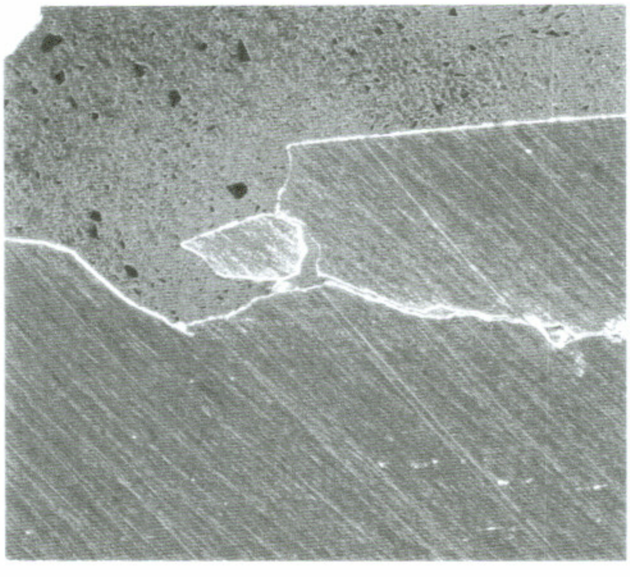

Figure 2.45b The side view of the spall. Magnification 30x.

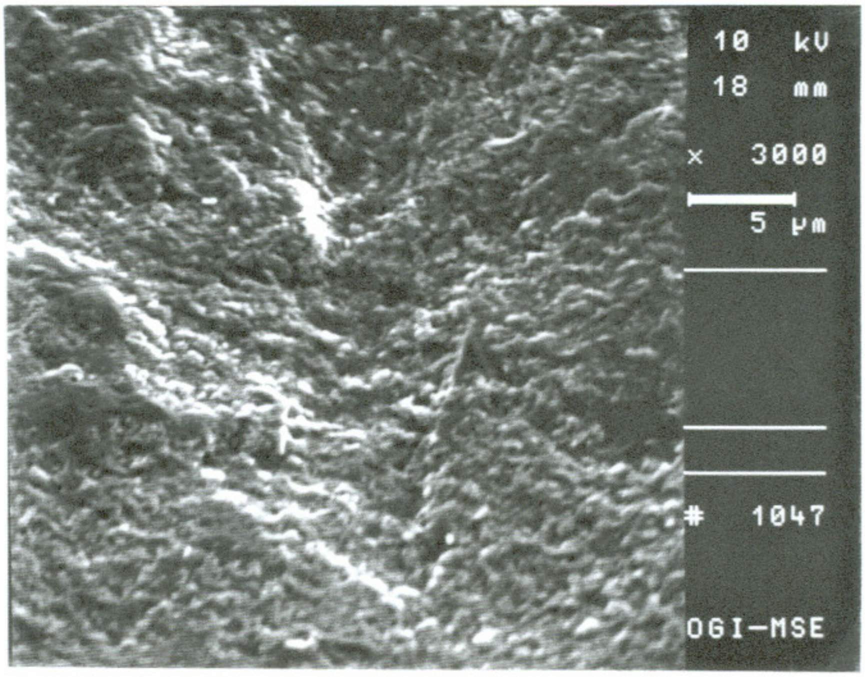

Figure 2.46a One location of the bottom of a typical type I spall. Magnification 3000 x.

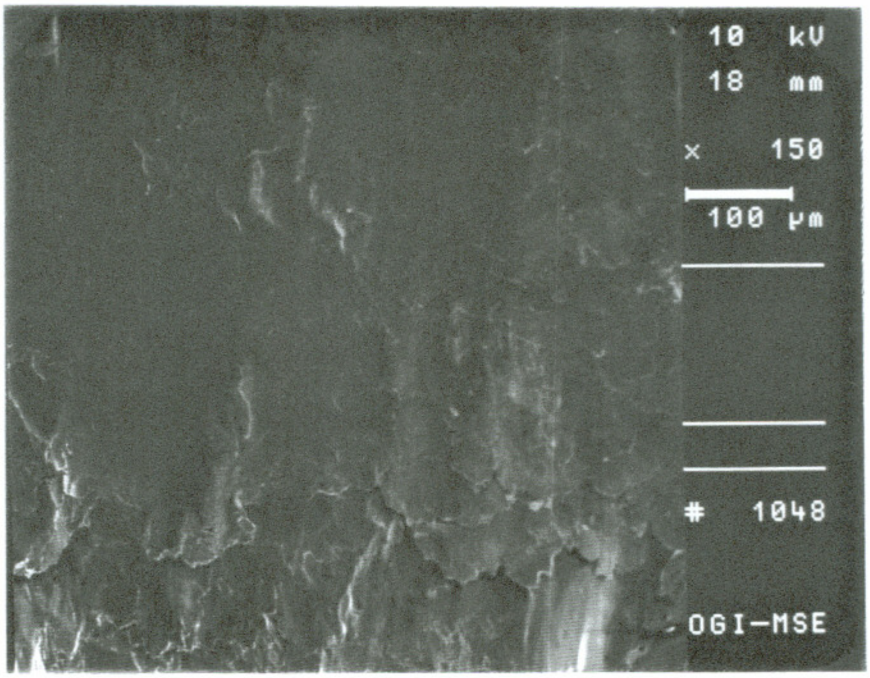

Figure 2.46b Another location of tongue-like feature on the bottom of the same spall. Magnification 200x.

Figure 2.47a A typical type II spall of an arrow head appearance. Magnification 15x.

Figure 2.47b The side view of the same spall, with a crack going inward at 25°.

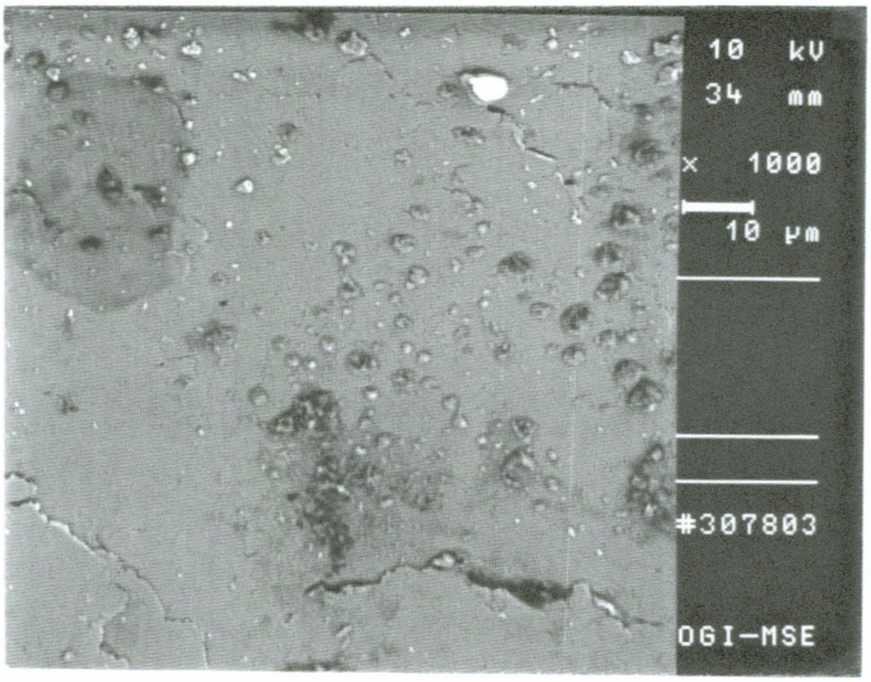

Figure 2.48 The flat and featureless bottom of a type II spall. Magnification 1000x.

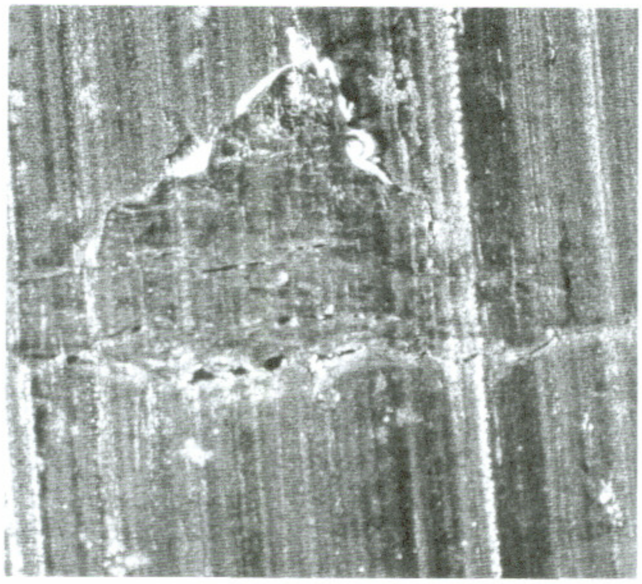

Figure 2.49 The early stage of a type II spall. Magnification 30x.

2.3.6 Spalling phenomena in the tests of the four FAST rail steels

Spall defects were a dominant cause of terminating the first seven tests of M3-C90 steel. Several spalls on the rolling surface of the M3-9004 roller were congregated and connected to one another (Figure 2.50). Spreading across the rolling surface and causing severe damage, a typical spall on the M3-9002 roller already grew to its final stage (Figure 2.51a). Although the full features of this spall were already deteriorated, the retained features suggested that this spall belonged to type I. In the cavity bottom a crack was still discernible. By a stepwise sectioning technique the metallographic examination displayed a series of the side views of this spall. As the sectioning advanced toward the spall center, the cavity went deeper. The deepest point of the bottom was at about 2 mm beneath the surface. Its similarities to the spall shown in Figure 2.45 and its difference from the spalls shown in Figure 2.47 are apparent. In addition, the metallographic examination revealed on the bottom a cluster of Al_2O_3 inclusions (Figure 2.51b), around which a cavity was formed.

Of the M2-C90 steel tests, only the M2-9001 roller suffered spalling (Figure 2.52). The spall had some features of a type I spall: the local surface surrounding the cavity was relatively smooth, and a radially oriented crack existed in the deepest location of the bottom. However, an attempt to investigate the origin of this spall was not successful; the metallographic examination failed to find any nonmetallic inclusions in the crack.

In testing M1-I90B steel, only the M1-9010B and M1-9003B rollers experienced spalling. As showed in Figure 2.53, adjacent to one edge of the rolling surface the cavity had a clear-cut border. The spall-related surface failure that led to terminate the M1-9002C test is shown in Figure 2.54.

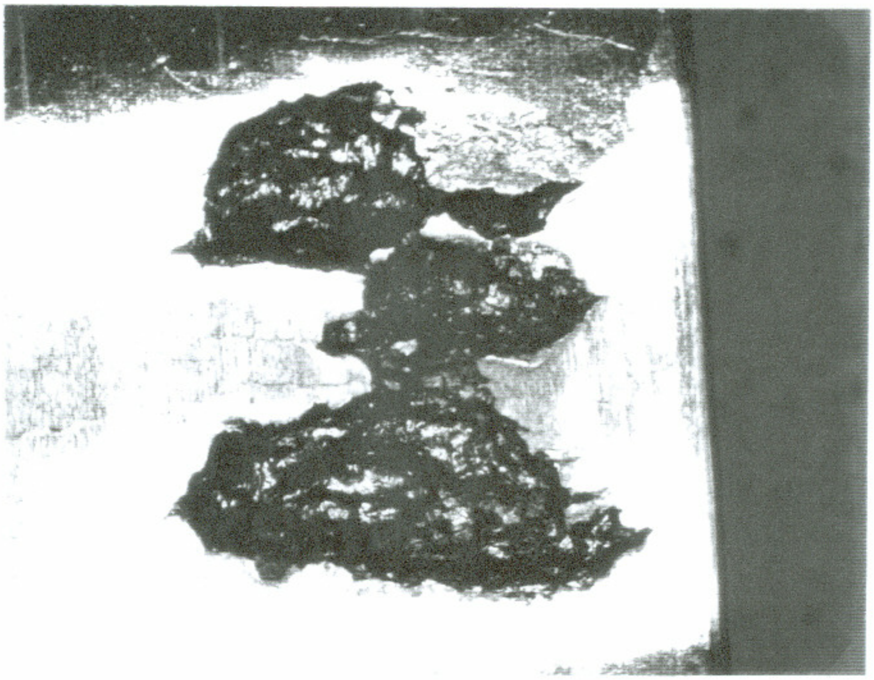

Figure 2.50 A cluster of spalls on the rolling surface of roller M3-9004.

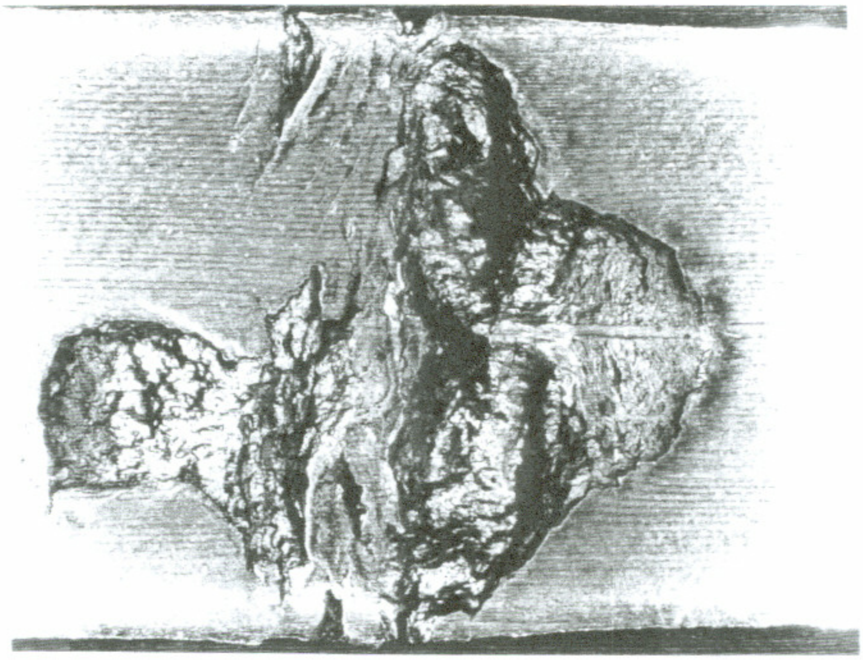

Figure 2.51a A spall across the entire rolling tread of roller M3-9002. Magnification 50x.

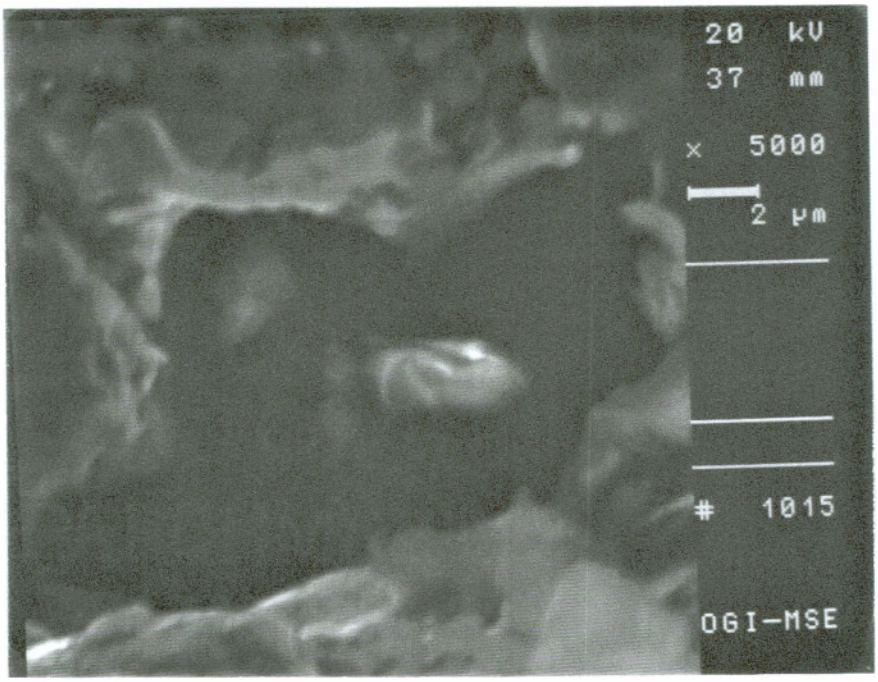

Figure 2.51b A cavity formed at Al_2O_3 inclusions on the bottom of the spall.

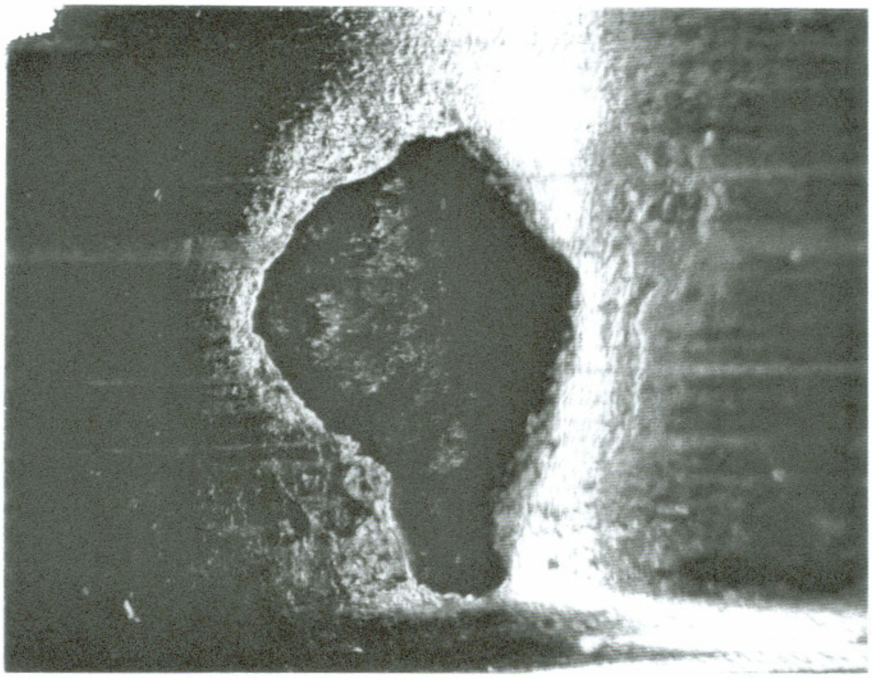

Figure 2.52 A type I spall on the rolling surface of roller M2-9001. Magnification 20x.

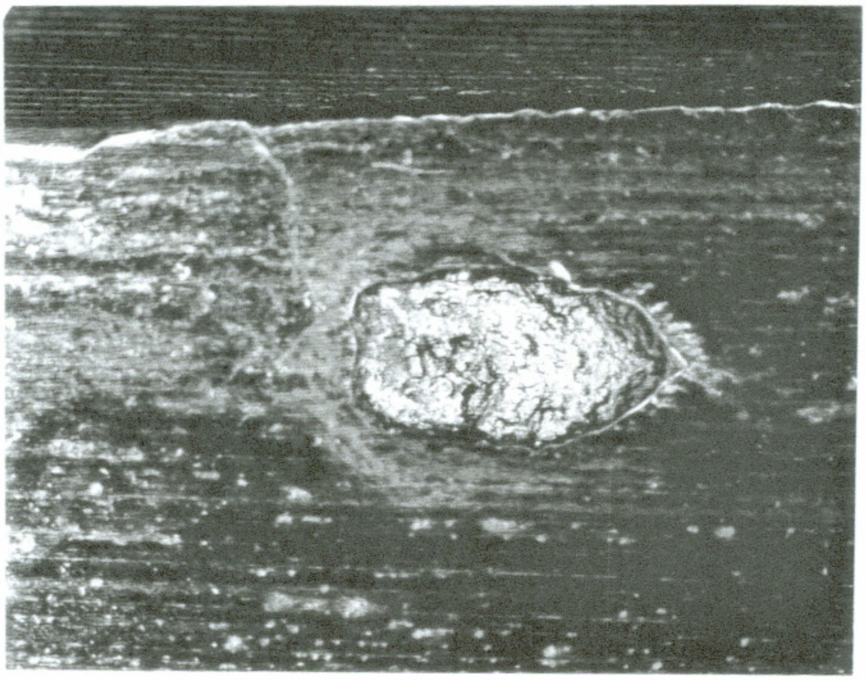

Figure 2.53 A type I spall on the rolling surface of roller M1-9010B. Magnification 20x.

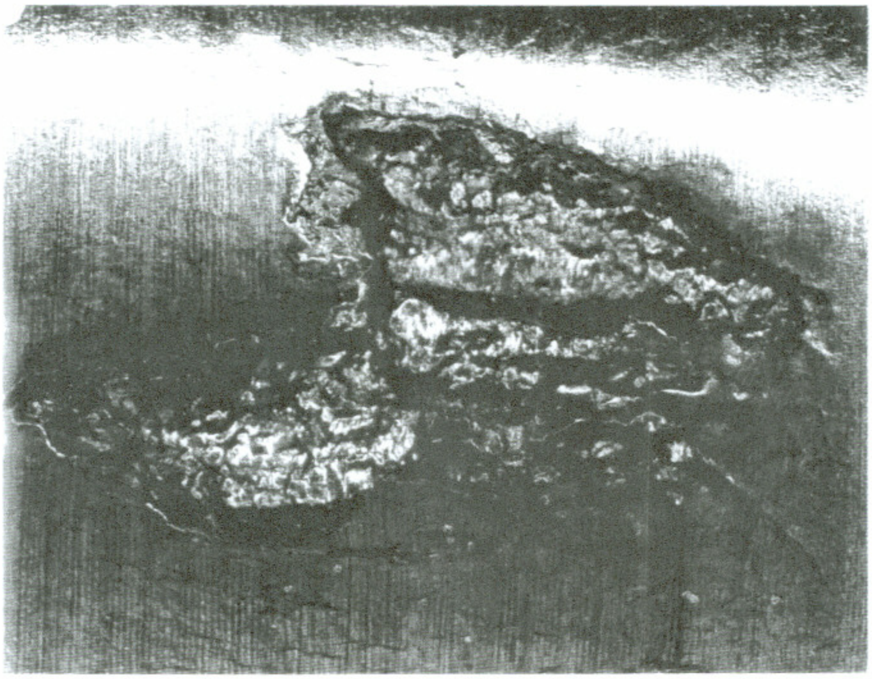

Figure 2.54 A spall failure on roller M1-9002C. Magnification 15x.

Chapter 3

ASSESSMENT OF NONMETALLIC INCLUSIONS

3.1 Experiemental procedures

3.1.1 Sampling and preparation of specimens

The steel blocks used for assessing nonmetallic inclusions were cut from a particular position in the rail head (Figure 3.1). This particular position is the most susceptible to subsurface initiated fatigue.[51] With the size of 20 x 10 x 10 mm, all specimens were sampled end to end from the heads of the M1-I79, M1-I90B, M1-I90C, M2-C88, M2-C90, and M3-C90 rails. Fifty specimens were cut from a four-foot piece of the M1-I79 rail; 30 specimens from a three-foot piece of the unused M2-C88 rail; 20 specimens from each of the M1-I90B, M1-I90C, M2-C90 and M3-C90 rails. These specimens were ground exactly to the dimension of 20 x 10 x 10 mm and mounted for further processing. The specimens were ground automatically and polished in compliance with a procedure recommended in the Standard Practice ASTM E 45 - 87. [116, 117] The grinding and polishing were carefully controlled so as to assure an acceptable quality of the metallographic specimens. During coarse grinding stages, nonmetallic inclusions in the specimens were not pitted, left in relief, dragged, removed or obscured. After their final grinding the specimens were cleaned thoroughly before being polished. The polishing was done using 6 μm and 1 μm diamond paste and completed by a 0.05 μm colloid slurry. During polishing caution was taken not to alter the true appearance of nonmetallic inclusions on the plane-of-polish and to avoid excessive relief, pitting, or pullout. Before microscopic examination the specimen surfaces were cleaned with ethanol.

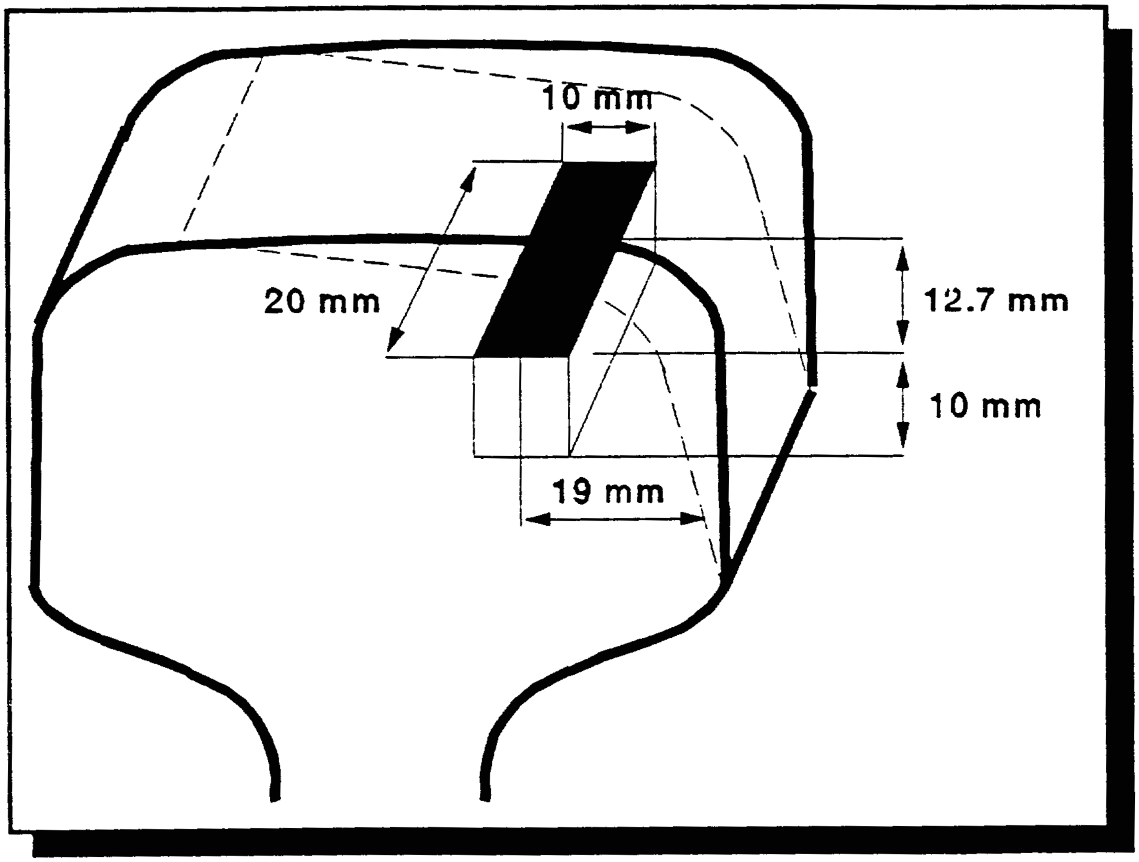

Figure 3.1 Specimens from the particular position in rail head.

3.1.2 Classification of nonmetallic inclusion types

The specimens were examined with an optical microscope in order to determine the types and distribution of nonmetallic inclusions in the rail steels. Typical nonmetallic inclusions were photographed. Those specimens containing typical nonmetallic inclusions were further investigated by SEM, and the types of nonmetallic inclusions were determined by X-ray energy dispersive spectrum (EDX).

3.1.3 Measurement of aggregation of oxide inclusions

The amounts and lengths of stringered oxide inclusions indicate the aggregation of oxide inclusions in the steels. A stringer of oxide inclusions was defined as a chain of individual oxide particles separated by at most 50 μm which together are longer than 100 μm, illustrated in Figure 3.2. The entire polished surface, 200 mm^2, of a specimen was surveyed using an optical microscope at a magnification of 100x, with a microscopic field area being as large as 0.50 mm^2. Lengths of oxide stringers were measured with a built-in microscale.

3.1.4 Practice for determining area fractions of oxide inclusions

The practice of determining volume fractions of oxide inclusions was based on stereological measurement methods. A *Leco* computer-aided image analyzer was used to identify oxide inclusions and to measure their areas. Nonmetallic inclusions of different types were detected and distinguished by gray-level intensity differences between one or another and an unetched matrix. There were differences in the morphologies of oxide inclusions and sulfides. Sulfides were elongated in the rail rolling direction whereas individual oxides were globular. By the differences in reflectivity and aspect ratio an image analyzer can distinguish between oxides and sulfides. In order to prevent the polished surfaces of specimens from being obscured and ensure a consistent grey level of polished surfaces, the measurements were always carried out immediately after polishing. Forty random field measurements were made on each of the 50 unetched M1-I79 specimens, and 50 random field measurements were performed on each of the 30 unetched M2-C88 specimens. For the four FAST rails, M1-

I90B, M1-I90C, M2-C90 and M3-C90, a total of 20 specimens for each steel were investigated, and 50 random field measurements were conducted on each of the specimens. Both the correctness of inclusion identification and the accuracy of the measurements depend on the inclusion identification routines, which were designed for the image analyzer to identify and measure inclusions of the steels under review.

3.1.5 Development of the routines

A few of the typical fields that contained oxides, sulfides, and oxy-sulfide duplex inclusions were chosen from several specimens of the M1-I79 rail. Types and compositions of those inclusions were determined with an optical microscope and EDX. Based on the types and compositions, a prototype routine for an image analyzer to distinguish and measure oxide inclusions was developed. The applicability of this prototype routine was repetitively tested on other specimens and was modified until its general applicability was acceptable. The test showed that this general routine worked well in differentiating the neighborhood sulfides and oxides (Figure 3.3). The routines applied to measuring volume fractions of oxide inclusions evolved from this prototype routine. The routine for M1-I79 steel is presented as an example (Figure 3.4), while the routines for the other rail steels are included in Appendix 1.

The M1-I79 routine was organized as a sequence of 30 analytical steps. The purpose of each step was to ensure the correct of identification of oxides and improve the accuracy of the measurement. The goal was to be as accurately as possible for oxide inclusions while excluding all sulfide inclusions. For a single field measurement focusing on such a large area as 0.0452 mm^2 at a magnification of 400x, a 386DX PC computer took approximately one minute to run through the routine.

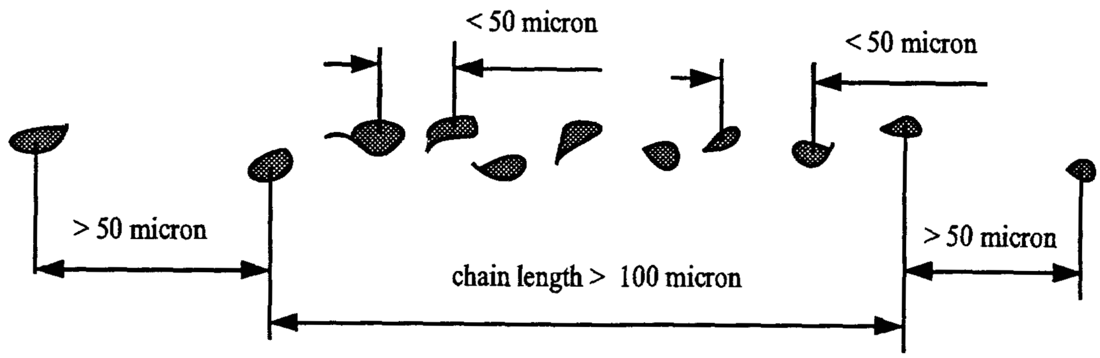

Figure 3.2 Illustrative definition of a stringer of oxide inclusions.

Figure 3.3a A stringer of oxy-sulfide inclusions(the darker phase is oxides).

Figure 3.3b Oxides(the red phase) were distinguished from the surrounding sulfide.

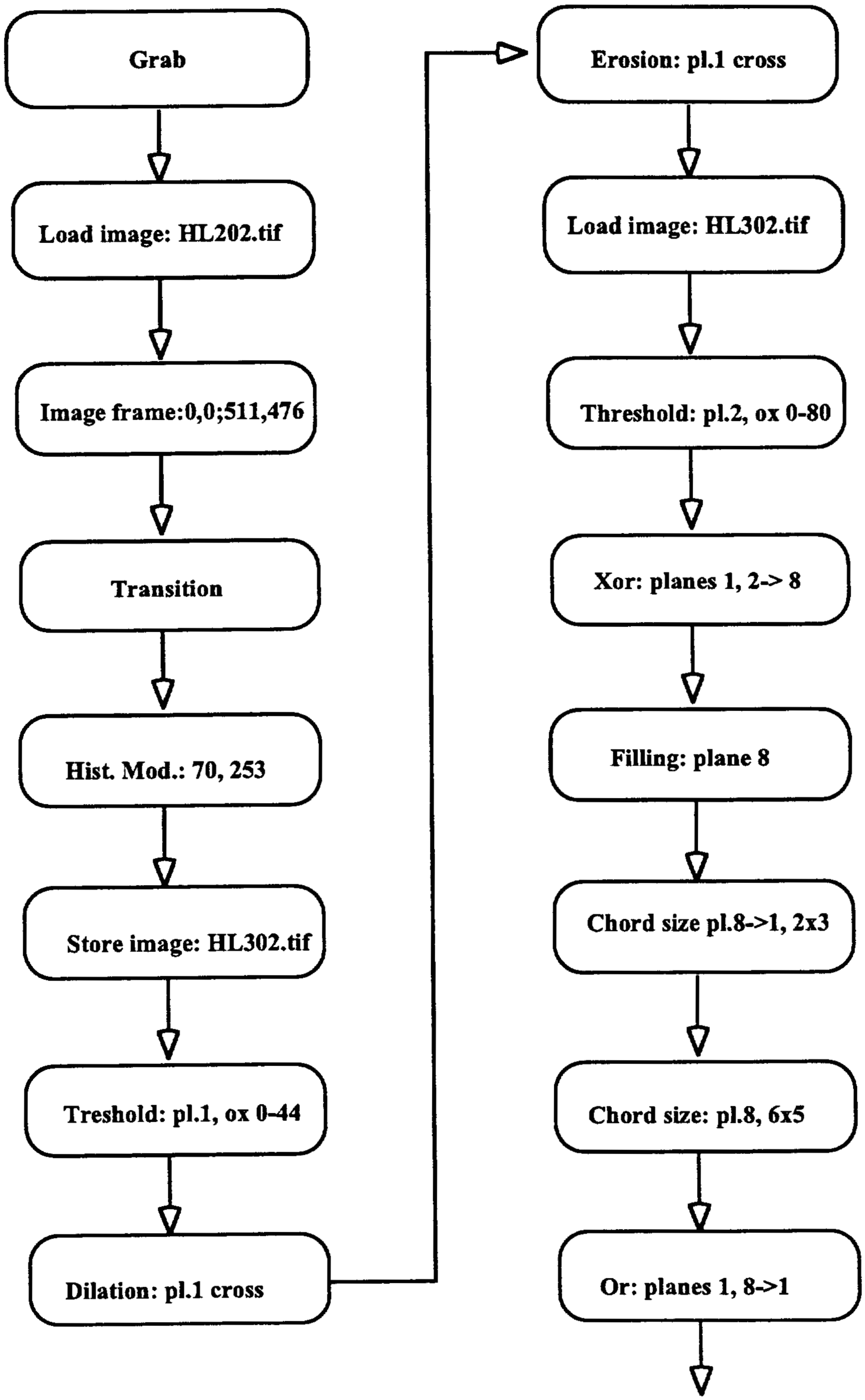

Figure 3.4 Analytical routine for identifying and measuring oxide inclusions in M1-I79 steel

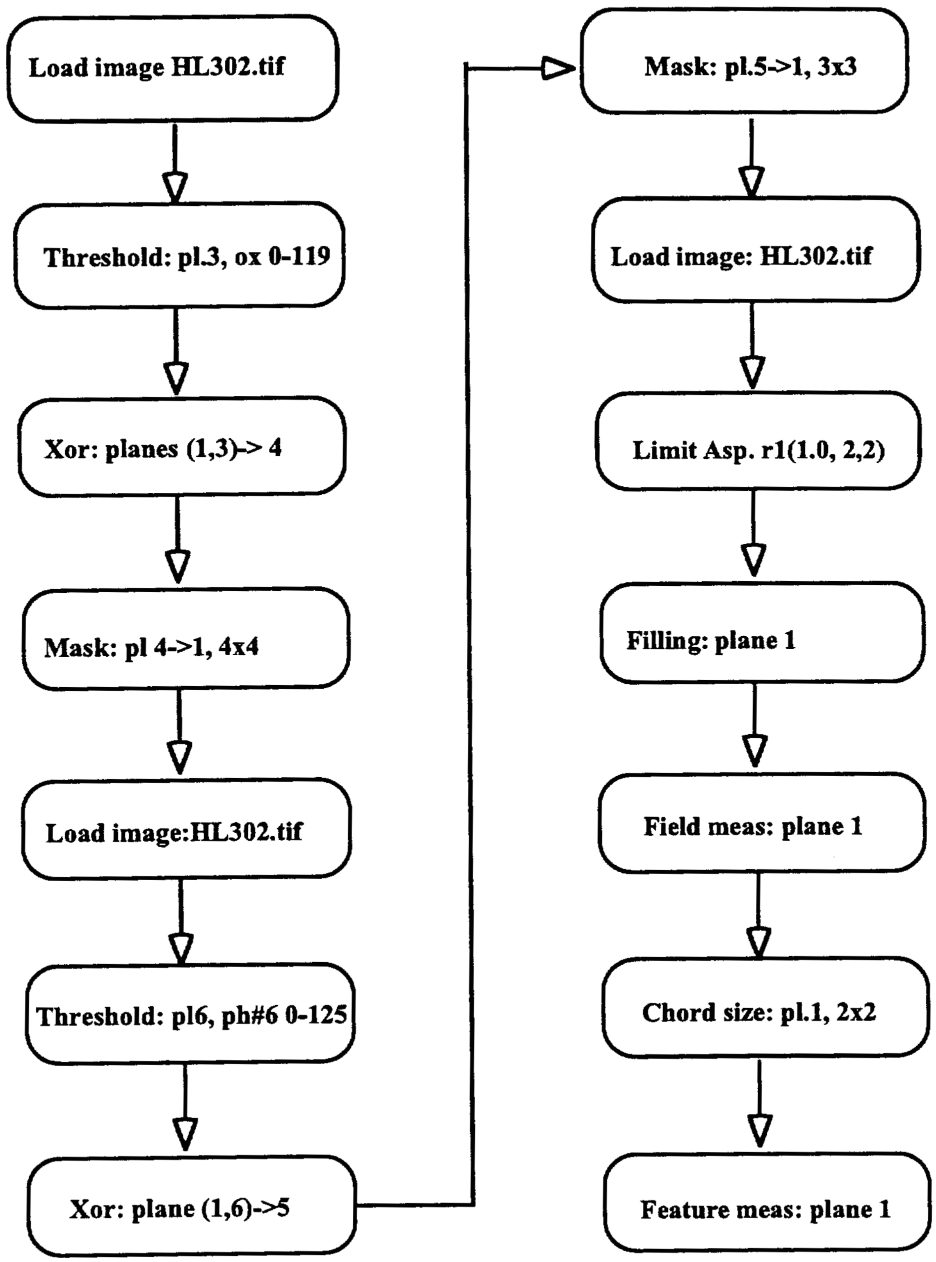

Figure 3.4 Analytical routine for identifying and measuring oxide inclusions in M1-I79 steel

3.2 Qualitative and quantitative characteristics of nonmetallic inclusions

3.2.1 Types and morphologies of nonmetallic inclusions

Based on the examinations by optical microscopy and EDX, nonmetallic inclusions in the rail steels were classified primarily as oxides and manganese sulfides. Oxide inclusions were alumina, calcium aluminate and titanium oxides. The types of oxide inclusions in the individual steels are listed in Table 3-1.

Table 3-1 Presence of oxide inclusions in the steels

steel	Al_2O_3	mAl_2O_3-nCaO	Al_2O_3-MgO-CaO	SiO_2	TiO_2
M1-I79	yes	yes	no	no	yes
M1-I90B	yes	yes	no	no	yes
M1-I90C	yes	yes	no	no	yes
M2-C88	yes	yes	no	no	yes
M2-C90	yes	yes	yes	no	yes
M3-C90	yes	no	no	yes	yes

Primary oxide inclusions in all steels but M3-C90 steel were alumina and calcium aluminate. There were no calcium aluminates in M3-C90 steel. Oxide inclusions in M1-I90B and M1-I90C steels were identical in type. Oxide inclusions existed in isolated particles or stringers (Figure 3.5), and in elongated oxy-sulfide duplex inclusions with oxide particles being surrounded by manganese sulfides (Figure 3.6). TiO_2 particles were sparsely distributed in the steels. Elongated MnS inclusions were aligned to the direction of rail forming. Alumina and calcium aluminate stringers in M1-I79 steel were coarse compared to those in the other rail steels.

3.2.2 Contents of oxides inclusions

The computer-aided image analyzer measured the area fractions of detected oxides by dividing the detected area of each by 0.045 mm^2 of the measurement field. According to stereological microscopy, the volume fractions of oxide inclusions in the rail steels were determined by the detected area fractions:

$$V_V = A_A = \frac{A_i}{A_T}$$

where V_V is a volume fraction; A_A is an area fraction of oxides; A_i is the area of detected oxides; A_T is equal to 0.045 mm^2, the measurement field. In a numerical sense, therefore, a detected area fraction of oxide inclusions is equivalent to a volume fraction of oxide inclusions. In total more than 10,000 microscopic fields were investigated for the six rail steels. As part of the quantitative analysis, 400 field measurements of the first 10 M1-I79 specimens and 500 field measurements of the first 10 M2-C88 specimens are presented in Tables 3.2 and 3.3, respectively. The field measurements of the remaining specimens are all included in Appendix 2. The oxide volume fractions of the 50 M1-I79 specimens and 30 M2-C88 specimens, which were based on the data in Table 3-2, Table 3-3 and Appendix 2, are shown in Tables 3-4 and 3-5, and the oxide volume fractions of the specimens of the other four steels, resulting from the total of 4000 field measurements, are presented in Table 3-6.

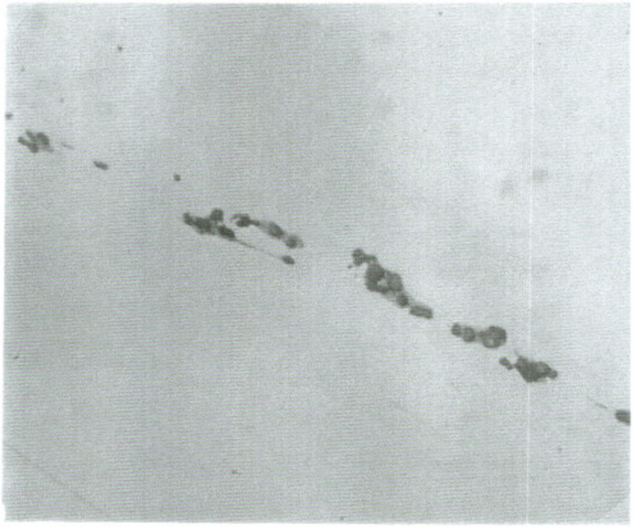

Figure 3.5 A stringer of alumina inclusions in M1-I79 steel. Magnification 400x.

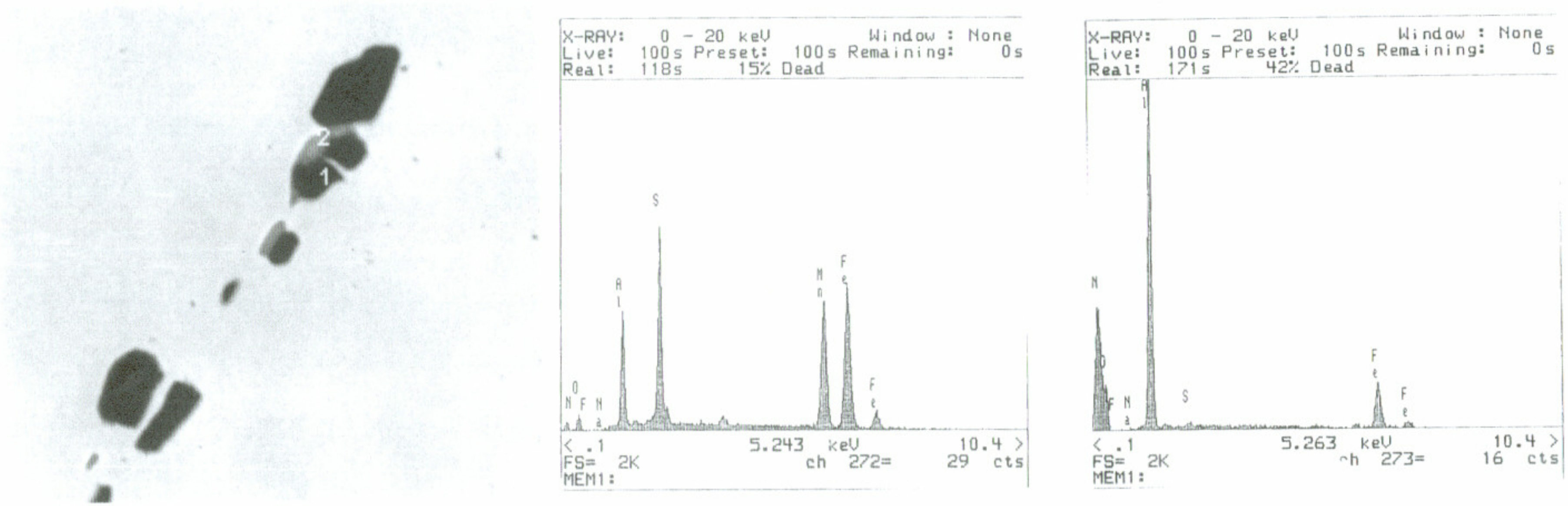

Figure 3.6 Duplex oxy-sulfide inclusions in M1-I79 steel; X-ray spectrum of spot 1; X-ray spectrum of spot 2

Table 3-2 Area fractions of oxide inclusions in 10 M1-I79 specimens

field #	specimen 1	specimen 2	specimen 3	specimen 4	specimen 5
1	.0091	.0000	.0239	.0000	.0000
2	.0000	.0000	.2382	.0000	.0000
3	.0128	.0000	.0000	.0000	.0000
4	.0000	.0000	.0000	.0000	.0215
5	.0000	.0000	.0000	.0425	.0000
6	.0144	.0252	.0000	.1705	.0000
7	.0153	.0000	.0000	.0000	.0000
8	.0000	.0000	.0000	.0000	.0000
9	.0066	.0000	.0211	.0000	.0000
10	.0871	.0305	.0206	.0000	.0000
11	.0000	.0074	.0541	.0000	.0000
12	.0025	.0004	.0144	.0458	.0000
13	.1050	.0033	.0000	.0000	.0000
14	.0037	.0000	.0000	.0000	.0000
15	.0384	.0000	.0000	.1362	.0000
16	.0235	.0248	.1152	.0000	.0570
17	.0116	.0054	.0000	.0000	.0000
18	.0227	.0045	.0000	.0000	.0000
19	.0087	.0103	.0000	.0000	.0000
20	.0066	.0033	.0000	.0000	.0450
21	.0000	.0078	.0000	.0000	.0000
22	.0000	.0050	.0000	.0000	.0000
23	.0000	.0083	.0000	.0000	.0000
24	.0000	.1030	.0000	.1940	.0000
25	.0000	.0681	.0000	.0000	.0000
26	.0000	.1040	.0450	.1907	.0000
27	.0000	.0594	.0000	.0000	.0000
28	.0000	.0000	.0111	.0000	.0000
29	.0810	.0202	.0879	.0000	.0099
30	.0000	.0326	.0000	.0000	.0000
31	.0099	.0314	.0520	.0000	.0000
32	.0037	.0000	.0516	.0000	.0648
33	.0000	.0066	.0000	.0000	.0000
34	.0103	.1030	.0000	.1783	.0000
35	.0078	.0004	.0000	.0000	.1536
36	.0285	.0025	.0000	.0000	.0000
37	.0008	.0078	.0541	.0000	.0000
38	.0000	.0000	.0000	.0000	.0281
39	.0533	.0107	.0000	.0000	.0000
40	.0000	.0169	.0000	.0000	.0698
$\bar{x}$	.0141	.0176	.0197	.0239	.0112

(continued)

field #	specimen 6	specimen 7	specimen 8	specimen 9	specimen 10
1	.0000	.1313	.0000	.0000	.0000
2	.0194	.1936	.0000	.0821	.0000
3	.0223	.0000	.0000	.0000	.0314
4	.0103	.0000	.0599	.0169	.0000
5	.0000	.0103	.0000	.0128	.0095
6	.0012	.0182	.0000	.0974	.0000
7	.0000	.0095	.0000	.0000	.0000
8	.0623	.0000	.0000	.0314	.0000
9	.2642	.0000	.1094	.0000	.0487
10	.0000	.0000	.0000	.0000	.0677
11	.0120	.0000	.0000	.2126	.0000
12	.0640	.0000	.0000	.0000	.0384
13	.0095	.0128	.0883	.0000	.0000
14	.0182	.0153	.0000	.0000	.0000
15	.0735	.0000	.0000	.0268	.0000
16	.0000	.1329	.0268	.0318	.0305
17	.0095	.0000	.0000	.0000	.0000
18	.0000	.0000	.0000	.0417	.0000
19	.0000	.0330	.1065	.0000	.0000
20	.0293	.0000	.0000	.0925	.0256
21	.5507	.0239	.0000	.0114	.0000
22	.0351	.0438	.0000	.0801	.0223
23	.1135	.0000	.0000	.0000	.0000
24	.0000	.0000	.0000	.0305	.0149
25	.0202	.0000	.0000	.0000	.0475
26	.0000	.0000	.0355	.0000	.0000
27	.1300	.0223	.0000	.1907	.2056
28	.0000	.0000	.0000	.0442	.0000
29	.0343	.0632	.0330	.0000	.0000
30	.0107	.0000	.0000	.0000	.0739
31	.0000	.0000	.0000	.0000	.6204
32	.0000	.0000	.0087	.1825	.0000
33	.0000	.0000	.0949	.0706	.0000
34	.0000	.0244	.0165	.0223	.0000
35	.0000	.0442	.0326	.0000	.0516
36	.0000	.0000	.0071	.0326	.0000
37	.0293	.1606	.0000	.0000	.0000
38	.0285	.0000	.0194	.0000	.1189
39	.0000	.0480	.0000	.0000	.0107
40	.0000	.0000	.0553	.0710	.0000
$\bar{x}$	.0390	.0247	.0189	.0345	.0354

Table 3-3 Area fractions of oxide inclusions in the first ten M2-C88 specimens

field #	specimen 1	specimen 2	specimen 3	specimen 4	specimen 5
1	.0000	.0000	.0000	.0000	.0000
2	.0000	.0000	.0000	.0000	.0000
3	.0000	.0000	.0000	.0000	.0000
4	.0000	.0000	.0000	.0000	.0000
5	.0000	.0000	.0000	.0000	.0000
6	.0000	.0000	.0000	.0000	.0000
7	.0000	.0000	.0000	.0000	.0000
8	.0000	.0582	.0000	.0000	.0000
9	.0000	.0000	.0000	.0000	.0000
10	.0000	.0000	.0000	.0000	.0000
11	.0000	.0000	.0000	.0000	.0000
12	.0000	.0000	.0000	.0000	.0000
13	.0000	.0000	.0000	.0000	.0000
14	.0000	.0000	.0000	.0000	.0000
15	.0000	.0000	.0000	.0000	.0000
16	.0000	.0000	.0000	.0000	.0000
17	.0285	.0000	.0000	.0000	.0000
18	.0000	.0000	.0000	.0000	.0000
19	.0000	.0000	.0000	.0000	.0227
20	.0000	.0000	.0000	.0000	.0000
21	.0000	.0000	.0000	.0000	.0000
22	.0000	.0000	.0995	.0000	.0000
23	.0000	.0000	.0801	.0000	.0000
24	.0000	.0000	.0000	.0000	.0000
25	.0000	.0000	.0000	.0000	.0000
26	.0000	.0000	.0000	.0000	.0000
27	.0000	.0000	.0000	.0000	.0000
28	.0000	.0000	.0000	.0000	.0000
29	.1752	.0000	.0000	.0000	.0194
30	.0000	.0000	.0000	.0000	.0000
31	.0000	.0000	.0000	.0000	.0000
32	.0000	.0561	.1511	.0000	.0000

(continued)

field #	specimen 1	specimen 2	specimen 3	specimen 4	specimen 5
33	.0000	.0000	.0000	.0000	.0066
34	.0078	.0000	.0000	.0066	.0000
35	.0000	.0000	.0000	.0000	.0000
36	.0000	.0000	.0000	.0000	.0000
37	.0000	.0000	.0000	.0000	.0000
38	.0000	.0000	.0000	.0000	.0000
39	.0000	.0409	.0000	.0000	.0000
40	.0000	.0000	.0000	.0000	.0000
41	.0000	.0409	.0000	.0000	.0000
42	.0000	.0000	.0000	.0000	.0000
43	.0000	.0000	.0000	.0499	.0000
44	.0000	.0000	.0000	.0000	.0000
45	.0000	.0000	.0000	.0000	.0000
46	.0000	.0000	.0000	.0000	.0000
47	.0000	.0000	.0000	.0000	.0000
48	.0000	.0000	.0000	.0000	.0000
49	.0000	.0000	.0000	.0000	.0603
50	.0000	.0000	.0000	.0000	.0000
$\bar{x}$	.0041	.0039	.0068	.0011	.0022

(continued)

field #	specimen 6	specimen 7	specimen 8	specimen 9	specimen 10
1	.0000	.0000	.1601	.0000	.0000
2	.0000	.0000	.0000	.0000	.0561
3	.0000	.0396	.0000	.0000	.0000
4	.0000	.0206	.0000	.0000	.0000
5	.0000	.0000	.0000	.0000	.0000
6	.0000	.0000	.0000	.0000	.0000
7	.0000	.0000	.0000	.0000	.0000
8	.0000	.0000	.0000	.0000	.0000
9	.0000	.0000	.0000	.0000	.0363
10	.0000	.0173	.0000	.0000	.0000
11	.0000	.0000	.0000	.0000	.0000
12	.0000	.0000	.0000	.0000	.0000
13	.0000	.0000	.0000	.0000	.0000
14	.0000	.0000	.0000	.0000	.0000
15	.0000	.0157	.0000	.0000	.0074
16	.0000	.0000	.0000	.0000	.0000
17	.0000	.0202	.0000	.0000	.0000
18	.0000	.0000	.0000	.0000	.0000
19	.0000	.0000	.0000	.0000	.0000
20	.0000	.0000	.0000	.0000	.0000
21	.0000	.0000	.0000	.0285	.0000
22	.0000	.0000	.0000	.0000	.0000
23	.0000	.0000	.0000	.0000	.0000
24	.0000	.0000	.0000	.0000	.0000
25	.0000	.0000	.0000	.0000	.0000
26	.0000	.0000	.0000	.0000	.0000
27	.0000	.0000	.0000	.0000	.0000
28	.0000	.0000	.0000	.0000	.0000
29	.1540	.0000	.0000	.0000	.0000
30	.0000	.0000	.0000	.0000	.0000
31	.0000	.0000	.0301	.1139	.0000
32	.0000	.0000	.0000	.0000	.0000

(continued)

field #	specimen 6	specimen 7	specimen 8	specimen 9	specimen 10
33	.0000	.0000	.0000	.0000	.0000
34	.0000	.0000	.0000	.0000	.0000
35	.0813	.0000	.0000	.0000	.0000
36	.0000	.0190	.0000	.0140	.0000
37	.0000	.0000	.0078	.0000	.0000
38	.0000	.0000	.0000	.0000	.0000
39	.0000	.0000	.0000	.0000	.0000
40	.0376	.0000	.0000	.0000	.0000
41	.0000	.0000	.0000	.0000	.0000
42	.0000	.0000	.0157	.0000	.0000
43	.0000	.0000	.0000	.0000	.0000
44	.0000	.0000	.0000	.0000	.0000
45	.0000	.0314	.0000	.0000	.0000
46	.0000	.0000	.0000	.0000	.0000
47	.0000	.0000	.0000	.0000	.0285
48	.0000	.0000	.0000	.0198	.0000
49	.0000	.0000	.0000	.0227	.0000
50	.0000	.0000	.0000	.0000	.0000
$\bar{x}$	.0054	.0021	.0043	.0040	.0026

Table 3-4. Oxide volume fractions of fifty M1-I79 specimens

I.D #	Vol.%	I.D #	Vol.%	I.D #	Vol.%	I.D #	Vol.%
1	.0141	14	.0139	27	.0164	40	.0107
2	.0176	15	.0240	28	.0150	41	.0378
3	.0197	16	.0106	29	.0161	42	.0136
4	.0239	17	.0115	30	.0330	43	.0177
5	.0112	18	.0407	31	.0154	44	.0201
6	.0390	19	.0028	32	.0188	45	.0181
7	.0247	20	.0376	33	.0316	46	.0234
8	.0189	21	.0156	34	.0189	47	.0191
9	.0345	22	.0203	35	.0341	48	.0153
10	.0354	23	.0042	36	.0032	49	.0316
11	.0330	24	.0087	37	.0075	50	.0465
12	.0123	25	.0114	38	.0174		
13	.0218	26	.0027	39	.0459		

Table 3-5 Oxide volume fractions of thirty M2-C88 specimens

I.D #	Vol.%	I.D #	Vol.%	I.D #	Vol.%	I.D #	Vol.%
1	.0041	9	.0040	17	.0026	25	.0035
2	.0039	10	.0026	18	.0087	26	.0088
3	.0068	11	.0070	19	.0119	27	.0034
4	.0011	12	.0076	20	.0058	28	.0048
5	.0022	13	.0044	21	.0010	29	.0067
6	.0054	14	.0064	22	.0040	30	.0052
7	.0021	15	.0102	23	.0000		
8	.0043	16	.0049	24	.0020		

Table 3-6 Oxide volume fractions of the M1-I90B, M1-I90C, M2-C90 and M3-C90 specimens

I.D #	M1-I90B Vol.%	M1-I90C Vol.%	M3-C90 Vol.%	M2-C90 Vol.%
1	.0049	.0041	.0013	.0032
2	.0040	.0045	.0030	.0038
3	.0006	.0048	.0064	.0003
4	.0049	.0179	.0032	.0039
5	.0043	.0213	.0069	.0026
6	.0115	.0097	.0160	.0023
7	.0064	.0060	.0031	.0052
8	.0103	.0164	.0180	.0041
9	.0041	.0022	.0105	.0038
10	.0059	.0110	.0049	.0082
11	.0031	.0154	.0066	.0054
12	.0034	.0213	.0118	.0076
13	.0073	.0137	.0141	.0051
14	.0084	.0197	.0079	.0041
15	.0052	.0081	.0034	.0081
16	.0077	.0118	.0123	.0020
17	.0025	.0092	.0090	.0030
18	.0090	.0086	.0073	.0037
19	.0030	.0118	.0074	.0025
20	.0009	.0092	.0053	.0022

3.1.3 Length measurements of oxide stringers

Finally, the length measurements of oxide stringers in the steels are given in Table 3.7.

Table 3-7 Lengths of oxide stringers in the specimens

I.D #	$L_{CF\&I-79}$, µm	$L_{CF\&I-90B}$, µm	$L_{CF\&I-90C}$, µm	$L_{beth-90}$, µm	$L_{rodan-90}$, µm
1	0	0	0	0	0
2	0	4950	0	0	0
3	1875	0	0	0	0
4	0	0	0	0	0
5	925	0	970	0	0
6	0	0	0	205	100
7	0	0	0	0	0
8	0	0	0	0	0
9	350	0	0	0	0
10	0	0	0	0	0
11	450	0	0	0	0
12	0	0	160	0	125
13	0	0	1084	150	0
14	150	0	0	0	0
15	0	0	0	0	0
16	2500	0	175	0	0
17	0	1722	0	0	125
18	1350	125	0	0	0
19	0	0	0	0	0
20	2650	0	787	0	0

<u>Chapter 4</u>

ANALYSIS AND DISCUSSION I

4.1 Population characteristics of oxide inclusions

4.1.1 Estimation of population characteristics

By the means of statistical analysis unknown population characteristics of oxide inclusions can be inferred from a statistical sample, which is composed of information about an oxide inclusion population.

From the data presented in Tables 3.2-3.6, means $\bar{x}$ and standard deviations s of the samples are calculated by the equations:

$$\bar{x} = \frac{1}{n}\sum_{i=1}^{n} x_i \qquad (4\text{-}1)$$

$$s = \sqrt{\frac{1}{n-1}\sum_{i=1}^{n}(x_i-\bar{x})^2} \qquad (4\text{-}2)$$

where x_i is the ith specimen measurement, and n the number of specimens. If a population of nonmetallic inclusions conforms to a normal distribution, the mean μ of the population can be estimated using the t-distribution, and the variances σ, representing the spread of the sample mean about μ, can be estimated using the χ^2-distribution [120].

$$\bar{x}-t_{\alpha/2,n-1}*\frac{s}{\sqrt{n}}<\mu<\bar{x}+t_{\alpha/2,n-1}*\frac{s}{\sqrt{n}} \qquad (4\text{-}3)$$

in which, $t_{\alpha/2,n-1}$ is the upper 100(α/2) percentile point of a *t*-distribution, and *n* the number of degrees of freedom, which corresponds to the sample size.

$$\frac{(n-1)\,s^2}{\chi^2_{\alpha/2,n-1}}<\sigma^2<\frac{(n-1)\,s^2}{\chi^2_{1-\alpha/2,n-1}} \qquad (4\text{-}4)$$

in which $\chi^2_{\alpha/2,n-1}$ and $\chi^2_{1-\alpha/2,n-1}$ are the upper 100(α/2) percentile point and the lower 100(1-α/2) percentile point of a χ^2-distribution, respectively. But if *n* in a χ^2-distribution is greater than 30, the values of χ^2 are estimated instead by

$$\chi^2=n\,(1-\frac{2}{9n}+z_\alpha\sqrt{\frac{2}{9n}}\,)^3 \qquad (4\text{-}5)$$

in which z_α is obtainable from the Standard Normal Distribution included in Appendix 3. [121]

As a result, the means and variances of oxide inclusion populations of the rail steels as well as the means and variances of the samples are presented in Table 4-1. The results assert with 95% confidence that volume fractions of oxide inclusions in the rail steels must be within the intervals defined by their own 95% C.I.

Table 4-1 Statistical characteristics of oxide inclusion distribution in the steels

steel	s	σ (95% C.I)	$\bar{x}$	μ (95% C.I)
M1-I79	0.011	0.009 - 0.013	0.021	0.018 - 0.026
M1-I90B	0.0029	0.0022-0.0042	0.0054	0.0038-0.0070
M1-I90C	0.0057	0.0043-0.0083	0.0113	0.0082-0.0145
M2-C88	0.003	0.002-0.004	0.005	0.003-0.005
M2-C90	0.0020	0.0015-0.0029	0.0039	0.0029-0.0051
M3-C90	0.0079	0.0060-0.0110	0.0045	0.0054-0.0104

4.1.2 The statistical distribution of oxide inclusions

It has been presumed that the population characteristics of nonmetallic inclusions in steel, such as the content and the size, would always conform to a normal distribution. Procedures of determining the population characteristics of nonmetallic inclusions has been established on the basis of this presumption. A measurement of nonmetallic inclusions is carried out on each field of view selected, and a statistical analysis of population characteristics is based on the field-to-field variability of measurements. [122] For a long time very few people except G. Moore [105] have ever questioned this presumption, and actually most practices in assessment of nonmetallic inclusions in steel still were carried on using such procedures. The omission of whether the presumption is always sound and true and whether a practicing procedure is proper for determining the population characteristics is probably due to the lack of a large enough database. The database of oxide inclusion established by the present work makes it possible to question the presumption and review practicing procedures.

The two thousand field measurements of oxide inclusions in M1-I79 steel are all plotted in Figure 4.1. The volume fractions of oxide inclusions vary from 0 to 0.968. Since three quarters of the 2000 field measurements are zero, the distribution of the 2000 field measurements about their mean is highly skewed toward the left extreme, exhibiting the mode of a log-normal distribution (Figure 4.2). Obviously such a distribution does not conform to a normal distribution. The highly skewed distribution signifies that the average of the 2000 field measurements does not represent the statistical mean of the 2000 volume fractions so the 2000 points do not converge to this average. The lack of conformity to a normal distribution makes the population characteristics of oxide inclusions indeterminable. If a conventional practicing procedure based on a normal distribution had been arbitrarily applied to determining oxide population characteristics, the results would have been misleading. The same problem was addressed in Moore's work. [105] To eliminate this problem and perform a sound statistical analysis, Moore's practice was to group field measurements into a number of sets consisting of 30 $\sim$ 100 sequential field measurements. Alternatively, the present work regarded a specimen as the measurement unit, and thus considered a specimen measurement

—— the average of 40-50 field measurements —— to be one contribution. As a result of this practice, volume fractions of the specimens randomly fluctuate about their means (Figures 4.3 ~ 4.8) and statistical distributions of oxide inclusions in the rail steels complied with normal distributions as shown by the cases of M1-I79 and M2-C88 steels (Figure 4.9 and Figure 4.10). Therefore, as long as enough specimens were surveyed for each steel and thus enough volume fractions measured, the volume fractions would statistically converge to their mean. The population characteristics of oxide inclusions can be evaluated according to normal distributions of inclusion populations.

The present experimental evidence has called conventional procedures into question. Conventional procedures are statistically correct only if the content of nonmetallic inclusions is so large that at a certain magnification every field measurement can yield a nonzero volume fraction. However, provided that an inclusion measurement is restricted to sporadic oxides or that a steel contains a slight amount of nonmetallic inclusions, conventional procedures based on the presumption are not applicable because a distribution of individual field measurements need not be a normal distribution. Under the circumstances a correct approach is to group field measurements or to regard a specimen as the measurement unit.

4.1.3 Average lengths of oxide stringers

The congregation of oxide inclusions was indicated by lengths of oxide stringers. From surveying 20 specimens, the average length of oxide stringers in each steel was used as an indicator of the congregation. This characteristic number is calculated through equation 4-6:

$$\overline{L} = \frac{1}{n}\sum_{i=1}^{n} L_i \qquad (4\text{-}6)$$

in which n is equal to 20, the total of examined specimens; and L_i the total length of oxide stringers in the I standard specimen. The average lengths of the rail steels are shown in Figure 4.11.

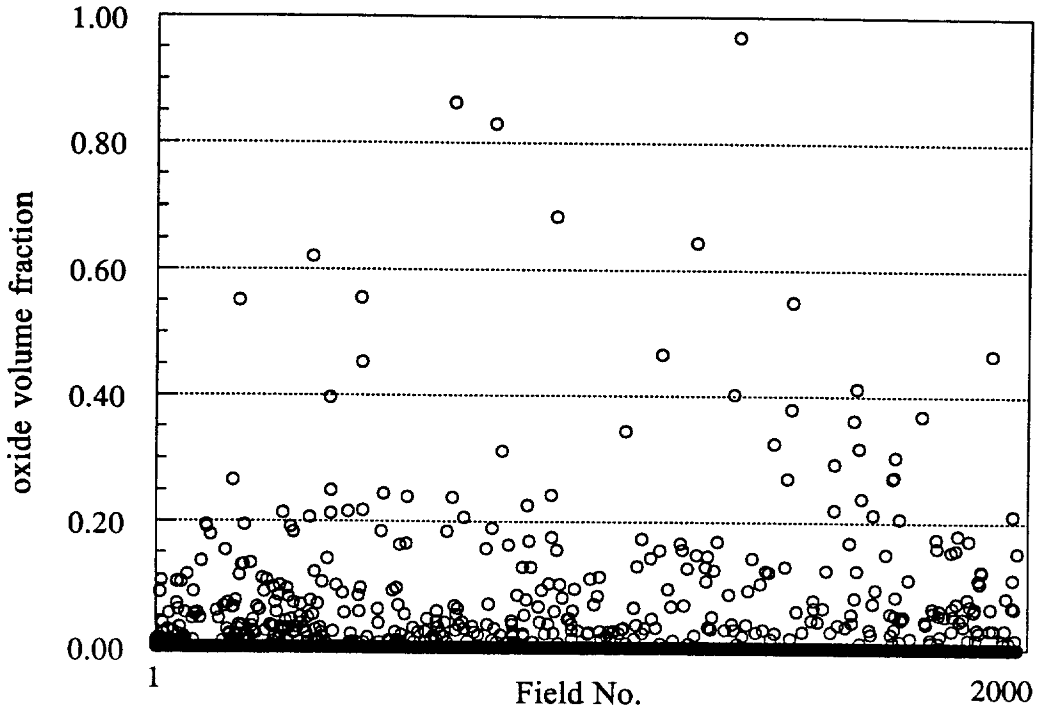

Figure 4.1a 2000 field measurements of oxide inclusions in M1-I79 steel

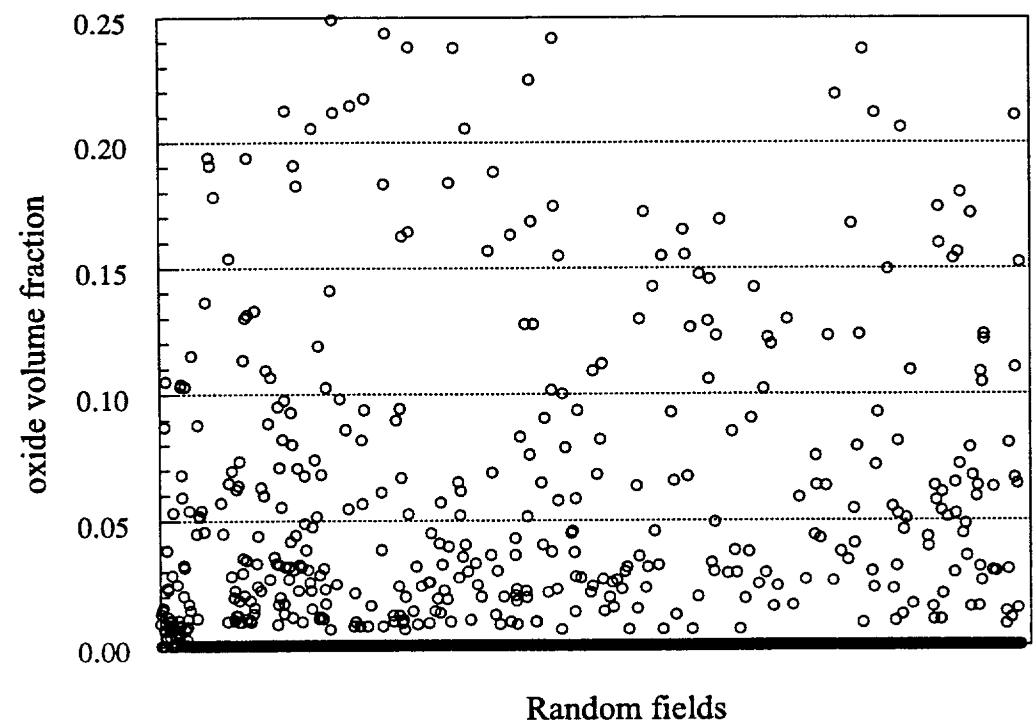

Figure 4.1b Most of the 2000 field measurements are distributed between 0 and 0.25.

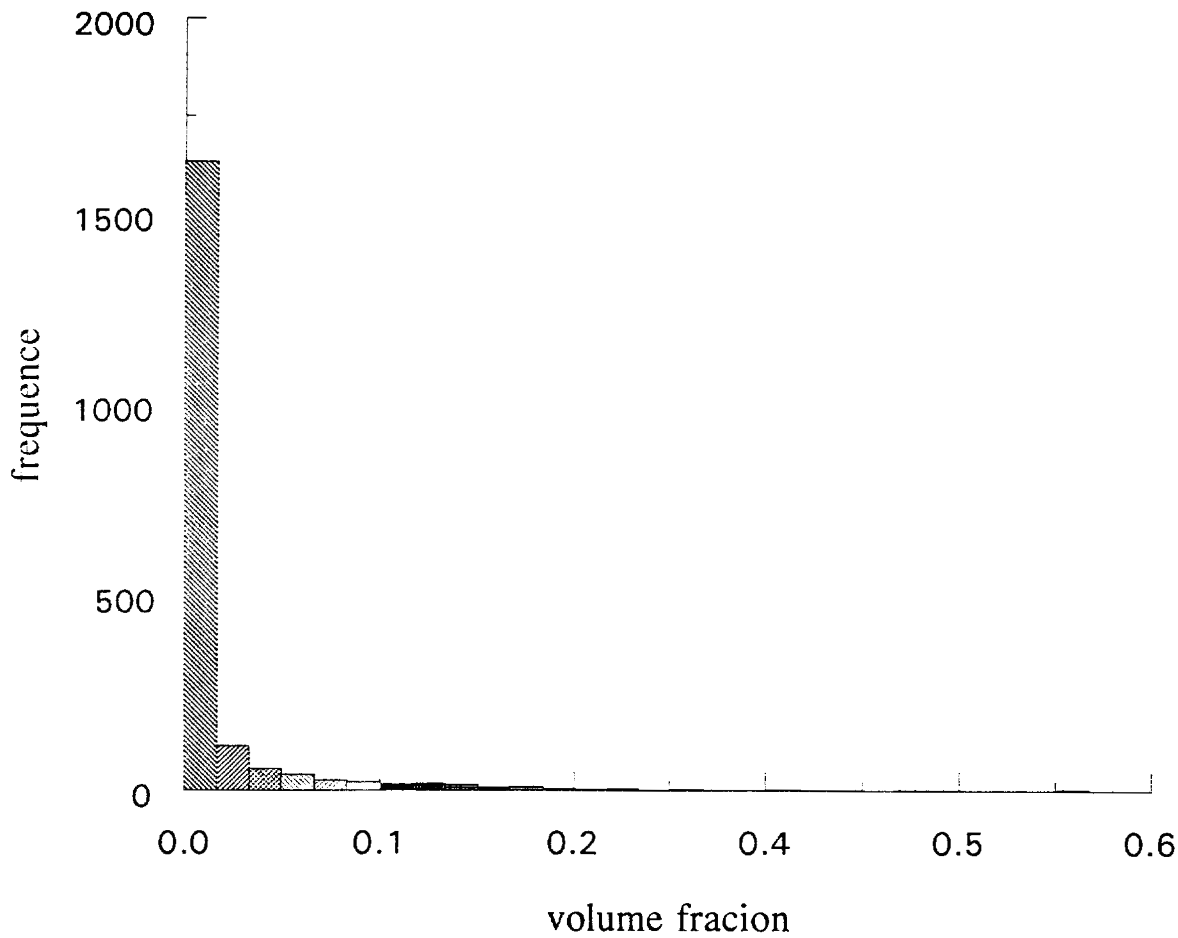

Figure 4.2 2000 field measurements of oxide inclusions were skewed toward zero.

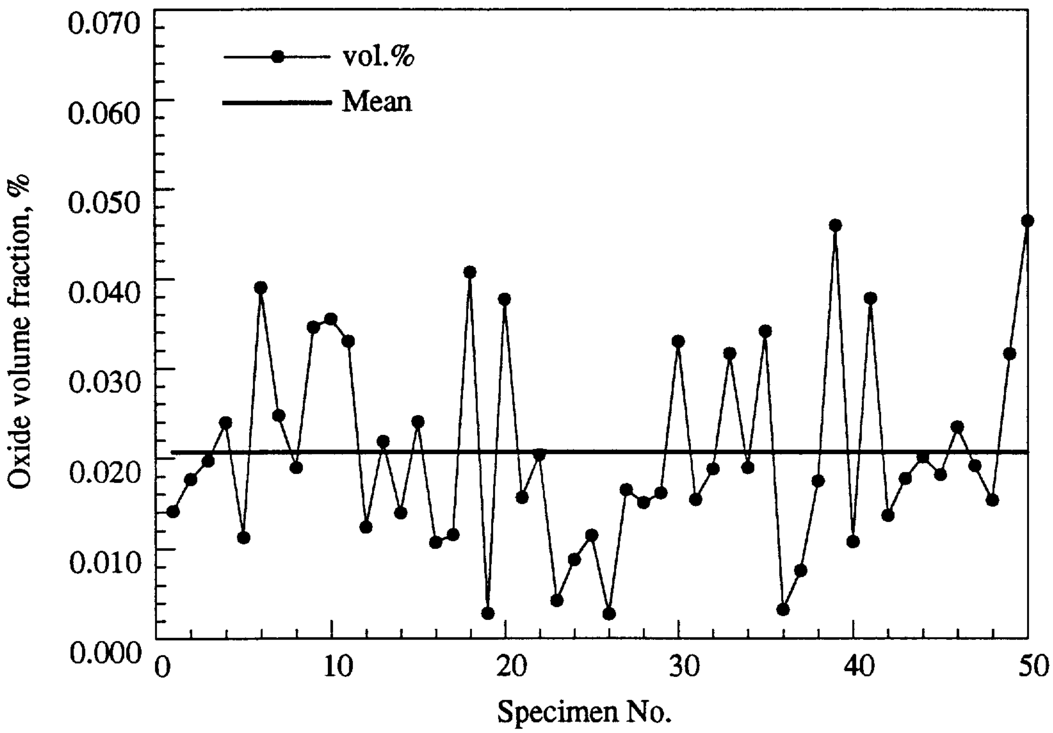

Figure 4.3 Oxide volume fractions of the M1-I79 specimens fluctuate about their mean.

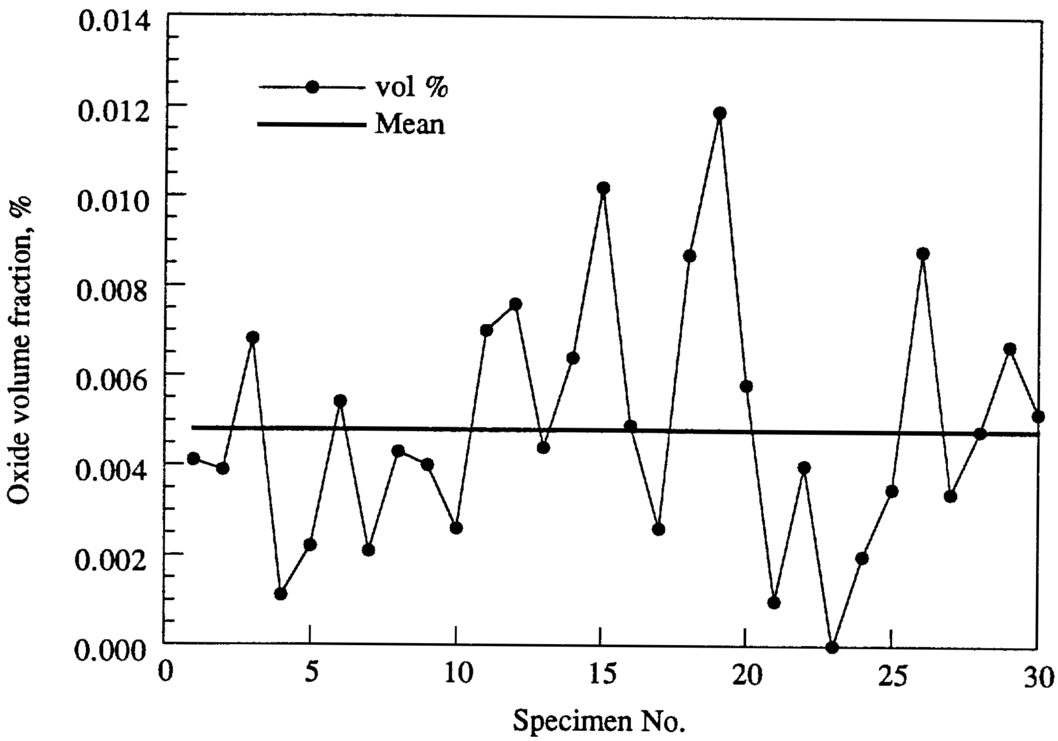

Figure 4.4 Oxide volume fractions of the M2-C88 specimens fluctuate about their mean.

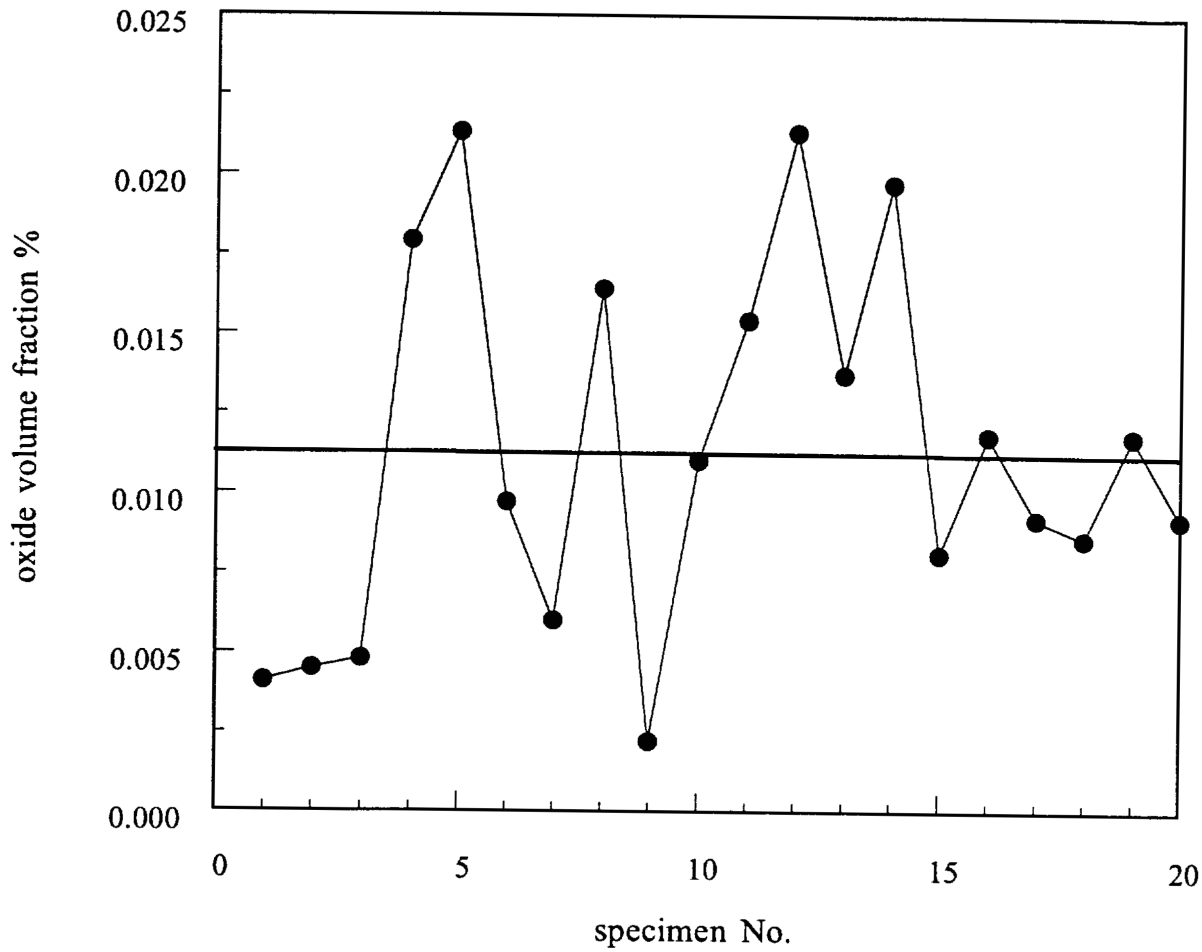

Figure 4.5 Distribution of oxide volume fractions of the M1-I90B specimens.

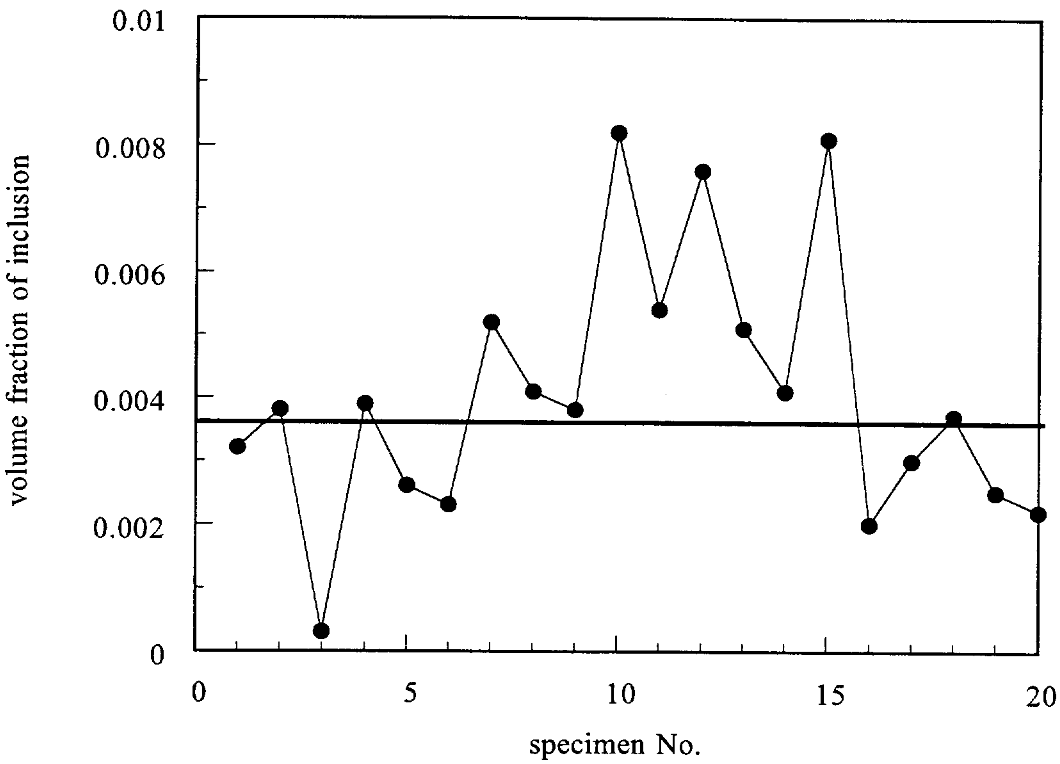

Figure 4.6 Distribution of oxide volume fractions of the M1-I90C specimens.

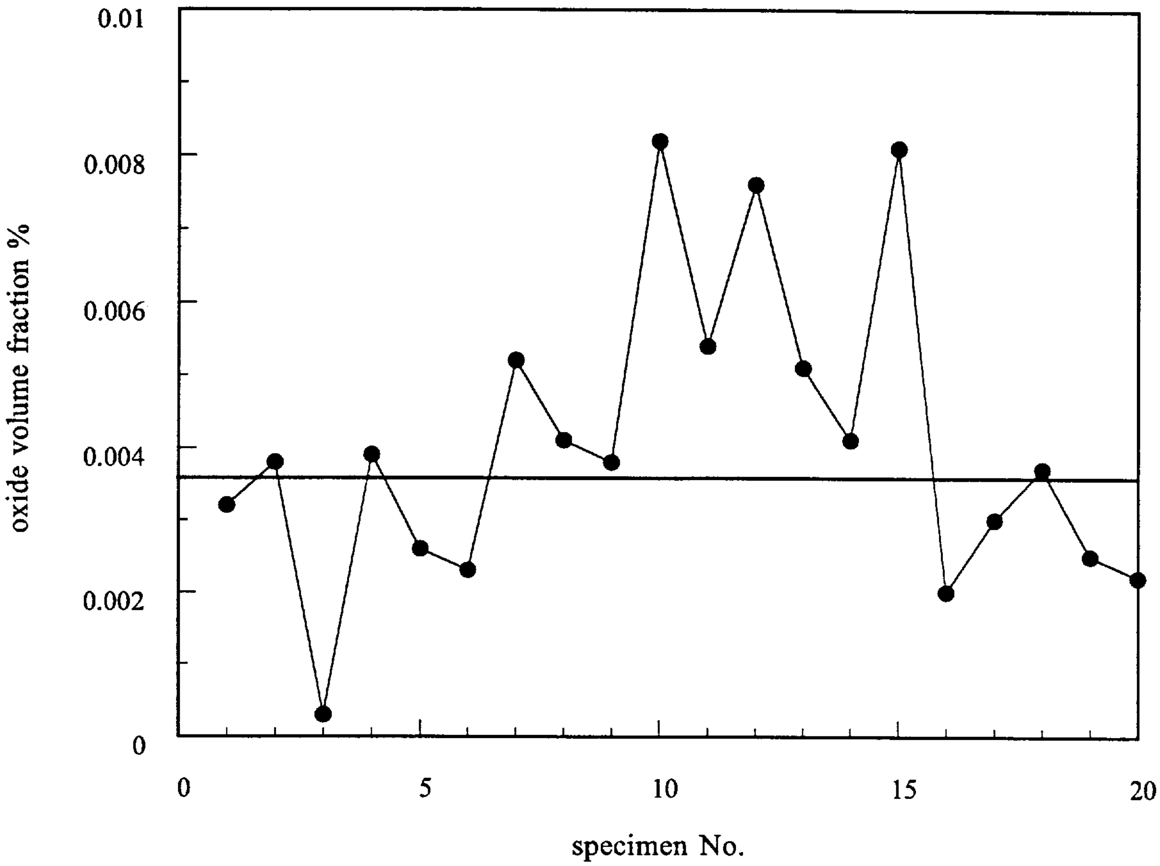

Figure 4.7 Distribution of oxide volume fractions of the M2-C90 specimens.

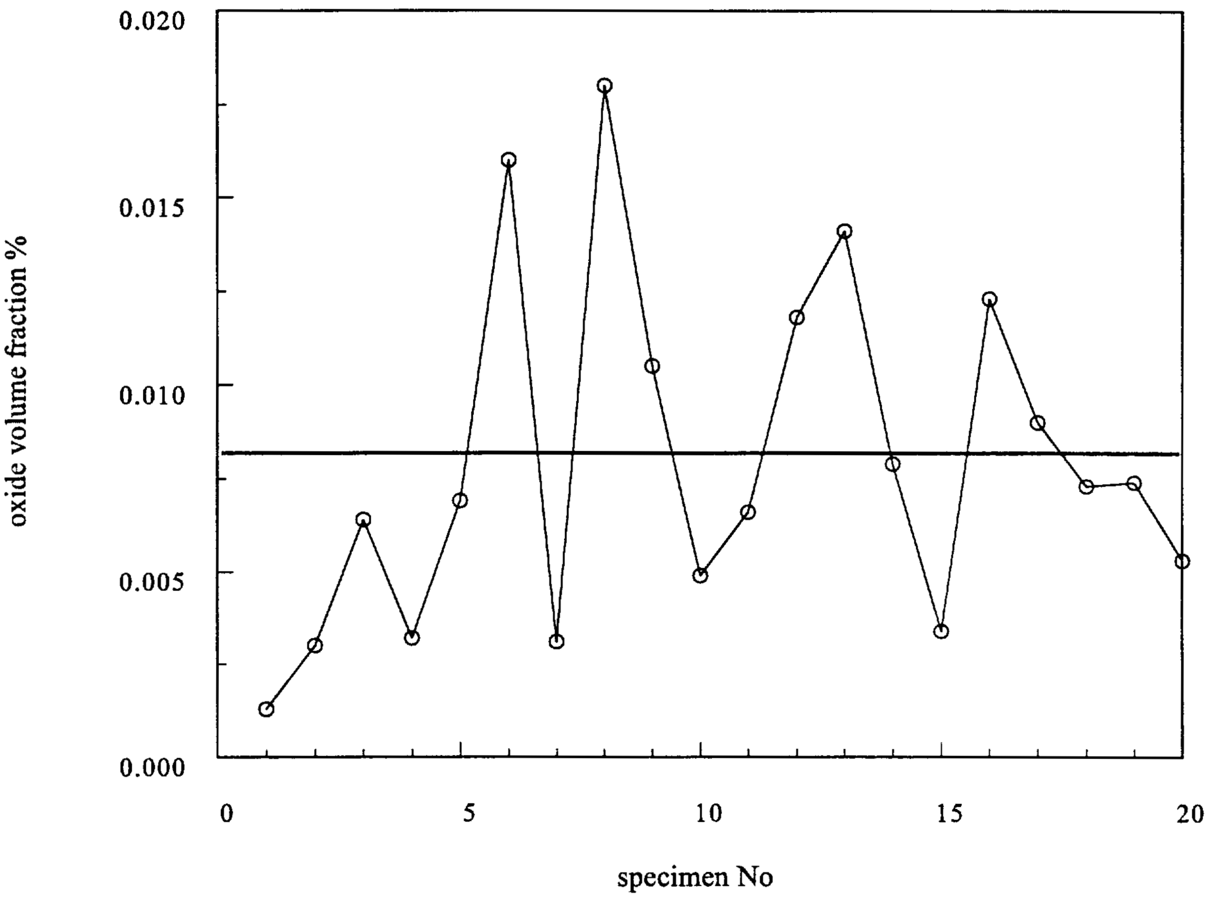

Figure 4.8 Distribution of oxide volume fractions of the M3-C90 specimens.

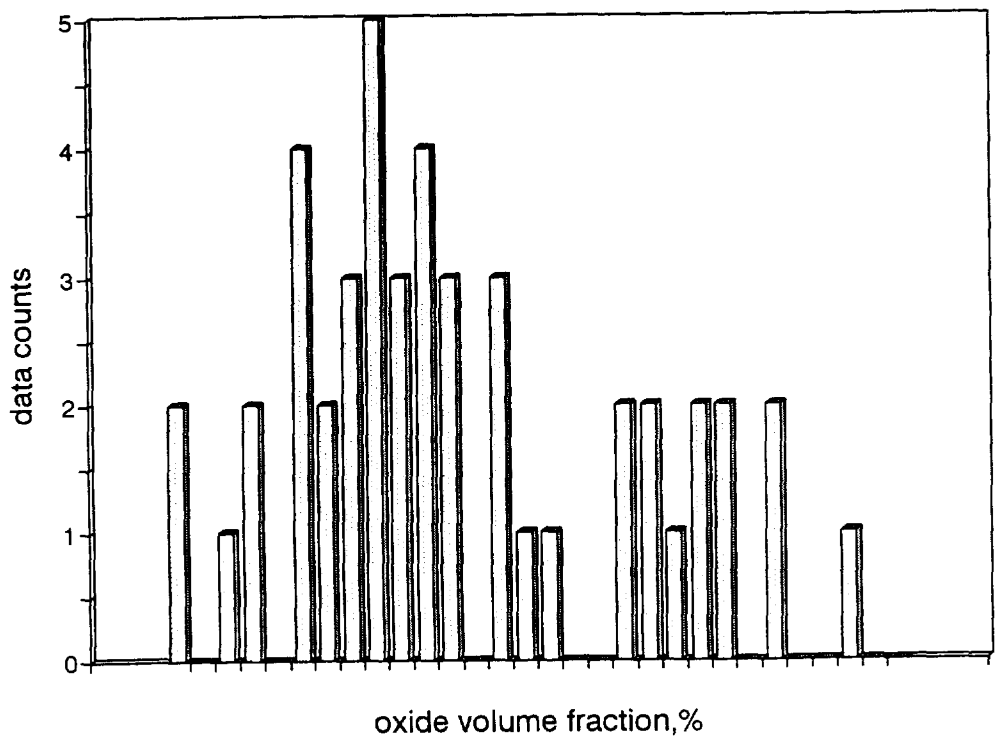

Figure 4.9 Approximate normal distribution of oxide volume fractions of M1-I79 steel.

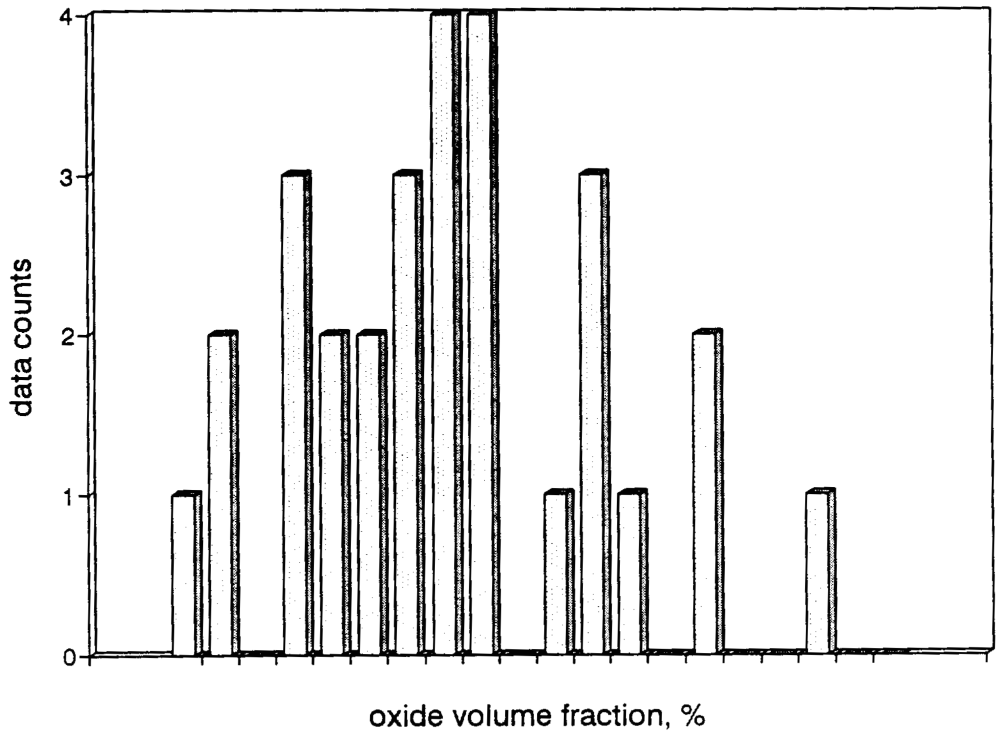

Figure 4.10 Approximate normal distribution of oxide volume fractions of M2-C88 steel.

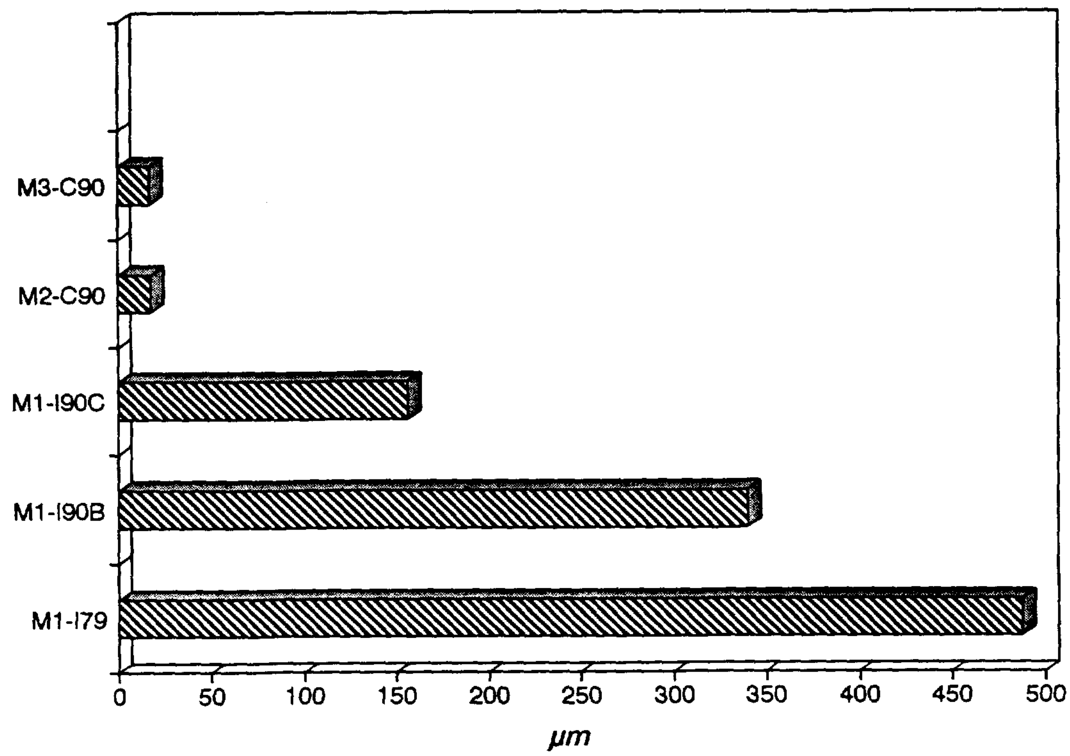

Figure 4.11 Average length of stringers.

4.2 The significance and statistical nature of rail cleanliness

The oxide volume fractions of the four FAST steels, M1-I90B, M2-I90C, M2-C90 and M3-C90, varied widely from specimen to specimen. Even the variation of the volume fractions between the M1-I90B and M1-I90C rails, which were made from the different parts of a single heat, was as high as a factor of two. The stringer lengths of M1-I90B and M1-I90C rail steels are even more variable with many specimens containing no stringers while others contained stringers of total lengths measured in micrometers. One observation that stands out is that the M2-C90 and M3-C90 rails exhibit very low stringer tendencies. In the FAST experiment the fatigue performance of the M2-C90 rails was superior to the M1-I90 rails by a considerable margin.[48] Although the FAST experiments were only conducted over a 178 MGT period, the evidence clearly shows the benefits to be derived from modern rail manufacturing practices. In view of the great difference in stringer length of the two steels, it is considered reasonable to suggest that modern rails should be fully evaluated in the field before any further moves are made to tighten the specification of inclusion contents any further. In the same field experiment the M1-I90C rails were significantly better than the M1-I90B rails. From the data in Table 4-1 and Figure 4.2 it is tempting to conclude that only the stringer lengths are significant in this regard. Furthermore, since the M3-C90 rails suffered the highest shell defect rate of the four steels (attributed to high gauge corner contact stresses caused by the mismatch of wheel and rail profiles) with so few stringers it is not yet possible to say that individual oxides cannot play a role in initiating subsurface fatigue defects. There are two possibilities: either shells can be formed with high enough contact stresses without oxide assistance as claimed by some workers [123] or as the contact stresses increase the critical oxide size for assisting in fatigue initiation is reduced to that of individual oxide inclusions.

The distributions of the volume fractions of both fields and specimens corresponded to variations of the oxide content along the longitudinal direction of rail because the specimens were taken end to end from the rails. Obviously, sampling from a single location in rail cannot represent the statistical characteristics of oxide contents in a full rail. In order to represent the characteristics of inclusion populations, specimens must be taken from different locations and the assessment must be done by means of statistical analysis.

There is also the evidence that the volume fractions vary significantly over very small distances in a vertical sense. The influence of both different depth locations in the same specimens and the different operators on the results are presented in Table 4-3. When the two operators made measurements on exactly the same polished face, the results were almost identical. However, when the specimen surface was reground and repolished —— a practice that involved the removal of a few thousands of an inch, the results could vary by up to a factor of two. This experimental evidence confirmed that sampling locations influenced the result of cleanliness assessment. The variations of the oxide content in both the longitudinal and the vertical directions strongly suggest that specimens for a good estimation of the content must come from different locations. These findings exhibit the statistical nature of rail cleanliness.

Table 4-3 Oxide volume fractions in the four specimens of M1-I79 steel

	specimen 20	specimen 21	specimen 22	specimen 23	remark
vol. %	0.009	0.012	0.015	0.020	prepared and counted by operator A
	0.011	0.026	0.022	0.040	reprepared and recounted by operator A
	0.014	0.018	0.016	0.024	repolihsed and counted by operator B
	0.016	0.017	0.015	0.026	recounted by operator A following operator B

By the ratings of oxide content, M2-C90 steel was the best whereas M1-I79 steel the worst. The progress the rail manufacturers have made in the last 15 years in reducing the oxide inclusions can also be judged by comparing the oxide contents of M1-I79 steel and M2-C90 steel. The old standard carbon ingot rails contained about 5 times as many oxides as did the modern continuously cast intermediate strength standard carbon rails. It is also evident that the latter process reduces the stringer content by an even greater margin with respect to ingot rail steel.

Because of the distribution characteristics of oxide inclusions in the steels, the assessment of rail cleanliness undoubtedly is a statistical issue; the unknown population characteristics of oxide inclusions are inferred by the means of a statistical sample. The validity of the inferences depends on whether a statistical sample can represent a population from which it is drawn. A good sample must reflect the true characteristics of a population; a sample size has to be small enough to be practical but large enough to represent the characteristics of a population. In fact, to determine an appropriate sample size for cleanliness assessment is to decide how many specimens are required to obtain a specific level of accuracy at a certain confidence level. While the metallographic determination of oxide inclusion levels for rail steels could follow different routes, the number of specimens required to obtain a reasonable, reproducible result is of general concern.

4.3 The size of a statistical sample

For a normal distribution of a single population, a sample size of 4 or 5 specimens is usually adequate to estimate the population statistics. [107] Since the present M1-I79 and M2-C88 samples consisted of as many as 50 specimens and 30 specimens respectively, it is not groundless to assume that the two samples can be regarded, in effect, as the infinitely large populations of the heats of rails they represent. In fact, the randomness with which volume fractions of these specimens was distributed about their means has justified the assumption. The randomness of these specimen measurements can be tested by a randomness test. [124]

$$r_{\frac{N}{2},\frac{1-\alpha}{2}} < R < r_{\frac{N}{2},\frac{\alpha}{2}} \quad (4\text{-}7)$$

where R is the number of runs relative to the sample means. The number of runs for M1-I79 steel and M2-C88 steel are shown in Figures 4.2 and 4.3. From a statistical perspective, the points of the specimen measurements are considered randomly distributed about their mean if the number of the runs meets inequality 4-7. There are a total of 28 runs in Figure 4.2 and 14 runs in Figure 4.3. In Table 4-4 the randomness tests mean that, to a 95% level of confidence, the fluctuations of the specimen measurements are randomly distributed about the sample means. Thus, the distributions of oxide volume fractions are random with respect to longitudinal location; that is, the two samples were already so large that the statistics of the two samples were not restricted to the longitudinal direction and can be regarded as random samples.

Table 4-4 Randomness tests of the specimen estimates of M1-I79 and M2-C88.

Rail steel	No. of specimens, N	$r_{N/2,1-0.05/2}$	r*	$r_{N/2,0.05/2}$
M1-I79	50	18	28	33
M2-C88	30	10	14	21

Note: the values of $r_{N/2,1-\alpha/2}$ and $r_{N/2,\alpha/2}$ are constants given by Ref [124].

To determine the size of a sample is to resolve the minimum number of specimens that are, if selected at random, required to estimate reliably the statistics of a population. Because the population characteristics of oxide inclusions in M1-I79 and M2-C88 steels have already been shown to conform to normal distributions, the sample sizes can be determined using the known statistical parameters of their distributions.

A sample mean $\bar{x}$ is the best unbiased estimator of a population mean μ. The absolute error in estimating μ by $\bar{x}$ is $|\bar{x} - \mu|$. It is desirable to control this absolute error at a certain level so this requirement can be stated as:

$$P(|\bar{x}-\mu|<c)\geq 1-\alpha \tag{4-8}$$

where c and α are prechosen positive constants. It is possible to choose n to meet the condition defined by inequality 4-8. If a population conforms to a normal distribution (μ, σ^2), then a sample from this population must follow such a normal distribution as (μ, σ^2/n) also, where n is the degrees of freedom.[120] According to the characteristics of a normal distribution (μ, σ^2/n), the sample size that is able to meet inequality 4-8 is given by:

$$|\mu-\bar{x}|\leq Z_{\alpha/2}*\frac{\sigma}{\sqrt{n}} \tag{4-9}$$

On assumption that the fifty M1-I79 specimen measurements and thirty M2-C88 specimen measurements can be statistically regarded as the infinitely large populations from which they were drawn, σ and μ on the right side of equation 4-9 can be replaced with s and $\bar{x}$ respectively. Thus,

$$|\mu-\bar{x}|\leq Z_{\alpha/2}*\frac{s}{\sqrt{n}} \tag{4-10}$$

Equation 4-10 is rearranged as:

$$\frac{|\mu-\bar{x}|}{\mu}\leq\frac{Z_{\alpha/2}}{\sqrt{n}}*[\frac{s}{\mu}] \tag{4-11}$$

Clearly, a sample size is a function of the prechosen accuracy (the term on the left of inequality 4-11) for the estimation of the distribution characteristics, μ and σ. Finally, the sample sizes for the M1-I79 and M2-C88 rails are determined by using equation 4-11.

The means and variations of the samples have already been resolved by the experiment and are given in Table 4-1, $s_{M1\text{-}I79} = 0.0111$ and $s_{M2\text{-}C88} = 0.0027$. $z_{\alpha/2}$ is a constant, which is obtained from the Standard Normal Distribution, [121] equal to 1.96 for $\alpha = 0.05$. Therefore, if a relative error ($|\mu - \bar{x}| / \mu$) is set as 25% or 0.25 the number of specimens required for M1-I79 steel is

$$n=[\frac{1.96}{25\%}*\frac{0.0111}{0.0207}]^2\approx 17 \qquad (4\text{-}12)$$

and the number of M2-C88 specimens is required to be

$$n=[\frac{1.96}{25\%}*\frac{0.0027}{0.0048}]^2\approx 20 \qquad (4\text{-}13)$$

The relations between the sample sizes and the preset relative errors are demonstrated in Table 4-5.

Table 4-5 Sample sizes for M1-I79 and M2-C88 steels

relative err.	30%	25%	20%
M1-I79 steel	12	17	27
M2-C88 steel	14	20	(31)

If the relative errors need to be less than 20%, the sample size increases considerably. Meanwhile the results assert with 95% confidence that by taking a sample size of 20 specimens, 95 times out of a 100 this sample can give an estimate of the population mean that is within ± 25% of the true value. Further, M1-I79 steel and M2-C88 steel were produced by the old and current steel making processes, respectively. If the distributions of the oxide contents in the two steels typically represented the characteristics of oxide inclusions in steels made by the two melting and casting processes, the sample sizes given in Table 4-5 are probably applicable to rail steels that are made in the same kind of processes.

The large values of σ suggest that the distribution of oxide inclusions in the rails were so scattered that it is necessary to question the normal practice of determining oxide content with only six specimens.[107] According to the present work and the statistical analysis a sample of six specimens is too small to represent the population characteristics of oxide inclusions in rails, and thus a result derived from such a small sample would be not only incorrect but also misleading. If the computer-aided image analysis is to become a standard method of assessing the cleanliness of rails, then it is apparent that the size of a sample must be more than 6 specimens.

Finally, since several specimens could be selected at random, even for the ingot-made rails, which would have revealed no stringers at all, the same argument could be applied to the counting of stringers.

4.4 Influence of steel making process

Most of the oxide inclusions in the rails resulted from Al deoxidation of liquid steels.

$$2\,[Al] + 3\,[o] \rightarrow (Al_2O_3)$$

In precipitation deoxidation —— a practice in which Al is added on its own as the initial deoxidant, Al_2O_3 inclusions are formed as products of the deoxidation. Some of the Al_2O_3 inclusions are floated out of liquid steel but some are trapped at the dendrites of steel during solidification of the liquid steel. These retained inclusions tend to form Al_2O_3 clusters when they encounter one another. [70] The clusters of Al_2O_3 inclusions are broken apart during the process of rail rolling, resulting in Al_2O_3 stringers aligned to the direction of rail forming. In addition to pure Al_2O_3 stringers, complex oxides such as Al_2O_3-CaO or Al_2O_3-CaO-MgO observed in the rails are also products of Al precipitation deoxidation but formed through inhomogeneous nucleation on exogenous CaO or MgO particles (Figures 4.12 and 4.13).

The content, size, and morphology of oxide inclusions in rail steels are influenced by steel melting, deoxidizing and casting. In particular, oxide inclusions in M1-I79 steel were distinct from those in the other steels by size and morphology. The variances of these characteristic parameters in the rail steels probably were related to the methods of steel making and casting. M1-I79 steel was Al-deoxidized and ingot-cast. As opposed to the deoxidation process of M1-I79 steel, vacuum degassing was applied to deoxidization of the other five steels —— a reaction of forming gaseous carbon monoxide. The fundamental difference between the two deoxidation processes was responsible for differences in size and morphology of oxide inclusions in the rail steels. The pronounced comparison of oxide inclusions in M1-79 steel and M1-I90 steel was a proof of the influence. M1-I90 steel was also ingot-cast but vacuum-degassed. Globular and stringered oxide inclusions were present in both the steels. However, the content of oxide inclusions in M1-I79 steel was higher than that of oxides in M1-I90C steel approximately by factor of two; the average size of oxide inclusions was larger, and oxide stringers were coarser and longer in the former too (Figures 4.14 and 4.15). Owing to vacuum degassing a lower content of oxygen in M2-I90 steel was available for oxide formation when or if alloying elements such as CaSi or Al were added in the ladle so both globular and clustered oxide inclusions were less and smaller, whereas inherently the precipitation deoxidation of M1-I79 steel by Al produced a larger number of Al_2O_3 products. The morphology of oxide stringers in M2-C88, M2-C90 and M3-C90 steels had the same comparison with oxide inclusions in M1-I79 steel. In effect, the types of inclusions were not changed by vacuum degassing, but the content and the size were reduced and the aggregation of inclusions was alleviated. On the other hand, the practice of vacuum deoxidation increased the ladle-holding time of the liquid steels, and the steels treated by vacuum degassing were therefore vulnerable to trapping slag and refractories. The trapped nonmetallic materials were the reason why the vacuum-treated steels still contained complex oxide inclusions such as Al_2O_3-CaO, SiO_2-CaO and Al_2O_3-CaO-MgO.

The comparisons of the size, morphology, and amount of oxide inclusions in the rail steels and no great differences in the chemical compositions of the steels strongly suggested that the steel making methods influenced the types, morphology and size of inclusions more than the chemical compositions of the steels. Although the methods of steel melting, deoxidizing, teeming and casting operations all had a great effect on the formation of inclusions, it was the deoxidation processes that fundamentally controlled the size, morphology and amount of oxide inclusions.

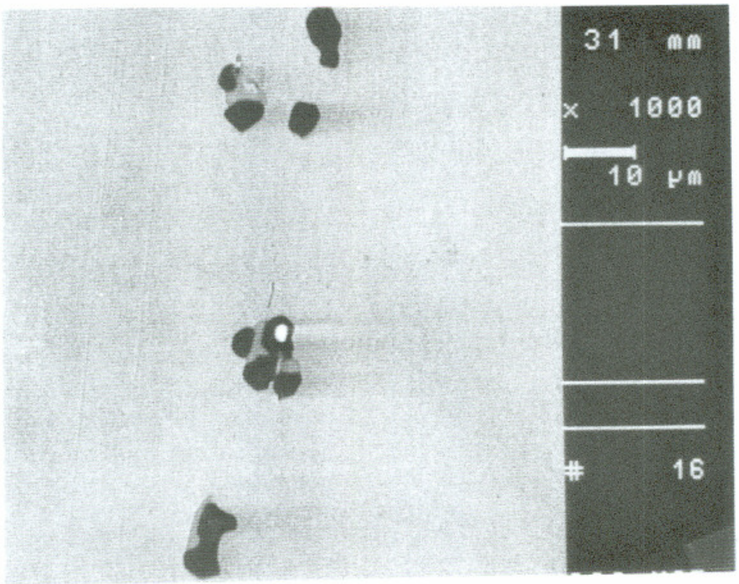

Figure 4.12a Calcium aluminate inclusions in M1-I79 steel

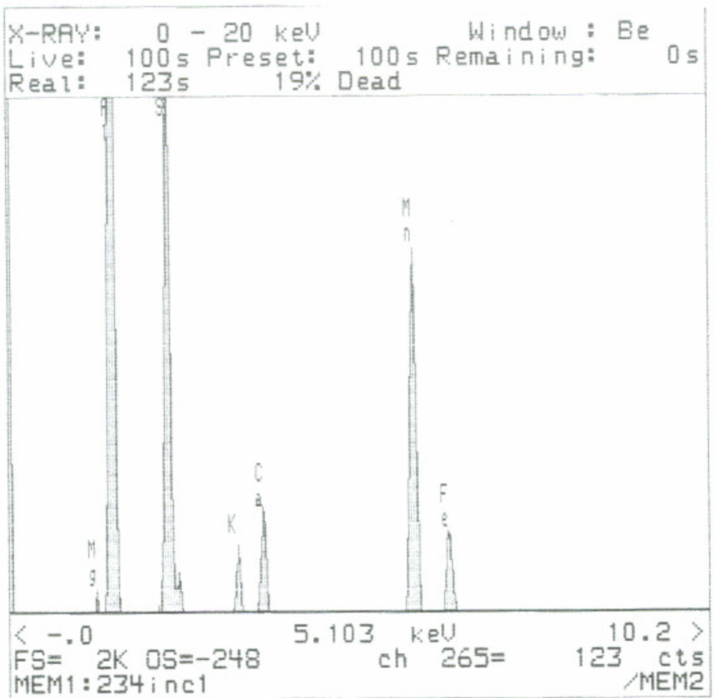

Figure 4.12b EDX analysis spectrum

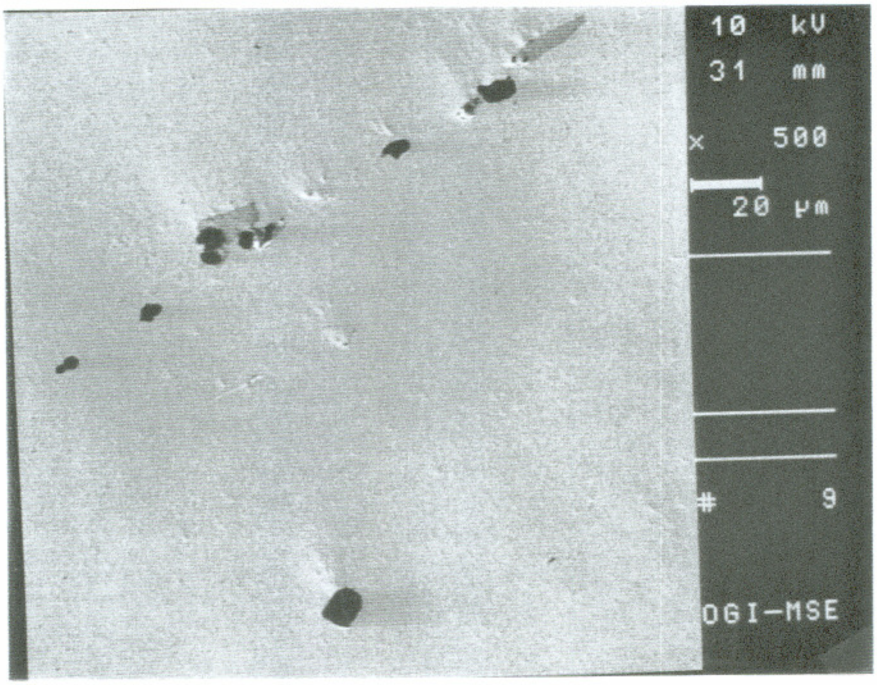

Figure 4.13a Al_2O_3-CaO-MgO compound inclusions in M2-C90 steel

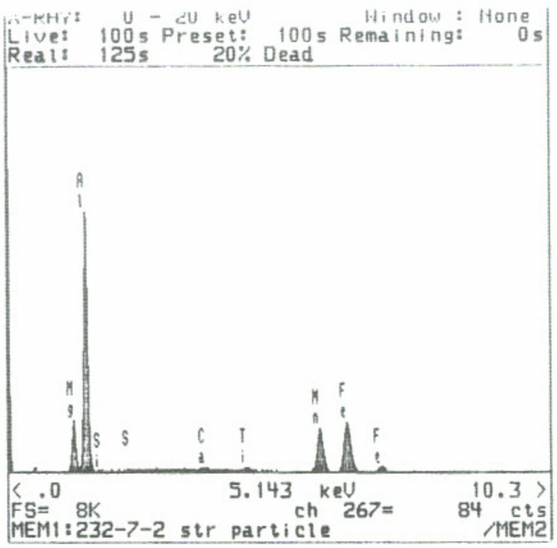

Figure 4.13b EDX analysis spectrum.

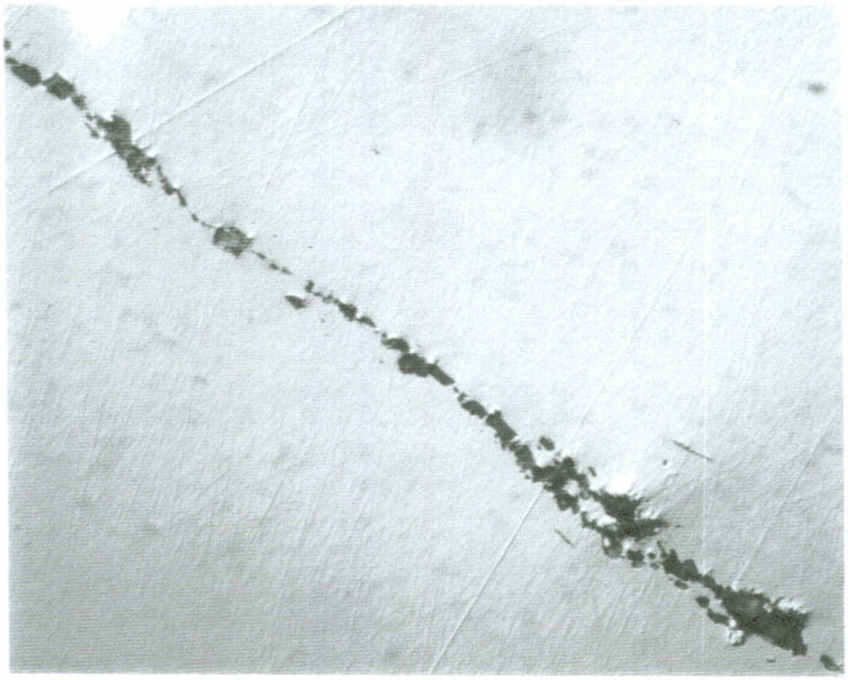

Figure 4.14 A stringer of oxide inclusions in M1-I79 steel. Magnification 200x.

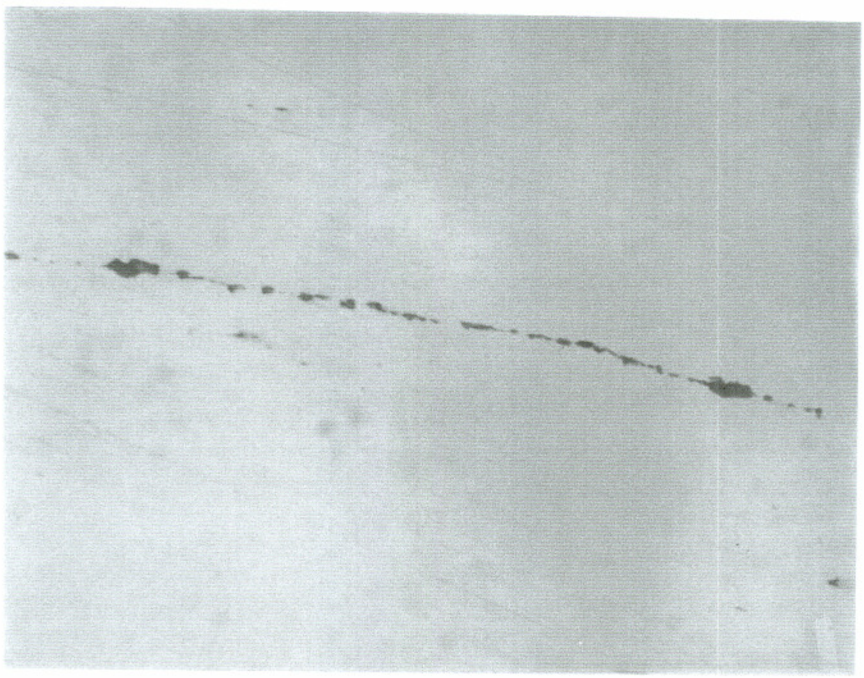

Figure 4.15 A stringer of oxide inclusions in M1-I90 steel. Magnification 200x.

Chapter 5

ANALYSIS AND DISCUSSION II

5.1 Ratings of the rail steels by the incidence of subsurface initiated defects

From the perspective of materials, the propensity to fatigue is related to the number of weak points that are situated in a highly stressed region, such as detrimental nonmetallic inclusions, defective grains, and dislocations. The volume of steel at risk to fatigue is governed by contact load and mechanical properties of the materials. As a highly stressed region increases in volume the number of weak points is multiplied, and the likelihood of fatigue occurrence increases. In effect, the number of weak points is in proportion to the number of material defects. Material defects are randomly distributed, but only those situated, by chance, in the highly stressed subsurface are possibly responsible for the occurrence of subsurface fatigue. No doubt, a subsurface fatigue failure tends to occur selectively at weak points. If a distribution of weak points is known or a distribution of subsurface fatigue defects is known, the propensity of materials to subsurface fatigue can be evaluated accordingly.

Based on the results presented in Table 2-8, the likelihood that subsurface initiated fatigue defects occurred in rail steels was estimated and is given in Table 5-1. The likelihood that fatigue defects could occur in the subsurface subjected to contact stresses is expressed as a probability, θ. Since θ actually represented the chance by which a subsurface crack was located by using the metallographic examination, $1/\theta$ was proportional to the density of subsurface initiated defects in the tested steels. Because the likelihood of subsurface fatigue occurrence is known to be a probability θ, on the average $1/\theta$ trials need to be conducted in order that at least one subsurface crack was observed in the trials. For the purpose of distinctly rating the rail steels in subsurface fatigue, $1/\theta$ is now defined as the return period of a subsurface initiated fatigue defect, $T(x)$. The return periods of the rail steels are given in Table 5-2. The return period of M2-C90 steel indicates that its resistance to subsurface fatigue was superior to that of the other steels; the number of the trials for locating a subsurface crack would be at least 10, or at contact loads of $p_o/k < 7$ the chance for a subsurface crack to occur was virtually zero. In comparison, M1-I79 steel had the highest risk to subsurface fatigue; its shortest return period was 2 trials at $p_o/k = 5.7$. M1-I90B steel was inferior to M2-C90 steel but better than M1-I90C steel by comparison of the return period. This latter conclusion, however, contradicted the result of the FAST experiment that the performance of the M1-I90C rail was superior to that of the M1-I90B rail. Concrete reasons for this contradiction were not clear, but a stochastic behavior of fatigue occurrence probably was one factor.

Table 5-1 Probability (θ) of subsurface crack occurrence at the different contact loads

p_o/k	$\theta_{M3\text{-}C90}$	$\theta_{M2\text{-}C90}$	$\theta_{M1\text{-}I90B}$	$\theta_{M1\text{-}I90C}$	$\theta_{M1\text{-}I79}$
4.0	0.00	0.00	0.00	0.00	0.00
5	///	0.00	0.00	0.1	0.0
5.5	///	0.00	0.1	0.2	0.5
5.7	///	0.00	0.2	0.4	0.6
6	///	0.00	///	///	///
6.5	///	0.00	///	///	///
7.0	///	0.10	///	///	///

Table 5-2 Return period, $T_{(x)}$, of the occurrence of subsurface crack

p_o/k	$T_{M1\text{-}C90}$	$T_{M2\text{-}C90}$	$T_{M1\text{-}I90B}$	$T_{M1\text{-}I90C}$	$T_{M1\text{-}I79}$
5	///	∞	∞	10	∞
5.5	///	∞	10	5	2
5.7	///	∞	5	3	2
6.0	///	∞	///	///	///
6.5	///	∞	///	///	///
7	///	10	///	///	///

Note: the notation "/// " means that no tests were carried out under the conditions.

5.2 A statistical model for predicting the propensity of rails to subsurface fatigue

5.2.1 The stochastic behavior of subsurface initiated fatigue occurrence

Material fatigue is known to be statistical in nature. Even if a population of apparently identical rolling specimens is subjected to an identical load, speed, and lubrication and environmental conditions, they do not exhibit the same life in fatigue. In the present experiment the stochastic behavior of subsurface fatigue was reflected through the complex consequences of the tests.

Subsurface initiated fatigue is governed by properties of materials as well as contact loads and contact cycles. For a given contact load and a given contact duration, variations in subsurface initiated fatigue life can be ascribed to influences of the coherence between nonmetallic inclusions and a steel matrix, distributions, types and sizes of nonmetallic inclusions, and the chance for detrimental inclusions to be unfavorably situated in the highly stressed subsurface. Indisputably, the influence of these material defect-related factors are all stochastic so the occurrence of subsurface initiated fatigue is stochastic in the location at which a subsurface fatigue crack would be initiated and in the number of material defects that would be able to initiate subsurface cracks. Therefore, subsurface initiated fatigue life of rail steels can be regarded as a random function of metallurgical and mechanical properties of rail steels, as well as contact loads and other testing conditions.

5.2.2 Subsurface fatigue life

Subsurface initiated fatigue life is consumed by the nucleation of a fatigue crack. Accordingly, the concept of subsurface initiated fatigue life is defined as a period in which a fatigue defect is nucleated and developed to a critical size. However, because of the limit of current detection techniques the so-defined subsurface fatigue life actually is not amenable to experimental determination. As the findings of the present tests demonstrated, neither changes in the subsurface microstructure nor hardening of the subsurface uniquely indicated the imminence of subsurface fatigue. This uncertainty involved in testing subsurface fatigue life made it unlikely to correlate subsurface fatigue life with the number of contact cycles. Probably the fact that no effective means are available for determining subsurface fatigue life is a primary reason why very few workers have ever tried to evaluate materials solely by comparing the susceptibility of subsurface to fatigue. Previous work on testing subsurface fatigue only dealt with testing durability of materials; every fatigue failure on the surface was considered to have been initiated in the subsurface. [125] The widely applied Weibull model was a typical example in this regard. However, the present experimental evidence shows that in free rolling subsurface initiated fatigue cracks tended to propagate parallel to the rolling surface (Figure 2.21). In addition, even under free rolling and lubricated conditions not all failures on the rolling surface were initiated from the subsurface. Some of the failures were apparently initiated on the surface. Thus, Weibull's theory cannot be directly applied to testing subsurface fatigue life. Instead, an attempt was made in the present experiment to evaluate the propensity of the rail steels to subsurface fatigue by directly comparing the probabilistic behavior of subsurface initiated fatigue rather than by correlating subsurface fatigue life with the number of rolling cycles.

5.2.3 Statistically modeling the propensity to subsurface initiated fatigue

It is well recognized that oxide inclusions in rails are primarily responsible for rail shells. The results of the present experiment also confirmed that the incidence of subsurface initiated fatigue defects in rails is a function of cleanliness of rail steels, characteristics of stringered oxide inclusions and contact loads. Generally, in free rolling, the occurrence of RCF is governed by numerous tribological and material variables, such as Hertz pressure, EHD film ratio, asperity traction coefficient, asperity height, fatigue limit stress, and a stress concentrator factor. In prediction of the occurrence of subsurface initiated fatigue, however, the characteristics of material defects and the severity of defects are significantly influential factors. With the applicability of a model considered, parameters used in modeling must have a strong effect on subsurface fatigue life and must be widely used. In addition, these parameters are amenable to experimental determination.

The Shell Index represented the first attempt to model the influence of oxide inclusions and effects of the microstructure upon the occurrence of subsurface initiated fatigue in rails.

$$SI = \ln[\frac{Vol_{oxide}\% * L_{stringer}}{BH^2}] \qquad (5\text{-}1)$$

It quantifies the influence of the metallurgical properties of rail steels on initiation of subsurface initiated fatigue. Moreover, the simplicity of the Shell Index and the usage of the measurable parameters make this formula practical. The shell indices of M1-I90B, M1-I90C, M2-C90 and M3-C90 steels have been calculated from the experimental results.

Table 5-3 Shell indices of the rail steels

steel	Vol. %	$L_{stringer}$, μm	Brinell hardness	[SI]
M2-C90	0.0039	18	310	-14.20
M3-C90	0.0079	17	270	-13.20
M1-I90B	0.0054	340	300	-10.39
M1-I90C	0.0113	156	300	-10.78

By comparing their susceptibility to shelling, the shell indices rate M2-C90 steel the best and rate M1-I90B steel the worst. This conclusion agrees with the results of the FAST experiment. The influence of metallurgical properties of rail steels are illustrated in Figure 5.1 with respect to the incidence of shells per rail MGT(million gross tonnage). The exceptional behavior of the M3-C90 rail was attributed to an exceptionally high contact pressure caused by the mismatch of wheel and rail profiles. The incidence of subsurface fatigue defects was beyond the correlation of the Shell Index. On the other hand, this case suggested that contact pressure had such a dominant effect upon the incidence of subsurface fatigue defects that it should not be excluded. The relations between likelihoods of subsurface fatigue defect occurrence and contact loads are shown in Figure 5.2. To modify the Shell Index, the effect of a contact load is taken into account:

$$[NSI] = [-SI] * (P_o / k) \qquad (5\text{-}2)$$

where P is contact pressure; k is shear yield strength. This new formula considers both metallurgical properties and effects of contact load. The *NSI*s of the rail steels are given in Table 5-4.

Table 5-4 *NSI*s of the rail steels at the different contact pressures

P_o / k	M2-C90	M3-C90	M1-I90B	M1-I90C	M1-I79
4.0	56.8	52.8	41.6	43.1	35.5
5.0	71.0	66.0	51.95	53.9	44.4
5.5	78.1	72.6	57.14	59.3	48.8
5.7	80.9	75.2	59.22	61.6	50.6
6.0	85.2	79.2	62.3	64.7	53.3

Further, to model the likelihood that a subsurface crack could occur in a roller subjected to a contact load, the probability of subsurface failure, *F(N)*, is correlated with *[NSI]* and normalized as :

$$F(N) = C * [SI]^a * \left[\frac{P_o}{k}\right]^b, \quad 0 \le F(N) \le 1 \qquad (5\text{-}4)$$

where *C*, *a* and *b* are correcting factors of normalizing *F(N)*, and *N* rolling cycles. All remaining parameters of this model are experimentally determinable. This probabilistic model establishes a correlation among contact pressures (P_o), material properties (k), and metallurgical properties (SI). It can be used in predicting the propensity of rail steels to subsurface fatigue. Besides, the modeling method is a worthy attempt to approach the life prediction by following the stochastic behavior of subsurface-initiated fatigue occurrence.

By substituting the resultant data of M1-I90B and M1-I90C steels into equation 5-4 so as to determine the correcting factors, this model is specified as (Figure 5.3):

$$F_{N=1\,million} = 0.028\,[SI]^2 * [\frac{P_o}{k}]^{1.7} - 0.445\,[SI] * [\frac{P_o}{k}] \qquad (5\text{-}5)$$

For a component subjected to free rolling contact for one million cycles, the survival likelihood is $(1 - F_{N=1\,million})$. Every improvement in decreasing the chance for a fatigue crack to occur increases the survival probability. To improve the cleanliness or disperse stringered oxide inclusions lessens the risk of rails to shell formation.

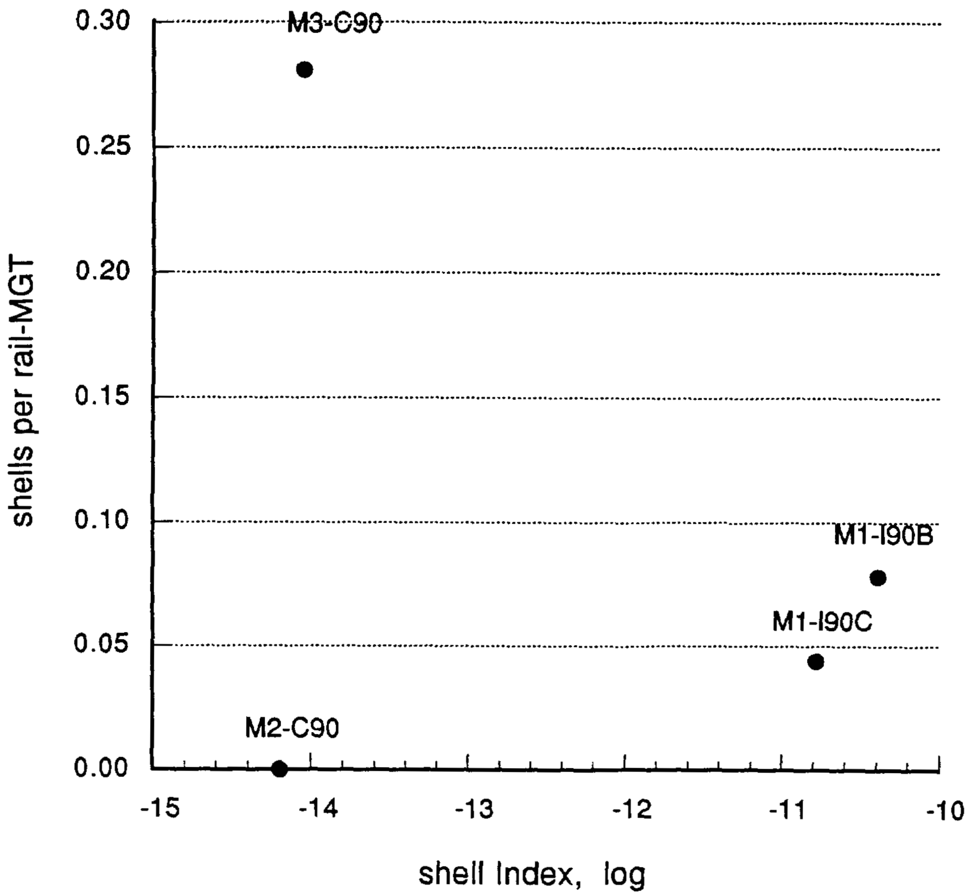

Figure 5.1 Incidence of shell defects versus shell index, log.

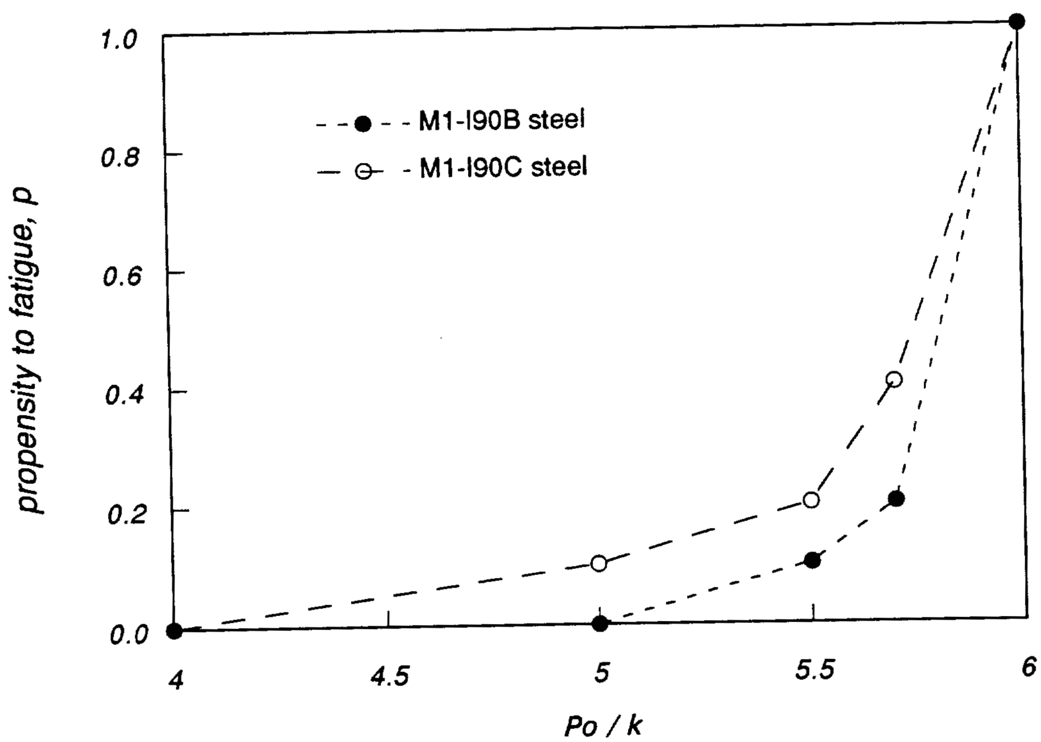

Figure 5.2 Probabilistic relation between propensity to fatigue and contact load.

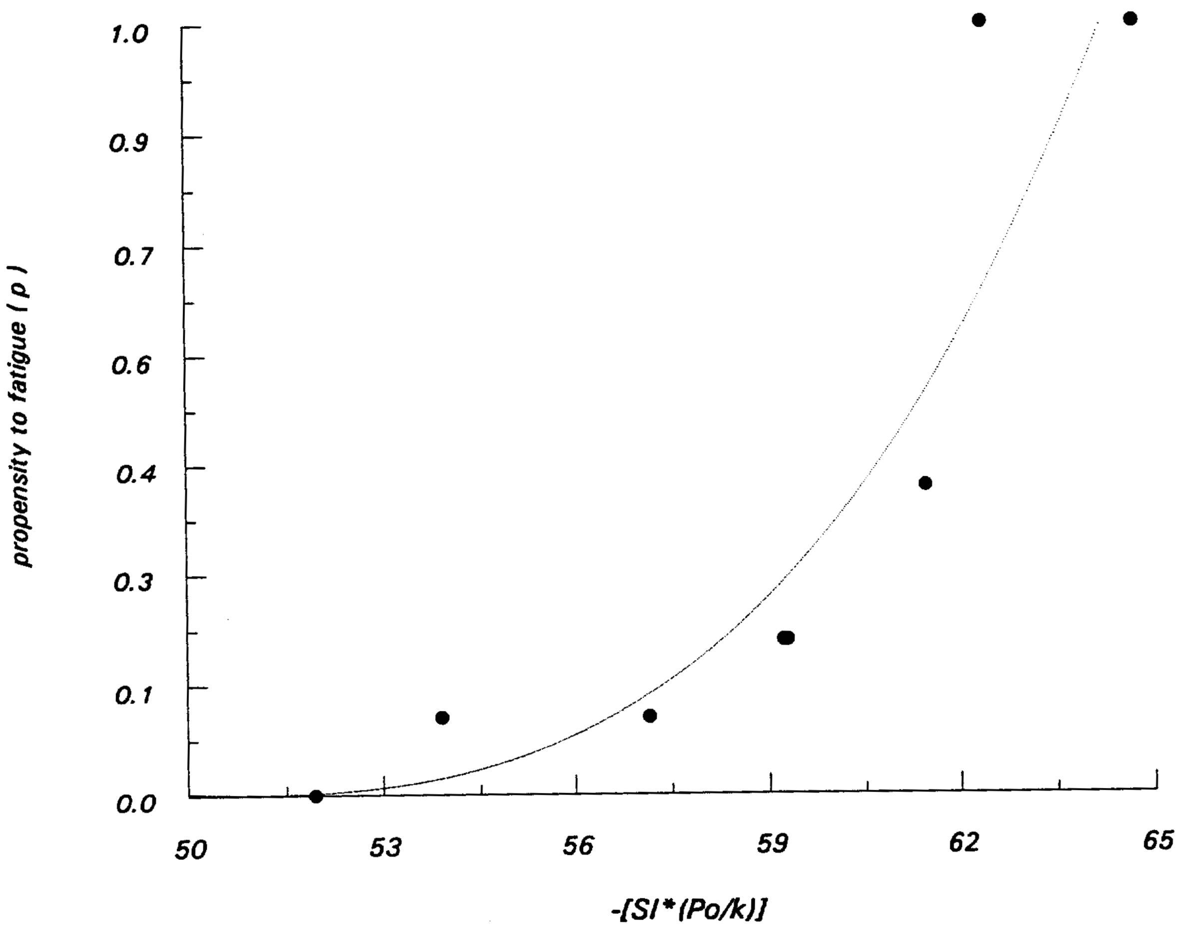

Figure 5.3 Probabilistic relation derived from the experimental results, as a function of SI and contact load.

5.3 Rolling contact conditions of subsurface fatigue occurrence

5.3.1 Appropriate contact loads

In free rolling, the subsurface is the most vulnerable with respect to the distribution of stresses, and thus fatigue failure would first be initiated in the subsurface. But the evidence of the present experiment showed that in a rolling test surface initiated fatigue and subsurface initiated fatigue competed each other and that subsurface initiated fatigue occurred only at appropriate contact loads as well as in favorable tribological conditions. A low contact load could not induce subsurface fatigue, but a high contact load caused either damage to the rolling surface or bulk deformation of the top rollers. To ensure a primary failure mode related to subsurface initiated fatigue, the present experiment tried a wide range of contact loads on each steel. According to the theory of shakedown, $P_o = 4.0k$, the limit would be the minimum contact pressure required to provoke subsurface deformation. Subjected to the minimum contact load, however, the subsurface did not show plastic deformation after 1 million cycles, and the response of the subsurface was still predominantly elastic. Appreciable plastic deformation in the subsurface did not occur until a contact pressure increased above a limit(P_{lower}). But once a contact load was further increased beyond an upper limit(P_{upper}) surface damage such as flaking, pitting, and cracking and corrugation occurred. Failures related to subsurface initiated fatigue were found only in the rollers subjected to loads that varied between P_{lower} and P_{upper}. The P_{lower} and P_{upper} for each rail steel are given in Table 5-5.

Table 5-5 The contact load limits for the steels

steel	M1-I79	M1-I90	M2-C90	M3-C90
$\sigma_{0.02}$, MPa	482	529	444	669
k, MPa	278	305	256	386
P_o, MPa	1112	1220	1024	1544
P_{lower}, MPa	///	1525	1279	1930
P_{uppper}, MPa	1578	1738	1792	///

5.3.2 Tribological conditions

Surface roughness of test specimens and lubrication conditions were the two key factors that suppressed surface-initiated fatigue so as to promote subsurface-initiated fatigue. In a rolling system, fluid lubricant films can separate rolling surfaces subjected to extremely high pressures in the zones of contact. A most useful engineering quantity is the λ ratio, which is defined as the ratio of total surface roughness to calculated film thickness of a lubricant oil

$$\lambda = h/\sigma_c$$

in which

$$\sigma_c = \sqrt{\sigma_t + \sigma_b}$$

The roughness of the specimens used in the present experiment was R_a = 0.8 μm on average. Under the testing conditions, the thickness of oil between a top roller and a bottom roller was around 1.7 μm (its calculation procedure is included in appendix 4). Thus the λ ratio was just greater than 2, the critical value below which surface asperities of the rollers are in contact in a test and above which these extraneous effects are eliminated. [125] This less than perfect tribological condition probably was the reason why the rolling surface sometimes suffered indenting and pitting (Figure 5.4). Surface initiated fatigue was not entirely suppressed in a test, and in fact it was competing with subsurface initiated fatigue. If the incubation of subsurface fatigue took a longer time than the incubation of surface fatigue, surface initiated fatigue took priority, resulting in pits, cracks and flakes on the rolling surface. Otherwise, subsurface initiated fatigue occurred. Subsurface initiated fatigue in a clean steel must take a long time to occur because it is lacking in nonmetallic inclusions crack initiators. It is tempting to conclude that RCF mode of a clean steel may primarily be related to surface initiated fatigue. This is also the reason why subsurface cracks were seldom nucleated in M2-C90 steel.

An effective contact load, good lubrication conditions, and the good surface finish of test specimens are essential for fatigue to occur in the subsurface rather than on the surface. The present tests on subsurface fatigue were conducted under these constraints.

5.4 Discussion on some results of subsurface fatigue testing

5.4.1 Formation mechanism of type I spalls

The two types of spalls were different from both top and side view, suggesting that possibly the two types of spalls were formed through different mechanisms. In fact, it is commonly accepted in research of ball bearings that type I spalls are attributed to stress concentration only and are subsurface initiated whereas type II spalls are caused by surface wear and surface initiated. [125]

Radial-oriented cracks were usually associated with type I spalls, extending to the deepest bottom. It is conjectured that type I spalls were developed from the origin of a radial-oriented subsurface crack. In a process of rolling contact, micro cracks could be initiated in the vicinity of nonmetallic inclusions. While a rolling test preceded, such micro cracks grew and radially propagated outward. A propagating crack might be the source for the formation of a spall (Figure 5.5), resulting in a round or near oblong failure spalling out on the rolling surface. In order to further investigate the origin of type I spalls, every effort was made in the present experiment but difficulties associated with preparation of metallographic specimens always thwarted the attempts.

5.4.2 Work hardening versus plastic deformation in the subsurface

The microhardness profiles peaked at a depth of about 300 μm, which corresponded to the location where the maximum shear stresses were supposed to be. In view of this fact, the shear stresses must have been responsible for work hardening. Therefore, the effect of work hardening was in proportion to the magnitude of the shear stresses or the contact loads (Figures 2.41 ~ 2.43). In addition, the experimental evidence demonstrated that the effect of work hardening was related to contact durations too. The M2-9008 roller was subjected to a contact load for 29,690 cycles while the M2-9004 roller subjected to an identical load for 1 million cycles. The hardening of the subsurface of the two rollers was significantly different (Figure 2.40). Work hardening is caused by an increased density of dislocations. The higher contact loads and longer rolling contact duration boosted the movement and aggregation of dislocations in the subsurface, enhancing the effect of work hardening.

Work hardening-affected zones extended as deep as 1.2 mm in the subsurface. The effect of work hardening was appreciable even in the subsurface of rollers that were subjected to a relatively low contact load of $P_o/k = 4.0$. But discernible forward plastic flow in subsurface existed in the shallower zone of the subsurface and was observed in M1-I79 steel only. Compared to clear plastic flow in M1-I79 steel, plastic flow induced in the other steels was less clear. For example, the near surface plastic zone and the subsurface plastic zone of the M2-C9004 roller were actually inseparable (Figure 2.36), and plastic deformation in M1-I90 steel did not develop as well as plastic deformation in M1-I79 steel either. Therefore, the development of plastic flow was governed by the initial hardness of the materials as well as the yield strengths of the steels. Such a phenomenon has been reported by other workers. [126]

Supposedly, when contact loads exceeded the shakedown limits of the individual steels, plastic yield should first occur at 0.3 mm depth beneath the rolling surface, where the maximum shear stresses existed according to the distribution of the shear stresses (the calculation included in appendix 5). However, the highly plastic deformation zone was situated instead at a deeper location (Figure 2.35). The reason for this discrepancy could be attributed to work harding of the subsurface. As Figure 2.35 shows, the upper boundary of the highly plastic zone was situated at a depth of 0.3 mm below the rolling surface—approximately corresponding to where the microhardness profiles peaked. Therefore, it could be that initially work hardening took place at the upper boundary so that the material in that depth became harder than the other area of the subsurface. The stresses transmitted through this already hardened layer forced plastic flow to develop inward only. As a process of rolling contact preceded, the lower boundary of the highly plastic zone continued to move inward, resulting in the highly plastic zone being away from a depth of 0.3 mm beneath the surface.

5.4.3 MnS inclusions as internal crack initiators

The present experiment confirmed that oxide inclusions such as Al_2O_3 and MAl_2O_3-NCaO acted as crack initiators, and also discovered that some manganese sulfides took part in initiating subsurface cracks (Figure 5.6). Although many researchers firmly believe that sulfides hardly participate in initiation of internal fatigue cracks or question the role of sulphide inclusions in initiating a fatigue defect, [2, 31] the present experimental evidence revealed that manganese sulfides in the highly stressed zone are capable of initiating subsurface cracks. The decohesion between sulphide inclusions and a steel matrix was responsible for crack initiation. In effect, once nucleated at MnS inclusions, fatigue cracks probably propagated more rapidly than those cracks nucleated by oxide inclusions, because elongated sulfide inclusions were ideal weaker paths and facilitated crack growth. Therefore, the influence of sulphide inclusions upon rail fatigue life needs reconsidering.

Figure 5.4a An indentation on the rolling surface. Magnification 12x.

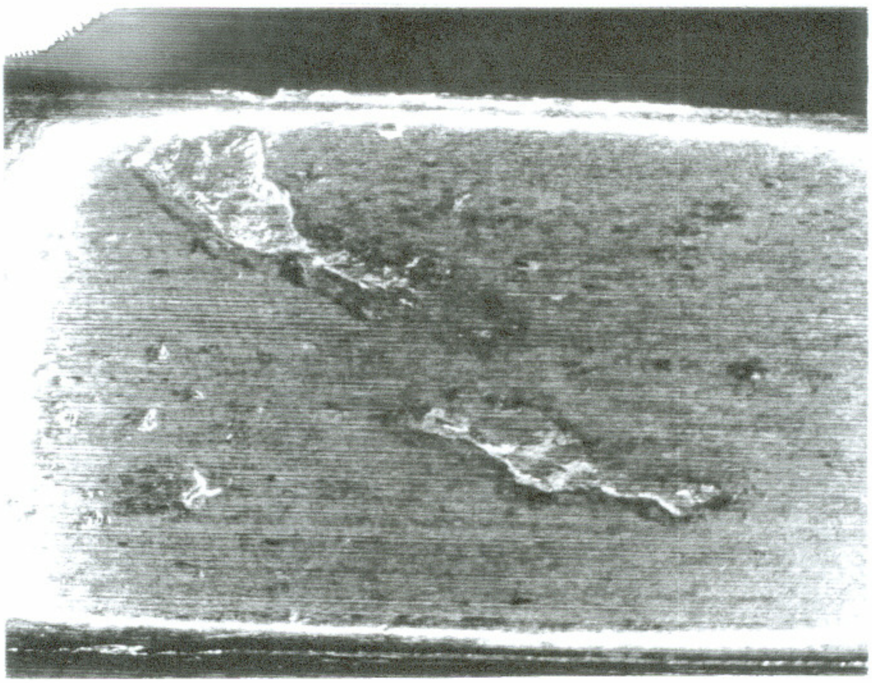

Figure 5.4b Pits on the rolling surface. Magnification 10x.

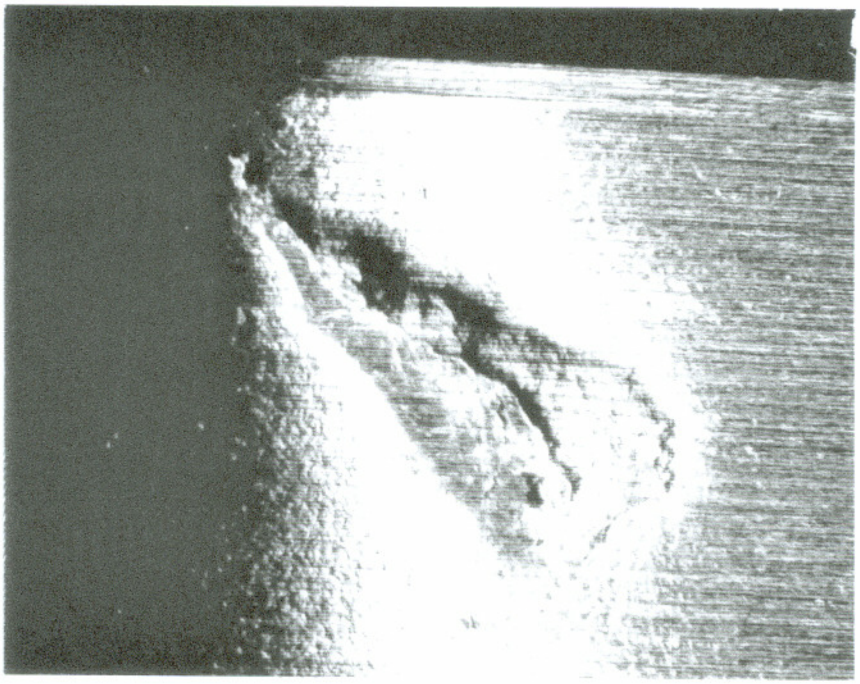

Figure 5.5 The origin of a developing spall. Magnification 25x.

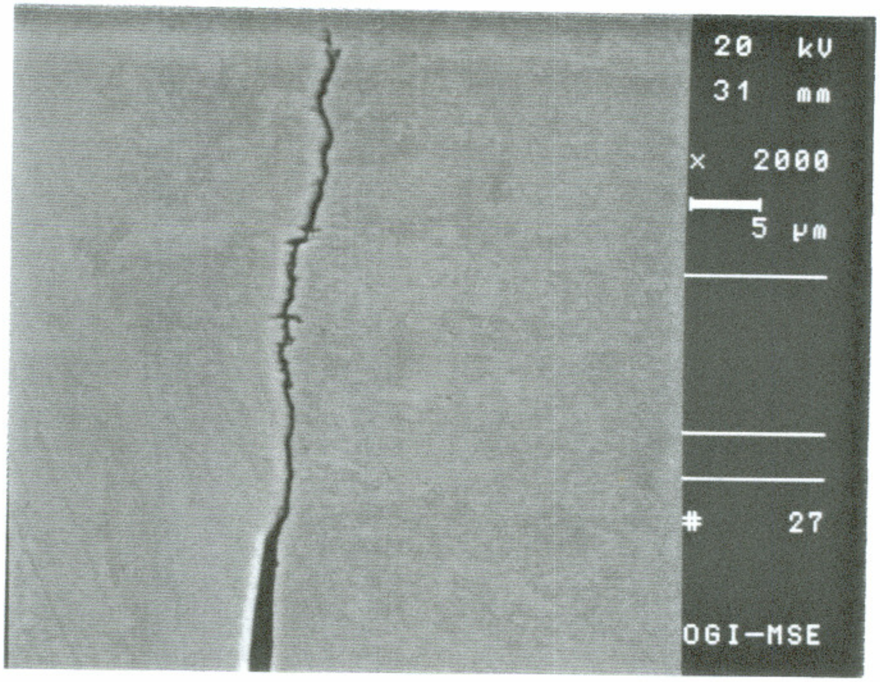

Figure 5.6a A crack emanated from a sulfide inclusion near to the rolling surface.

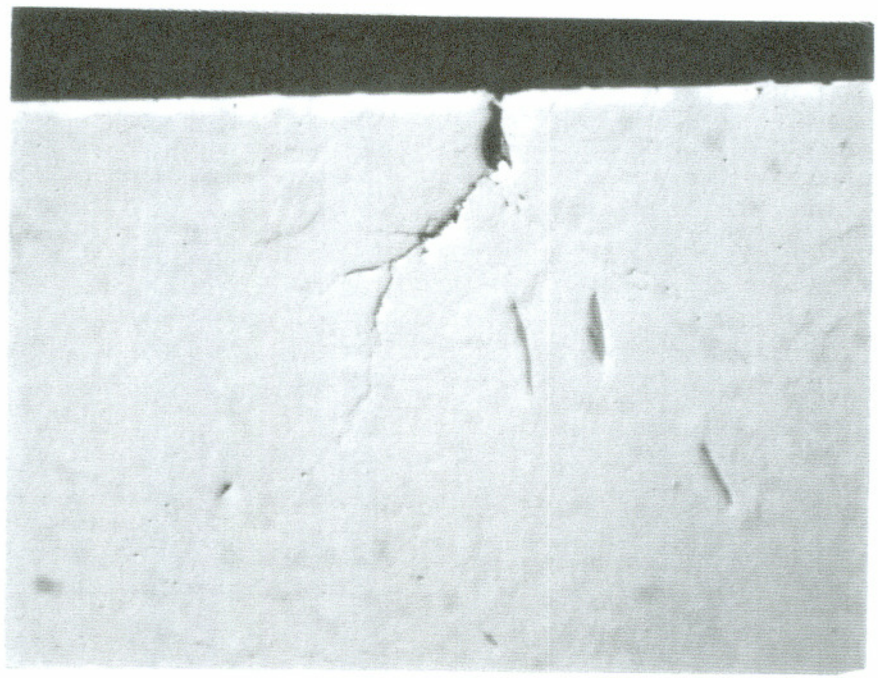

Figure 5.6b A crack was developing at the tip of a sulfide inclusion and propagating toward the rolling surface. Magnification 400x.

Chapter 6

CONCLUSIONS

1. The degree of variability in oxide volume fraction within short spatial separations in rails means that conventional procedures of taking only six or so specimens to characterize cleanliness is inadequate. For a relative error of ±25%, 18 random specimens are required to determine oxide volume fractions in the M1-I79 rail and 19 random specimens for the cleaner, M2-C88 rail. Further, 20 random specimens are considered appropriate for assessing the cleanliness of rails manufactured in modern production processes if at least 40 random fields are surveyed for each specimen.

2. The population characteristics of oxide inclusions should be examined fully before an assessment procedure is applied to determine the content of oxide inclusions. The size of a statistical sample is a matter of primary concern in this regard. A statistical sample should be composed of measurements of specimens rather than measurements of individual fields.

3. The low oxide volume fractions in the rails manufactured by modern manufacturing processes strongly suggest that a heavy weighting should be given to the stringer length rather than to the oxide volume fraction in a model that quantitatively characterizes the influence of oxide inclusions upon subsurface fatigue at normal contact pressures.

4. The method of vacuum deoxidation had a great advantage over Al precipitation deoxidization, not only reducing the content of oxide inclusions but also countering the clustering of oxide inclusions. However, the types of nonmetallic inclusions were not changed by vacuum degassing.

5. Subsurface initiated fatigue can be generated with a laboratory-scale apparatus. To ensure failures primarily related to subsurface-initiated fatigue, an appropriate contact load is critical. For M1-I79, M1-I90 and M2-C90 rail steels the maximum contact loads are $P_o / k = 5.9$, 5.7 and 7, respectively.

6. The incidence of subsurface fatigue defects of M1-I79, M1-I90B, M1-I90C and M2-C90 steels was a function of the Shell Index. Of the four FAST rail steels, M2-C90 steel was rated superior to the other steels in propensity to subsurface failure. This result agrees with that of the FAST experiment. However, the conclusion about M1-I90B and M1-I90C steels is different from the result of the FAST experiment.

7. The statistical model

$$F_{N=1\,million} = 0.028\,[SI]^2 * [\frac{P_o}{k}]^{1.7} - 0.445\,[SI] * [\frac{P_o}{k}]$$

can be applied to predicting the probability of subsurface fatigue with the measurable parameter *SI*, providing a novel approach to evaluating materials in subsurface fatigue. Under the circumstances in which the capability of available means to detect a subsurface crack is limited, this approach is particularly promising.

8. The experimental findings confirmed that oxide inclusions participated in initiating fatigue cracks in the subsurface and also revealed that sulfide inclusions in the stressed subsurface are able to initiate subsurface cracks. The effect of sulfide inclusions upon rail fatigue needs to

be reconsidered.

9. Type I spalls are due to subsurface initiated fatigue. This type of spall can only be a sufficient criterion for judging the occurrence of subsurface initiated fatigue. The Weibull model is not directly applicable to testing subsurface fatigue life.

REFERENCES

1. P. Ola, E. Aulaire, Freight trains are back and they're on a roll, *Smithsonian*, No.6, 1995, 36-48.

2. D. H. Stone, Rail developments and requirements for heavy haul railways, *Rail Quality And Maintenance For Modern Railway Operation*, KLUWER ACADEMIC PUBLISHERS, 1992, pp. 15-26.

3. R. K. Steele, Strategies for maximizing rail life, *Rail Quality And Maintenance For Modern Railway Operation*, KLUWER ACADEMIC PUBLISHERS, 1992, pp. 77-96.

4. E. Savage, R. K. Steele, and J. M. Morris, A failure analysis of railroad rail, *Prevention of Structural Failures - The Role of NDT, Fracture Mechanics And Failure Analysis: Proceedings Of Two Annual Forums*, Tarpon Spring, Florida, June 1977, pp. 29 - 48.

5. O. Orringer, Rail testing: Strategies for safe and economical rail quality assurance, *Transportation Research Record 1174: Rail Replacement and Maintenance Management,* Transportation Research Board, National Research Council, Washington DC, 1988, pp. 28-42.

6. P. M. Besuner, D. H. Stone, K. W. Schoeneberg, and M. A. Herrera, Probability analysis of rail defect data, *Proceedings Of Heavy Haul Railways Conference*, Perth, Western Australia, September 1978, Session 308.

7. F. D. Acord, Heavy rail loading by locomotive and cars, *Proceedings Of Heavy Haul Railways Conference,* Perth, Western Australia, September 1978, Session 504.

8. R. K. Steele, Requirements for the reliability assessment of railroad rail in service, *Railroad Track Mechanics & Technology*, Pergamon Press, 1975, pp. 303 - 320

9. ERRI Question D173, *Rolling Contact Fatigue (Report Number 5)*, European Railway Research Institute, Utrecht, Netherlands, 1993.

10. J. M. Hyzak and I. M. Bernstein, The effect of defects on the fatigue crack initiation process in two P/M superalloys: part I. fatigue origins, *Metallurgical Transactions A*, Vol. 13A, January 1982, pp. 33 - 42.

11. R. K. Steele, Metallurgical cleanliness improves rail life, *Railway Gazette International,*

March 1987, pp. 175 - 179.

12. Nakamura, The rail shelly crack in Japan, *Quarterly Report of The RTRI*, Vol. 6, No. 3, pp. 34-44.

13. S. Marich and P. Curicio, Development of high-strength alloyed rail steels suitable for heavy duty applications, *Rail Steels - Developments, Processing And Use*, ASTM Special Technical Pub. 644, 1977, pp. 167 -160.

14. K. L. Johnson, *Contact Mechanics*, Cambridge University Press, 1992.

15. S. P. Timosenko and J. N. Goodier, *Theory Of Elasticity*, 3rd ed., New York, McGraw-Hill, 1951.

16. B. Paul, A review of rail - wheel contact stress problems, *Railroad Track Mechanics & Technology*, Pergamon Press, 1975, pp. 323 - 351.

17. T. O. Smith and C. K. Liu, Stresses due to tangential and normal loads on an elastic solid with application to some contact stress problems, *ASME Journal of Applied Mechanics*, Vol. 5, No.2, 1953, pp. 157-166.

18. S. G. Sampath and T. G. Johns, Stresses around transverse fissure flaws in rails due to service loads, *Rail Steels - Developments, Processing And Use*, ASTM Special Technical Pub. 644, 1977, pp. 330 - 341.

19. T. G. Johns, K. B. Davies, P. M. McGuire, and S. G. Sampath, *Engineering analysis of stresses in railroad rail*, Battelle Columbus Lab Report, June, 1977, DOT-TSC-1038.

20. B. Paul, Surface and subsurface stresses associated with non-Hertzian wheel-rail contact, *Contact Mechanics And Wear of Rail/Wheel Systems*, Pergamon Press, 1982, pp. 197-207.

21. R. K. Steele and M. W. Joerms, *A Fatigue Analysis Of The Effects Of Wheel Load On Rail Life*, American Association of Railroad Report, R-689, September, 1988.

22. R. C. Rice, R. Rungta and D. Broek, *Post-service Rail Defect Analysis*, Third Interim Report, DOT, Battelle , Columbus Laboratories, Ohio, 1989.

23. A. P. Voskamp, R. Osterlund, P. C. Becker and O. Vingsbo, Gradual changes in residual stress and microstructure during contact fatigue in ball bearings, *Metals Technology*, Vol. 7, January 1980, pp. 14 - 21.

24. H. Swahn, P. C. Becker and O. Vingsbo, Martensite decay during rolling contact fatigue in

ball bearing, *Metallurgical Transactions A*, Vol. 7A, pp. 1099-1110.

25. V. A. Dikshit, *Rolling Contact Fatigue Behavior Of Pearlitic Rail Steels,* Ph.D. Thesis, Oregon Graduate Institute of Science & Technology, 1992.

26. K. L. Johnson, The mechanics of plastic deformation of surface and subsurface layers in rolling and sliding contact, *The Role Of Subsurface Zones In The Wear Of Materials*, Trans Tech Publications Ltd., USA, 1988, pp. 17 - 33.

27. K. L. Johnson, *The Strength Of Surface In Rolling Contact*, Third Annual BP/I Mech. E., Tribology Lecture, Dec. 1988.

28. H. P. Lieurade, R. Y. Deroche, B. Derboule and R. Conti, A study of the shelling mechanism of rails, *The Second International Symposium On Contact Mechanics And Wear of Rail/Wheel Systems*, Univ. of R.I., July 8-11, 1986, pp. 376 - 396.

29. V. Bhargava, G. T. Hahan, and C. A. Rubin, Rolling contact deformation, etching effects, and failure of high-strength bearing steel, *Metallurgical Transactions A*, 21A, 1990, pp. 1921-1931.

30. *Rail Defect Manual*, Sperry Rail Service, 1964.

31. D. Y. Jeong, O. Orringer, A. B. Perlman and R. Rice, Beam theory predictions of shell nucleation life, *Proceedings Of International Symposium On Contact Mechanics And Wear Of Rail/Wheel Systems II*, Univ. of R.I., July 8-11, 1986, pp. 394 - 404.

32. R. K. Steele, Recent North American experience with shelling in railroad rails (part I observations), *AREA Bulletin*, No. 722, 1989, pp. 311-345.

33. D. H. Skinner and P. A. Judd, A metallographic study of fatigue defects in rails, *Metals in Mining*, Australia Institute of Metal, 34th Annual Conference, Queensland, 1981, pp. 68 - 72.

34. R. K. Steele, Rail: its behavior and relationship to total system wear, *The Second International Heavy Haul Railway Conference*, Colorado Springs, Colorado, USA, 1982, pp. 115-159.

35. P. Mutton, Rail assessment, *The Second International Heavy Haul Railway Conference*, Colorado Springs, Colorado, USA, 1982, pp. 99 - 114.

36. D. E. Sonon, J. V. Pellegrino and J. M. Wandrisco, A metallurgical examination of control-cooled, carbon-steel rails with service-developed defects, *Rail Steels - Developments, Processing And Use*, ASTM Special Technical Pub. 644, 1977, pp. 99-117.

37. E. E. Laufer, H. Ghonem, J. Kalousek and D. H. Stone, Aspects of plastic deformation and fatigue damage in pearlitic rail steel, *The Second International Heavy Haul Railway Conference, Colorado Springs, Colorado, USA*, 1982, pp.233-256.

38. B. N. Leis and R. C. Rice, Rail fatigue resistance - increased tonnage and other factors of consequence, *The Second International Heavy Haul Conference*, Colorado Springs, Colorado, September 1982, pp. 55-67.

39. G. Lundberg and A. Palmgren, Dynamic capacity of roller bearings, *Acta Polytech.*, No. 210, 1952, pp.23-45.

40. G. C. Martin and W. W. Hay, *Influence Of Wheel/Rail Contact Forces On The Formation Of Rail Shells*, University of Illinois, Department of Civil Engineering, Reprots 70-102, Trans Series Number 5, December 1970, and Trans Series ASME 72-WA/RT-8, 1972.

41. A. K. Hellier, D. J. H. Corderoy and M. B. McGirr, A study of subsurface rail/wheel contact stresses with application to modeling rail fatigue, *The Second International Symposium On Contact Mechanics And Wear of Rail/Wheel System II*, Univ. of R.I., July 8 - 11, 1986, pp. 421 - 434.

42. C. G. Chipperfield and A. S. Blickblau, Modeling rolling contact fatigue in rails, *Rail International*, Vol. 15, No.1, pp. 25 - 31.

43. M. Tokuda, Observations of the peeling mode of failure and surface-originated flaking from a ring-to-ring rolling contact fatigue test rig, *Rolling Contact Fatigue Testing of Bearing Steels*, ASTM Special Technical Pub. 771, 1981, pp.151 - 165.

44. R. K. Steele, Recent North American experience with shelling in railroad rails (part II analytical treatment), *AREA Bulletin No.723*, 1989, pp.395-408.

45. S. Marich, J. W. Cottam and P. Curcio, Laboratory investigation of transverse defects in rails, *Proceedings Of The Heavy Haul Railway Conference*, Perth, Western Australia, 1978, Session 303.

46. P. J. Mutton, C.J. Epp and J. Dudek, Rolling contact fatigue in railway under high axle loads, *Wear*, Vol. 144, 1991, pp. 139-152.

47. D. H. Skinner and P. A. Judd, A metallographic study of fatigue defects in rails, *34th Australian Inst. Metals Conference*, Queensland, 1981, 68-72

48. P. Clayton and G. Brave, *Fatigue Defect Origination And Growth Experiment*, Report

FRA/ORD-91/18, Federal Railroad Administration, DOT, 1981.

49. D. E. Sonon, J. V. Pellegrino and J.M.Wandrisco, A metallurgical examination of control cooled, carbon-steel rails with service developed defects, *Rail Steels - Developments, Processing And Use*, ASTM Special Technical Pub. 644, 1978, pp. 99-117.

50. R. C. Rice, R. Rungta and D.Broek, *Post-service Rail Defect Analysis*, Battelle Columbus Laboratories Third Interim Report, US Dept of Transportation, July 1983.

51. K. Sugino, H. Kageyama and H. W. Newell, Detection method for harmful inclusions in rail steels, *AREA Bulletin No 716*, 1989, pp. 230-259.

52. *Draft Report RP7,* ERRI D173 Committee on Rolling Contact Fatigue, European Railway Research Institute, Utrech, Netherlands, 1994.

53. S. Jahanmir and N.P.Suh, Mechanics of subsurface void nucleation in delamination wear, *Wear*, Vol.44, 1977, pp. 17-38.

54. J. Gurland and J.Plateau, The mechanism of ductile rupture of metals containing inclusions, *Transactions of ASM*, Vol. 56, 1963, pp. 442-454.

55. M. F. Ashby, Work hardening of dispersion-hardened crystals, *Phil Mag*, Vol. 14, 1966, pp. 1157-1178.

56. P. H. Dawson, Rolling contact fatigue crack initiation in a 0.3 per cent carbon steel, *Journal Of The Institution Of Mechanical Engineers*, Vol. 46, 1969, pp. 36-45.

57. P. C. Bastias, G. T. Hahn, C. A. Rubin, V.Gupta and X. Leng, Analysis of rolling contact spall life in 440C bearing steel, *Wear* 171, 1994, pp. 169-178.

58. J. J. Wert, The role microstructure in subsurface damage induced by sliding contact, *The Role Of Subsurface Zones In The Wear Of Materials*, Trans Tech Publications Ltd., USA, 1988, pp. 105 -129.

59. F. A. McClintock and A.S.Argon, *Mechanical Behavior of Materials*, Addison-Wesley, Reading, MA, 1966.

60. H. Frost and M. F. Ashby, *Deformation-Mechanism Maps*, Pergamon Press, 1982.

61. H. Sunwoo, Cyclic deformation of pearlitic eutectoid rail steel, *Metallurgical Transactions A*, Vol.13A, pp. 1982 - 2035.

62. J. F. Braza, M. E. Fine, A. K. Gangopadhyay, L. M. Keer, and R. E. Worden, Mechanical failure mechanisms in ceramic sliding and rolling contacts, *Tribology Transactions*, Vol. 32, No.1, 1989, pp. 1-8.

63. L. M. Keer, Subsurface and surface cracking due to Hertzian contact, *Journal Of Lubrication Technology*, Vol. 104, 1982, No. 7, pp. 251 - 247.

64. J. Ruppen, P. Bhowal, D. Eylon, and A. J. McEvily, On the process of subsurface fatigue crack initiation in Ti-6Al-4V, *Fatigue Mechanisms*, ASTM Special Technical Pub. 675, pp. 47 - 64.

65. J. L. Gilbert and H. R. Piehler, On the nature and crystallographic orientation of subsurface cracks in high cycle fatigue of Ti-6Al-4V, *Metallurgical Transactions* A, Vol. 24A, 1993, pp. 669-680.

66. D.F. Neal and P. A. Blenkinsop, Internal fatigue origin in alphi-beta titanium alloys, *Acta Metallurgica, Vol. 24, 1976, pp. 59 - 63.*

67. N. Y. Jin, C. Zhong and X. Chen, Cyclic deformation of AISI-310 stainless steel - II. saturation dislocation structures, *Acta Metallurgica et Materials*, Vol. 38, No. 11, pp. 2141 - 2148.

68. Meredith and F. J. Sewell, Assessment of nonmetallic inclusion content and the relationship to fatigue life of one percent carbon-chrome steels, *Bearing Steels: The Rating of Nonmetallic Inclusions*, ASTM Special Technical Pub 575, 1974, pp. 66-95.

69. K.Asano and T. Nakano, Deoxidation of molten steel with deoxidizer containing aluminum, *Transactions Of The Iron And Steel Of Japan*, Vol. 210, 1972, No.12, pp. 343-349.

70. E. T. Turkdogan, Deoxidation of steel, *Japanese Journal Of The Iron And Steel Institute*, No.1 , Vol. 210, 1972, pp. 21-36.

71. H. Li, *Modification Of Oxide Inclusions In Rail Steels*, Master Thesis, Beijing University of Science & Technology, China, 1988.

72. R. J. Fruehan, Deoxidization of molten steel, *Iron & Steelmaking*, No.3, 1983, pp. 33-37.

73. T. Malkiewica and S. Rudnik, Deformation of non-metallic inclusions during rolling of steel, *Japanese Journal Of The Iron And Steel Institute*, Vol. 201, 1963, pp. 33-38.

74. D. Brooksbank and K. W. Andrews, Stress fields around inclusions and their relation to mechanical properties, *Japanese Journal Of The Iron And Steel Institute*, 210, 1972, pp.

246-255.

75. H. Salehizadeh and N. Sake, The mechanics of crack initiation at hard particle in rolling line contact, *Journal of Tribology*, April, 1992, pp. 341-347.

76. W. E. Duckworth, The effects of externally introduced alumina particles on the fatigue life of En24 steel, *Clean Steel 77*, pp. 87 - 103.

77. L. O. Uhrus, Through hardening steels for ball bearings - effect of inclusions on endurance, *Clean Steel 77*, pp. 104 -109.

78. J. M. Barsom and E. J. Imhof, Fatigue and fracture behavior of carbon-steel rails, *Rail Steels - Developments, Processing And Use*, ASTM Special Technical Pub. 644, 1978, pp. 387-410.

79. S. Marich and R. Beolen, Revised rail selection criteria, *Fourth International Heavy Haul Railway Conference*, Brisbane, Australia, 11-15 September 1989, pp. 25-34.

80. E. A. Starke Jr., Fatigue cracks: resistance to initiation, *Encyclopedia of Materials Science And Engineering*, Pergermon Press, 1986, pp. 1666 - 1669.

81. K. Kiessling, *Non-metallic Inclusion In Steel*, The Metals Society, London, 1971.

82. R. F. Johnson and J. F. Sewell, The bearing properties of 1%C-Cr steel as influenced by steelmaking practice, *Japanese Journal Of The Iron And Steel Institute*, Vol. 198, 1960, pp. 414-444.

83. S. J. Goodwin, Inclusion nucleated ductile fracture in stainless steel, *Acta Metallurgica*, No.5, 1989, pp. 1389-1398.

84. Metals Handbook, 9th ed, Vol.11, pp.133-134.

85. K. W. Andrews and D. Brooksbank, Stresses associated with inclusions in steel: a photoelastic analogue and the effects of inclusions in proximity, *Japanese Journal Of The Iron And Steel Institute*, Vol. 210, 1972, pp. 765-776.

86. A. S. Argon, J. IM and R. Safoglu, Cavity formation from inclusions in ductile fracture, *Metallurgical Transactions A*, 6A, 1975, pp. 825-837.

87. R. Chattopadhyay, Effect of sulfide inclusions on the fracture of a low-carbon aluminum-killed steel, *Microstructural Science, ASM*, Vol 12, pp. 488-493.

88. D. T. Llewellyn, *Steel: Metallurgy & Application*, Butterworth-Heinemann Ltd, Great

Britain, 1992, p.196.

89. J. Kalousek, D. M. Fegredo and E. E. Laufer, The wear resistance and worn metallography of pearlite, bainite, and tempered martensite rail steel microstructure of high hardness, *Proceedings Of The International Conference On Wear Of Materials,* Vancouver, 14-18 April 1985, ASME, pp.213-245.

90. P. J. Mutton, *The Influence Of Microstructure On The Wear Behavior Of Rail And Wheel Materials,* Master of Applied Science Thesis, University of Melbourne, 1985.

91. E. Hornbogen, *Physical Metallurgy*, American Elsevier Publishing Company, Inc , New York, 1970, p. 629.

92. W. H. Hodgson, The development of a second generation of alloy steel rails for heavy haul applications, *The Second International Heavy Haul Railway Conference*, Colorado Spring, Colorado, USA, 1992, pp. 1-14.

93. Bouse, Role of alloying and microstructure on the strength and toughness of experimental rail steels, *Rail Steels-Developments, Processing And Use*, ASTM Special Technical Pub 644, 1976, p. 152.

94. Y. Murakami, S. Kodama and S. Konuma, Quantitative evaluation of effects of non-metallic inclusions on fatigue strength of high strength steels I: basic fatigue mechanism and evaluation of correlation between the fatigue fracture stress and the size and location of non-metallic inclusions, *International Journal Of Fatigue*, No.9, 1989, pp. 291-298.

95. M. Dollar, I. M. Bernstein and A. W. Thompson, Influence of deformation substructure on flow and fracture of fully pearlitic steel, *Acta Metallurgica*, Vol.36, 1988, pp. 311-320.

96. M. Dollar, I. M. Bernstein, M. Daeubler and A. W. Thompson, The effect of cyclic loading on the dislocation structure of fully pearlitic steel, *Metallurgical Transactions A*, 20 A, 1989, pp. 447-451.

97. D. J. Alexander and I. M. Bernstein, *Phase Transformation In Ferrous Alloys,* AIME, New York, 1984, p.243

98. *Standard Recommended Practice For Determining The Inclusion Content Of Steel,* ASTM E45, 1984.

99. *Microscopic Testing Method For The Non-metallic Inclusions In Steel,* Japanese Standard JIM-G-0555, *JIM Handbook,* 1994.

100. A. Koyanagi, Microscopic testing method for the non-metallic inclusions in bearing steels in Japan, *Bearing Steels: The Rating of Nonmetallic Inclusion*, ASTM Special Technical Pub. pp. 22 - 37.

101. A. G. Framlom, Comparison between a quantitative microscope and chemical methods for assessment of non-metallic inclusions, *Japanese Journal Of The Iron And Steel Institute*, Vol. 207, 1969, pp. 181 - 186.

102. *Standard Practice For Determining Inclusion Content Of Steel And Other Metals By Automatic Image Analysis*, ASTM E 1245-89, 1989.

103. R. A. Rege, *Microcleanliness of steel -- a new quantitative TV rating method*, ASTM Special Technical Pub. 480, 1970, pp. 249 - 272.

104. G. F. Vander Voort, Inclusion measurement, *Metallography As A Quality Control Tool*, Plenum Press, 1979, pp. 1 - 88.

105. P.Clayton, Fatigue behavior of rail steels in a 33 kip wheel load experiment at FAST, *AREA Bulletin 731*, Vol. 92, 1991, pp. 189-217.

106. H. Li and P. Clayton, A statistical analysis of the oxide content of rail steel, *Symposium Of Rail Steels For The 21st Century*, AIME ISS Mechanical Working and Steel Conference, Baltimore, Oct. 1994.

107. C. V. Darragh, J. D. Stover, R. J. High, Quality steels for the twenty-first century, *Symposium of Rail Steels For The 21st Century*, AIME ISS Mechanical Working and Steel Conference, Baltimore, Oct. 1994.

108. J. D. Stover, R. V. Kolarisk and M. D. Keener, The detection of aluminum oxide stringers in steel using an ultrasonic measuring method, *Proceedings Of AIME 31st Mechanical Working And Steel Conference, 1989*, pp. 145-53.

109. R. F. Johnson, *Japanese Journal Of The Iron And Steel Institute*, No.12, 1966, p. 414.

110. R. F. Johnson, Fatigue in rolling contact: some metallurgical aspects, *Symposium on Fatigue in Rolling Contact, London*, 1963, pp. 95-102.

111. M. Atkinson, The influence of non-metallic inclusions on the fatigue properties of ultra-high-tensile steels, *Japanese Journal Of The Iron And Steel Institute*, Vol. 195, 1957, pp. 64 - 75.

112. Y. Murakami and H. Usuki, Quantitative evaluation of effects of nonmetallic inclusions on

fatigue strength of high strenght steels II: fatigue limit evaluation based on statistics for extreme values of inclusion size, *International Journal Of Fatigue*, No.5, 1989, pp. 299-307.

113. Y. P. Chiu, An engineering model of spalling fatigue failure in rolling contact, *Wear*, Vol. 17, 1971, pp. 433 - 446.

114. A. W. Thompson, D. E. Albert and G. T. Gray, Fatigue crack growth in rail steels, *Rail Quality and Maintenanace For Modern Railway Opertion*, KLUWER ACADEMIC PUBLISHERS, 1992, pp. 361-372.

115. *Standard Practice For Determining Inclusion Content Of Steel*, ASTM E412, 1987.

116. *Standard Practice For Preparing And Evaluating Specimens For Automatic Inclusion Assessment Of Steel, ASTM E 768 - 80*, 1985.

117. *Standard Test Methods For Microhardness Of Materials*, ASTM E384, 1984.

118. *Standard Test Methods For Brinell Hardness of Materials*, ASTM E10, 1984.

119. J. E. Freund, *Mathematical Statistics*, Prentice-Hall, Englewood Cliffs, New Jersey, 1980.

120. W. H. Beyer, *Handbook of Mathematical Siences*, CRC Press, New York, 1992.

121. *Standard Practice For Determining Inclusion Content Of Steel And Other Metals By Automatic Image Analysis*, ASTM E 1245 - 89, 1989.

122. K. Sugino, H. Kageyama, C. Urashima and T. Kuroki, Metallurgical investigation of transvers defects in worn rails in service, *Proceedings Of Contact Mechanics And Wear of Wheel/Rail Systems*, Vancouver 1994, 324-348.

123. J. S. Bendat and A. G. Piersol, *Random Data: Analysis And Measurement Procedures*, Wiley-Interscience, New York, 1971.

124. T. A. Harris, *Rolling Bearing Analysis*, John Wiley & Sons,Inc, New York, 1994.

125 V. Bhargava, G. T. Hahn and C. A. Rubin, Analysis of rolling contact with kinematic hardening for rail steel properties, *Wear*, Vol 122, 1988, pp. 267-283.

APPENDICES

Appendix 1 Analysis Routines

1.1 Analysis Routine for M2-C88 Steel

1>	Live
2>	Image frame: 0, 0, 511, 476
3>	Transition
4>	Hist. Mod. : 70, 253
5>	Store image: M2-C88.TIF
6>	Threshold: pl. 1, oxide 0-70
7>	Dilation: pl. 1 Cross
8>	Erosion: pl 1 Cross
9>	Load image: M2-C88.TIF
10>	Threshold: pl 2, oxide 0-80
11>	Xor: planes 1, 2 -> 8
12>	Filling: plane 8
13>	Chord size: pl 8->1, 4 x 5
14>	Load image: M2-C88.TIF
15>	Threshold: pl 3, oxide 0-119
16>	Xor: planes 1, 3 -> 4
17>	Mask: pl 4 -> 1, 4 x 4
18>	Load image: M2-C88.TIF
19>	Threshold: pl 6. Phase #6 0-125
20>	Xor: planes 1, 6 -> 5
21>	Mask: pl 5 -> 1, 3 x 3
22>	Load image: M2-C88.TIF
23>	Limit Asp. r 1 1.00 2.00
24>	Filling: plane 1
25>	Field meas: plane 1
26>	Chord size: pl 1, 1 x 1
27>	Feature meas: plane 1

1.2 Analysis Routine for M3-C90 Steel

1> Live
2> Image frame: 0, 0, 511, 476
3> Transition
4> Hist. Mod. : 70, 253
5> Store image: M3-C90.TIF
6> Threshold: pl. 1, oxide 0-66
7> Dilation: pl. 1 Cross
8> Erosion: pl 1 Cross
9> Load image: M3-C90.TIF
10> Threshold: pl 2, oxide 0-80
11> Xor: planes 1, 2 -> 8
13> Chord size: pl 8->1, 3 x 4
13> Filling: plane 1
14> Load image: M3-C90.TIF
15> Threshold: pl 3, oxide 0-100
16> Xor: planes 1, 3 -> 4
17> Mask: pl 4 -> 1, 4 x 4
18> Load image: M3-C90.TIF
19> Threshold: pl 6. Phase #6 0-110
20> Xor: planes 1, 6 -> 5
21> Mask: pl 5 -> 1, 3 x 3
22> Load image: M3-C90.TIF
23> Limit Asp. r 1 1.00 2.20
24> Filling: plane 1
25> Field meas : plane 1
26> Chord size: pl 1, 2 x 2
27> Feature meas: plane 1

1.3 Analysis Routine for M2-C90 Steel

1> Live
2> Image frame: 0 0 511 476
3> Transition
4> Hist. Mod. : 70, 253
5> Store image: M2-C90.TIF
6> Threshold: pl. 1, oxide 0-52
7> Filling: plane 1
8> Threshold: pl 1, oxide 0-64
9> Xor: planes 1, 2 -> 8
10> Chord size : pl 8 -> 1, 2 x 3
11> Load image : M2-C90. TIF
12> Threshold : pl 3, oxide 0-90
13> Xor : planes 1, 3 -> 4
14> Disconnect : plane 4
15> Chord size : pl 4 -> 1, 3 x 3
16> Load image : M2-C90.TIF
17> Threshold : pl 6, Phase #6 0-100
18> Xor: planes 1, 6 -> 5
19> Mask: pl 5 -> 1, 3 x 3
20> Load image: M2-C90.TIF
21> Limit Asp. r 1 1.00 2.20
22> Field meas. : plane 1
23> Chord size: pl 1, 2 x 2
24> Feature meas.: plane 1

1.4 Analysis Routine for M1-I90C Steel

1>	Live
2>	Image frame: 0 0 511 476
3>	Transition
4>	Hist. Mod. : 63, 253
5>	Store image: M1-I90C.TIF
6>	Threshold: pl. 1, oxide 0-60
7>	Dilation : pl 1 Cross
8>	Erosion : pl 1 Cross
9>	Load image : M1-I90C. TIF
10>	Threshold : pl 2, oxide 0-70
11>	Xor : planes 1, 2 -> 8
12>	Chord size : pl 8 -> 1, 3 x 3
13>	Filling : plane 1
13>	Load image : M1-I90C.TIF
14>	Field meas. : plane 1
15>	Load image : M1-I90C.TIF

1.5 Analysis Routine for M1-I90B Steel

1> Live
2> Image frame: 0, 0, 511, 476
3> Transition
4> Hist. Mod. : 70, 253
5> Store image: M1-I90B.TIF
6> Threshold: pl. 1, oxide 0-90
7> Dilation: pl. 1 Cross
8> Erosion: pl 1 Cross
9> Load image: M1-I90B.TIF
10> Threshold: pl 2, oxide 0-105
11> Xor: planes 1, 2 -> 8
12> Filling: plane 8
13> Chord size: pl 8->1, 2 x 3
14> Chord size: pl 8 8, 6 x 5
15> Or : planes 1, 8 -> 1
16> Load image: M1-I90B.TIF
17> Threshold: pl 3, oxide 0-119
18> Xor: planes 1, 3 -> 4
19> Mask: pl 4 -> 1, 4 x 4
20> Load image: M1-I90B.TIF
21> Threshold: pl 6. Phase #6 0-125
22> Xor: planes 1, 6 -> 5
23> Mask: pl 5 -> 1, 3 x 3
24> Load image: M1-I90B.TIF
25> Limit Asp. r 1 1.00 2.20
26> Filling: plane 1
27> Field meas : plane 1
28> Chord size: pl 1, 2 x 2
29> Feature meas: plane 1

Appendix 2 Oxide Volume Fractions of the Rail Steels

Oxide Volume Fractions(%) of M1-I79 Steel

No.1	No.8	No.15	No.22	No.29	No.36	No.43	No.49
0.0091	0	0	0	0.0066	0	0	0
0	0	0.0896	0	0.466	0	0	0
0.0128	0	0	0	0	0	0	0
0	0.0599	0	0.076	0	0	0	0
0	0	0	0.225	0	0	0	0.142
0.0144	0	0	0	0	0	0	0
0.0153	0	0.0239	0	0	0	0.0433	0
0	0	0	0	0	0	0.0396	0
0.0066	0.1094	0.012	0.1684	0	0.059	0	0
0.0871	0	0.0941	0	0	0	0	0
0	0	0	0	0	0	0	0.019
0.0025	0	0	0	0	0	0	0
0.105	0.0883	0.0669	0.1276	0	0	0	0
0.0037	0	0.0091	0	0	0	0	0
0.0384	0	0	0	0	0	0	0
0.0235	0.0268	0.1626	0.0095	0	0	0	0
0.0116	0	0.0103	0	0	0	0.0153	0
0.0227	0	0	0.0095	0.0925	0	0	0
0.0087	0.1065	0	0	0	0	0.0103	0
0.0066	0	0.0066	0	0	0	0	0.0293
0	0	0.0198	0	0	0	0	0
0	0	0	0	0	0.0264	0.0636	0.0512
0	0	0	0	0	0	0	0
0	0	0	0	0.0656	0	0.0578	0.0384
0	0	0	0	0	0	0	0
0	0.0355	0	0	0	0	0	0
0	0	0	0	0	0	0	0
0	0	0.0524	0	0.0124	0	0	0
0.081	0.033	0	0.0648	0	0	0	0
0	0	0.1643	0	0	0	0.1742	0
0.0099	0	0.2382	0	0	0	0.1598	0
0.0037	0.0087	0	0.0405	0	0	0	0
0	0.0949	0	0	0	0	0	0.0652
0.0103	0.0165	0	0	0	0	0.0103	0
0.0078	0.0326	0	0	0	0	0.0537	0
0.0285	0.071	0	0.0904	0	0	0	0.9197
0.0008	0	0	0	0	0	0.0611	0
0	0.0194	0.014	0	0	0	0.0206	0
0.0533	0	0	0	0	0	0	0
0	0.0553	0	0	0	0.0442	0	0

Ave.	0.0141	0.01894	0.0241	0.0203	0.0161	0.0032	0.0177	0.0316
Std.de	0.0252	0.0329	0.0537	0.0503	0.0751	0.0121	0.0397	0.146

	No.2	No.9	No.16	No.23	No.30	No.37	No.44	No.50
	0	0	0	0	0	0	0	0
	0	0.0821	0	0.0215	0	0	0	0
	0	0	0	0	0.1651	0.0755	0	0
	0	0.0169	0.0318	0	0	0	0	0
	0	0.0128	0	0	0	0.064	0	0
	0.0252	0.0974	0.0087	0	0	0	0	0
	0	0	0	0	0.1552	0	0.0512	0
	0	0.0314	0	0	0	0	0	0
	0	0	0	0.0376	0	0	0	0.1486
	0.0305	0	0	0.1015	0	0	0	0
	0.0074	0.2126	0	0	0.0673	0	0	0
	0.0004	0	0	0	0	0	0	0
	0.0033	0	0	0	0	0.0429	0	0.2774
	0	0	0	0.2415	0	0	0	0
	0	0.0268	0.0239	0	0	0	0	0
	0.0248	0.0318	0	0.1746	0	0	0	0
	0.0054	0	0	0	0	0	0	0
	0.0045	0.0417	0	0	0.1263	0	0	0.1713
	0.0103	0	0	0	0	0	0	0
	0.0033	0.0925	0	0.0227	0	0	0.1536	0
	0.0078	0	0	0	0.0066	0	0	0
	0.005	0.01143	0	0.684	0	0	0.0293	0
	0.0083	0.0801	0	0.0578	0	0	0.0648	0
	0.103	0	0	0	0	0	0.0524	0
	0.0681	0.0305	0	0	0	0.0636	0	0
	0.104	0	0	0.1548	0	0	0	0
	0.0594	0	0	0	0	0	0	0
	0	0.1907	0	0	0	0	0	0
	0.0202	0.0442	0	0	0	0	0	0.0244
	0.0326	0	0.0256	0	0	0.0533	0.1564	0.0239
	0.0314	0	0.0091	0.0066	0	0	0	0
	0	0	0.0256	0	0	0	0.0721	0
	0.0066	0.1825	0	0.0999	0.0198	0	0	0
	0.103	0.0706	0	0	0.644	0	0	0
	0.0004	0.0223	0.045	0	0	0	0.18	0
	0.0025	0	0	0	0	0	0	0
	0.0078	0.0326	0	0	0.1474	0	0	0.1247
	0	0	0	0	0	0	0	0
	0.0107		0	0.0788	0	0	0	0
	0.0169		0	0	0	0	0.0446	0
Ave.	0.0176	0.0345	0.0042	0.042	0.0333	0.0075	0.0201	0.0192
Std.de	0.0292	0.0558	0.0106	0.1179	0.1091	0.0204	0.0458	0.0578

	No.3	No.10	No.17	No.24	No.31	No.38	No.45
	0.0239	0	0	0	0	0.123	0
	0.2382	0	0.014	0	0	0	0
	0	0.0314	0	0	0	0	0
	0	0	0	0	0	0	0
	0	0.0095	0	0	0	0	0.0483
	0	0	0	0	0	0	0
	0	0	0.019	0	0	0	0.0359
	0	0	0	0	0	0	0
	0.0211	0.0487	0	0.045	0	0	0
	0.0206	0.0677	0	0	0	0.026	0
	0.0541	0	0	0	0	0	0
	0.0144	0.0384	0.0409	0	0	0	0
	0	0	0.0132	0.0458	0	0	0
	0	0	0.057	0	0	0	0
	0	0	0	0	0	0	0.0788
	0.1152	0.0305	0	0	0.1288	0	0.0153
	0	0	0.0326	0.0372	0.1057	0.2192	0.1717
	0	0	0	0.0136	0	0.2914	0
	0	0	0	0.0277	0	0	0
	0	0	0	0.0586	0.1453	0	0.0677
	0	0.0256	0.0223	0	0	0	0
	0	0	0	0	0.0334	0	0
	0	0.0223	0	0	0	0	0
	0	0	0	0.0933	0	0	0
	0	0.0149	0	0	0	0	0
	0.045	0.0475	0	0	0	0.0376	0
	0	0	0	0	0.0297	0	0
	0.0111	0.2056	0.0186	0	0	0	0.0594
	0.0879	0	0	0	0.0491	0	0
	0	0	0	0	0	0	0
	0.052	0.0739	0.0396	0.0272	0	0	0.0636
	0.0516	0.6204	0	0	0	0	0
	0	0	0	0	0.123	0	0.0157
	0	0	0.1837	0	0	0	0
	0	0	0.0095	0	0	0	0.0314
	0	0.0516	0	0	0	0	0
	0.0541	0	0	0	0	0	0
	0	0	0	0	0	0	0.1086
	0	0.1189	0	0	0	0	0
	0	0.0107		0	0	0	0.026
Ave.	0.0197	0.0354	0.0115	0.0087	0.0154	0.0107	0.0181
Std.de	0.0445	0.1016	0.0315	0.02045	0.0389	0.0594	0.0366

	No.4	No.11	No18	No.25	No.32	No.39	No.46
	0	0.0285	0	0	0	0.0343	0.1044

	0	0	0	0	0	0	0
	0	0.0116	0	0	0.1692	0	0
	0	0	0	0	0	0	0.1234
	0.0425	0.0681	0.2378	0	0	0	0.1214
	0.1705	0	0	0	0	0	0
	0	0	0.8623	0	0	0	0
	0	0	0	0	0	0	0
	0	0.0107	0	0	0	0.1676	0
	0	0.031	0	0.0215	0	0	0
	0	0	0.0652	0	0	0	0
	0.0458	0	0	0	0	0	0
	0	0.0227	0.0272	0	0	0.0545	0
	0	0.0169	0	0.0239	0	0	0
	0.1362	0.1024	0.052	0	0	0.0409	0
	0	0	0	0.109	0	0	0
	0	0	0.0615	0	0	0.3612	0
	0	0	0	0	0	0	0
	0	0	0	0	0.0289	0	0
	0	0	0	0	0	0.0793	0
	0	0	0.0355	0	0	0	0
	0	0	0	0	0	0	0.0301
	0	0.0066	0	0	0	0.412	0
	0.194	0	0	0.0681	0	0	0.0632
	0	0.1408	0	0	0	0.1234	0
	0.1907	0	0	0	0	0	0.466
	0	0	0.0405	0	0	0	0
	0	0	0	0	0.085	0	0
	0	0	0	0	0	0.317	0.0297
	0	0.3963	0.2056	0	0	0	0
	0	0	0	0.0821	0	0	0
	0	0.2489	0.0297	0	0	0.0091	0
	0	0.2118	0	0	0	0	0
	0.1783	0	0	0	0.038	0.2374	0
	0	0	0	0.1119	0	0	0
	0	0	0	0.0268	0.4021	0	0
	0	0	0	0	0	0	0
	0	0.0248	0.0103	0	0.0293	0	0
	0	0	0	0.014	0	0	0
	0	0	0	0	0	0	0
Ave.	0.0239	0.033	0.0407	0.0114	0.0188	0.0459	0.0234
Std.de	0.0587	0.0814	0.142	0.0289	0.0691	0.0105	0.0787
	No5.	No.12	No19	No.26	No.33	No.40	No.47
	0	0	0	0	0	0	0
	0	0	0	0	0.968	0	0
	0	0	0	0	0	0	0

	0.0215	0.0978	0	0	0.0066	0	0
	0	0	0	0	0	0	0
	0	0	0	0	0	0	0
	0	0	0.033	0	0	0	0
	0	0	0	0	0	0	0
	0	0	0	0.0194	0	0	0
	0	0	0	0	0	0	0.0136
	0	0	0.0244	0	0	0	0.0087
	0	0	0	0	0	0.0297	0
	0	0	0	0	0	0	0
	0	0	0	0.0256	0	0	0.0305
	0	0	0	0	0.019	0.0231	0
	0.057	0	0	0	0	0	0.0805
	0	0.0859	0	0.0153	0	0	0
	0	0	0	0	0	0.2118	0
	0	0	0.0198	0	0	0.0718	0
	0.045	0	0	0	0	0	0
	0	0	0	0	0	0	0.0111
	0	0.0545	0	0	0	0	0
	0	0	0	0	0.0376	0	0
	0	0	0	0.0264	0	0.0925	0
	0	0	0	0	0	0	0
	0	0	0	0	0	0	0
	0	0	0	0	0	0	0
	0	0	0	0	0.0904	0	0.0665
	0.0099	0.2147	0	0	0	0	0.1102
	0	0	0	0	0	0	0.2109
	0	0	0	0	0	0	0
	0.0648	0	0	0	0	0	0
	0	0.0078	0	0	0	0	0.0644
	0	0	0	0	0	0	0
	0.1536	0	0	0.0227	0.142	0	0.0149
	0	0.0211	0	0	0	0	0
	0	0	0	0	0	0	0
	0.0281	0.0095	0	0	0	0	0
	0	0	0.0363	0	0	0	0.1523
	0.0698	0	0	0	0	0	0
Ave.	0.0112	0.0123	0.0028	0.0027	0.03159	0.0107	0.0191
Std.de	0.03	0.0394	0.0089	0.0075	0.1541	0.0377	0.0458
	No.6	No.13	No.20	No.27	No.34	No.41	No.48
	0	0	0	0.0297	0	0	0.107
	0.0194	0	0.0689	0	0.0248	0	0
	0.0223	0	0	0	0	0	0
	0.0103	0	0	0.0314	0	0	0
	0	0	0	0	0	0.1494	0

	0.012	0.0078	0	0	0	0	0
	0	0	0	0.343	0	0	0
	0.0623	0	0.1882	0	0	0	0
	0.2642	0	0.0124	0	0	0	0
	0	0.0817	0	0.0066	0	0	0
	0.012	0	0.8289	0	0	0	0.0966
	0.064	0.0566	0	0	0	0	0.0144
	0.0095	0.5544	0.0301	0	0.102	0	0
	0.0182	0	0	0	0	0	0
	0.0735	0.0937	0	0	0	0.0553	0
	0	0.4528	0	0	0	0.0227	0
	0.0095	0	0	0	0	0	0
	0	0	0	0	0.0293	0	0
	0	0.2175	0.0087	0	0	0.27	0
	0.0293	0	0	0	0	0.0099	0
	0.5507	0	0	0	0	0.2712	0
	0.0351	0.0078	0	0	0	0	0
	0.1135	0	0	0	0.1222	0.0318	0.3373
	0	0	0	0	0	0.3026	0
	0.0202	0	0	0	0	0.0524	0
	0	0	0	0.0636	0	0.0813	0
	0.13	0	0.0198	0	0	0	0
	0	0	0	0.0149	0	0	0
	0.0343	0	0	0	0	0	0.0223
	0.0107	0.0161	0	0	0.1197	0	0
	0	0	0.3108	0	0	0	0
	0	0	0	0.0359	0	0	0
	0	0	0	0	0	0	0
	0	0	0	0.1296	0.0157	0.206	0
	0	0	0	0	0	0.0124	0
	0	0	0	0	0	0	0
	0.0293	0		0		0	0
	0.0285	0	0	0	0	0.0462	0.0338
	0	0	0	0	0	0	0
	0	0	0	0	0.324	0	0
Ave.	0.039	0.0372	0.0376	0.01637	0.0189	0.0378	0.0153
Std.de	0.0964	0.1158	0.1424	0.058	0.059	0.0819	0.0571
	No.7	No.14	No.21	No.28	No.35	No.42	No.49
	0.1313	0	0	0	0	0	
	0.1936	0	0	0.1721	0.0239	0.0508	
	0	0	0	0	0	0	
	0	0	0.0095	0.0231	0	0	
	0.0103	0	0	0	0	0	
	0.0182	0	0.1631	0	0	0	
	0.0095	0	0	0	0	0	

	0	0	0	0	0	0
	0	0	0	0.0314	0	0
	0	0	0	0	0	0
	0	0.0611	0	0	0	0
	0	0.0384	0	0	0	0.1094
	0.0128	0	0.0429	0	0	0
	0.0153	0.0078	0.0363	0	0	0
	0	0	0.0202	0	0	0
	0.1329	0	0.0178	0	0	0.0165
	0	0	0.0227	0	0	0
	0	0.1833	0.0087	0	0	0
	0.033	0	0	0	0	0
	0	0	0	0	0	0
	0.0239	0	0	0.1424	0	0
	0.0438	0.2436	0	0	0	0
	0	0	0	0	0	0
	0	0	0	0.0458	0.1296	0
	0	0	0.083	0	0	0
	0	0	0	0	0	0
	0.0223	0	0	0	0	0
	0	0	0	0	0	0
	0.0632	0	0	0	0.2683	0
	0	0	0	0	0	0
	0	0	0	0	0	0
	0	0	0	0.0322	0	0
	0	0	0	0	0	0
	0.0244	0	0	0	0	0
	0.0442	0	0	0	0.0161	0
	0	0.012	0.1276	0	0.3785	0
	0.1602	0	0.0219	0	0	0
	0	0.0099	0.0194	0	0.549	0
		0	0	0	0	0
		0	0.0516	0.1548	0	0.3682
Ave.	0.0247	0.0139	0.0156	0.0154	0.0341	0.01362
Std.de	0.0641	0.04823	0.0351	0.0422	0.1118	0.06055

Oxide Volume Fractions (%) of M2-C88 Steel

Field #	No.1	No.5	No.9	No.13	No.17	No.21	No.25	No.29
1	0	0	0	0	0	0	0	—
2	0	0	0	0	0	0	0.0095	—
3	0	0	0	0	0	0	0.0124	—
4	0	0	0	0	0	0	0	—
5	0	0	0	0	0	0	0	—
6	0	0	0	0	0	0	0	—
7	0	0	0	0	0	0	0.0351	—
8	0	0	0	0	0	0	0	—
9	0	0	0	0	0	0	0	—
10	0	0	0	0	0	0	0	—
11	0	0	0	0	0	0	0	—
12	0	0	0	0	0	0	0	—
13	0	0	0	0	0	0	0	—
14	0	0	0	0	0	0	0	—
15	0	0	0	0	0	0	0	—
16	0	0	0	0	0.0272	0	0	—
17	0.0285	0	0	0	0	0	0.0305	—
18	0	0	0	0	0	0	0	—
19	0	0.0227	0	0	0	0	0	—
20	0	0	0	0	0	0	0	—
21	0	0	0.0285	0	0	0.0433	0	—
22	0	0	0	0	0	0	0	—
23	0	0	0	0.0652	0	0	0.0083	—
24	0	0	0	0	0	0	0	—
25	0	0	0	0	0	0	0	—
26	0	0	0	0	0.0256	0	0	—
27	0	0	0	0	0	0	0	—
28	0	0	0	0	0	0	0	—
29	0.1752	0.0194	0	0	0	0	0	—
30	0	0	0	0	0	0	0	—
31	0	0	0.1139	0	0	0	0	—
32	0	0	0	0	0	0	0	—
33	0	0.0066	0	0	0	0	0	—
34	0.0078	0	0	0	0	0	0	—
35	0	0	0	0	0.0334	0	0	—
36	0	0	0.014	0	0	0	0	—
37	0	0	0	0	0.0277	0	0	—
38	0	0	0	0	0	0	0	—
39	0	0	0	0	0	0	0	—
40	0	0	0	0	0	0	0.0264	—
41	0	0	0	0.0239	0	0	0	—

42	0	0	0	0	0	0	0	—
43	0	0	0	0	0	0	0	—
44	0	0	0	0	0	0	0	—
45	0	0	0	0	0.0149	0	0	—
46	0	0	0	0	0	0	0	—
47	0	0	0	0	0	0	0	—
48	0	0	0.0198	0.0904	0	0	0.0512	—
49	0	0.0603	0.0227	0	0	0	0	—
50	0	0	0	0	0	0	0	—
Ave.	0.0041	0.0022	0.004	0.0044	0.0026	0.001	0.0035	
Std.dev	0.0248	0.0094	0.0168	0.0167	0.008	0.0062	0.0103	
Ave.	0.0041	0.0022	0.004	0.0044	0.0026	0.001	0.0035	0.0067
Std.dev	0.0248	0.0094	0.0168	0.0167	0.008	0.0062	0.0103	—

Field #	No.2	No.6	No.10	No.14	No.18	No.22	No.26	No.30
1	0	0	0	0	0	0	0	—
2	0	0	0.0561	0	0	0	0.0351	—
3	0	0	0	0	0	0	0	—
4	0	0	0	0	0	0	0	—
5	0	0	0	0	0	0	0.0252	—
6	0	0	0	0	0	0	0	—
7	0	0	0	0.0425	0	0	0	—
8	0.0582	0	0	0	0	0	0	—
9	0	0	0.0363	0.0045	0	0	0	—
10	0	0	0	0	0.0351	0	0.0136	—
11	0	0	0	0	0	0	0.0499	—
12	0	0	0	0.0272	0	0	0	—
13	0	0	0	0	0.0215	0	0	—
14	0	0	0	0	0	0	0	—
15	0	0	0.0074	0	0	0	0	—
16	0	0	0	0	0	0.0277	0	—
17	0	0	0	0	0	0	0	—
18	0	0	0	0	0	0	0.0132	—
19	0	0	0	0	0	0	0	—
20	0	0	0	0.0132	0.0056	0	0	—
21	0	0	0	0	0	0	0	—
22	0	0	0	0	0	0	0.0206	—
23	0	0	0	0	0	0	0	—
24	0	0	0	0	0	0	0.0107	—
25	0	0	0	0	0.0194	0	0	—
26	0	0	0	0.0698	0.0409	0	0.0429	—
27	0	0	0	0	0	0	0.0144	—
28	0	0	0	0.0178	0	0	0	—
29	0	0.154	0	0	0	0	0	—
30	0	0	0	0	0.0153	0	0	—

31	0	0	0	0	0	0	0	—
32	0.0561	0	0	0	0.0111	0	0	—
33	0	0	0	0	0.0264	0	0	—
34	0	0	0	0	0	0	0	—
35	0	0.0813	0	0	0.0322	0.1725	0	—
36	0	0	0	0	0	0	0.014	—
37	0	0	0	0	0.0264	0	0.0214	—
38	0	0	0	0	0	0	0.0091	—
39	0.0409	0	0	0.0516	0	0	0.0409	—
40	0	0.0376	0	0	0.0669	0	0	—
41	0.0409	0	0	0.0272	0	0	0	—
42	0	0	0	0	0	0	0.0838	—
43	0	0	0	0	0	0	0	—
44	0	0	0	0	0	0	0	—
45	0	0	0	0	0.0198	0	0	—
46	0	0	0	0	0	0	0.045	—
47	0	0	0.0285	0	0.012	0	0	—
48	0	0	0	0	0	0	0	—
49	0	0	0	0	0.0206	0	0	—
50	0	0	0	0	0.0206	0	0	—
Ave.	0.0039	0.0024	0.0026	0.0064	0.0087	0.0006	0.0088	
Std.dev	0.0136	0.0127	0.0101	0.0172	0.0164	0.0039	0.0174	
Ave.	0.0039	0.0054	0.0026	0.0064	0.0087	0.004	0.0088	0.0052
Std.dev	0.0136	0.0248	0.0101	0.0172	0.0164	0.0246	0.0174	—

Field #	No.3	No.7	No.11	No.15	No.19	No.23	No.27
1	0	0	0	0	0	0	0.0144
2	0	0	0	0.0949	0	0	0.0107
3	0	0.0396	0	0	0.0297	0	0
4	0	0.0206	0	0	0	0	0
5	0	0	0	0	0	0	0.0107
6	0	0	0	0	0	0	0
7	0	0	0	0	0	0	0
8	0	0	0	0	0.0421	0	0
9	0	0	0	0	0	0	0
10	0	0.0173	0	0	0	0	0
11	0	0	0	0	0.0045	0	0
12	0	0	0	0	0.011	0	0
13	0	0	0	0	0.0178	0	0
14	0	0	0	0	0.0116	0	0
15	0	0.0157	0	0	0	0	0
16	0	0	0	0	0	0	0
17	0	0.0202	0	0	0	0	0
18	0	0	0	0	0.0392	0	0
19	0	0	0	0	0	0	0

20	0	0	0	0.0355	0.0043	0	0
21	0	0	0	0.031	0	0	0
22	0.0995	0	0	0	0.0091	0	0
23	0.0801	0	0	0	0	0	0
24	0	0	0	0	0	0	0
25	0	0	0	0	0	0	0
26	0	0	0	0	0.0372	0	0
27	0	0	0	0	0	0	0
28	0	0	0	0	0	0	0.052
29	0	0	0.1168	0	0	0	0
30	0	0	0	0.0161	0.0533	0	0
31	0	0	0	0	0	0	0
32	0.1511	0	0	0	0	0	0
33	0	0	0	0.0974	0	0	0
34	0	0	0.038	0	0.0056	0	0
35	0	0	0	0	0	0	0
36	0	0.019	0	0.1697	0	0	0
37	0	0	0	0	0.0178	0	0
38	0	0	0	0	0	0	0.0504
39	0	0	0	0	0	0	0
40	0	0	0	0	0	0	0
41	0	0	0	0	0	0	0
42	0	0	0	0.0425	0	0	0
43	0	0	0	0	0	0	0
44	0	0	0.1969	0	0	0	0
45	0	0.0314	0	0	0	0	0
46	0	0	0	0	0	0	0
47	0	0	0	0	0	0	0.0091
48	0	0	0	0	0	0	0.0215
49	0	0	0	0.0248	0	0	0
50	0	0	0	0	0	0	0
Ave.	**0.0037**	**0.0021**	**0.0031**	**0.0102**	**0.0119**	**0**	**0.0034**
Std.dev	**0.0181**	**0.0065**	**0.0174**	**0.031**	**0.0265**	**0**	**0.0107**
Ave.	**0.0068**	**0.0021**	**0.007**	**0.0102**	**0.0119**	**0**	**0.0034**
Std.dev	**0.0274**	**0.0065**	**0.0324**	**0.031**	**0.0265**	**0**	**0.0107**

Field #	No.4	No.8	No.12	No.16	No.20	No.24	No.28
1	0	0.1601	0	---	0	0	
2	0	0	0	---	0.0239	0	
3	0	0	0	---	0	0	
4	0	0	0	---	0	0	
5	0	0	0	---	0	0	
6	0	0	0	---	0	0	
7	0	0	0	---	0.0191	0	
8	0	0	0	---	0	0.0149	

9	0	0	0	---	0	0	
10	0	0	0	---	0	0	
11	0	0	0	---	0	0	
12	0	0	0	---	0	0	
13	0	0	0	---	0.0293	0	
14	0	0	0	---	0	0	
15	0	0	0	---	0	0	
16	0	0	0	---	0.0541	0	
17	0	0	0	---	0	0	
18	0	0	0	---	0	0	
19	0	0	0	---	0.0677	0	
20	0	0	0	---	0	0	
21	0	0	0	---	0	0	
22	0	0	0	---	0	0	
23	0	0	0	---	0	0.0227	
24	0	0	0	---	0	0	
25	0	0	0.0405	---	0	0	
26	0	0	0	---	0	0	
27	0	0	0	---	0	0	
28	0	0	0.306	---	0.0578	0	
29	0	0	0	---	0	0.0322	
30	0	0	0	---	0	0	
31	0	0.0301	0	---	0	0	
32	0	0	0	---	0	0	
33	0	0	0	---	0.0099	0	
34	0.0066	0	0	---	0	0	
35	0	0	0	---	0	0.0297	
36	0	0	0	---	0	0	
37	0	0.0078	0	---	0.0264	0	
38	0	0	0.0066	---	0	0	
39	0	0	0	---	0	0	
40	0	0	0	---	0	0	
41	0	0	0.0211	---	0	0	
42	0	0.0157	0.0066	---	0	0	
43	0.0499	0	0	---	0	0	
44	0	0	0	---	0	0	
45	0	0	0	---	0	0	
46	0	0	0	---	0	0	
47	0	0	0	---	0	0	
48	0	0	0	---	0	0	
49	0	0	0	---	0	0	
50	0	0	0	---	0	0	
Ave.	**0.0011**	**0.0011**	**0.0015**		**0.0058**	**0.002**	
Std.dev	**0.0071**	**0.0049**	**0.0065**		**0.0155**	**0.0071**	
Ave.	**0.0011**	**0.0043**	**0.0076**	**0.0049**	**0.0058**	**0.002**	**0.0048**

Std.dev	0.0071	0.0231	0.0436	---	0.0155	0.0071	---

Oxide Volume Fractions of M3-C90 Steel

Field #	231-1	231-2	231-3	231-4	231-5	231-6	231-7	231-8
1.0000	0.0000	0.0859	0.0000	0.0000	0.0000	0.0000	0.0000	0.0000
2.0000	0.0000	0.0000	0.0000	0.0000	0.0000	0.0000	0.0652	0.0000
3.0000	0.0000	0.0000	0.0000	0.0000	0.0000	0.0000	0.0000	0.0000
4.0000	0.0000	0.0000	0.0000	0.0000	0.0000	0.0000	0.0000	0.0000
5.0000	0.0000	0.0000	0.0000	0.0000	0.0000	0.0000	0.0000	0.0000
6.0000	0.0000	0.0087	0.0000	0.0000	0.0000	0.0000	0.0000	0.0000
7.0000	0.0000	0.0000	0.0000	0.0000	0.0000	0.0000	0.0000	0.0000
8.0000	0.1544	0.0000	0.0000	0.0000	0.0000	0.0000	0.0000	0.0000
9.0000	0.0000	0.0000	0.0000	0.0000	0.0000	0.0000	0.0000	0.0000
10.0000	0.0000	0.0000	0.0000	0.0000	0.0000	0.0000	0.0000	0.0000
11.0000	0.0000	0.0000	0.0000	0.0000	0.0000	0.1981	0.0235	0.0000
12.0000	0.0000	0.0000	0.0000	0.0000	0.0000	0.0000	0.0000	0.0000
13.0000	0.0000	0.0000	0.0000	0.0000	0.0000	0.0000	0.0000	0.0000
14.0000	0.0000	0.0000	0.0000	0.0000	0.0000	0.0000	0.0000	0.0000
15.0000	0.0000	0.0000	0.0000	0.0000	0.0000	0.0000	0.0000	0.0000
16.0000	0.0788	0.0000	0.0000	0.0000	0.0000	0.0000	0.0000	0.0000
17.0000	0.0000	0.0000	0.0000	0.0000	0.0000	0.0000	0.0483	0.0516
18.0000	0.0000	0.0000	0.0000	0.0000	0.0000	0.0000	0.0000	0.0000
19.0000	0.0000	0.0000	0.0000	0.0000	0.0000	0.0000	0.0000	0.0000
20.0000	0.0000	0.0000	0.0000	0.0000	0.0000	0.0000	0.0000	0.0277
21.0000	0.0000	0.0793	0.0000	0.0000	0.0000	0.0000	0.0000	0.0000
22.0000	0.0165	0.0000	0.0000	0.0000	0.0000	0.0000	0.0000	0.0000
23.0000	0.0000	0.0000	0.0000	0.0000	0.0000	0.0000	0.0000	0.0000
24.0000	0.0000	0.0000	0.0000	0.0000	0.0000	0.0000	0.0144	0.0000
25.0000	0.0000	0.0000	0.0000	0.0466	0.0000	0.0000	0.0000	0.0000
26.0000	0.0000	0.0000	0.0000	0.0000	0.0000	0.0000	0.0000	0.0483
27.0000	0.0000	0.0000	0.0000	0.0000	0.0000	0.0000	0.0000	0.0000
28.0000	0.0000	0.0000	0.0000	0.0000	0.0000	0.0000	0.0000	0.0132
29.0000	0.0000	0.0000	0.0000	0.0000	0.0000	0.0000	0.0000	0.0000
30.0000	0.0000	0.0000	0.0000	0.0000	0.0000	0.0000	0.0000	0.0000
31.0000	0.0000	0.0000	0.0000	0.0000	0.0000	0.0000	0.0000	0.0000
32.0000	0.0000	0.0000	0.0000	0.0000	0.0000	0.0000	0.0000	0.0000
33.0000	0.0000	0.0000	0.0000	0.0000	0.0000	0.0000	0.0000	0.0000
34.0000	0.2658	0.0000	0.0000	0.0000	0.0000	0.0000	0.0000	0.0037
35.0000	0.0000	0.0000	0.0000	0.0000	0.0710	0.0000	0.0000	0.0000
36.0000	0.0409	0.0000	0.0000	0.0000	0.0000	0.0000	0.0000	0.0000

37.0000	0.0000	0.0000	0.0000	0.0000	0.0000	0.0000	0.0000	0.0000
38.0000	0.0000	0.0000	0.0000	0.0000	0.0000	0.0863	0.0000	0.0689
39.0000	0.0000	0.0000	0.0000	0.0000	0.0000	0.0000	0.0000	0.0425
40.0000	0.0000	0.0000	0.0000	0.0000	0.0000	0.0000	0.0000	0.0438
41.0000	0.0000	0.0000	0.0000	0.0000	0.1057	0.0000	0.0000	0.0000
42.0000	0.0000	0.0000	0.0000	0.0000	0.0000	0.0000	0.0000	0.0000
43.0000	0.0000	0.0000	0.0000	0.0000	0.0000	0.0231	0.0000	0.0000
44.0000	0.0000	0.0000	0.0685	0.0000	0.0000	0.0000	0.0000	0.0000
45.0000	0.0000	0.0000	0.0000	0.0000	0.0000	0.0000	0.0000	0.0000
46.0000	0.0000	0.0000	0.0000	0.0000	0.0000	0.0000	0.0000	0.0000
47.0000	0.0186	0.0000	0.0000	0.0000	0.0000	0.0000	0.0144	0.0000
48.0000	0.0000	0.0000	0.0000	0.0000		0.0000	0.0000	0.0000
49.0000	0.0000	0.0000	0.0372	0.0000		0.0000	0.0000	0.0000
50.0000	0.0000	0.0000	0.0000	0.0000		0.0000	0.0000	0.0000
51.0000	0.0000	0.0000	0.0000	0.0000				
52.0000	0.0000	0.0000	0.0000	0.0000				
53.0000	0.0000	0.0000	0.0000	0.0000				
54.0000	0.0000	0.0000	0.0000	0.0000				
55.0000	0.0000	0.0000	0.0000	0.0000				
56.0000	0.0000	0.0000	0.0000	0.0000				
57.0000	0.0000	0.0000	0.0000	0.0000				
58.0000	0.0000	0.0000	0.0000	0.0000				
59.0000	0.0000	0.0000	0.0190	0.0000				
60.0000	0.0000	0.0000	0.0000	0.0000				
Ave. %	0.0096	0.0029	0.0021	0.0008	0.0037	0.0062	0.0033	0.0060
Std. dev	0.0403	0.0149	0.0101	0.0060	0.0182	0.0301	0.0118	0.0159

Field #	231-9	231-10	231-11	231-12	231-13	231-14	231-15	231-16
1.0000	0.0025	0.0000	0.0000	0.0000	0.0000	0.0000	0.0000	0.0000
2.0000	0.0000	0.0000	0.0153	0.0000	0.0000	0.0000	0.0000	0.0000
3.0000	0.0000	0.0000	0.0000	0.0116	0.0000	0.0000	0.0000	0.0000
4.0000	0.0008	0.0000	0.0000	0.0000	0.0000	0.0000	0.0000	0.0000
5.0000	0.0000	0.0000	0.0000	0.0000	0.0000	0.0248	0.0000	0.0000
6.0000	0.0000	0.0000	0.0000	0.0466	0.0000	0.0000	0.0000	0.0000
7.0000	0.0000	0.0000	0.0173	0.0000	0.0000	0.0000	0.0220	0.0000
8.0000	0.0000	0.0000	0.0000	0.0000	0.0000	0.0000	0.0000	0.0000
9.0000	0.0000	0.0000	0.0000	0.0000	0.0000	0.0000	0.0000	0.0000
10.0000	0.0000	0.0000	0.0000	0.0000	0.0000	0.0000	0.0000	0.0000

11.0000	0.0000	0.0000	0.0000	0.0000	0.0000	0.0000	0.0000	0.0000
12.0000	0.0000	0.0000	0.0000	0.0000	0.0000	0.0000	0.0000	0.0000
13.0000	0.0000	0.0000	0.0000	0.0227	0.0000	0.0000	0.0000	0.0000
14.0000	0.0000	0.0000	0.0252	0.0000	0.0000	0.0000	0.0549	0.0000
15.0000	0.0000	0.0000	0.0000	0.0000	0.0000	0.0000	0.0000	0.0000
16.0000	0.0000	0.0000	0.0000	0.0000	0.0000	0.0318	0.0000	0.0000
17.0000	0.0272	0.0000	0.0000	0.0000	0.0000	0.0000	0.0000	0.0000
18.0000	0.0000	0.0000	0.0000	0.0000	0.0000	0.0000	0.0021	0.0000
19.0000	0.0000	0.0000	0.0000	0.0000	0.0000	0.0000	0.0000	0.0000
20.0000	0.0000	0.0000	0.0000	0.0000	0.0000	0.0000	0.0000	0.0466
21.0000	0.0000	0.0000	0.0095	0.0000	0.0000	0.0000	0.0000	0.0169
22.0000	0.0000	0.0000	0.0400	0.0116	0.0000	0.0706	0.0000	0.0000
23.0000	0.0000	0.0000	0.0000	0.0000	0.2485	0.0000	0.0000	0.0000
24.0000	0.0000	0.2039	0.0178	0.0000	0.0000	0.0000	0.0000	0.0000
25.0000	0.0000	0.0000	0.0000	0.0000	0.0442	0.0000	0.0000	0.0000
26.0000	0.0000	0.0000	0.0000	0.0949	0.0000	0.0136	0.0000	0.0000
27.0000	0.0000	0.0000	0.0000	0.0000	0.0000	0.0000	0.0480	0.0000
28.0000	0.0000	0.0000	0.0000	0.0000	0.0000	0.0000	0.0000	0.0000
29.0000	0.0223	0.0149	0.0000	0.0000	0.0000	0.0000	0.0000	0.0000
30.0000	0.0000	0.0000	0.0000	0.0000	0.0000	0.0000	0.0100	0.0157
31.0000	0.0000	0.0000	0.0000	0.0000	0.0000	0.0000	0.0000	0.0000
32.0000	0.0000	0.0000	0.0000	0.0000	0.0000	0.0000	0.0000	0.0000
33.0000	0.0000	0.0000	0.0000	0.0165	0.0000	0.0000	0.0000	0.0144
34.0000	0.0000	0.1065	0.0000	0.0000	0.0000	0.0000	0.0180	0.0000
35.0000	0.0000	0.0000	0.0000	0.0000	0.0000	0.0000	0.0000	0.0000
36.0000	0.0000	0.0000	0.0037	0.0000	0.0000	0.0000	0.0250	0.0000
37.0000	0.0000	0.0000	0.2857	0.0000	0.0000	0.0000	0.0000	0.0000
38.0000	0.0000	0.0966	0.0000	0.0091	0.0000	0.0000	0.0000	0.0000
39.0000	0.0000	0.0256	0.0000	0.0000	0.0000	0.0000	0.0000	0.0000
40.0000	0.0421	0.0000	0.0000	0.0000	0.0000	0.0215	0.0000	0.0000
41.0000	0.0000	0.0000	0.0211	0.0004	0.0000	0.0000	0.0000	0.0000
42.0000	0.1044	0.0000	0.0000	0.0359	0.0000	0.0000	0.0000	0.0000
43.0000	0.0000	0.0000	0.0000	0.0000	0.0000	0.0000	0.0000	0.0000
44.0000	0.0000	0.0000	0.0000	0.0000	0.0000	0.0000	0.0000	0.0194
45.0000	0.0000	0.0000	0.0000	0.0124	0.0000	0.0000	0.0000	0.0000
46.0000	0.0000	0.0000	0.0372	0.0211	0.0219	0.0000	0.0000	0.0000
47.0000	0.0000	0.0000	0.0000	0.0330	0.0000	0.0000	0.0000	0.0000
48.0000	0.0000	0.0000	0.0000	0.0165	0.0206	0.0000	0.0150	0.0000
49.0000	0.0000	0.0000	0.0000	0.0000	0.0000	0.0000	0.0000	0.0000
50.0000	0.0000	0.0000	0.0000	0.0000	0.0000	0.0000	0.0000	0.0000

Ave. %	0.0040	0.0089	0.0095	0.0066	0.0067	0.0032	0.0039	0.0023
Std.dev.	0.0162	0.0344	0.0405	0.0163	0.0353	0.0116	0.0112	0.0078

Field #	231-17	231-18	231-19	231-20	231-21	231-22	231-23
1.0000	0.0000	0.0000	0.0000	0.0000	0.0000	0.0000	0.0370
2.0000	0.0000	0.1070	0.0000	0.0000	0.0000	0.0000	0.0000
3.0000	0.0000	0.0000	0.0000	0.0066	0.0000	0.0000	0.0000
4.0000	0.0000	0.0000	0.0000	0.0099	0.0000	0.0000	0.0000
5.0000	0.0000	0.0000	0.0000	0.0000	0.0157	0.0000	0.1061
6.0000	0.0000	0.0227	0.0000	0.0000	0.0000	0.0000	0.0000
7.0000	0.0000	0.0000	0.0000	0.0000	0.0000	0.0000	0.0045
8.0000	0.0000	0.0000	0.0000	0.0801	0.0000	0.0000	0.0000
9.0000	0.0000	0.0000	0.0000	0.0107	0.0000	0.0182	0.0000
10.0000	0.0000	0.0000	0.0000	0.0000	0.0000	0.0062	0.0000
11.0000	0.0000	0.0000	0.0000	0.0000	0.0091	0.0000	0.0074
12.0000	0.0000	0.0000	0.0000	0.0074	0.0000	0.0111	0.0050
13.0000	0.0260	0.0000	0.0000	0.0000	0.0000	0.0000	0.0000
14.0000	0.0000	0.0000	0.0000	0.0000	0.0000	0.0000	0.0000
15.0000	0.0000	0.0000	0.0000	0.0000	0.0000	0.0000	0.0000
16.0000	0.0000	0.0000	0.0000	0.0000	0.0000	0.0000	0.0000
17.0000	0.0000	0.0000	0.0000	0.1049	0.0000	0.0619	0.0000
18.0000	0.0000	0.0000	0.0000	0.0000	0.0000	0.0916	0.0000
19.0000	0.0000	0.0000	0.0000	0.0000	0.0000	0.0000	0.0000
20.0000	0.0000	0.0000	0.0000	0.0000	0.0000	0.0000	0.0000
21.0000	0.0000	0.0000	0.0000	0.0000	0.0000	0.0000	0.0000
22.0000	0.0000	0.0000	0.0000	0.0000	0.0000	0.0372	0.0000
23.0000	0.0000	0.0000	0.0000	0.0103	0.0000	0.0000	0.0000
24.0000	0.0000	0.0301	0.0000	0.0107	0.0000	0.0000	0.0000
25.0000	0.0000	0.0103	0.0000	0.0000	0.0000	0.0000	0.0000
26.0000	0.0000	0.0000	0.0000	0.0000	0.0000	0.0000	0.0000
27.0000	0.0000	0.0000	0.0500	0.0000	0.0000	0.0000	0.0000
28.0000	0.0000	0.0000	0.0000	0.0000	0.0000	0.0000	0.0000
29.0000	0.0281	0.0000	0.0000	0.0037	0.0000	0.0058	0.0000
30.0000	0.0066	0.0000	0.0000	0.0161	0.0000	0.0000	0.0000
31.0000	0.0000	0.0000	0.0520	0.0000	0.0000	0.0000	0.0215
32.0000	0.0000	0.0000	0.0000	0.0000	0.2535	0.0000	0.0000
33.0000	0.0000	0.0000	0.0000	0.0000	0.0000	0.0000	0.0000
34.0000	0.0000	0.0000	0.0000	0.0000	0.1086	0.0000	0.0000

35.0000	0.0000	0.0000	0.0000	0.0000	0.0000	0.0000	0.0000
36.0000	0.0000	0.0000	0.0000	0.0000	0.0000	0.0000	0.0000
37.0000	0.0000	0.0000	0.0900	0.0487	0.0000	0.0000	0.0000
38.0000	0.0000	0.0000	0.0000	0.0000	0.0000	0.0000	0.0000
39.0000	0.0000	0.0000	0.0000	0.0000	0.0000	0.0000	0.0000
40.0000	0.0582	0.0000	0.0000	0.0000	0.0000	0.0000	0.0000
41.0000	0.0000	0.0000	0.0000	0.0000	0.0000	0.0000	0.0000
42.0000	0.0000	0.0450	0.0000	0.0000	0.0000	0.0091	0.0000
43.0000	0.0198	0.0078	0.0359	0.0000	0.0000	0.0000	0.0000
44.0000	0.0000	0.0000	0.0000	0.0000	0.0000	0.0000	0.0000
45.0000	0.0206	0.0000	0.0000	0.0000	0.0000	0.0000	0.0091
46.0000	0.0000	0.0000	0.0000	0.0000	0.0000	0.0000	0.0000
47.0000	0.0000	0.0000	0.0000	0.0000	0.0000	0.0000	0.0091
48.0000	0.0000	0.0000	0.0000	0.0000	0.0000	0.0000	0.0000
49.0000	0.0000	0.0000	0.0000	0.0000	0.0000	0.0000	0.0000
50.0000	0.0000	0.0000	0.0248	0.0000	0.0000	0.0000	0.0000
Ave. %	0.0032	0.0025	0.0042	0.0062	0.0770	0.0048	0.0033
Std.dev.	0.0102	0.0168	0.0167	0.0193	0.0383	0.0162	0.0158

Oxide Volume Fractions of M2-C90 Steel

Field	232-1	232-2	232-3	232-4	232-5	232-6	232-7	232-8
1	0.0000	0.0000	0.0000	0.0000	0.0000	0.0000	0.0000	0.0000
2	0.0000	0.0000	0.0000	0.0000	0.0000	0.0000	0.0000	0.0000
3	0.0293	0.0000	0.0000	0.0000	0.0000	0.0000	0.0173	0.0000
4	0.0000	0.0000	0.0000	0.0000	0.0000	0.0000	0.0000	0.0000
5	0.0000	0.0000	0.0000	0.0000	0.0000	0.0000	0.0000	0.0000
6	0.0000	0.0000	0.0000	0.0000	0.0000	0.0000	0.0000	0.0000
7	0.0000	0.0656	0.0000	0.0000	0.0000	0.0000	0.0000	0.0000
8	0.0000	0.0000	0.0000	0.0000	0.0000	0.0000	0.0000	0.0000
9	0.0000	0.0000	0.0000	0.0000	0.0000	0.0590	0.0706	0.0000
10	0.0000	0.0378	0.0000	0.0000	0.0000	0.0000	0.0000	0.0000
11	0.0000	0.0000	0.0000	0.0000	0.0000	0.0000	0.0000	0.0000
12	0.0000	0.0417	0.0000	0.0000	0.0000	0.0000	0.0000	0.0173
13	0.0000	0.0000	0.0000	0.0000	0.0000	0.0000	0.0000	0.0000
14	0.0000	0.0000	0.0000	0.0000	0.0000	0.0000	0.0000	0.0000
15	0.0000	0.0000	0.0000	0.0000	0.0000	0.0460	0.0000	0.0000
16	0.0000	0.0000	0.0144	0.0000	0.0000	0.0000	0.0000	0.0000
17	0.0000	0.0000	0.0000	0.0000	0.0000	0.0000	0.0000	0.0132
18	0.0000	0.0000	0.0000	0.0000	0.0000	0.0000	0.0000	0.0000
19	0.0235	0.0000	0.0000	0.0000	0.0000	0.0000	0.0000	0.0000
20	0.0000	0.0000	0.0000	0.0000	0.0000	0.0000	0.0000	0.0000
21	0.0000	0.0000	0.0000	0.0000	0.0000	0.0000	0.0000	0.0000
22	0.0000	0.0000	0.0000	0.0000	0.0000	0.0000	0.0000	0.0000
23	0.0000	0.0000	0.0000	0.0000	0.0000	0.0092	0.0000	0.0000
24	0.0000	0.0128	0.0000	0.0000	0.0223	0.0000	0.0000	0.0000
25	0.0000	0.0000	0.0000	0.0000	0.0735	0.0000	0.0000	0.0000
26	0.0000	0.0000	0.0000	0.0000	0.0000	0.0000	0.0000	0.0000
27	0.0000	0.0000	0.0000	0.0000	0.0000	0.0000	0.0000	0.0223
28	0.0000	0.0000	0.0000	0.0000	0.0000	0.0000	0.0000	0.0000
29	0.0000	0.0000	0.0000	0.0000	0.0000	0.0000	0.0169	0.0000
30	0.0000	0.0000	0.0000	0.0000	0.0000	0.0000	0.1102	0.0000
31	0.0000	0.0000	0.0000	0.0000	0.0000	0.0000	0.0000	0.0000
32	0.0000	0.0297	0.0000	0.0000	0.0000	0.0000	0.0000	0.0000
33	0.0000	0.0000	0.0000	0.0000	0.0000	0.0000	0.0000	0.0000
34	0.0000	0.0000	0.0000	0.0000	0.0000	0.0000	0.0000	0.0000
35	0.0140	0.0000	0.0000	0.0000	0.0000	0.0000	0.0000	0.0000
36	0.0000	0.0000	0.0000	0.0000	0.0000	0.0000	0.0000	0.0000
37	0.0124	0.0000	0.0000	0.0000	0.0000	0.0000	0.0000	0.0000

38	0.0000	0.0000	0.0000	0.0000	0.0000	0.0000	0.0442	0.0000
39	0.0000	0.0000	0.0000	0.0000	0.0000	0.0008	0.0000	0.0000
40	0.0000	0.0000	0.0000	0.0000	0.0000	0.0000	0.0000	0.0000
41	0.0000	0.0000	0.0000	0.0000	0.0000	0.0000	0.0000	0.0347
42	0.0800	0.0000	0.0000	0.0000	0.0000	0.0000	0.0000	0.0000
43	0.0000	0.0000	0.0000	0.0000	0.0000	0.0000	0.0000	0.0000
44	0.0000	0.0000	0.0000	0.0000	0.0000	0.0020	0.0000	0.0000
45	0.0000	0.0000	0.0000	0.1928	0.0000	0.0000	0.0000	0.0000
46	0.0000	0.0000	0.0000	0.0000	0.0328	0.0000	0.0000	0.0000
47	0.0000	0.0000	0.0000	0.0000	0.0000	0.0000	0.0000	0.1197
48	0.0000	0.0000	0.0000	0.0000	0.0000	0.0000	0.0000	0.0000
49	0.0000	0.0000	0.0000	0.0000	0.0000	0.0000	0.0000	0.0000
50	0.0000	0.0000	0.0000	0.0000	0.0000	0.0000	0.0000	0.0000
Ave. %	0.0032	0.0038	0.0003	0.0039	0.0026	0.0023	0.0052	0.0041
Std. dev.	0.0124	0.0125	0.0020	0.0273	0.0115	0.0104	0.0193	0.0179

Field	232-9	232-10	232-11	232-12	232-13	232-14	232-15	232-16
1	0.0000	0.0000	0.0000	0.0000	0.0182	0.0000	0.0000	0.0000
2	0.0000	0.0000	0.0000	0.0000	0.0000	0.0000	0.0000	0.0000
3	0.0000	0.0000	0.0000	0.0000	0.0000	0.0000	0.0000	0.0000
4	0.0000	0.0858	0.0000	0.0000	0.0000	0.0173	0.0000	0.0000
5	0.0000	0.0103	0.0000	0.0000	0.0000	0.0000	0.0000	0.0000
6	0.0000	0.0000	0.0000	0.0000	0.0000	0.0000	0.0000	0.0000
7	0.0000	0.0000	0.0000	0.1441	0.0000	0.0000	0.0000	0.0000
8	0.0000	0.0000	0.0396	0.0000	0.0000	0.0000	0.0000	0.0000
9	0.0000	0.0000	0.0000	0.0000	0.0000	0.0000	0.0000	0.0000
10	0.0000	0.0000	0.0149	0.0000	0.1321	0.0000	0.0000	0.0000
11	0.0000	0.0000	0.0000	0.0000	0.0000	0.0000	0.0000	0.0000
12	0.0000	0.0000	0.0000	0.0000	0.0264	0.0000	0.0000	0.0000
13	0.0000	0.0000	0.0000	0.0000	0.0000	0.0000	0.0066	0.0000
14	0.0421	0.0000	0.0000	0.0000	0.0000	0.0000	0.0000	0.0000
15	0.0000	0.0000	0.0000	0.0000	0.0000	0.0000	0.1061	0.0244
16	0.0541	0.0000	0.0091	0.0000	0.0000	0.0000	0.0000	0.0000
17	0.0000	0.0070	0.0153	0.0000	0.0000	0.0000	0.0000	0.0000
18	0.0000	0.2449	0.0000	0.0000	0.0000	0.0000	0.0000	0.0000

19	0.0000	0.0000	0.0140	0.0000	0.0000	0.0000	0.0000	0.0000
20	0.0000	0.0213	0.0000	0.0000	0.0000	0.0000	0.0000	0.0000
21	0.0000	0.0000	0.0000	0.0000	0.0000	0.0000	0.0000	0.0000
22	0.0000	0.0000	0.0000	0.0000	0.0000	0.0000	0.0000	0.0000
23	0.0000	0.0000	0.0000	0.0000	0.0000	0.0000	0.0000	0.0000
24	0.0000	0.0000	0.0244	0.0000	0.0000	0.0000	0.0000	0.0000
25	0.0000	0.0000	0.0000	0.0000	0.0000	0.0000	0.0000	0.0000
26	0.0000	0.0000	0.0000	0.0000	0.0000	0.0000	0.0000	0.0000
27	0.0000	0.0000	0.0000	0.1544	0.0000	0.0000	0.0000	0.0000
28	0.0000	0.0000	0.0078	0.0000	0.0000	0.0000	0.0000	0.0000
29	0.0000	0.0000	0.0000	0.0000	0.0000	0.0000	0.1201	0.0000
30	0.0000	0.0000	0.0000	0.0000	0.0000	0.0000	0.0000	0.0508
31	0.0000	0.0000	0.0000	0.0000	0.0000	0.0000	0.0000	0.0000
32	0.0000	0.0000	0.0000	0.0000	0.0656	0.0000	0.0000	0.0244
33	0.0471	0.0000	0.0000	0.0000	0.0000	0.0000	0.0000	0.0000
34	0.0000	0.0000	0.0000	0.0000	0.0000	0.0000	0.0000	0.0000
35	0.0000	0.0000	0.0219	0.0000	0.0000	0.0000	0.0000	0.0000
36	0.0000	0.0000	0.0000	0.0165	0.0000	0.0000	0.0000	0.0000
37	0.0000	0.0406	0.0120	0.0000	0.0000	0.0000	0.0000	0.0000
38	0.0000	0.0000	0.0000	0.0000	0.0000	0.0000	0.0000	0.0000
39	0.0000	0.0000	0.0355	0.0000	0.0000	0.0000	0.0359	0.0000
40	0.0000	0.0000	0.0000	0.0000	0.0000	0.0000	0.0000	0.0000
41	0.0000	0.0000	0.0000	0.0000	0.0000	0.0000	0.0000	0.0000
42	0.0000	0.0000	0.0000	0.0000	0.0000	0.0797	0.0000	0.0000
43	0.0000	0.0000	0.0000	0.0000	0.0000	0.0000	0.0000	0.0000
44	0.0000	0.0000	0.0000	0.0190	0.0000	0.0120	0.0000	0.0000
45	0.0000	0.0000	0.0281	0.0000	0.0000	0.0970	0.0000	0.0000
46	0.0000	0.0000	0.0000	0.0000	0.0000	0.0000	0.0000	0.0000
47	0.0000	0.0000	0.0000	0.0000	0.0000	0.0000	0.0000	0.0000
48	0.0475	0.0000	0.0000	0.0000	0.0000	0.0000	0.1350	0.0000
49	0.0000	0.0000	0.0000	0.0475	0.0144	0.0000	0.0000	0.0000
50	0.0000	0.0000	0.0454	0.0000	0.0000	0.0000	0.0000	0.0000
Ave. %	0.0038	0.0082	0.0054	0.0076	0.0051	0.0041	0.0081	0.0020
Std. dev.	0.0131	0.0364	0.0113	0.0302	0.0210	0.0177	0.0293	0.0085

Field	232-17	232-18	232-19	232-20	232-21
1	0.0000	0.0000	0.0000	0.0000	0.0000
2	0.0000	0.0000	0.0000	0.0000	0.0000
3	0.0000	0.0000	0.0000	0.0000	0.0000
4	0.0000	0.0000	0.0000	0.0000	0.0000
5	0.0000	0.0000	0.0000	0.0000	0.0000
6	0.0000	0.0000	0.0000	0.0000	0.0000
7	0.0000	0.0359	0.0000	0.0000	0.0000
8	0.0000	0.0000	0.0000	0.0000	0.0380
9	0.0000	0.0000	0.0000	0.0000	0.0000
10	0.0000	0.0000	0.0000	0.0000	0.0000
11	0.0000	0.0000	0.0000	0.0000	0.0000
12	0.0000	0.0000	0.0000	0.0000	0.0000
13	0.0000	0.0000	0.0000	0.0000	0.0000
14	0.0000	0.0000	0.0000	0.0000	0.0000
15	0.0000	0.0000	0.0504	0.0000	0.0000
16	0.0000	0.0000	0.0000	0.0000	0.0000
17	0.0000	0.0000	0.0000	0.0520	0.0471
18	0.0000	0.0140	0.0000	0.0173	0.0000
19	0.0000	0.0000	0.0541	0.0000	0.0000
20	0.0000	0.0000	0.0182	0.0000	0.0000
21	0.0000	0.0000	0.0000	0.0000	0.0000
22	0.0000	0.0000	0.0000	0.0000	0.0000
23	0.0000	0.1003	0.0000	0.0186	0.0000
24	0.0000	0.0000	0.0000	0.0000	0.0000
25	0.0000	0.0000	0.0000	0.0000	0.0000
26	0.0000	0.0000	0.0000	0.0000	0.0000
27	0.0000	0.0000	0.0000	0.0000	0.0000
28	0.0000	0.0000	0.0000	0.0000	0.0000
29	0.0000	0.0000	0.0000	0.0000	0.0000
30	0.0438	0.0091	0.0000	0.0000	0.0000
31	0.0000	0.0000	0.0000	0.0000	0.0000
32	0.0000	0.0000	0.0000	0.0000	0.0000
33	0.0000	0.0000	0.0000	0.0000	0.0000
34	0.0000	0.0000	0.0000	0.0000	0.0000
35	0.0000	0.0000	0.0000	0.0000	0.0000
36	0.0000	0.0169	0.0000	0.0000	0.0000
37	0.0000	0.0000	0.0000	0.0000	0.0000
38	0.0000	0.0000	0.0000	0.0200	0.0000

39	0.0000	0.0000	0.0000	0.0000	0.0000
40	0.0000	0.0000	0.0000	0.0000	0.0000
41	0.1044	0.0000	0.0000	0.0000	0.0000
42	0.0000	0.0000	0.0000	0.0000	0.0000
43	0.0000	0.0000	0.0000	0.0000	0.0000
44	0.0000	0.0107	0.0000	0.0000	0.0000
45	0.0000	0.0000	0.0000	0.0000	0.0000
46	0.0000	0.0000	0.0000	0.0000	0.0000
47	0.0000	0.0000	0.0000	0.0000	0.0000
48	0.0000	0.0000	0.0000	0.0000	0.0000
49	0.0000	0.0000	0.0000	0.0000	0.0000
50	0.0000	0.0000	0.0000	0.0000	0.0000
Ave. %	0.0030	0.0037	0.0025	0.0022	0.0017
Std. dev.	0.0159	0.0152	0.0106	0.0084	0.0084

Oxide Volume Fractions of M1-I90C Steel

Field #	233-1	233-2	233-3	233-4	233-5	233-6	233-7	233-8
1	0.0000	0.0000	0.0000	0.0000	0.0000	0.0000	0.0000	0.0000
2	0.0000	0.0000	0.0000	0.0000	0.0149	0.0000	0.0231	0.0689
3	0.0000	0.0000	0.0000	0.0000	0.2931	0.0000	0.0000	0.0000
4	0.0000	0.0000	0.0000	0.0000	0.0000	0.0149	0.0000	0.0000
5	0.0000	0.0396	0.1218	0.0000	0.0000	0.0000	0.0000	0.0000
6	0.0000	0.0000	0.0153	0.0000	0.0000	0.1540	0.0000	0.0000
7	0.0000	0.0000	0.0000	0.0000	0.0611	0.0000	0.0000	0.0000
8	0.0000	0.0000	0.0000	0.0000	0.0520	0.0186	0.0000	0.1404
9	0.0000	0.0000	0.0000	0.0000	0.0000	0.0000	0.0495	0.0000
10	0.0000	0.0000	0.0000	0.0454	0.0000	0.0169	0.0000	0.0157
11	0.0000	0.0000	0.0000	0.0442	0.0157	0.0446	0.0000	0.0000
12	0.0000	0.0000	0.0000	0.0392	0.0000	0.0000	0.0000	0.0000
13	0.0000	0.0187	0.0000	0.0165	0.0000	0.0000	0.0000	0.0615
14	0.0000	0.0000	0.0000	0.0000	0.0000	0.0000	0.0140	0.0277
15	0.0000	0.0000	0.0000	0.0367	0.0000	0.0182	0.0000	0.0000
16	0.0000	0.0467	0.0000	0.0392	0.0000	0.0000	0.0000	0.0000
17	0.0000	0.0000	0.0000	0.0000	0.0000	0.0000	0.0000	0.1965
18	0.0000	0.0000	0.0479	0.0000	0.0458	0.0000	0.0000	0.0000
19	0.0000	0.0000	0.0000	0.0182	0.0636	0.0619	0.0000	0.0000
20	0.0392	0.0000	0.0000	0.0000	0.0000	0.0000	0.0000	0.0000
21	0.0000	0.0000	0.0000	0.0000	0.0194	0.0000	0.0000	0.0000
22	0.0178	0.0000	0.0000	0.0000	0.0000	0.0000	0.0124	0.0301
23	0.0000	0.0000	0.0000	0.0000	0.0198	0.0000	0.0640	0.0000
24	0.0301	0.0000	0.0000	0.0000	0.0000	0.0099	0.0173	0.0000
25	0.0000	0.0000	0.0000	0.0000	0.0000	0.0000	0.0706	0.0000
26	0.0000	0.0295	0.0000	0.0054	0.0169	0.0178	0.0000	0.0504
27	0.0000	0.0000	0.0000	0.0000	0.0367	0.0000	0.0000	0.0000
28	0.0000	0.0000	0.0409	0.0000	0.0000	0.0000	0.0000	0.0000
29	0.0000	0.0000	0.0083	0.0000	0.0153	0.0421	0.0475	0.0813
30	0.0000	0.0000	0.0000	0.0000	0.0409	0.0000	0.0000	0.0702
31	0.0000	0.0000	0.0000	0.1300	0.0111	0.0000	0.0000	0.0000
32	0.0000	0.0000	0.0000	0.0000	0.0000	0.0000	0.0000	0.0000
33	0.0896	0.0000	0.0000	0.0508	0.0000	0.0000	0.0000	0.0000
34	0.0000	0.0000	0.0000	0.0000	0.0648	0.0000	0.0000	0.0000
35	0.0000	0.0000	0.0000	0.0000	0.0000	0.0000	0.0000	0.0000
36	0.0000	0.0000	0.0000	0.0000	0.0000	0.0000	0.0000	0.0000
37	0.0169	0.0633	0.0000	0.0000	0.0000	0.0000	0.0000	0.0000

38	0.0000	0.0000	0.0000	0.0495	0.0000	0.0000	0.0000	0.0000
39	0.0000	0.0000	0.0000	0.0000	0.0000	0.0000	0.0000	0.0000
40	0.0000	0.0000	0.0000	0.0000	0.0202	0.0000	0.0000	0.0000
41	0.0000	0.0000	0.0000	0.1387	0.0962	0.0000	0.0000	0.0000
42	0.0000	0.0000	0.0050	0.0656	0.0000	0.0000	0.0000	0.0603
43	0.0099	0.0000	0.0000	0.0000	0.1243	0.0198	0.0000	0.0000
44	0.0000	0.0000	0.0000	0.0000	0.0235	0.0157	0.0000	0.0000
45	0.0000	0.0000	0.0000	0.0883	0.0000	0.0000	0.0000	0.0000
46	0.0000	0.0000	0.0000	0.0000	0.0000	0.0000	0.0000	0.0149
47	0.0000	0.0000	0.0000	0.0000	0.0111	0.0000	0.0000	0.0000
48	0.0000	0.0000	0.0000	0.0074	0.0000	0.0000	0.0000	0.0000
49	0.0000	0.0000	0.0000	0.0516	0.0054	0.0491	0.0000	0.0000
50	0.0000	0.0274	0.0000	0.0669	0.0124	0.0000	0.0000	0.0000
Ave. %	0.0041	0.0045	0.0048	0.0179	0.0213	0.0097	0.0060	0.0164
Std. dev	0.0145	0.0132	0.0192	0.0331	0.0471	0.0253	0.0164	0.0387

Field #	233-9	233-10	233-11	233-12	233-13	233-14	233-15	233-16
1	0.0000	0.0000	0.0000	0.0000	0.0000	0.0000	0.0000	0.0000
2	0.0000	0.0698	0.0000	0.0512	0.0000	0.0000	0.0000	0.0153
3	0.0000	0.0000	0.0099	0.0000	0.0000	0.0111	0.0000	0.0000
4	0.0000	0.0000	0.0900	0.0244	0.0000	0.0124	0.0153	0.0000
5	0.0000	0.0190	0.0491	0.0000	0.0000	0.0206	0.0173	0.0136
6	0.0000	0.0000	0.0099	0.0128	0.0000	0.0000	0.0124	0.0000
7	0.0000	0.0000	0.0392	0.0128	0.0000	0.0000	0.0149	0.0231
8	0.0235	0.0000	0.0000	0.0405	0.0000	0.0000	0.0173	0.0153
9	0.0000	0.0000	0.0000	0.0227	0.0153	0.0000	0.0388	0.0000
10	0.0000	0.0000	0.0508	0.0244	0.0000	0.0429	0.0000	0.0343
11	0.0000	0.0000	0.0149	0.0310	0.0153	0.0574	0.0000	0.0219
12	0.0000	0.0000	0.2118	0.0000	0.0409	0.0206	0.0000	0.0000
13	0.0000	0.0000	0.0000	0.0000	0.0000	0.0000	0.0000	0.0169
14	0.0000	0.0000	0.0000	0.0256	0.0000	0.0293	0.0000	0.0409
15	0.0000	0.0000	0.0000	0.0656	0.0000	0.0000	0.0000	0.0000
16	0.0000	0.0000	0.0000	0.0537	0.0000	0.0000	0.0000	0.0000
17	0.0000	0.0000	0.0000	0.0000	0.1321	0.0000	0.0326	0.0454
18	0.0000	0.0000	0.0000	0.0000	0.0000	0.0000	0.0000	0.0239

19	0.0000	0.0000	0.0000	0.0219	0.0000	0.0000	0.0248	0.0000
20	0.0099	0.0000	0.0099	0.1713	0.0000	0.0000	0.0000	0.0173
21	0.0128	0.0000	0.0000	0.0512	0.0000	0.0363	0.0000	0.0000
22	0.0000	0.0000	0.0710	0.0000	0.0000	0.0099	0.0000	0.0334
23	0.0000	0.0524	0.0285	0.0000	0.0000	0.0528	0.0578	0.0000
24	0.0000	0.0000	0.0000	0.0929	0.0000	0.0285	0.0223	0.0260
25	0.0128	0.0000	0.0000	0.0215	0.0000	0.0136	0.0000	0.0000
26	0.0000	0.0000	0.0000	0.0000	0.0747	0.0000	0.0260	0.0293
27	0.0000	0.0000	0.0000	0.0000	0.0000	0.0157	0.0000	0.0165
28	0.0000	0.0000	0.0000	0.0124	0.0000	0.0338	0.0000	0.0000
29	0.0000	0.0000	0.0000	0.0314	0.0516	0.0607	0.0000	0.0235
30	0.0000	0.0000	0.0000	0.0000	0.0000	0.0219	0.0000	0.0338
31	0.0000	0.0000	0.0000	0.0520	0.0000	0.0000	0.0111	0.0000
32	0.0000	0.1503	0.0000	0.0314	0.0153	0.0157	0.0000	0.0124
33	0.0000	0.0000	0.0788	0.0000	0.0297	0.0000	0.0000	0.0000
34	0.0000	0.0611	0.0000	0.0454	0.0000	0.0338	0.0277	0.0000
35	0.0000	0.0000	0.0178	0.0000	0.0000	0.0165	0.0000	0.0000
36	0.0000	0.0000	0.0000	0.0000	0.0239	0.0000	0.0000	0.0000
37	0.0000	0.0834	0.0000	0.0244	0.0000	0.1771	0.0000	0.0000
38	0.0000	0.0000	0.0000	0.0000	0.0388	0.0227	0.0553	0.0000
39	0.0000	0.0000	0.0000	0.0000	0.0000	0.0219	0.0000	0.0153
40	0.0000	0.0000	0.0351	0.0260	0.0000	0.0594	0.0000	0.0702
41	0.0000	0.0000	0.0194	0.0000	0.0231	0.0000	0.0000	0.0000
42	0.0000	0.0000	0.0107	0.0099	0.0421	0.0000	0.0000	0.0252
43	0.0000	0.0000	0.0000	0.0000	0.0000	0.0000	0.0000	0.0260
44	0.0000	0.0000	0.0000	0.0000	0.0000	0.0417	0.0227	0.0000
45	0.0533	0.0000	0.0000	0.0149	0.0000	0.0310	0.0099	0.0000
46	0.0000	0.0916	0.0099	0.0000	0.0000	0.0954	0.0000	0.0000
47	0.0000	0.0000	0.0124	0.0099	0.0000	0.0000	0.0000	0.0000
48	0.0000	0.0206	0.0000	0.0140	0.0000	0.0000	0.0000	0.0099
49	0.0000	0.0000	0.0000	0.0000	0.0000	0.0000	0.0000	0.0000
50	0.0000	0.0000	0.0000	0.0000	0.0099	0.0000	0.0000	0.0000
Ave. %	0.0022	0.0110	0.0154	0.0199	0.0103	0.0197	0.0081	0.0118
Std. dev	0.0084	0.0300	0.0354	0.0302	0.0237	0.0313	0.0143	0.0156

Field #	233-17	233-18	233-19	233-20
1	0.0000	0.0136	0.0000	0.0165
2	0.0149	0.0000	0.0000	0.0264
3	0.0268	0.0000	0.0000	0.0000
4	0.0264	0.0000	0.0000	0.0751
5	0.0000	0.0000	0.0000	0.0000
6	0.0099	0.0111	0.0000	0.0000
7	0.0000	0.0256	0.0000	0.0000
8	0.0157	0.0000	0.0301	0.0000
9	0.0000	0.0000	0.0000	0.0706
10	0.0000	0.0153	0.0000	0.0000
11	0.0000	0.0000	0.0000	0.0124
12	0.0000	0.0000	0.0000	0.0000
13	0.0000	0.1077	0.0000	0.0000
14	0.0000	0.0000	0.0954	0.0000
15	0.0000	0.0000	0.0000	0.0000
16	0.0330	0.0355	0.0000	0.0000
17	0.0442	0.0000	0.0000	0.0000
18	0.0000	0.0000	0.0000	0.0000
19	0.0479	0.0260	0.0000	0.0000
20	0.0310	0.0000	0.0000	0.0000
21	0.0000	0.0000	0.0000	0.0000
22	0.0000	0.0000	0.0000	0.0000
23	0.0479	0.0000	0.0260	0.0000
24	0.0000	0.0000	0.0000	0.0149
25	0.0000	0.0268	0.0111	0.0000
26	0.0182	0.0194	0.1205	0.0000
27	0.0111	0.0000	0.0442	0.0000
28	0.0000	0.0000	0.0099	0.0619
29	0.0000	0.0000	0.0000	0.0586
30	0.0000	0.0000	0.0272	0.0000
31	0.0462	0.0223	0.0000	0.0376
32	0.0000	0.0000	0.0000	0.0000
33	0.0000	0.0000	0.0524	0.0000
34	0.0000	0.0000	0.0632	0.0000
35	0.0000	0.0000	0.0000	0.0000
36	0.0000	0.0000	0.0367	0.0425
37	0.0293	0.0000	0.0182	0.0000
38	0.0000	0.0000	0.0223	0.0000

39	0.0000	0.0000	0.0000	0.0000
40	0.0000	0.0318	0.0000	0.0000
41	0.0000	0.0000	0.0000	0.0000
42	0.0000	0.0107	0.0000	0.0000
43	0.0000	0.0000	0.0000	0.0000
44	0.0355	0.0157	0.0124	0.0000
45	0.0000	0.0111	0.0000	0.0000
46	0.0000	0.0314	0.0000	0.0000
47	0.0223	0.0000	0.0000	0.0000
48	0.0000	0.0260	0.0000	0.0413
49	0.0000	0.0000	0.0000	0.0000
50	0.0000	0.0000	0.0198	0.0000
Ave. %	0.0092	0.0086	0.0118	0.0092
Std. dev	0.0153	0.0178	0.0250	0.0202

Oxide Volume Fractions of M1-I90B Steel

Field #	235-1	235-2	235-3	235-4	235-5	235-6	235-7	235-8
1	0.0000	0.0000	0.0000	0.0000	0.0000	0.0000	0.0000	0.0000
2	0.0000	0.0000	0.0000	0.0000	0.0000	0.0000	0.0000	0.0000
3	0.0000	0.0000	0.0000	0.0000	0.0000	0.0000	0.0000	0.0000
4	0.0149	0.0140	0.0000	0.0000	0.0000	0.0627	0.0000	0.0000
5	0.0000	0.0000	0.0000	0.0409	0.0000	0.0165	0.0000	0.0000
6	0.0000	0.0000	0.0000	0.0000	0.0227	0.0000	0.0000	0.0000
7	0.0000	0.0000	0.0000	0.0000	0.0000	0.0854	0.0000	0.0000
8	0.0173	0.0000	0.0000	0.0000	0.0000	0.0000	0.0000	0.0000
9	0.0000	0.0000	0.0000	0.0000	0.0000	0.0252	0.0466	0.0000
10	0.0128	0.0768	0.0000	0.0000	0.0000	0.0000	0.0000	0.0000
11	0.0000	0.0000	0.0000	0.0000	0.0000	0.0252	0.0157	0.0466
12	0.0000	0.0446	0.0000	0.0297	0.0000	0.0000	0.0000	0.0000
13	0.0000	0.0000	0.0000	0.0000	0.0000	0.0392	0.0000	0.0000
14	0.0000	0.0000	0.0000	0.0000	0.0000	0.0000	0.0000	0.0000
15	0.0000	0.0000	0.0000	0.0000	0.0000	0.0000	0.0000	0.0000
16	0.0000	0.0000	0.0000	0.0000	0.0000	0.0425	0.0000	0.0194
17	0.0000	0.0000	0.0000	0.0000	0.0000	0.0206	0.0330	0.0000
18	0.0000	0.0260	0.0000	0.0000	0.0000	0.0000	0.0000	0.0520
19	0.0000	0.0000	0.0000	0.0000	0.0000	0.0000	0.0000	0.0000
20	0.0000	0.0000	0.0000	0.0000	0.0173	0.0000	0.0000	0.0000
21	0.0000	0.0000	0.0000	0.0000	0.0000	0.0000	0.0351	0.0925
22	0.0000	0.0000	0.0000	0.0107	0.0000	0.0000	0.0000	0.0000
23	0.0140	0.0000	0.0000	0.0000	0.0000	0.0000	0.0000	0.0211
24	0.0000	0.0000	0.0000	0.0000	0.0000	0.0227	0.0000	0.0000
25	0.0244	0.0000	0.0000	0.0000	0.0000	0.0000	0.0000	0.0000
26	0.0000	0.0000	0.0000	0.0000	0.0066	0.0000	0.0351	0.0000
27	0.0000	0.0000	0.0000	0.0000	0.0000	0.0000	0.0000	0.0000
28	0.0000	0.0000	0.0000	0.0000	0.0000	0.0000	0.0000	0.0219
29	0.0000	0.0000	0.0000	0.0277	0.0343	0.0594	0.0000	0.0000
30	0.0000	0.0000	0.0000	0.0000	0.0000	0.1325	0.0000	0.0788
31	0.0000	0.0219	0.0000	0.0000	0.0095	0.0000	0.0000	0.0000
32	0.0000	0.0000	0.0000	0.0000	0.0000	0.0000	0.0227	0.0000
33	0.1164	0.0000	0.0000	0.0000	0.0066	0.0660	0.0136	0.0000
34	0.0000	0.0000	0.0000	0.0000	0.0000	0.0116	0.0000	0.0194
35	0.0000	0.0000	0.0000	0.0000	0.0000	0.0000	0.0169	0.0516
36	0.0301	0.0000	0.0219	0.0000	0.0272	0.0000	0.0409	0.0528
37	0.0000	0.0000	0.0000	0.0000	0.0000	0.0116	0.0000	0.0000

38	0.0000	0.0000	0.0000	0.0297	0.0338	0.0000	0.0000	0.0000
39	0.0000	0.0000	0.0000	0.0000	0.0363	0.0000	0.0000	0.0000
40	0.0000	0.0111	0.0000	0.0000	0.0000	0.0322	0.0000	0.0000
41	0.0640	0.0000	0.0000	0.0140	0.0000	0.0173	0.0000	0.0000
42	0.0000	0.0000	0.0000	0.0487	0.0318	0.0000	0.0103	0.0553
43	0.0000	0.0000	0.0000	0.0186	0.0000	0.0000	0.0000	0.0000
44	0.0000	0.0000	0.0000	0.0285	0.0000	0.0000	0.0000	0.0000
45	0.0000	0.0144	0.0000	0.0000	0.0000	0.0000	0.0000	0.0000
46	0.0000	0.0000	0.0157	0.0000	0.0000	0.0000	0.0000	0.0392
47	0.0000	0.0182	0.0000	0.0000	0.0000	0.0000	0.0000	0.0000
48	0.0000	0.0000	0.0000	0.0000	0.0182	0.0000	0.0000	0.0182
49	0.0000	0.0000	0.0000	0.0000	0.0140	0.0074	0.0000	0.0000
50	0.0000	0.0000	0.0000	0.0000	0.0000	0.0000	0.0256	0.0338
51	0.0000	0.0000	0.0000	0.0000	0.0000	0.0000	0.0000	0.0000
52	0.0000	0.0000	0.0000	0.0000	0.0000	0.0000	0.0000	0.0000
53	0.0000	0.0000	0.0000	0.0000	0.0000	0.0000	0.0000	0.0000
54	0.0000	0.0116	0.0000	0.0000	0.0000	0.0000	0.0000	0.0000
55	0.0000	0.0000	0.0000	0.0140	0.0000	0.0000	0.0000	0.0000
56	0.0000	0.0000	0.0000	0.0000	0.0000	0.0285	0.0000	0.0000
57	0.0000	0.0000	0.0000	0.0000	0.0000	0.0000	0.0000	0.0000
58	0.0000	0.0000	0.0000	0.0132	0.0000	0.0000	0.0000	0.0000
59	0.0000	0.0000	0.0000	0.0000	0.0000	0.0000	0.0194	0.0165
60	0.0000	0.0000	0.0000	0.0165	0.0000	0.0000	0.0000	0.0000
Ave. %	0.0049	0.0040	0.0006	0.0049	0.0043	0.0115	0.0064	0.0103
Std. dev.	0.0177	0.0124	0.0034	0.0111	0.0099	0.0249	0.0131	0.0213

Field #	235-9	235-10	235-11	235-12	235-13	235-14	235-15	235-16
1	0.0000	0.0264	0.0248	0.0000	0.0000	0.0000	0.0000	0.0000
2	0.0000	0.0000	0.0000	0.0000	0.0000	0.0000	0.0000	0.0000
3	0.0000	0.0000	0.0000	0.0000	0.0000	0.0400	0.0000	0.0000
4	0.0000	0.0000	0.0000	0.0000	0.0000	0.0000	0.0000	0.3856
5	0.0000	0.0000	0.0000	0.0000	0.0000	0.0000	0.0000	0.0000
6	0.0000	0.0000	0.0000	0.0293	0.0000	0.0000	0.0272	0.0107
7	0.0000	0.0000	0.0000	0.0000	0.0000	0.0000	0.0000	0.0000
8	0.0000	0.0000	0.0000	0.0000	0.0000	0.0000	0.0000	0.0000
9	0.0834	0.0000	0.0000	0.0000	0.0000	0.0000	0.0000	0.0293

10	0.0000	0.0000	0.0000	0.0000	0.0000	0.0000	0.0000	0.0000
11	0.0000	0.0091	0.0000	0.0574	0.0318	0.0421	0.0000	0.0000
12	0.0000	0.0000	0.0000	0.0000	0.0000	0.0000	0.0000	0.0000
13	0.0000	0.0000	0.0000	0.0000	0.0000	0.0000	0.0000	0.0219
14	0.0000	0.0000	0.0000	0.0458	0.0314	0.0000	0.0000	0.0000
15	0.0000	0.0000	0.0202	0.0000	0.0000	0.0000	0.0000	0.0000
16	0.0000	0.0000	0.0000	0.0000	0.0000	0.0000	0.0000	0.0000
17	0.0000	0.0000	0.0000	0.0000	0.0000	0.0000	0.0000	0.0000
18	0.0000	0.0000	0.0355	0.0000	0.0000	0.0000	0.0000	0.0000
19	0.0000	0.0000	0.0000	0.0000	0.0000	0.0665	0.0000	0.0000
20	0.0000	0.0000	0.0000	0.0000	0.0000	0.0409	0.0000	0.0000
21	0.0000	0.0136	0.0000	0.0000	0.0000	0.0000	0.0000	0.0000
22	0.0000	0.0000	0.0000	0.0000	0.0000	0.0000	0.0000	0.0000
23	0.0000	0.0000	0.0000	0.0000	0.0000	0.0000	0.0888	0.0000
24	0.0000	0.0217	0.0000	0.0000	0.0000	0.0000	0.0000	0.0000
25	0.0000	0.0000	0.0000	0.0000	0.0000	0.0000	0.0000	0.0000
26	0.0000	0.0338	0.0000	0.0000	0.0665	0.0000	0.0000	0.0000
27	0.0000	0.0000	0.0000	0.0000	0.0000	0.0000	0.0000	0.0000
28	0.0000	0.0000	0.0000	0.0000	0.0000	0.0124	0.0000	0.0000
29	0.0000	0.0504	0.0000	0.0000	0.0000	0.0000	0.0000	0.0000
30	0.0000	0.0000	0.0000	0.0000	0.1292	0.0000	0.0000	0.0000
31	0.0000	0.0000	0.0000	0.0000	0.0000	0.0095	0.0000	0.0000
32	0.0000	0.0000	0.0000	0.0000	0.0000	0.0318	0.0000	0.0000
33	0.0000	0.0000	0.0000	0.0000	0.0000	0.0116	0.0000	0.0000
34	0.0000	0.0000	0.0000	0.0305	0.0000	0.0000	0.0000	0.0000
35	0.0000	0.0000	0.0000	0.0000	0.0000	0.0000	0.0078	0.0000
36	0.0000	0.0000	0.0268	0.0000	0.0000	0.0000	0.0322	0.0169
37	0.0000	0.0000	0.0000	0.0000	0.0000	0.0000	0.0330	0.0000
38	0.0000	0.0000	0.0000	0.0000	0.0000	0.0522	0.0000	0.0000
39	0.0586	0.0000	0.0000	0.0000	0.0165	0.0000	0.0000	0.0000
40	0.0000	0.0000	0.0495	0.0438	0.0000	0.0000	0.0000	0.0000
41	0.0000	0.0000	0.0000	0.0000	0.0000	0.0000	0.0000	0.0000
42	0.0314	0.0053	0.0000	0.0000	0.0000	0.0351	0.0198	0.0000
43	0.0000	0.0000	0.0000	0.0000	0.0000	0.0000	0.0000	0.0000
44	0.0000	0.0000	0.0281	0.0000	0.0235	0.0000	0.0000	0.0000
45	0.0231	0.0287	0.0000	0.0000	0.0227	0.0359	0.0000	0.0000
46	0.0000	0.0000	0.0000	0.0000	0.0000	0.0656	0.0000	0.0000
47	0.0000	0.0024	0.0000	0.0000	0.0314	0.0000	0.0000	0.0000
48	0.0000	0.0000	0.0000	0.0000	0.0000	0.0000	0.0495	0.0000
49	0.0000	0.0090	0.0000	0.0000	0.0000	0.0000	0.0000	0.0000

50	0.0000	0.0000	0.0000	0.0000	0.0223	0.0000	0.0000	0.0000
51	0.0000	0.0052	0.0000	0.0000	0.0000	0.0252	0.0000	0.0000
52	0.0000	0.0000	0.0000	0.0000	0.0000	0.0000	0.0000	0.0000
53	0.0000	0.0058	0.0000	0.0000	0.0000	0.0215	0.0000	0.0000
54	0.0000	0.0068	0.0000	0.0000	0.0000	0.0178	0.0000	0.0000
55	0.0000	0.0260	0.0000	0.0000	0.0000	0.0000	0.0000	0.0000
56	0.0380	0.0033	0.0000	0.0000	0.0483	0.0000	0.0000	0.0000
57	0.0000	0.0144	0.0000	0.0000	0.0000	0.0000	0.0528	0.0000
58	0.0000	0.0059	0.0000	0.0000	0.0161	0.0000	0.0000	0.0000
59	0.0000	0.0353	0.0000	0.0000	0.0000	0.0000	0.0000	0.0000
60	0.0000	0.0480	0.0000	0.0000	0.0000	0.0000	0.0000	0.0000
Ave. %	0.0041	0.0059	0.0031	0.0034	0.0073	0.0084	0.0052	0.0077
Std. dev.	0.0144	0.0120	0.0098	0.0119	0.0207	0.0171	0.0159	0.0499

Field #	235-17	235-18	235-19	235-20
1	0.0000	0.0000	0.0000	0.0161
2	0.0000	0.0000	0.0000	0.0000
3	0.0000	0.0000	0.0000	0.0000
4	0.0000	0.0000	0.0000	0.0000
5	0.0000	0.0000	0.0000	0.0000
6	0.0000	0.0000	0.0000	0.0000
7	0.0000	0.0000	0.0000	0.0000
8	0.0000	0.0000	0.0000	0.0000
9	0.0000	0.0000	0.0755	0.0000
10	0.0000	0.0000	0.0000	0.0000
11	0.0656	0.0000	0.0000	0.0000
12	0.0000	0.0000	0.0000	0.0000
13	0.0000	0.0000	0.0000	0.0000
14	0.0000	0.0000	0.0000	0.0000
15	0.0000	0.0000	0.0000	0.0000
16	0.0000	0.0000	0.0000	0.0000
17	0.0000	0.0000	0.0000	0.0000
18	0.0000	0.0000	0.0000	0.0000
19	0.0000	0.0000	0.0000	0.0000
20	0.0000	0.0000	0.0000	0.0000
21	0.0000	0.0000	0.0000	0.0000

22	0.0000	0.0000	0.0000	0.0000
23	0.0000	0.0000	0.0000	0.0000
24	0.0000	0.0000	0.0000	0.0000
25	0.0000	0.0000	0.0000	0.0206
26	0.0000	0.0000	0.0000	0.0000
27	0.0000	0.0000	0.0000	0.0000
28	0.0000	0.0000	0.0000	0.0000
29	0.0000	0.0000	0.0000	0.0000
30	0.0000	0.0000	0.0000	0.0000
31	0.0000	0.0000	0.0000	0.0000
32	0.0000	0.0000	0.0000	0.0000
33	0.0000	0.0000	0.0000	0.0000
34	0.0000	0.0000	0.0000	0.0000
35	0.0652	0.0165	0.0000	0.0000
36	0.0000	0.0000	0.0178	0.0190
37	0.0000	0.0000	0.0000	0.0000
38	0.0000	0.0000	0.0000	0.0000
39	0.0000	0.0000	0.0417	0.0000
40	0.0000	0.0000	0.0000	0.0000
41	0.0000	0.0000	0.0169	0.0000
42	0.0000	0.0000	0.0000	0.0000
43	0.0000	0.0000	0.0000	0.0000
44	0.0000	0.0000	0.0000	0.0000
45	0.0000	0.0000	0.0000	0.0000
46	0.0000	0.0000	0.0000	0.0000
47	0.0000	0.0000	0.0000	0.0000
48	0.0000	0.0000	0.0000	0.0000
49	0.0000	0.0000	0.0153	0.0000
50	0.0000	0.0000	0.0000	0.0000
51	0.0000	0.0000	0.0000	0.0000
52	0.0000	0.0000	0.0000	0.0000
53	0.0000	0.0000	0.0116	0.0000
54	0.0000	0.0000	0.0000	0.0000
55	0.0000	0.0000	0.0000	0.0000
56	0.0194	0.0000	0.0000	0.0000
57	0.0000	0.0000	0.0000	0.0000
58	0.0000	0.0367	0.0000	0.0000
59	0.0000	0.0000	0.0000	0.0000
60	0.0000	0.0000	0.0000	0.0000

Ave. %	0.0025	0.0009	0.0030	0.0009
Std. dev.	0.0120	0.0052	0.0116	0.0041

Appendix 3

Normal Distribution

$$F(x) = \int_{-\infty}^{x} \frac{1}{\sqrt{2\pi}} \exp -\frac{t^2}{2}\, dt$$

x	.00	.01	.02	.03	.04	.05	.06	.07	.08	.09
.0	.5000	.5040	.5080	.5120	.5160	.5199	.5239	.5279	.5319	.5359
.1	.5398	.5438	.5478	.5517	.5557	.5596	.5636	.5675	.5714	.5753
.2	.5793	.5832	.5871	.5910	.5948	.5987	.6026	.6064	.6103	.6141
.3	.6179	.6217	.6255	.6293	.6331	.6368	.6406	.6443	.6480	.6517
.4	.6554	.6591	.6628	.6664	.6700	.6736	.6772	.6808	.6844	.6879
.5	.6915	.6950	.6985	.7019	.7054	.7088	.7123	.7157	.7190	.7224
.6	.7257	.7291	.7324	.7357	.7389	.7422	.7454	.7486	.7517	.7549
.7	.7580	.7611	.7642	.7673	.7704	.7734	.7764	.7794	.7823	.7852
.8	.7881	.7910	.7939	.7967	.7995	.8023	.8051	.8078	.8106	.8133
.9	.8159	.8186	.8212	.8238	.8264	.8289	.8315	.8340	.8365	.8389
1.0	.8413	.8438	.8461	.8485	.8508	.8531	.8554	.8577	.8599	.8621
1.1	.8643	.8665	.8686	.8708	.8729	.8749	.8770	.8790	.8810	.8830
1.2	.8849	.8869	.8888	.8907	.8925	.8944	.8962	.8980	.8997	.9015
1.3	.9032	.9049	.9066	.9082	.9099	.9115	.9131	.9147	.9162	.9177
1.4	.9192	.9207	.9222	.9236	.9251	.9265	.9279	.9292	.9306	.9319
1.5	.9332	.9345	.9357	.9370	.9382	.9394	.9406	.9418	.9429	.9441
1.6	.9452	.9463	.9474	.9484	.9495	.9505	.9515	.9525	.9535	.9545
1.7	.9554	.9564	.9573	.9582	.9591	.9599	.9608	.9616	.9625	.9633
1.8	.9641	.9649	.9656	.9664	.9671	.9678	.9686	.9693	.9699	.9706
1.9	.9713	.9719	.9726	.9732	.9738	.9744	.9750	.9756	.9761	.9767
2.0	.9772	.9778	.9783	.9788	.9793	.9798	.9803	.9808	.9812	.9817
2.1	.9821	.9826	.9830	.9834	.9838	.9842	.9846	.9850	.9854	.9857
2.2	.9861	.9864	.9868	.9871	.9875	.9878	.9881	.9884	.9887	.9890
2.3	.9893	.9896	.9898	.9901	.9904	.9906	.9909	.9911	.9913	.9916
2.4	.9918	.9920	.9922	.9925	.9927	.9929	.9931	.9932	.9934	.9936
2.5	.9938	.9940	.9941	.9943	.9945	.9946	.9948	.9949	.9951	.9952
2.6	.9953	.9955	.9956	.9957	.9959	.9960	.9961	.9962	.9963	.9964
2.7	.9965	.9966	.9967	.9968	.9969	.9970	.9971	.9972	.9973	.9974
2.8	.9974	.9975	.9976	.9977	.9977	.9978	.9979	.9979	.9980	.9981
2.9	.9981	.9982	.9982	.9983	.9984	.9984	.9985	.9985	.9986	.9986
3.0	.9987	.9987	.9987	.9988	.9988	.9989	.9989	.9989	.9990	.9990
3.1	.9990	.9991	.9991	.9991	.9992	.9992	.9992	.9992	.9993	.9993
3.2	.9993	.9993	.9994	.9994	.9994	.9994	.9994	.9995	.9995	.9995
3.3	.9995	.9995	.9995	.9996	.9996	.9996	.9996	.9996	.9996	.9997
3.4	.9997	.9997	.9997	.9997	.9997	.9997	.9997	.9997	.9997	.9998

x	1.282	1.645	1.960	2.326	2.576	3.090	3.291	3.891	4.417
$F(x)$	.90	.95	.975	.99	.995	.999	.9995	.99995	.999995
$2[1 - F(x)]$	.20	.10	.05	.02	.01	.002	.001	.0001	.00001

By permission from "Introduction to the Theory of Statistics," by A. M. Mood, McGraw-Hill, New York, 1950.

Appendix 4 Isothermal Elastohydrodynamic (EHD) Lubrication

Rolling surfaces deform appreciably in proportion to the thickness of a fluid film between them. The combination of a deformable surface with a hydrodynamic lubrication action enable the elastohydrodynamic lubrication to occur. Based upon analytical studies and experimental results, Dowson et al [133] established the following formula to calculate the minimum film thickness

$$\overline{H}^0 = \frac{2.65\overline{U}^{0.7} G^{0.54}}{\overline{Q}_Z^{0.13}} \qquad (1)$$

in which $\overline{U}$ and $\overline{Q}$ are the dimensionless speed and the dimensionless load, defined by:

$$\overline{U}_i = \frac{\eta_0 * U}{2 * E' * R} \qquad (2)$$

$$\overline{Q}_Z = \frac{Q_z}{L * E' * R} \qquad (3)$$

$$E' = \frac{E}{1 - \xi^2} \qquad (4)$$

n equations (2), (3) and (4), η_o is lubricant viscosity, cp or lb.sec/inch^2; U is the entrainment velocity, mm/sec or in./sec; E is modulus of elasticity, N/mm^2 or psi; ξ is Poisson's ratio; R is equivalent radius, mm or inches. On the present testing conditions, $\eta_o = 6.9 \times 10^{-8}$ N sec /mm^2, $U = 1.435 \times 10^4$ mm/sec, $\xi = 0.3$, $R = 18.97$/mm, $E' = 2.274 \times 10^5$ N/mm^2 and $G = \lambda * E' = 5000$ for steel rollers and mineral oil lubricant, the dimensionless speed and load are equal to 1.148×10^{-10} and $1.623 \times 10^{-7} \times Q_z$, respectively. The lubricant film thickness, h, is expressed as a function of contact load Q_z in the following table:

Q_z, lb	1600	1700	1800	1900	2000	2100	2200	2300	2400
h, μm	1.76	1.75	1.74	1.72	1.71	1.7	1.7	1.7	1.70

Appendix 5 The Depth of Maximum Shear Stresses

The compressive stress is defined by equation (1):

$$P = 0.418\left[\frac{W*E*(R_T+R_B)}{R_T*R_B}\right]^{\frac{1}{2}} \qquad (1)$$

where W is the load per unit of axial length, E is Young's modulus, R_T and R_B are the top and bottom roller radii respectively. In case of two parallel cylinders of the same material in contact without friction, the half-width of the contact area, b, is given by

$$b=1.13\sqrt{(W*\nabla*R)}$$

$$R=\frac{R1+R2}{R1*R2}$$

$$\nabla=\frac{1-\nu_1}{E_1}+\frac{1-\nu_2}{E_2}$$

Since the two cylinders in the present experiments are the same material and Poisson's ratio ν is taken equal to 0.3, the equation above is simplified as

$$b=1.52\sqrt{\frac{W*R}{E}} \qquad (2)$$

According to the theory of free rolling contact, the maximum shear stress is at the depth of 0.78b underneath the contact surface. Given the other testing conditions, the depth is dependent upon contact load. This dependence is shown in the following table.

load, lb	W, lb/in.	R_T, in.	R_B, in.	b, in.	0.78b, mm
1600	3200	1.4	1.6	0.014	0.27
1700	3400	1.4	1.6	0.014	0.28
1800	3600	1.4	1.6	0.014	0.28
1900	3800	1.4	1.6	0.015	0.29
2000	4000	1.4	1.6	0.015	0.30
2100	4200	1.4	1.6	0.015	0.30
2200	4400	1.4	1.6	0.016	0.30

VITA

Hua Li was born in the Southwest of China on November 1961, and earned his B.S. in metallurgical engineering from Northeastern University, China, in 1982 and M.S. in metallurgy from Beijing University of Science & Technology in 1985. After school studies, He devoted seven years of his prime time to the Pearl River Steel Corporation of South China. In fall 1992, Hua Li started his doctoral study at the Oregon Graduate Institute of Science & Technology.